Safety in Mines Research Advisory Committee

Final Project Report

Preliminary Investigation into the Zone of Support Influence and Stable Span between Support Units

A. Daehnke, K.B. Le Bron and M. van Zyl

Research agency: CSIR Mining Technology

Project number: GAP 627

Date: October 1999

Executive Summary

The current methodology to design stope support systems in South African gold and platinum mines is based on the tributary area concept. The discontinuous nature of the hangingwall is not adequately addressed and the mechanisms governing the support-rock mass interaction are poorly understood. In the past relatively little progress has been made in quantifying the effect of support spacing on the rock mass stability and, at present, it is the responsibility of the rock engineer to estimate support spacing based upon experience. In order to improve safety and continue mining at increasing depth, it is important to improve the understanding of support mechanisms, zones of support influence and the role of rock mass discontinuities.

The aim of this project is to formulate a basis for quantifying support mechanisms, and specifically to gain insights into the influence of rock discontinuities on stable spans. The work gives a preliminary analysis of the support interaction with a discontinuous rock mass, and the understanding thereof will ultimately result in an optimised support system design methodology.

It is emphasised that, due to the preliminary nature of the work, the support design methodology proposed here is untried in the field. Before its full acceptance, the methodology should be subjected to field trials, and assessed and calibrated under actual rockfall and rockburst conditions. It is highly recommended to conduct further research work focussing on in situ evaluations of the proposed design methodology. This is considered an essential extension to this work.

The project comprises the following four enabling outputs:

EO 1 Identify relevant rock mass parameters to characterise the hangingwall integrity in various geotechnical areas.

EO 2 Using analytical and numerical techniques, establish models to quantify the zone of support influence in a discontinuous rock mass.

EO 3 Establish a procedure to verify and calibrate theoretical models (describing the zone of support influence) by means of underground data.

EO 4 Characterise input parameters and design charts for support methodologies leading to improved support system design for quasi-static (rockfall) and dynamic (rockburst) conditions.

It is found that the critical rock mass parameters governing the rock mass stability are (i) the number of discontinuities present in the rock mass, (ii) the orientation of the discontinuities, (iii) the perpendicular spacing of the discontinuities, which includes the beam thickness of hangingwall, (iv) the interface properties of the discontinuities, and (v) the horizontal hangingwall clamping stresses.

Analytical and numerical models are used to quantify zones of support influence. It is shown that the maximum extent of the zone of support influence is dependent on the bedding plane friction angle and the fallout thickness. The zones of influence of the stope face and backfill follow analogously to the support zones of influence. Various procedures to verify and calibrate the theoretical models are described.

This investigation has shown that mechanisms contributing towards hangingwall stability are (i) the zones of support influence, and (ii) keyblock stability between adjacent support units. The proposed design methodology combines both support mechanisms, thus potentially providing an improved and further optimised design tool. It is recommended that the design methodology proposed here be evaluated underground and, if applicable, be incorporated in a design program such as SDA II for use in the industry.

Acknowledgements

The authors would like to express their gratitude towards the Safety in Mines Research Advisory Committee (SIMRAC) for financial support of project GAP 627. The excellent co-operation of the personnel of the gold and platinum mines, which has contributed towards this project, specifically Western Area Gold Mine, Vaal Reefs and Hartebeestfontein, is gratefully acknowledged.

Finally, the authors are indebted to A.J. Jager, Dr M.K.C. Roberts and Dr T.O. Hagan for their guidance and valuable technical contribution, as well as C.A. Langbridge for editing this report.

Table of contents

List of figures

List of tables

Glossary of abbreviations and symbols

Abbreviations

BPM	Big Pebble Marker
UCS	Uni-axial Compressive strength
VCR	Ventersdorp Contact Reef

Symbols

J_r	Joint roughness number
J_a	Joint alteration number
s_n	Normal stress
t	Shear strength of the joint
JRC	Joint roughness coefficient
f_r	Residual friction angle for weathered joints
f_b	Basic friction angle for unweathered joints
JCS	Unconfined compression strength of joint surface
r	Dry density of rock (kg/m^3),
g	Acceleration due to gravity (9.8 m/s^2) and
r	Rebound on weathered joint surface (Schmidt Hammer Test)
R	Rebound on unweathered rock surface (Schmidt Hammer Test)
JRC_0 , JCS_0	Appropriate values for the length of joint actually rated
L_0	Length of joint actually rated
L_n	Total length of the joint
b	Height of bedding plane above hangingwall skin
j	Friction angle of bedding plane interface
f	Friction angle of extension and shear fracture interface
a	Angle of extension fracture (measured from h/wall skin)
b	Angle of shear fracture (measured from h/wall skin)
f	Spacing of discontinuities such as shear fractures & joints
F	Support load
r	Radius of cylindrical support unit
w	Width of rectangular support unit
$s\ (x)$	Zone of influence profile in two dimensions
$s\ (x,y)$	Zone of influence profile in three dimensions
x	Co-ordinate perpendicular to stope face
y	Co-ordinate parallel to stope face
z	Extent of zone of influence from support unit edge
z_x	Zone of influence extent extending in the x-direction from the support unit edge

z_y	Zone of influence extent extending in the *y*-direction from the support unit edge
F_v	Maximum vertical force
s_h^{crit}	Minimum stress
Ω	Scaling parameter
d	Distance from the edge of the support to the fracture
f	Fracture spacing
z_x^-	Extent of the zone of influence on the left-hand side of the support
H	Depth of mining
z_b	Effective zone of influence
c	Average of the measurements from backfill face to backfill - hangingwall contact
a- & *b*-values	Values associated with a backfill stress - strain graph
W	Weight of a block
s	Span between adjacent support units
s_x	Magnitude of compressive horizontal stress in the hangingwall
m	*C*oefficient of friction
V_I, V_{II}	Frictional resistance at abutments
E	Total energy to be absorbed by the support system
m	Mass of the hangingwall (dependent on fall-out height)
v	Initial hangingwall velocity
h	Downward hangingwall displacement
L	Actual unsupported span of the hangingwall beam
L_s	Maximum stable span
L_{max}	Maximum support spacing (centre to centre)
M_x	Mid-point of the support unit
A_p	Area of the panel
A_b	Area of a block
N	Number of blocks in the panel
f_x	Joint spacing in the x-direction
f_y	Joint spacing in the y-direction
S_x	Support spacing in the x-direction
S_y	Support spacing in the y-direction
P	Probability that a block is supported

1 Introduction

1.1 Background

In South African gold mines, rockfall and rockburst reportable injuries and fatalities began to exhibit a slowly rising upward trend during the 1950's, which was associated with steady increases in mining depth. Rock related accidents account for in excess of 50 per cent of all fatalities occurring in the mining industry. Of all rock related fatalities, slightly more than half are associated with rockfalls, whilst the remainder are a consequence of the failure of dynamically loaded rock during seismic events and rockbursts. In response to this challenge, a major expansion in research and development began in the 1960's. A significant research thrust was, and continues to be, directed at stope support, which is the ultimate strategy to combat the hazards of rockfalls and rockbursts. Stope support systems, typically consisting of combinations of props and packs, are used to stabilise the rock mass surrounding the mining excavation and reduce the risk of rockfalls and rockbursts.

The current methodology generally used by the South African gold and platinum mines to design stope support is based upon the tributary area concept. Here, a given weight of rock, determined by an area in the plane of the reef and the height of a possible fall, or the 'fall-out height', is divided between a fixed number of support elements according to the attributable area. The area is determined by the face layout, and the fall-out height is presumed to be known from previous observations. This simple concept takes care of the equilibrium requirements in a rudimentary sense, but it does not adequately address the fact that the rock being supported is likely to be fractured and jointed. Various authors (Klokow, 1999; Daehnke *et al.*, 1999a) have found that the majority of rock mass instabilities occur between support units, and the failure of individual support units is relatively uncommon. Clearly, in these circumstances, the distribution of the support elements is of paramount importance.

At present, it is the responsibility of the rock engineer to estimate support spacing based predominantly upon past experience. In order to improve safety and continue mining at increasing depth, an improved engineering approach is required to design effective support systems with optimum spacing of support units. To this end, an improved understanding of the mechanisms involved in the support - rock interaction, the zones of support influence, maximum stable spans, and the role of rock mass discontinuities is required.

Zones of support influence, broadly defined as the extent of the stress generated by a support unit in the hangingwall, contribute towards the hangingwall stability between adjacent support units. To optimise support spacing and ensure rock mass stability between adjacent support units, a quantification of the zones of support influence is required. To date, zones of support influence are poorly understood and, to the authors' knowledge, no rigorous scientific studies have yet been conducted to quantify zone of influence profiles in discontinuous hangingwall beams, as applicable to stopes in South African gold and platinum mines. A photograph illustrating the zone of influence of a pack during rockburst conditions is given in Figure 1.1, where it is apparent that the stabilising influence of the pack has extended no more than an estimated 10 – 30 cm to either side of the pack under prevailing conditions.

The present objective is to quantify stress profiles within zones of support influence and, specifically, to gain a deeper insight into the role of rock discontinuities such as joints, fractures and bedding planes. These planes of weakness are shown to affect the zone of influence and need to be considered when designing the spacing of support units.

Figure 1.1 The zone of influence of a mat pack after a seismic event (courtesy Hartebeestfontein Gold Mine)

The ultimate outcome of this work is a proposed design tool for the gold and platinum mining industry, to assist the rock mechanics engineer to improve support design, with emphasis on the estimation of optimised support spacing. These proposals are untried in practice, and thus they will have to be assessed and calibrated under practical conditions. This approach to support design should maximise support spacing, whilst maintaining a stable hangingwall span between support units, hence offering maximum safety at optimum cost.

1.2 Scope of Project

SIMRAC Project GAP 627, titled '*Preliminary investigation into the zone of support influence and stable span between support units*', is managed and co-ordinated by the CSIR: Division of Mining Technology. The project work forms the basis of a stope support design methodology with the objective of quantifying optimised support spacing, whilst maintaining stable hangingwall spans between adjacent support units for rockfall and rockburst conditions.

Four enabling outputs (EOs) have contributed towards this objective. These were defined in the project proposal, and are addressed in the relevant sections of this report, as follows.

EO 1 Identify relevant rock mass parameters to characterise the hangingwall integrity in various geotechnical areas.
(Addressed in Chapter 2 of this report)

Step 1.1 Using previous SIMRAC work (GAP 022, GAP 032, GAP 330, GAP 334 and GAP 416) as a basis, identify relevant rock mass parameters

governing the hangingwall stability across the various geotechnical areas of the gold and platinum reefs.
(Sections 2.1, 2.2, 2.4, 2.5 and 2.6)

Step 1.2 Assess the accuracy and extent to which the relevant rock mass parameters can be quantified.
(Section 2.3)

EO 2 Using analytical and numerical techniques, establish models to quantify the zone of support influence in a discontinuous rock mass.
(Addressed in Chapters 3, 4, 5 and 6 of this report)

Step 2.1 a) Quantify zones of support influence in a discontinuous rock mass using numerical techniques.
(Chapter 3)

Step 2.1 b) Quantify zones of support influence in a discontinuous rock mass using analytical techniques.
(Chapter 4)

Step 2.2 Conduct preliminary studies investigating the zone of influence of the stope face.
(Chapter 5)

Step 2.3 Conduct preliminary studies investigating the zone of influence of backfill.
(Chapter 6)

EO 3 Establishing a procedure to verify and calibrate theoretical models (describing the zone of support influence) by means of underground data.
(Addressed in Chapter 7 of this report)

Step 3.1 Investigate methods to quantify the effective *in situ* hangingwall strength.
(Section 7.2)

Step 3.2 Make use of CSIR's accident database and conduct preliminary back-analyses of rockburst and rockfall accidents to determine a statistical distribution of unstable hangingwall spans for various geotechnical areas.
(Section 7.3)

Step 3.3 Apply data gathered in Steps 3.1 & 3.2 and establish a procedure to calibrate and verify theoretical models describing the zones of influence.
(Section 7.4)

EO 4 Characterise input parameters and design charts for support methodologies leading to improved support system design for quasi-static (rockfall) and dynamic (rockburst) conditions.
(Addressed in Chapter 8 of this report)

Further work is conducted to investigate support design methodologies relating to shallow mining environments. These are discussed in Chapter 9 of this report.

The tenth chapter synthesises the main outcomes and new knowledge gained, and makes recommendations for further research work. For a brief overview and summary of the principal findings of this project, it is recommended that the reader focus his/her attention on Chapter 10.

The approach followed in this study involves the determination of relevant rock mass parameters that govern hangingwall stability from a review of previous SIMRAC projects. The

effects of these parameters on the zone of support influence are studied using numerical models, thus providing a qualitative understanding of zones of support influence and facilitating the formulation of mathematical models describing them. These analytical zone of influence models are then combined with keyblock analyses to form a comprehensive design methodology, suitable for support design in intermediate- and deep-level mines. Various methods of verifying and calibrating the zone of influence models are investigated. Due to the different conditions encountered in shallow mines, they are considered separately, and a novel probabilistic support layout design approach is suggested.

2 Identification of relevant rock mass parameters governing hangingwall stability

2.1 Introduction

The complex environments associated with the Witwatersrand and Bushveld mining operations require a careful consideration of geological, rock engineering and mining parameters when assessing the application of certain support types and support strategies.

To enable any design, input is required. In compiling a design procedure for the layout of support systems, the relevant parameters, which characterise or describe the problem, need to be established. The aim of this chapter is to identify the input parameters, which will ultimately be used in the design of a support system.

In order to determine the relevant input parameters, a brief review of previous applicable SIMRAC work, in particular the different approaches concerning support-rock mass interaction and its effect on hangingwall stability, is presented. These approaches give an indication of the rock mass parameters that affect the hangingwall stability and will thus need to be incorporated into the design methodology. Once the relevant input parameters have been established, the extent to which these parameters can be determined is assessed.

Finally, the most important geotechnical areas are identified, as the rock mass parameters used in the design are dependent on the geotechnical characteristics of these areas.

2.2 Support interaction with rock mass

A summary of relevant work done in previous SIMRAC projects is presented here. The purpose of this review is to establish which parameters have a significant influence on the stability of hangingwalls, as these parameters will be used as the input parameters in the design methodology proposed in Chapter 8 of this report.

2.2.1 Approach 1: GAP 334 (York *et al.*, 1998)

Using the Universal Distinct Element Code, UDEC, a stope model was established to investigate the stability of the rock mass as a function of the friction angles on the joints and joint orientations, which exist within the rock mass. The model consists of a horizontal parting plane, referred to as a bedding plane, and another joint set, of which the orientation was varied between 0° and 90°.

It was found that the joint orientations could be categorised according to the modes of failure that occur as a function of the joint friction angle and the panel length (span between pillars).

Joint orientations were grouped together if the rock mass became unstable at the same critical friction angle and panel length. Thus, the joint combination 0°/(75°-85°) exhibited similar behaviour for any joint orientation in the range 75° to 85°. From Figure 2.2.1, it is seen that the joint combination 0°/(75°-85°) is stable at a panel length of 50 m provided that the friction angle on all joints is greater than 20°.

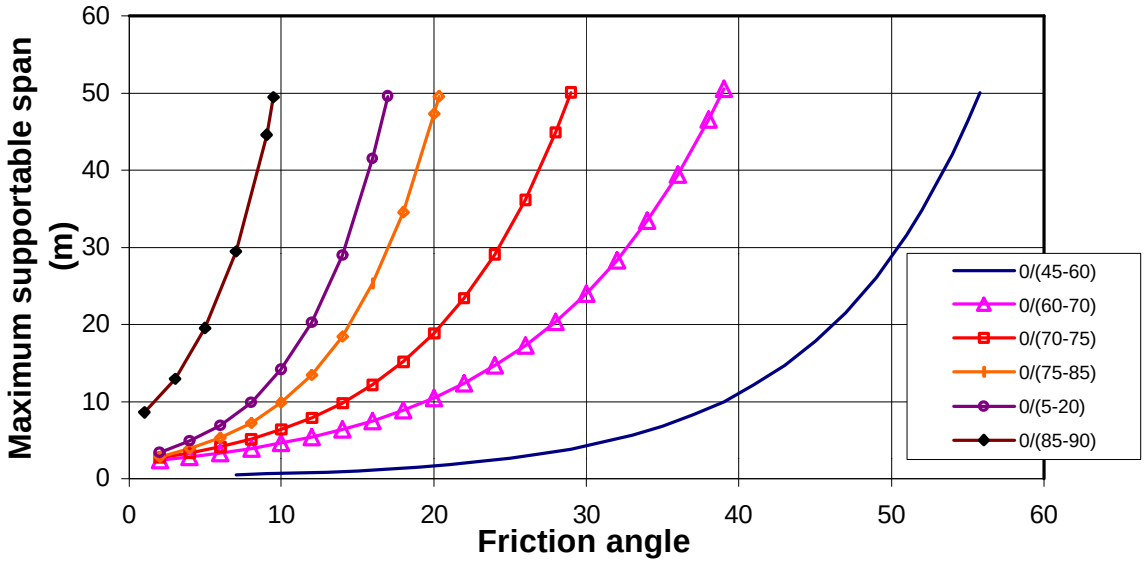

Figure 2.2.1 Influence of joint orientation and friction angle on the panel span for multiple stopes.

It was also found that a multiple (repeating) stope geometry resulted in less stable hangingwalls than the single stope geometry. The range of 20° – 45° joint orientations is completely unstable for the multiple stope geometry.

The different ranges were further divided into groups where the rock mass exhibits the following behaviour:

1) self supporting,
2) unsupportable, and
3) supportable.

Support spacing design charts were established for the supportable section. The design chart for the 85°-90° joint combinations is shown in Figure 2.2.2.

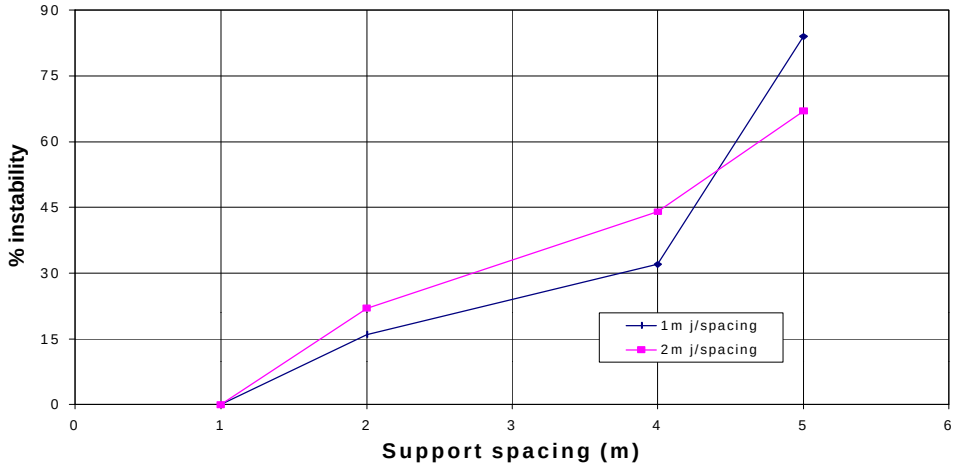

Figure 2.2.2 Percentage instability as a function of support spacing and joint spacing for 0°/(85°-90°) joint orientations with 10° friction angle for a 20m panel span.

This chart, however, is only applicable in a situation where only two joint sets exist in the rock mass. UDEC is a two dimensional program and the plane strain results should be interpreted with care. The existence, orientation and properties of possible fractures in the third dimension are completely ignored. The properties of both sets of fractures/joints are assumed to be the same throughout the model. In reality, the friction angle can be different at different positions along a joint. Although many assumptions were made to simplify the problem, the work done in GAP 334 gives an approximation of the zone of support influence for the different combinations of joint orientations.

The influence of the friction angle was investigated in detail, and the importance thereof with respect to the stability of the rock mass has been established. Neither the influence of horizontal clamping stress nor beam thickness was investigated.

A method for determining the friction angle of joints is presented in GAP 334 based on the results published by Barton (1978).

2.2.2 Approach 2: GAP 330 (Daehnke *et al.*, 1998)

The support-rock mass interaction was evaluated using the finite element code, ELFEN. The model consisted of three joint sets:

- horizontal (bedding plane),
- dipping towards the face (extension fractures), and
- dipping away from the face (shear fractures).

Extension fracture spacing was assumed to be approximately 0,2 m. Shear fractures were sparsely spaced to simulate the observed underground environment. A simplified schematic showing the three most prevalent discontinuity types in intermediate and deep-level mines is shown in Figure 2.2.3.

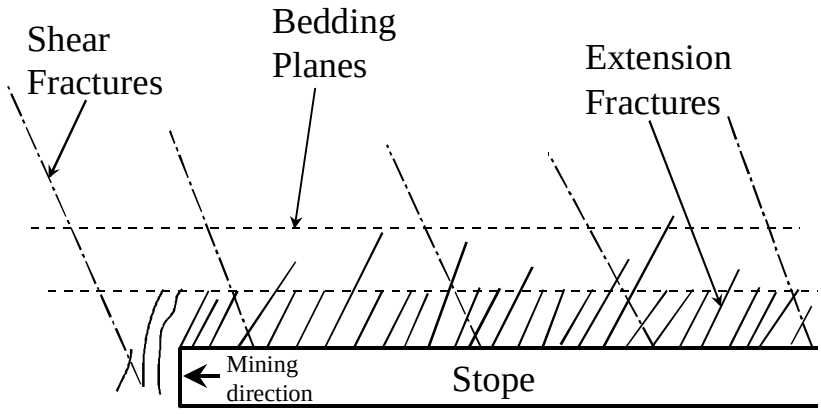

Figure 2.2.3 Discontinuity types in intermediate and deep-level mines (after Daehnke et al., 1998).

Two support units were placed under the beam and the beam was allowed to displace under the influence of gravity. The interaction between the support and the rock mass was then established by investigating the stress trajectories as shown in Figure 2.2.4. In this model the emphasis was placed on investigating the stress transfer from support units into a discontinuous hangingwall, and no horizontal stresses were applied.

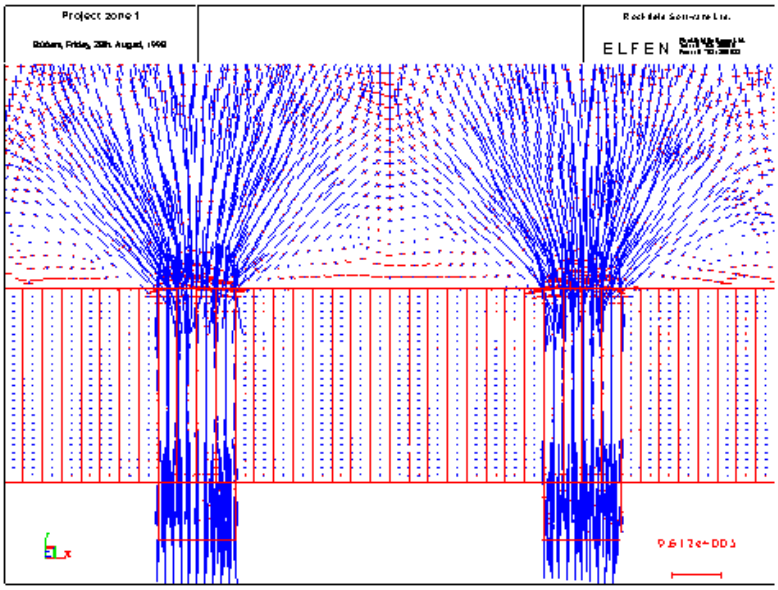

Figure 2.2.4 Schematic showing stress trajectories for fractures orientated 90°.

Stresses are transmitted parallel to discontinuities through a bedding plane into competent rock above. Low clamping stresses act on the slabs between the support units. In deep and intermediate level mines, fracturing ahead of the stope face causes dilation, which in turn gives rise to horizontal clamping stresses, which act parallel to the skin of the excavation (Jager and Roberts, 1996). The horizontal clamping stresses stabilise the slabs between the support units. Horizontal stresses at depths of 0,7 m and 2,2 m into the hangingwall were measured at 1 MPa and 10 MPa, respectively (Squelch, 1994).

By calculating the average stress in the hangingwall beam at different distances from the support units, the zone of support influence was established as a function of the fracture orientation. It was, however, not shown whether the zone of support influence is dependent on the position of the support with respect to the fractures in the unstable beam. This influence will be investigated in this study.

The zone of support influence, as indicated by the stress trajectories, is the exact zone of influence of the specific support unit. The stresses are concentrated parallel and perpendicular to the fracture orientations. The rock outside the area of influence can fall out under gravity since the support has no effect on the stability of this region. Sufficient horizontal stresses can, however, stabilise the rock outside the zone of support influence. The zone of influence can be extended by using headboards, which spread the support load over a greater area. The lateral area of the support unit, which is in contact with the unstable beam, and the horizontal clamping stress are extremely important with respect to the stability of the hangingwall beam.

Stability of the structures between support units was also analysed as part of the support-rock mass interaction investigation. Two failure mechanisms, namely beam buckling and shear failure due to slip at the abutments, were identified and are discussed in GAP 330. Figures 2.2.5 and 2.2.6 illustrate these failure mechanisms.

This study has shown that the horizontal clamping stress is important in stabilising the hangingwall. The influence of stress on the stability of a hangingwall, discretised by fractures of different orientations, was also considered in GAP 330. Further work indicated that, as the beam thickness increases, the hangingwall becomes less prone to fail in the buckling mode and the maximum stable span is increased (Figure 2.2.7). In addition, it was shown that the maximum stable span decreases as the number of joints per metre increases.

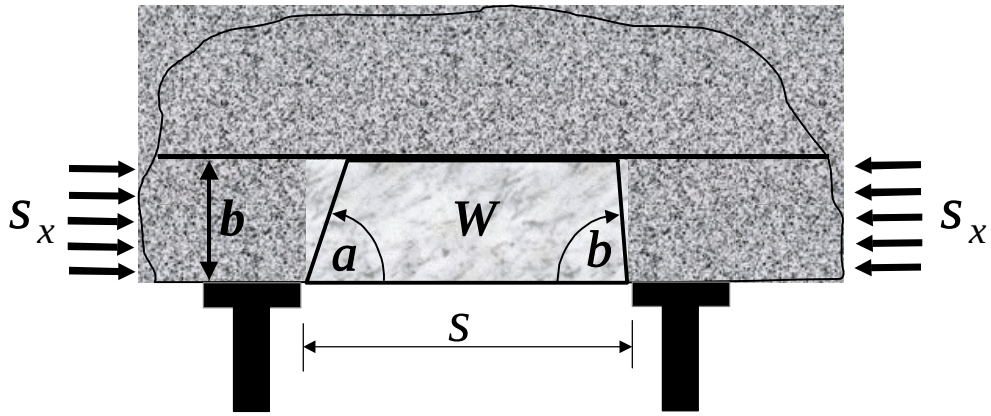

Figure 2.2.5 Rock mass instability due to shear failure at the abutments.

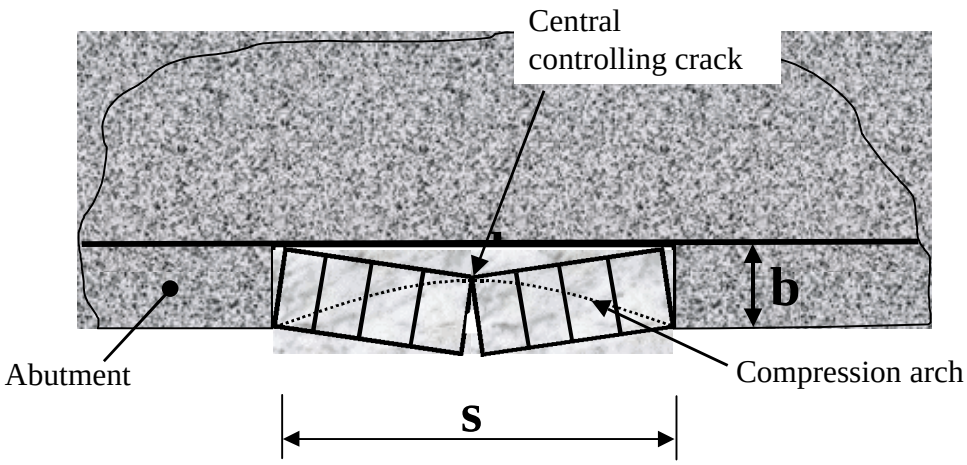

Figure 2.2.6 Buckling failure of beam.

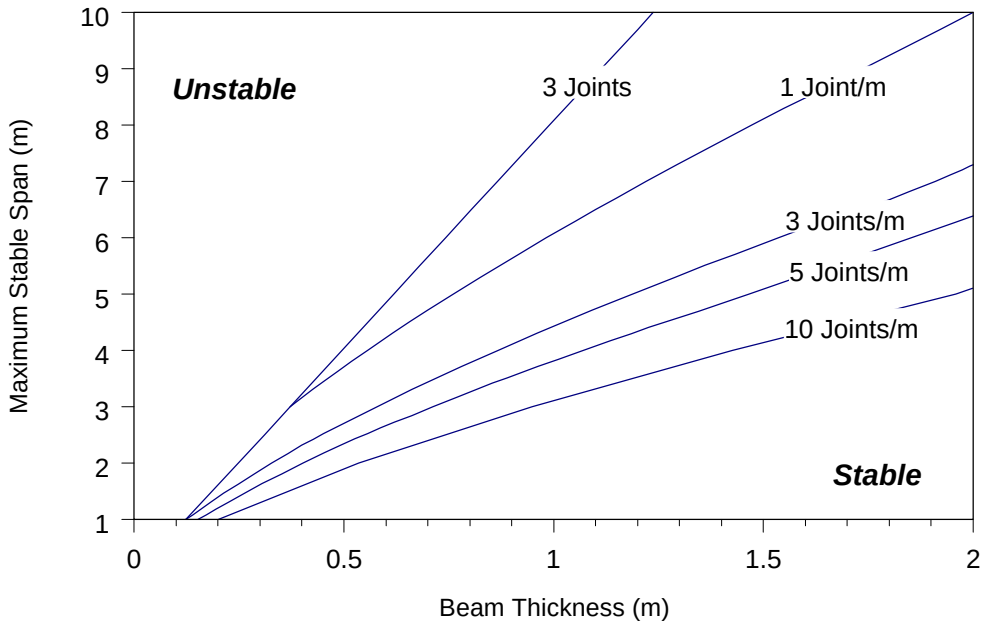

Figure 2.2.7 Influence of joint spacing and beam thickness on hangingwall stability.

2.2.3 Approach 3: GAP 330 (Daehnke *et al.*, 1998)

This study concentrated on failure mechanisms of layered rock mass. The effect of bedding planes on stress distribution and associated fracture formation has been addressed previously (Kuijpers, 1998; Sellers, 1997) and the effect of support pressure and resulting deformations was also investigated (Kuijpers, 1998). These efforts have not, however, led to conclusive results with respect to support requirements.

The analyses presented here concentrate on parameters such as layer thickness, interface friction and dilation (undulation), support pressure, stability of the hangingwall beam, etc.

It was concluded from the numerical model that a substantial amount of inelastic closure may be associated with the bedding planes. The parameter that controls this inelastic closure is the effective dilation associated with slip across these bedding planes. The number of bedding planes on which slip occurs affects the total closure to a great extent.

Slip and dilation are initiated at the abutments and cause separation of bedding planes over the full stope length. This mechanism of bedding plane separation may also explain the observations of Gürtunca *et al.* (1990). It was observed that up to a pressure of approximately 1 MPa in the supporting backfill, no differential movement was observed in the hangingwall across a strike gully. However, higher pressures induced a differential between the deformation of the hangingwall above the unsupported gully, and the lesser deformation of the hangingwall in direct contact with the pressurised backfill (Daehnke *et al*., 1998).

The study also suggested that closure of the bedding planes requires a certain stress; this stress depends on the thickness of the layer and possibly other parameters. Closure of all separated layers requires increased support pressures and has been observed by Gürtunca *et al*. (1990), who noted that at stresses above 3,5 MPa, no additional differential closure develops between the hangingwall above the unsupported gully, and the hangingwall subjected to the backfill pressure (Daehnke *et al*., 1998).

An observation by Herrmann (1987) showed that local support does not affect the (inelastic) closure in a longwall stope, but it was not possible to investigate the support interaction. Bed separation is a particular stability problem that can be associated with local support. Daehnke *et al*. (1998) indicated mechanisms leading to hangingwall instabilities induced by individual support units. If the support strength exceeds levels that may induce sliding across certain fractures in the immediate hangingwall, instabilities are possible.

Although it is difficult to quantify the support-rock mass interaction, it can be seen from many rock related accidents that the inability of the rock mass to bridge the span between individual support units is one of the main reasons for (local) instabilities and the consequences thereof. Under such circumstances, the rock mass requires additional support in order to assist it in bridging the gap between the (main) support units (Daehnke *et al*., 1998).

A decrease in the support spacing will increase the ability of the rock mass to bridge the (smaller) gaps. It may also be more efficient and cost effective to increase the load bearing capacity of the rock mass by providing it with extended areal support. The only function of the areal support is to assist the rock mass in bridging the distance between the main support units. This will enable more effective design of support units for their intended function, namely, to prevent the immediate stope hangingwall from detaching itself from the surrounding rock mass, thus inducing general hangingwall instabilities. (The current support design methodology assumes exactly that same function, without considering local stability; Daehnke *et al*., 1998.) Thus, a secondary support could fulfil the function of stabilising the rock between individual support units.

The requirements for a secondary support depend on the rock mass under consideration. Where a competent hangingwall is present, no secondary support may be required, whereas,

for cases in which highly fragmented hangingwall conditions prevail, a limited contribution towards load bearing capacity can be expected from the rock mass, and thus increasing support is required.

2.2.4 Approach 4: GAP 330 (Daehnke *et al*., 1998)

2.2.4.1 Fall of ground accident analysis

An analysis of fall of ground accidents in stopes was done for the Carletonville area. A study of the support failure modes showed that 59 per cent of falls of ground were due to dislodged (toppled) temporary support units, 17 per cent of falls were caused by dislodged permanent supports, and 24 per cent were due to failure of temporary and tendon support units. No cases of permanent support failure were reported (see Figure 2.2.8).

The location of falls of ground relative to the support units is extremely important and the results are shown in Figure 2.2.9. It can be seen that the largest number (44 per cent) of falls of ground occur in the face area, i.e. between the face and the first row of support. 13 per cent of falls of ground occur between permanent and temporary supports. Falls of ground that occur due to the failure or dislodgement of support units represent the remaining 43 per cent.

Evaluation of the dislodging of supports also showed that elongate type supports were the most likely to dislodge.

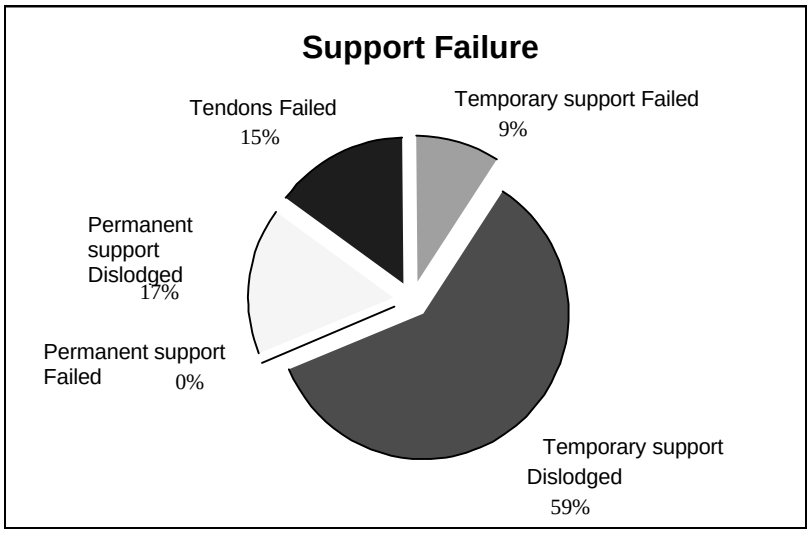

Figure 2.2.8 Modes of support failure (after Daehnke et al., 1998).

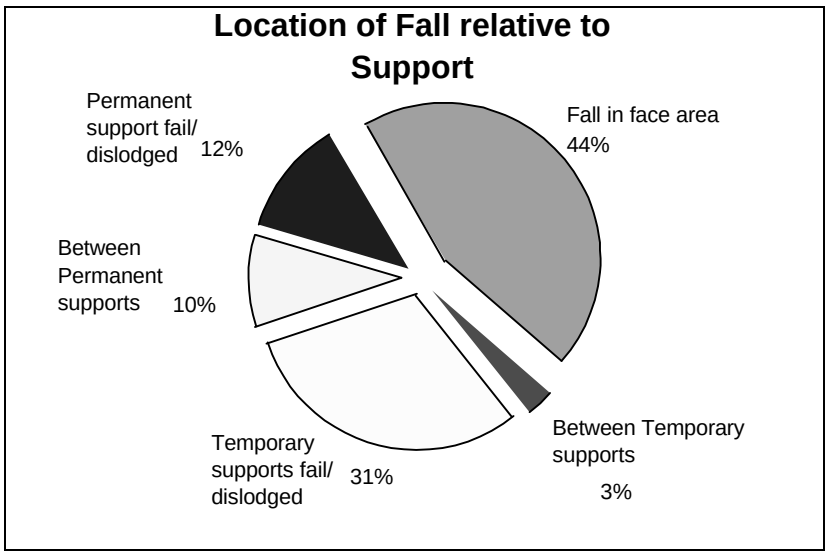

Figure 2.2.9 Location of falls relative to supports (after Daehnke et al., 1998).

2.2.4.2 Keyblock Analysis

The numerical code, JBLOCK, was used for a keyblock analysis. In this study (Daehnke *et al.*, 1998), the effect of different geotechnical parameters and variations thereof on keyblock stability was evaluated. To achieve this, a model, which consists of a stope excavation, was simulated. The objective was to determine, and possibly quantify, the reaction of the keyblocks to changes in parameters such as clamping stresses, dip of joints and spacing. The values of different parameters assumed in the model are shown in Table 2.2.1 and Table 2.2.2.

Table 2.2.1 Orientation data used in keyblock analysis models (after Daehnke et al., 1998).

Set	Dip	Dip direction	Scatter
1: Extension fractures	70°	270°	20°
2: Shear fractures	70°	90°	20°
3: Bedding	0°	180°	10°
4: Geological joints	90°	45°	10°
5: Stope hangingwall	0°	180°	10°

Table 2.2.2 Dimensions of discontinuities used in keyblock analysis models (after Daehnke et al., 1998).

Set	Spacing (m)	Min. spacing (m)	Max. spacing (m)	Trace Length (m)	Min. length (m)	Max. length (m)
1: Extension fractures	0,15	0,05	1,0	5,0	3,0	20,0
2: Shear fractures	3,0	2,0	10,0	10,0	5,0	30,0
3: Bedding	1,0	0.3	3,2	10,0	3,0	30,0
4: Geological joints	1,0	0,2	3,0	10,0	3,0	30,0

The fractures and joints were chosen such that the model would simulate the main features of a stope in a deep gold mine. The first set represents closely spaced extension fractures that are face parallel, dipping at 70°. The second set represents shear fractures that are less frequent and dip towards the back area of the stope. The third set represents a horizontal joint (bedding plane), spaced at an average of 1 m, parallel to the stope hangingwall. The fourth is a set of geological discontinuities that are vertical and strike at right angles to the face.

The effects of the various parameters were evaluated by modelling 5 000 keyblocks generated for each scenario, and testing each one for stability. In the absence of any support or clamping stresses, a keyblock can only be stable if it is held in place by friction. If a keyblock is able to simply drop out of the rock mass, it will do so. The presence of clamping stresses may cause a keyblock, which would have dropped out otherwise, to be held in position by friction (Daehnke *et al*., 1998).

The results of the analyses were compared by considering the volume of unstable keyblocks per 1 000 m^2 of hangingwall exposed. In this report, this is called the volume of failure. The failure volume is an indication of the amount – and not the severity – of failure, in terms of risk or hazard. Other parameters, such as the percentage of unstable keyblocks, were also considered (Daehnke *et al*., 1998).

All the stress related fractures were assumed to strike approximately parallel to the stope face, and therefore these cannot form keyblocks alone. A release surface is required, which defines the limits of the block.

Figure 2.2.10 shows the influence of fracture dip angle on the volume of failure. The clamping stress was assumed to be zero and no supports were present in the model. From Figure 2.2.10 it can be seen that if the fractures/joints are shallow dipping and form parallelepiped blocks (see Figure 2.2.11), the keyblocks are stable. In this case blocks fail by sliding along geological structures (Figure 2.2.11). As the dip of the fractures increases and wedge-shaped blocks are formed, a greater number of the keyblocks become unstable and fail by dropping out (Figure 2.2.11).

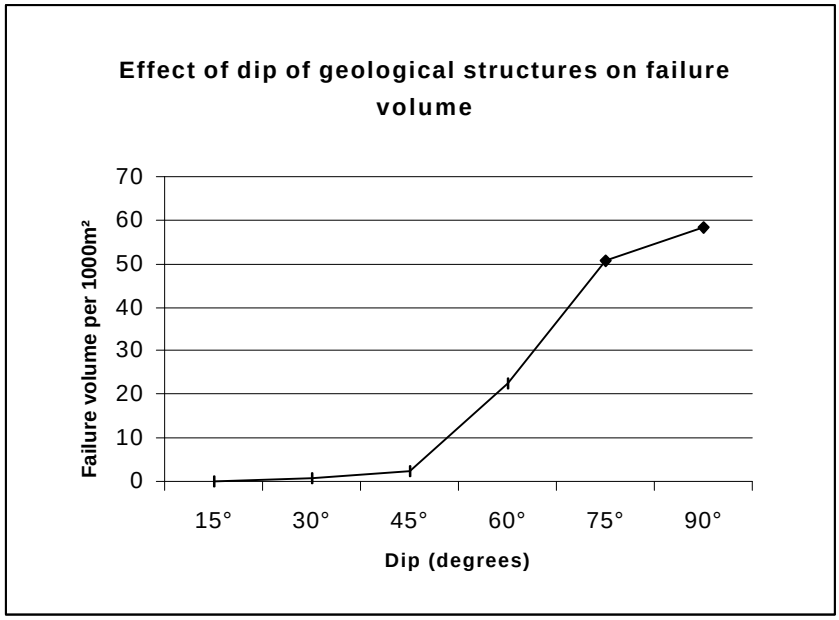

Figure 2.2.10 Graph showing the effect of the dip of geological structures on keyblock stability in the absence of clamping stresses (after Daehnke et al., 1998).

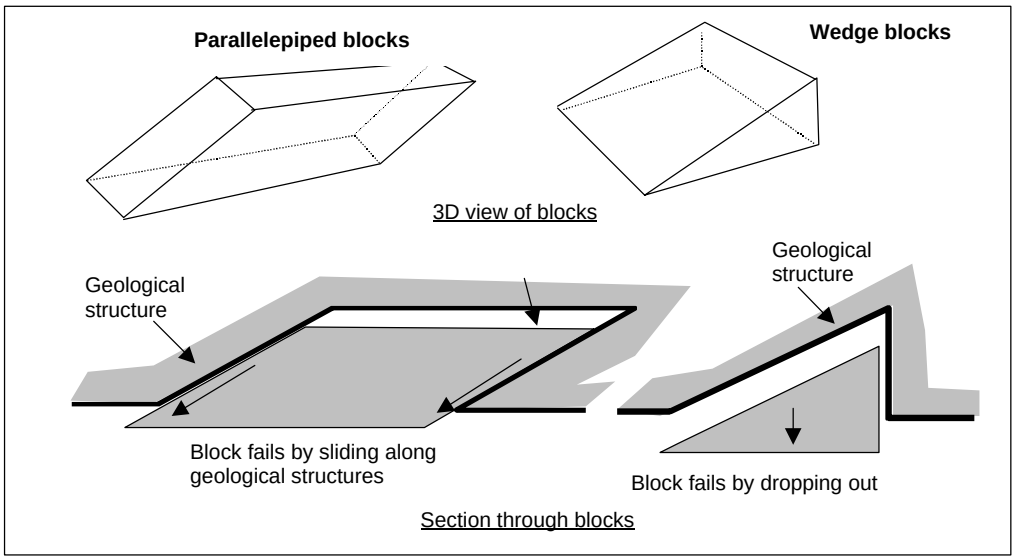

Figure 2.2.11 Sketch showing failure mode of two types of keyblocks (after Daehnke et al., 1998).

2.2.4.3 The effect of clamping stresses on keyblock stability

In deep mine excavations, horizontal clamping stresses exist in the hangingwalls of stopes. This is due to the dilation of the rock at the stope face. Horizontal clamping stresses increase the stability of the hangingwall. The effect of clamping stresses on wedge-shaped blocks was evaluated and the results are shown in Figure 2.2.12. The dip of the discontinuity was varied between 15° and 75° and the clamping stress was increased from 0 to 2 MPa.

The results show that clamping stresses as low as 200 kPa can stabilise most of the wedge-shaped blocks. Only the flat wedges, which are formed when the fracture dip angle is 15°, are unstable at high clamping stresses of 2 MPa. The results of these investigations show that relatively low clamping stresses stabilise keyblocks in the hangingwall.

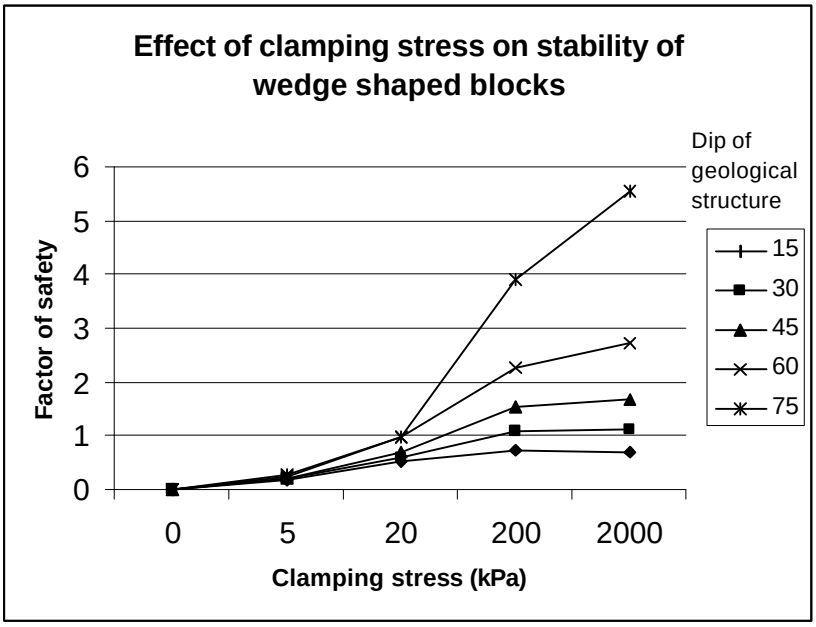

Figure 2.2.12 Graph showing the effect of clamping stresses on the factor of safety of wedge-shaped blocks (after Daehnke et al., 1998).

2.3 Quantification of rock mass parameters

From the previous section, it is clear that the following rock mass parameters govern the hangingwall stability:

1) The number of discontinuity sets present in the rock mass.
2) The dip angle/orientation of these discontinuities with respect to the horizontal.
3) The hangingwall beam thickness.
4) The interface properties of these discontinuities, such as apparent friction angle.
5) The horizontal clamping stress present in the rock mass.
6) The strength of the rock mass (including discontinuities).

In this section, the extent to which the above parameters can be determined is assessed.

Most of these parameters can be readily obtained by underground observations. When using these parameters in designing a support system, as much data as possible must be obtained to give a good representation of the rock mass conditions.

The number of discontinuities can be counted by inspecting the hangingwall surface. Although a good estimation can be obtained by observations only, the presence of other discontinuity sets, which are not exposed at the surface, can also be detected by drilling and examining core. Petroscopes and borehole cameras can be used to examine the actual hole for more discontinuities. The spacing of these discontinuities and the thickness of the hangingwall beam can also be determined using the same procedure. Thus, a fairly accurate assessment of the number of discontinuity sets and their perpendicular spacings can be made.

The dip angles of discontinuities are more difficult to obtain. These can be estimated (with great difficulty) from petroscope and borehole camera studies. The easiest way of measuring the dip angles is by using a clinorule on an exposed discontinuity surface. It is also difficult to measure sufficient numbers of these angles when there are only few or small areas of surfaces that are exposed. When a fall of ground occurs, there are usually a few discontinuity surfaces that are well exposed. Thus, depending on the conditions of the rock mass, the dip angles can be measured accurately (within 2 – 3 degrees).

Laboratory testing can be done to determine the strength of the rock. Using these results, the Hoek and Brown failure criterion can be used to estimate the strength of the rock mass. Other rock mass classification systems can also be used for this purpose. The strength of a rock mass is merely an estimate and is thus not very accurate.

A few methods exist to estimate the friction angles. The first method is a tilt test. A tilt test may be done by placing two rocks with a joint between them on a horizontal plane, one on top of the other. The lower rock is then tilted (increasing the angle between the discontinuity and the horizontal). The angle at which sliding on the joint between the rocks is initiated is measured and represents the joint friction angle.

Another methodology for determination of the friction angle is given below. This work was done for SIMRAC Project GAP 334. The study is reproduced in this report to emphasise that the determination of many parameters are merely approximations.

Barton (1978) presented a method to determine the effective friction angle on joints. The two cases that occur most frequently in hard rock mines are shown in Figure 2.3.1.

Figure 2.3.1 (a) Joint with in-filling. (b) Joint without in-filling.

The shear strength, t, of the joint shown in Figure 2.3.1(a) is given by:

$$t = s_n \tan (J_r/J_a) \qquad (2.3.1)$$

where J_r is the joint roughness number, J_a is the joint alteration number and s_n is the normal stress acting on the joint. The parameter, (J_r/J_a), is the effective friction angle of the joint. These values can be estimated from the Q-system parameter rating charts (Table 2.3.3).

The shear strength of the joint shown in Figure 2.3.1(b) is given by:

$$t = s_n \tan [JRC \log_{10} (JCS/s_n) + Z] \qquad (2.3.2)$$

Where: *JRC* is the joint roughness coefficient,
(JCS/s_n) is the joint wall compressive strength/normal stress,
Z (f_r) = residual friction angle for weathered joints, and
Z (f_b) = basic friction angle for unweathered joints.

The dilation angle of the joint is included in the term ($JRC \log_{10} (JCS/s_n)$). The friction angle of weathered joints is defined as the residual friction angle and the friction angle of unweathered joints is defined as the basic friction angle.

The proposed methodology is shown in Figure 2.3.2.

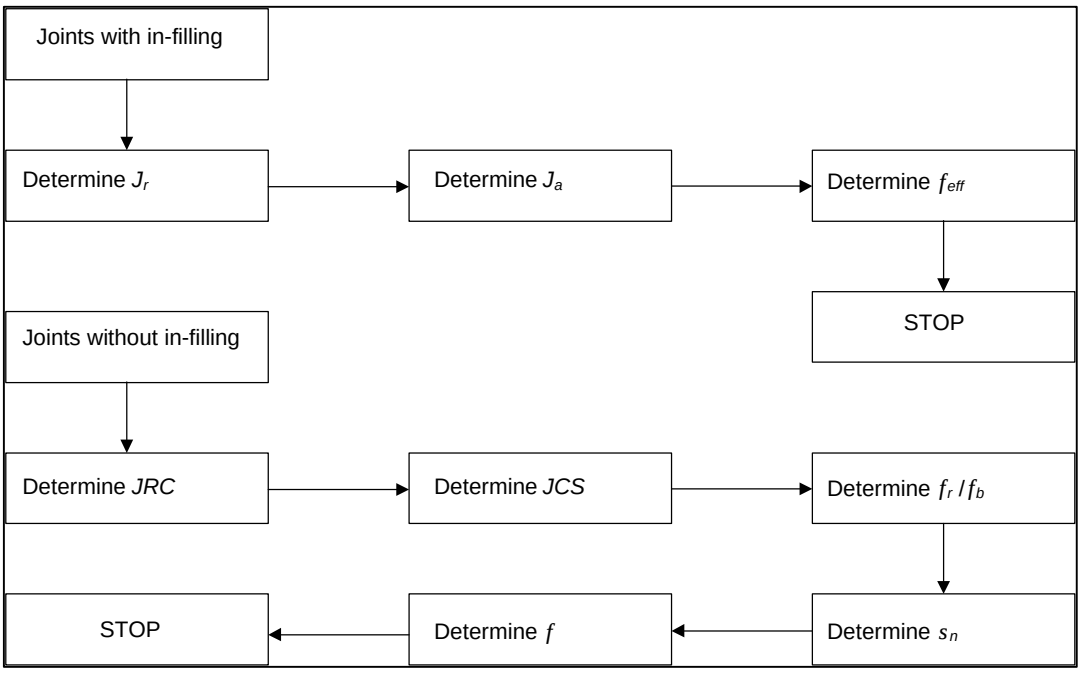

Figure 2.3.2 Proposed methodology for determination of joint friction angle.

The methods to determine the unknowns are discussed below.

The weathering process of a rock mass can be summarised as follows:

1) Formation of joint in intact rock; *JCS* value the same as σ_c (compressive strength of rock surface) since no weathering.
2) Slow reduction of joint wall strength if joints are water conducting; *JCS* becomes less than σ_c.
3) Common intermediate stage; weathered, water conducting joints, impermeable rock blocks; *JCS* some fraction of σ_c.
4) Advanced stage of weathering; more uniformly reduced σ_c finally drops to same level as *JCS*, rock mass permeable throughout.

The *JCS* values for stages 1 and 4 can be obtained by conventional unconfined compression tests on intact cylinders, or from point load tests on rock core or irregular lumps. The *JCS* values relevant to weathered, water conducting joints (stages 2 and 3) cannot be evaluated by standard rock mechanics tests.

The *JRC* for any joint can be estimated from Figure 2.3.3.

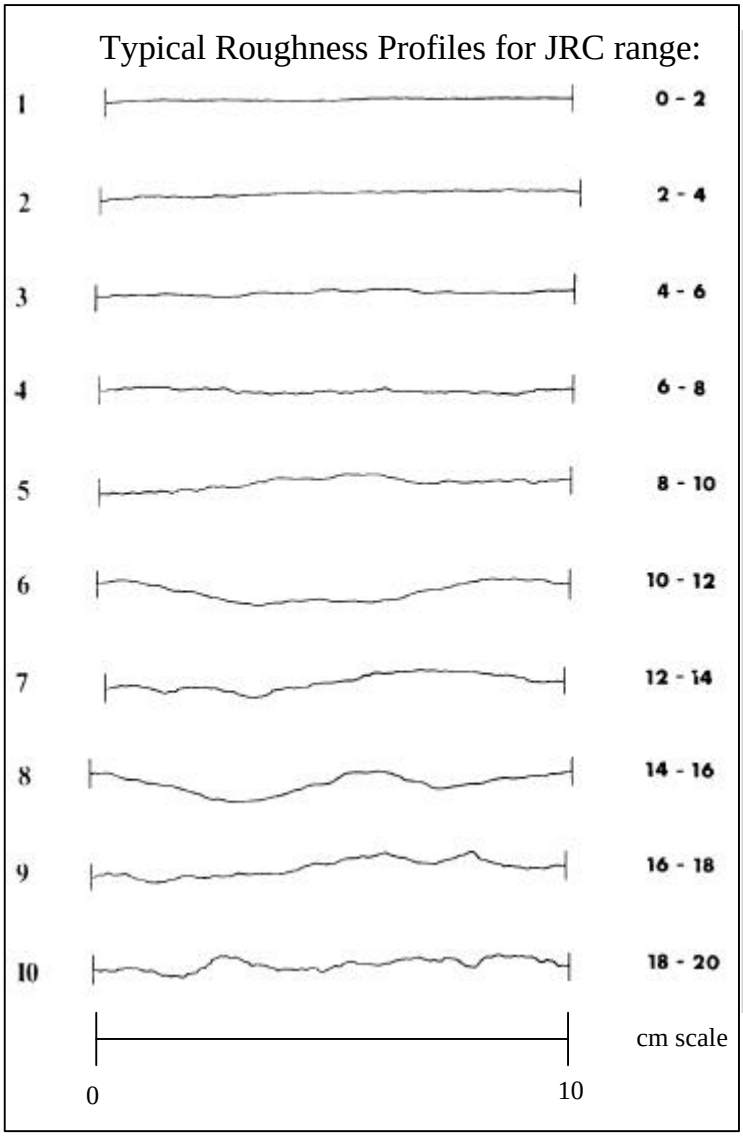

Figure 2.3.3 Joint roughness profile chart, after Barton (1978).

Schmidt Hammer Index test

A good estimation for the *JCS* can be obtained by multiplying the rebound number by the dry density of the rock.

$$\text{Log}_{10}\,(JCS) = 0{,}00088\; r\; g\; R + 1{,}01 \qquad (2.3.3)$$

where (*JCS*) = unconfined compression strength of joint surface (MPa),
r = dry density of rock (kg/m^3),
g = acceleration due to gravity (9.8 m/s^2), and
R = rebound number.

The above relationship and an approximate measure of the anticipated scatter are shown in Figure 2.3.4.

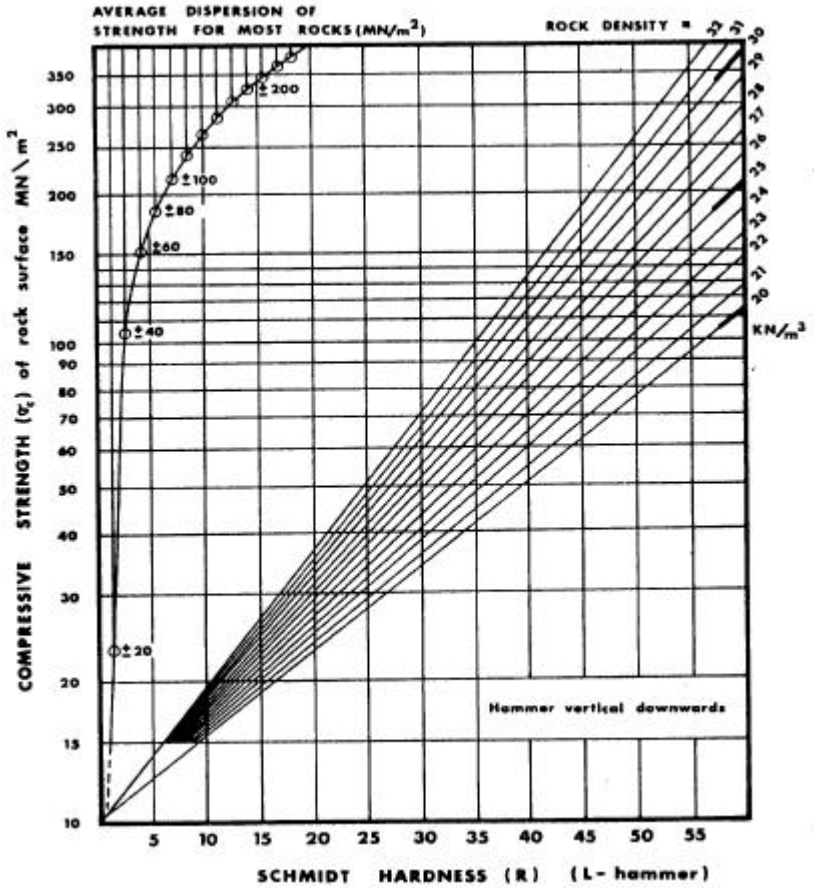

Figure 2.3.4 Correlation chart for Schmidt (L) hammer, relating rock density, compressive strength and rebound number.

For a given surface, the rebound number is a minimum when the hammer is used vertically downwards (rebound against gravity) and a maximum when used on horizontal surfaces. The corrections given in Table 2.3.1 below should be applied when the hammer is used in other directions. The hammer should be applied perpendicular to the surface in question.

A correct rebound measurement will not be obtained if the impulse of the Schmidt hammer is sufficient to move the rock sample being tested. If small samples such as rock core or small blocks are to be tested, they should be firmly seated or clamped on a heavy base. Larger blocks, extracted from rock slopes or tunnel walls, which are to be tested unclamped, should measure at least 20 cm in each direction.

Table 2.3.1 Corrections for Reduced Measured Schmidt Hammer Rebound (R) when the hammer is not used vertically downwards, after Barton (1978).

Rebound	Downwards		Upwards		Horizontal
R	α = - 90°	α = - 45°	α = + 90°	α = + 45°	α = 0°
10	0	-0.8	--	--	-3.2
20	0	-0.9	-8.8	-6.9	-3.4
30	0	-0.8	-7.8	-6.2	-3.1
40	0	-0.7	-6.6	-5.3	-2.7
50	0	-0.6	-5.3	-4.3	-2.2
60	0	-0.4	-4.0	-3.3	-1.7

Basic friction angles of different rock types are given in Table 2.3.2.

The residual friction angle, f_r, can be estimated from the results of Schmidt Rebound tests. The following empirical relationship may be used:

$$f_r = 10° + r/R\ (f_b - 10°) \tag{2.3.4}$$

Where: r = rebound on weathered joint surface, and
R = rebound on unweathered rock surface.

The basic friction angle is not affected by scale, but both the geometrical and asperity factors are. These factors decrease as the scale increases, as described by the following equations.

$$JRC_n = JRC_o\ [\ L_n / L_o\ ]^{-0.02\ JRCo} \tag{2.3.5}$$

$$JCS_n = JCS_o\ [\ L_n / L_o\ ]^{-0.03\ JCSo} \tag{2.3.6}$$

JRC_0 and JCS_0 are appropriate values for the length of joint actually rated, L_0. L_n is the total length of the joint. If, for example, only 10 cm (L_0) of a joint can be measured and this joint extends 2 m (L_n) into the hangingwall, JRC_0 can be determined by rating the joint that is exposed and JRC_n can be calculated by using Equation 2.3.5. JCS_0 and JCS_n can be determined following the same procedure.

In Equation 2.3.2, the determination of s_n causes difficulties, as this implies a proper modelling of the jointed rock mass, which can be complex and time consuming. To provide some guidelines, a sensitivity analysis was done to show the influence of normal stress on the effective friction angle. This is shown in Figure 2.3.5, where a typical *JCS* value of 30 MPa and a basic friction angle of 20° were assumed. For low values of *JRC*, the influence of normal stress is very limited, and where the normal stresses are above 15 MPa, the change in effective friction angle is negligible.

For high values of *JRC* (above 10), the influence of normal stress is more pronounced. A good estimation of the normal stress will give a more accurate value of the effective friction angle. Normal stress values lower than 5 MPa have a significant effect on the value of the effective friction angles.

Table 2.3.2 Basic Friction angles of various unweathered rocks, after Barton (1978).

Rock Type	Moisture Condition	Basic friction angle N_0	Reference
A. Sedimentary Rocks			
Sandstone	Dry	26 – 35	Patton, 1966
Sandstone	Wet	25 – 33	Patton, 1966
Sandstone	Wet	29	Ripley & Lee, 1962
Sandstone	Dry	31 – 33	Krsmanovi, 1967
Sandstone	Dry	32 – 34	Coulson, 1972
Sandstone	Wet	31 – 34	Coulson, 1972
Sandstone	Wet	33	Richards, 1975
Shale	Wet	27	Ripley & Lee, 1962
Siltstone	Wet	31	Ripley & Lee, 1962
Siltstone	Dry	31 – 33	Coulson, 1972
Siltstone	Wet	27 – 31	Coulson, 1972
Conglomerate	Dry	35	Krsmanovi, 1967
Chalk	Wet	30	Hutchinson, 1972
Limestone	Dry	31 – 37	Coulson, 1972
Limestone	Wet	27 – 35	Coulson, 1972
B. Igneous Rocks			
Basalt	Dry	35 – 38	Coulson, 1972
Basalt	Wet	31 – 36	Coulson, 1972
Fine-grained granite	Dry	31 – 35	Coulson, 1972
Fine-grained granite	Wet	29 – 31	Coulson, 1972
Coarse-grained granite	Dry	31 – 35	Coulson, 1972
Coarse grained granite	Wet	31 – 33	Coulson, 1972
Porphyry	Dry	31	Barton, 1971b
Porphyry	Dry	31	Barton, 1971b
Dolerite	Dry	36	Richards, 1975
Dolerite	Wet	32	Richards, 1975
C. Metamorphic Rocks			
Amphibolite	Dry	32	Wallace *et al.*, 1970
Gneiss	Dry	26 – 29	Coulson, 1972
Gneiss	Wet	23 – 26	Coulson, 1972
Slate	Dry	25 – 30	Barton, 1971b
Slate	Dry	30	Richards, 1975
Slate	Wet	21	Richards, 1975

Table 2.3.3 Updated Q-system parameter ratings (Grimstad et al., 1993 update)

1. Joint Roughness Number		J_r
a) Rock-wall contact, and b) rock-wall contact before 10 cm shear		
A	Discontinuous joints	4
B	Rough or irregular, undulating	3
C	Smooth, undulating	2
D	Slickensided, undulating	1.5
E	Rough or irregular, planar	1.5
F	Smooth, planar	1.0
G	Slickensided, planar	0.5
Note: i) Descriptions refer to small scale features and intermediate scale features, in that order.		
c) No rock-wall contact when sheared		
H	Zone containing clay minerals thick enough to prevent rock-wall contact	1.0
J	Sandy, gravelly or crushed zone thick enough to prevent rock-wall contact	1.0
Note: i) Add 1.0 if the mean spacing of the relevant joint set is greater than 3 m. ii) J_r = 0.5 can be used for planar slickensided joints having lineations, provided the lineations are oriented for minimum strength.		

2. Joint Alteration Number		f_r approx.	J_a
a) Rock-wall contact (no mineral fillings, only coatings)			
A	Tightly healed, hard, non-softening, impermeable filling, i.e., quartz or epidote	-	0.75
B	Unaltered joint walls, surface staining only	25-35^o	1.0
C	Slightly altered joint walls. Non-softening mineral coatings, sandy particles, clay-free disintegrated rock, etc.	25-30^o	2.0
D	Silty- or sandy-clay coatings, small clay fraction (non-softening)	20-25^o	3.0
E	Softening or low friction clay mineral coatings, i.e., kaolinite or mica. Also chlorite, talc, gypsum, graphite, etc., and small quantities of swelling clays	8-16^o	4.0
b) No rock-wall contact before 10 cm shear (thin mineral fillings)			
F	Sandy particles, clay-free disintegrated clay mineral	25-30^o	4.0
G	Strongly over-consolidated non-softening clay mineral fillings (continuous, but < 5 mm thickness)	16-24^o	6.0
H	Medium or low over-consolidation, softening, clay mineral fillings (continuous, but < 5 mm thickness)	12-16^o	8.0
J	Swelling-clay fillings, i.e., montmorillonite (continuous, but < 5 mm thickness). Value of J_a depends on per cent of swelling clay-size particles, and access to water, etc.	6-12^o	8-12
c) No rock-wall contact when sheared (thick mineral fillings)			
KLM	Zones or bands of disintegrated or crushed rock and clay (see G, H, J for description of clay condition)	6-24^o	6, 8, or 8-12
N	Zones or bands of silty- or sandy-clay, small clay fraction (non-softening)	-	5.0
OPR	Thick, continuous zones or bands of clay (see G, H, J for description of clay condition)	6-24^o	10, 13, or 13-20

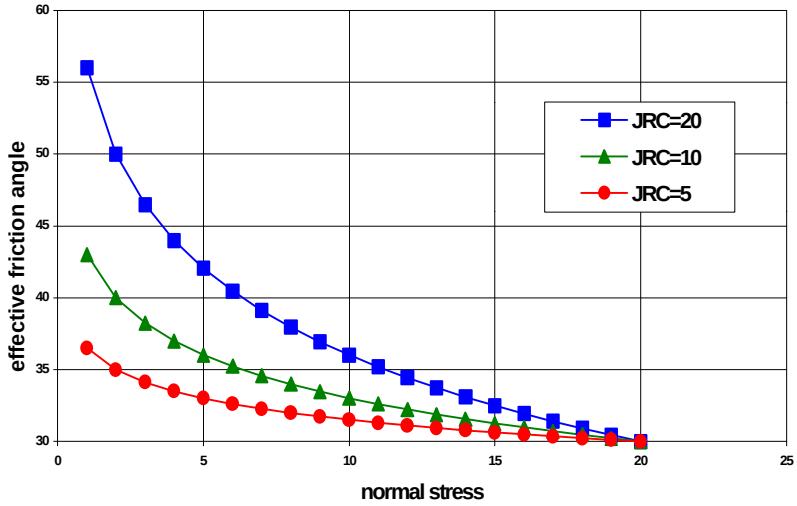

Figure 2.3.5 Influence of normal stress on effective friction angle.

From this analysis, it is clear that some parameters are easily quantified, whereas others are difficult to estimate.

2.4 Overview of mining environments and ground control districts in the Witwatersrand and Bushveld Complex

The purpose of this section is to provide an overview of the variation in conditions for which support has to be designed in the Witwatersrand and Bushveld mines. Geotechnical areas across the gold and platinum reefs are classified according to reef and rock mass behaviour. The main geotechnical areas across the Witwatersrand gold mines, delineated according to reef type, are:

1) Ventersdorp Contact Reef, VCR (West Rand)
2) Carbon Leader (West Rand)
3) Vaal Reef (Klerksdorp)
4) Leader reef, B-reef, Witpan reef, VS5, etc. (Free state)

Across the Bushveld platinum mines, the main reef types are:

1) Merensky reef
2) UG2

These reef types are deemed to be the most important, as in South Africa the highest proportion of gold and platinum reef exploitation occurs in them. The reefs can further be divided into ground control districts on the basis of various local rock mass behaviour characteristics. A brief overview of the main geotechnical areas is given below. For a more detailed description of these areas, the reader is urged to refer to SIMRAC GAP 330 Final Project Report (Daehnke *et al.*, 1998).

2.5 Rock mass parameters governing hangingwall stability associated with the Witwatersrand gold mines

A summary of relevant rock mass properties, which affect the relevant rock mass parameters that govern hangingwall stability across the various mining environments, is given here.

2.5.1 Carbon Leader

The immediate hangingwall consists of competent siliceous quartzite (medium-to-coarse grained). The thickness of the quartzite varies between 1,4 m and 4 m in the Carletonville area.
The immediate hangingwall of the Carbon Leader (up to 50 cm) appears to be either structureless or planar bedded.
A horizontal argillaceous layer, called the Green Bar, overlies the quartzite (see Figure 2.5.1). The thickness of the Green Bar varies between 1 m and 2,5 m. Bedding planes are prominent in the lower portion of the Green Bar, which grades upwards into more competent, less bedded siltstone.

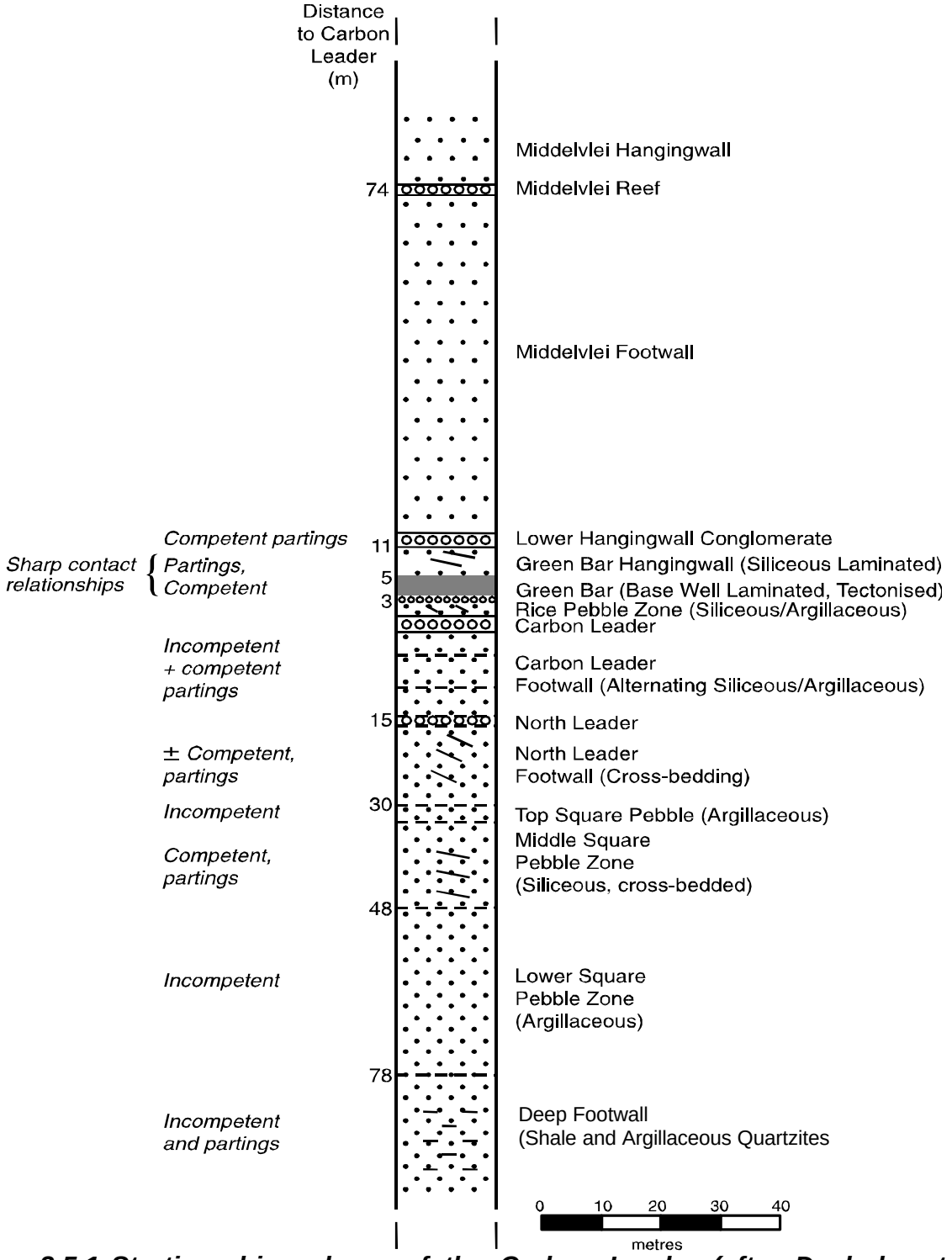

Figure 2.5.1 Stratigraphic column of the Carbon Leader (after Daehnke et al., 1998).

The Rice Pebble Marker, which has pronounced parting planes at its base and top, defines the transition from quartzite to Green Bar. These parting planes, which have low cohesion, control rock falls and it is suggested that the fall of ground thickness of the hangingwall strata is defined by the distance between the stope hangingwall, and the base of the Green Bar or RPM. This parting plane has been observed to reactivate as a bedding parallel fault during seismic events.

Due to the lack of cohesion between the Rice Pebble Marker and the quartzite, falls of ground occur as soon as the reef is mined. The Green Bar has a lower competency than the hangingwall of the Carbon Leader.

The mining induced fractures dip approximately 70° to the face in the quartzite. In some areas, planar cross-beds are prominent, weakening the rock and resulting in vertical extension fractures as shown in Figure 2.5.2.

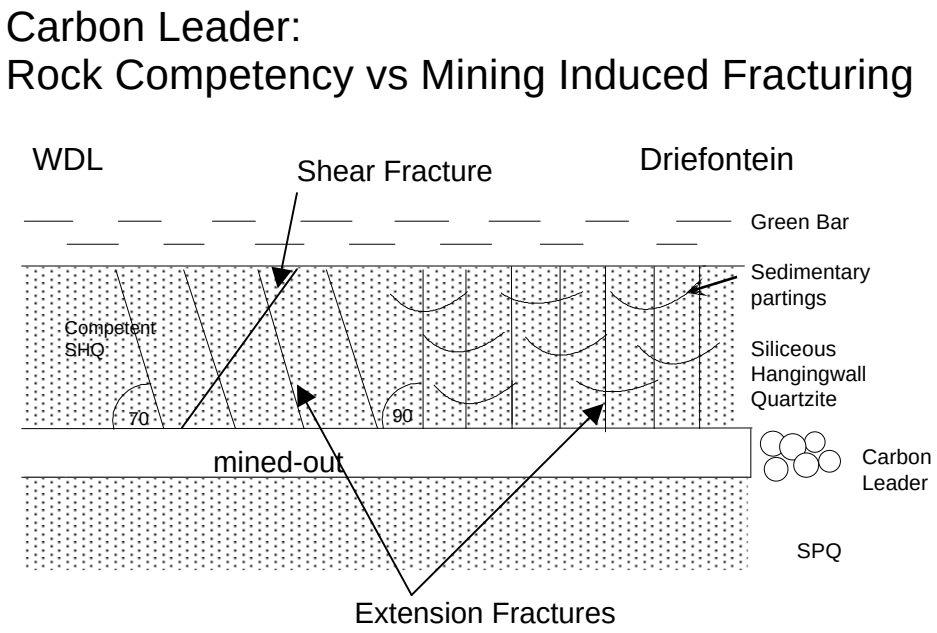

Figure 2.5.2 Variations in the mining induced fractures in the hangingwall of the Carbon Leader (after Daehnke et al., 1998).

2.5.2 Vaal Reef

The hangingwall of the Vaal Reef is a very competent siliceous (hard) quartzite, which has an average thickness of 0,5 m. Bedding planes in the quartzite are extremely prominent, and the quartzite is overlain by an argillaceous quartzite. These two lithologies are separated by a well-defined parting plane. The weak cohesion along this plane controls the stability of the hangingwall, and typical beam thickness is approximately 0,5 m.

The Zandpan Marker locally cuts down into the Vaal Reef or its footwall units, resulting in the Vaal Reef being overlain by argillaceous quartzites or being eroded. Parting planes in the MB5 zone range from 50 cm in the argillaceous quartzites to 200 cm in the siliceous quartzites.

Areas in which the Zandpan Marker cuts down in stratigraphy, however, are only known on Hartebeesfontein and the northeastern part of Vaal Reefs, but these localities are not well defined (Daehnke *et al.*, 1998). This is shown in Figure 2.5.3.

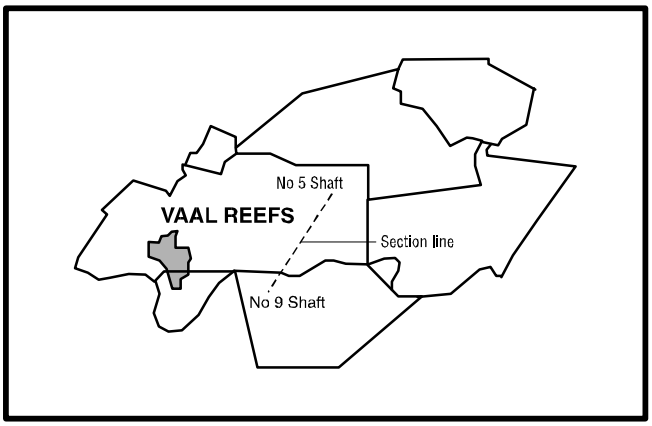

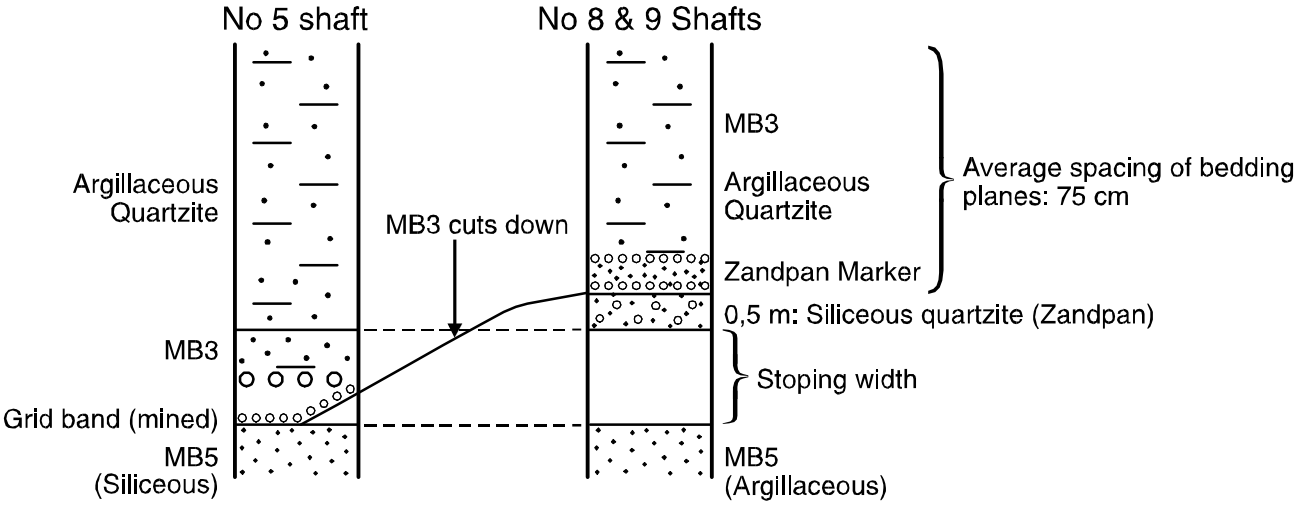

Figure 2.5.3 Section indicating the distribution of the Zandpan Marker (after Daehnke et al., 1998).

2.5.3 VCR

The stratigraphic column of the VCR is shown in Figure 2.5.4. This reef can be further divided into seven different ground control districts. The parameters governing the hangingwall stability of the three most distinct areas within the mining environments are described below.

The first area is a combination of hard lava and quartzite/conglomerate, the second a combination of soft lava and quartzite/conglomerate and the third a combination of soft lava and Jeppestown shale.

Different fracture orientations are observed in these areas. In the first geotechnical area, the extension fractures dip towards the stope face at a low angle (45°-55°) in the hangingwall. Sixty per cent of the extension fractures dip away from the face and 40 per cent dip towards the face in the second area. The extension fractures dip away steeply from the face in the third area.

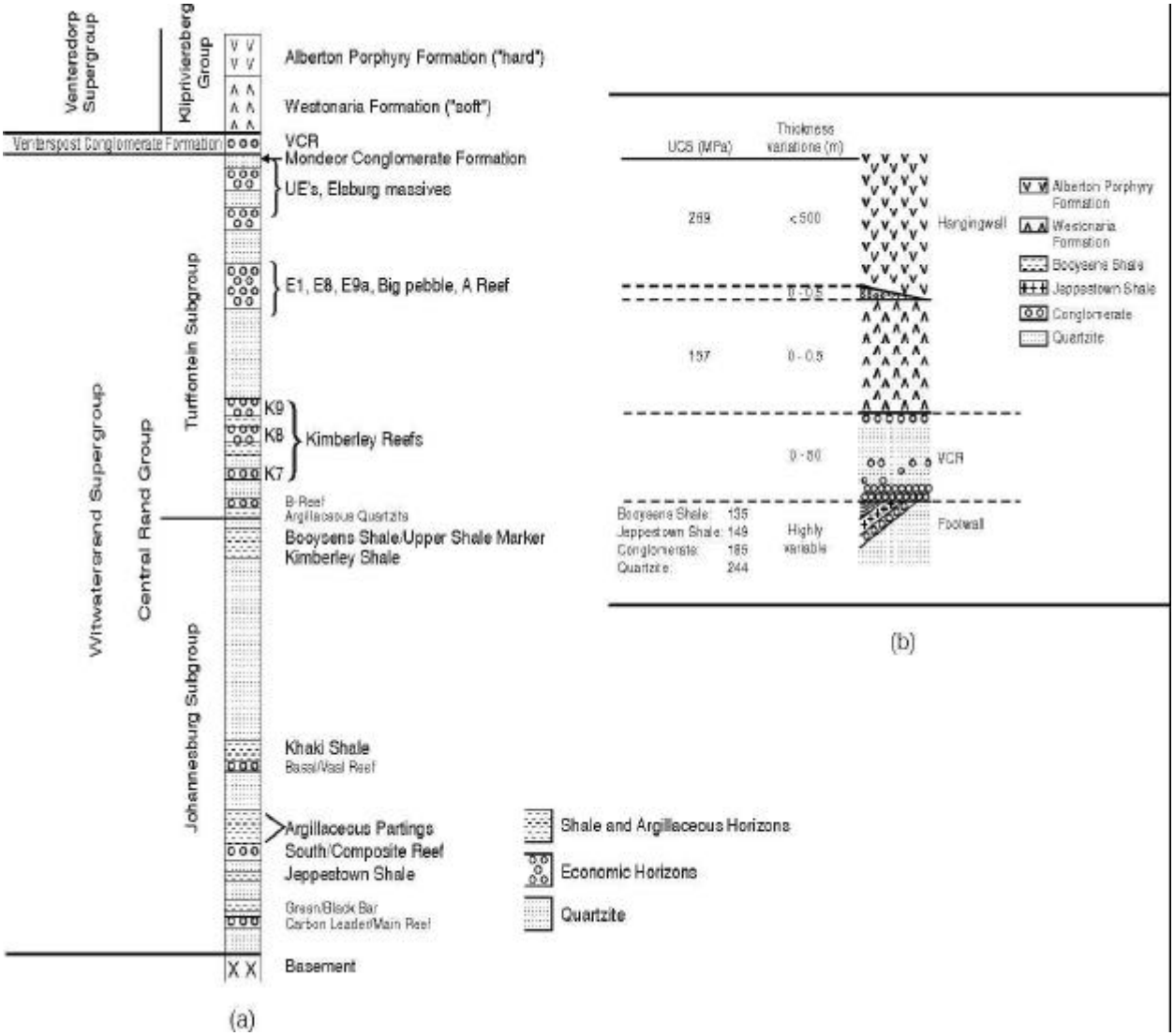

Figure 2.5.4 Stratigraphic columns of the VCR (a) Generalised and (b) More detailed (after Daehnke et al., 1998).

The hangingwall lavas, being volcanic in origin, do not possess any sedimentary structures. Flow contacts, however, are found sub-parallel to the reef plane and are better developed in the hard lavas. These contacts may separate fine-grained lava from amygdaloidal or brecciated lava and are often sites of alteration. Lava load casts referred to as pilloids occur locally, often near rolls causing poor hangingwall conditions. Parting planes may develop along flow contacts resulting in unsafe beams being formed. Horizontal, mining induced movement frequently occurs along the flow contacts resulting in fallouts between support units.

2.5.4 Geotechnical environment of the Kimberley Formation

Several orebodies are preserved within the Kimberley succession. This can be seen from the stratigraphic column shown in Figure 2.5.5. The B-Reef, Big Pebble Marker (BPM) and Witpan (8A) Reef are considered in this study. The orebodies contained within the Kimberley succession are generally situated in argillaceous (“soft”) strata, with siliceous ("hard") quartzites and conglomerates representing minority constituents. The succession is truncated towards the south, where only one Kimberley orebody is preserved, locally termed Sand River-, Kalkoonkrans-, or Beatrix Reef. Of note are locally developed shale channels. These may be developed in the hangingwall and the footwall of orebodies, also truncating the orebody itself (Daehnke *et al*., 1998).

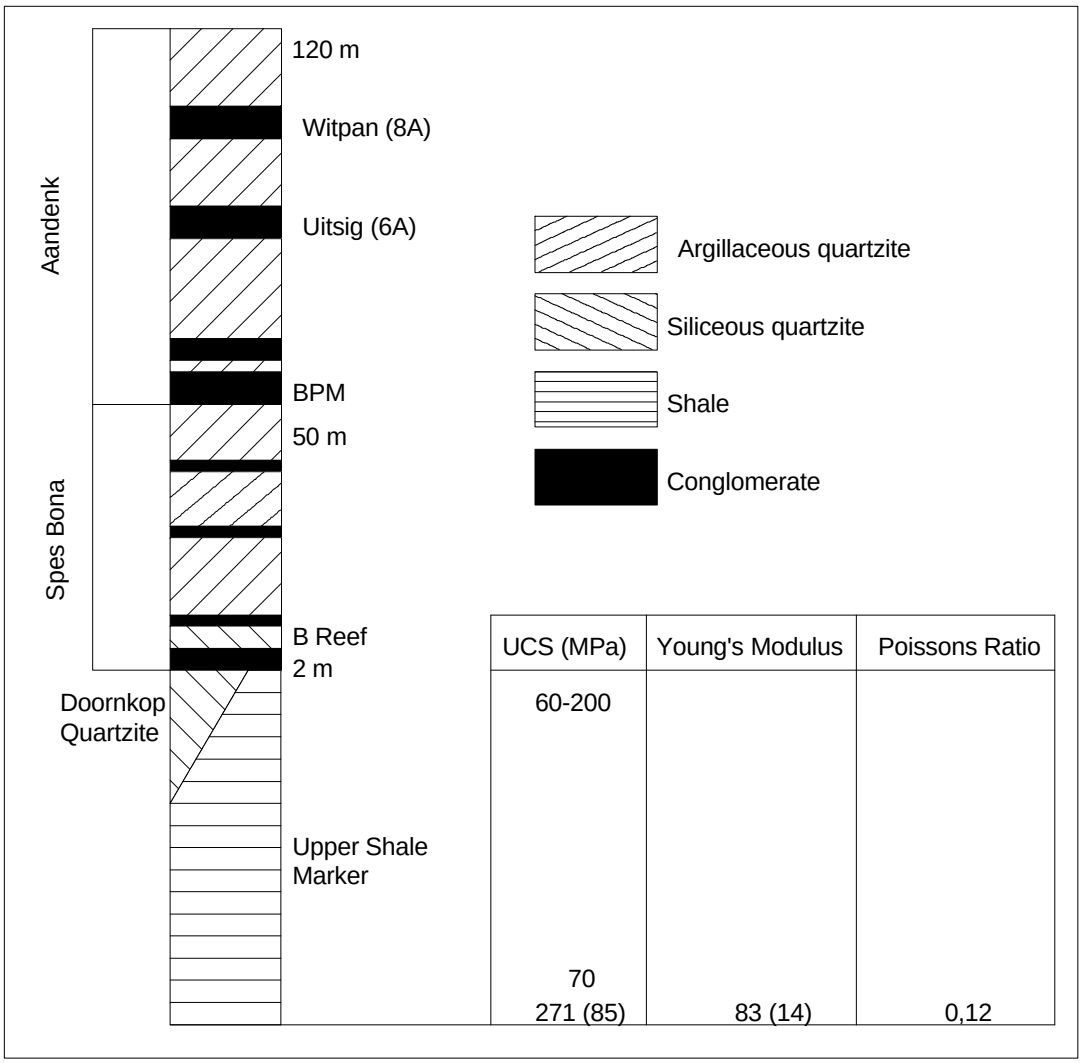

Figure 2.5.5 Stratigraphic column of the Kimberley succession.

2.5.4.1 B-Reef

The B-Reef is the basal orebody of the Kimberley succession. It overlies the Upper Shale Marker (similar to the Booysens Shale) over large areas. High UCS values may be associated with the Upper Shale Marker. In a bedding parallel orientation, however, the strengths of laminated shales are generally lower. This is due to the low cohesion between the fine shale laminae. Partings are also present in the argillaceous hangingwall quartzite.

The B-Reef is predominantly mined in a "soft", argillaceous environment. The footwall of the B-Reef is prone to bulging. The footwall rock of the B-Reef in the northeastern and south-western portion consist of siliceous and argillaceous quartzites, respectively. Two distinct geotechnical areas are distinguished. The footwall to the B-Reef is either hard or soft, whereas the hangingwall is always "soft".

2.5.4.2 Big Pebble Marker

The Big Pebble Marker (BPM) is mined predominantly in a "soft" environment, comprising argillaceous footwall and hangingwall rock types. Stoping widths can exceed 2 m. As the effects of seismicity are substantially increased with wider widths (Arnold *et al*., 1994), the increase in reef thickness towards the south-east should also be considered in an assessment of rock mass behaviour. Three mining environments are delineated for the Big Pebble Marker.

2.5.4.3 Witpan Reef

Two geotechnical environments are delineated for this reef. These areas are classified with respect to the different rock types comprising the footwall, such as argillaceous quartzites or conglomerates. The area where conglomerate (the Big Pebble Marker) underlies the Witpan is confined to the southern region of the Free State (Harmony area). It still has to be established, however, whether the conglomeratic footwall results in different rock mass behaviour, when compared to the northern argillaceous footwall.

2.5.5 Leader Reef

A single geotechnical environment is delineated for the Leader Reef over the extent of the Free State area. Both footwall and hangingwall lithologies are represented by argillaceous quartzites. Ground control districts characterised by siliceous quartzite bands in the hangingwall of the Leader Reef are, however, present, where uni-axial compressive strength values can exceed 300 MPa. Also of note is the Khaki Shale, which, on average, is encountered some 15 m into the footwall of the Leader Reef (Daehnke *et al*., 1998).

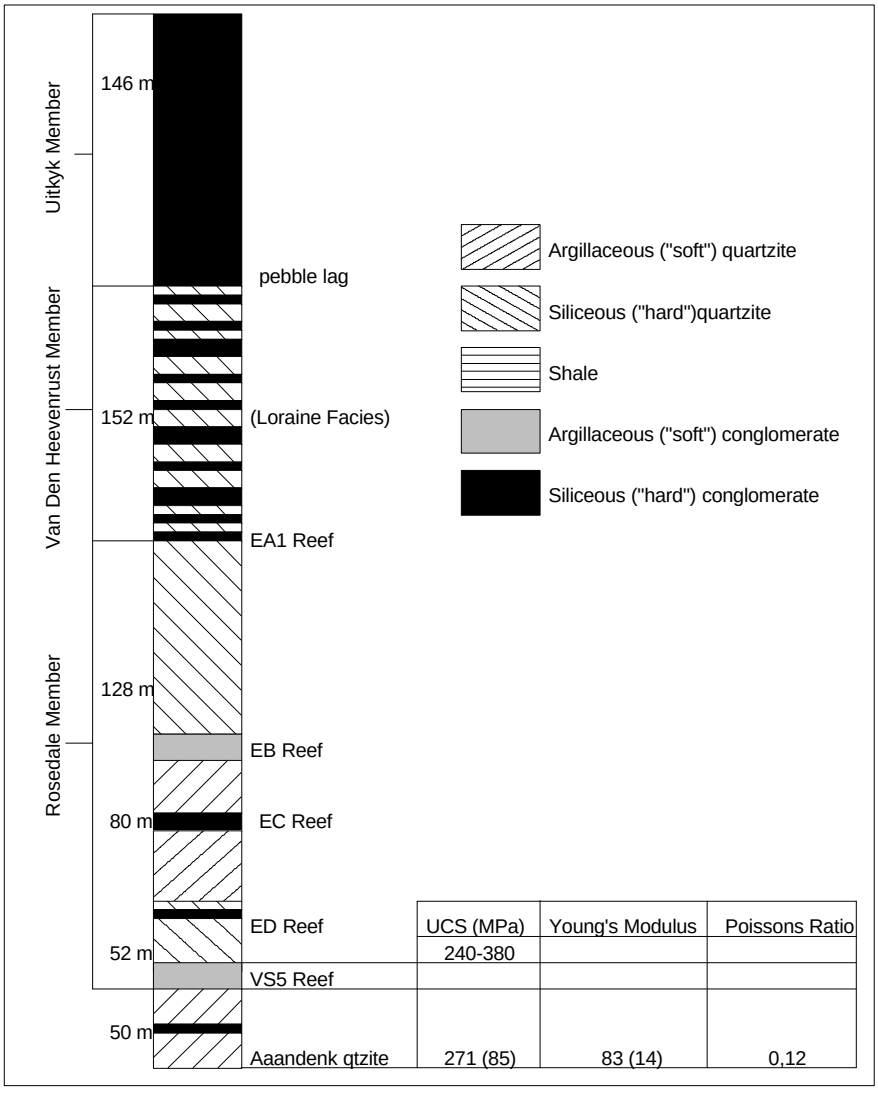

Figure 2.5.6 Stratigraphic column of the Elsburg succession.

2.5.6 VS5

The orebodies of the Elsburg succession are predominantly located in siliceous environments. The VS5, which immediately overlies the Kimberley succession, is considered to be an unusual Elsburg Reef (see Figure 2.5.6).

Five ground control districts are delineated for the VS5. Geotechnical areas are classified according to the combinations of siliceous conglomerates with argillaceous quartzite, argillaceous footwall and hangingwall quartzites. One of the ground control districts is defined by a sill, which is present in the hangingwall.

2.6 Rock mass parameters governing hangingwall stability associated with the Bushveld Complex

Two platinum reefs are considered in the Bushveld Complex. These are (i) the UG1 and UG2, and (ii) the Merensky reef. A summary of relevant rock mass properties, which affect the relevant rock mass parameters that govern hangingwall stability across the various geotechnical areas, is given here.

2.6.1 UG1 and UG2

The upper group chromitites are of great lateral extent and they usually consist of two chromitite layers, UG1 and UG2. The stratigraphy, thicknesses and compositions of these chromitite layers show variations throughout the Bushveld Complex.

The UG1, the lowermost of the upper chromitite layers, is one of the most distinctive and persistent chromitite layers within the Rustenburg Layered Suite (Viljoen and Hieber, 1986). On RPM, the main layer has an average thickness of 70 cm, which can, again, vary considerably (Daehnke *et al*., 1998). Anorthosite and pyroxenite are both found within the multiple chromitite layers of the UG1 and in the immediate hangingwall.

The pyroxenite passes sharply upwards into an anorthositic norite. The norite continues up to the UG2. Pyroxenite is again encountered above the UG2 chromitite layer, and norite is present above the pyroxenite up to the next unit, the Merensky Reef. Two thin chromitite layers are developed above and below the Merensky pegmatoid, a pegmatoidal pyroxenite in which platinum-group elements are concentrated (Daehnke *et al*., 1998).

The UG2 forms the uppermost of the substantial chromitite layers within the Rustenburg Layered Suite and on RPM it lies approximately 140 m below the Merensky Reef. Four footwall/hangingwall rock type assemblages can be distinguished for the UG2, which are:

- Norite/Norite;
- Pyroxenite/Pyroxenite;
- Norite/Pyroxenite;
- Pyroxenite/Norite.

2.6.2 Merensky Reef

The Merensky Reef unit, which includes the pyroxenitic Merensky Reef, is remarkably consistent in thickness across the whole Rustenburg Section, varying between 9 and 10 m (Viljoen and Hieber, 1986), unless potholes are encountered. The Merensky Reef unit

commences with the pyroxenite layer with associated chromitite layers, and is overlain by a differentiated suite consisting of norite, anorthositic norite, spotted anorthosite and, finally, mottled anorthosite.

Six hangingwall/footwall rock type assemblages are distinguished for the Merensky Reef. These are:

- Pyroxenite/Anorthosite;
- Norite/Norite;
- Pegmatitic Pyroxenite/Norite;
- Pyroxenite/Norite;
- Norite/Pyroxenite;
- Norite/Pegmatitic Pyroxenite.

Norite is the most abundant footwall lithology for the Merensky Reef. Norite and pyroxenite occur in equal proportions in the hangingwall of the Merensky Reef.

2.7 Conclusions

From the review it is evident that many factors need to be considered when assessing the hangingwall stability. The geology of the area and the related rock strength and rock mass characteristics need to be incorporated in the design of support systems.

The input parameters, which are to be used in the design of support systems (Chapter 8), are:

- Extent of fracturing – discontinuities per metre of hangingwall (applicable to intermediate- and deep-level mines)
- Orientation of extension (a) and shear fractures (b) (applicable to intermediate- and deep-level mines)
- Joint orientation and density (applicable to shallow mines)
- Instability thickness:
    i) Fallout thickness to prominent bedding plane (from rockfall/rockburst back-analyses), or
    ii) 95 % cumulative fallout thickness from fatality database (Roberts, 1995)
- Friction angle (j)
- Density of the rock mass (r)
- *In situ* compressive hangingwall stress (s_x)

Accurate data on the abovementioned parameters are often not easily attained, but need to be estimated in order to facilitate effective stope support designs.

The number of discontinuity sets and their spacing can be determined fairly accurately, as can the dip/orientation of these discontinuities and the beam thickness. Friction angles and horizontal clamping stresses, however, cannot be determined accurately and are only approximations.

Rock mass parameters are site specific and a good understanding of the geology of the area and delineation into ground control districts is required in order to estimate the rock mass parameters for the support design process.

3 Quantifying zones of support influence in a discontinuous rock mass using numerical techniques

3.1 Introduction

The objective of enabling output 2, which is discussed in this section, is a means of quantifying the zones of influence of support units, backfill and the stope face. To achieve this, numerical techniques are used to gain qualitative insights into stress trajectories through fractured hangingwall beams. This chapter focuses on the zones of influence of support units.

The influence of three discontinuity sets on the zone of support influence is investigated through the use of numerical methods. The models include various discontinuity types, namely horizontal bedding planes, extension fractures dipping towards the face and shear fractures dipping away from the face. The dip angle of the extension fractures is denoted by alpha (a) and the dip angle of the shear fractures by beta (b).

The distinct element code, UDEC, is used to investigate the mechanistic interaction between support and the rock mass. UDEC was chosen due to the ease of incorporating any number of fractures. In the UDEC model, the Mohr-Coulomb failure criterion is assigned to the fractures. A friction angle of 40 degrees was assumed on all fractures. The joint shear and normal stiffness were assumed to be 200 GPa.

Two approaches were followed in investigating the zone of support influence by means of numerical models. In the first approach, the zone of influence of a single support unit is studied while the second approach investigates the interaction between different support units with different spacings. A simplified deep mine stope model is used in the above-mentioned approaches. In this model, an elongate support unit is installed at different positions with respect to the joint-hangingwall surface interface (in an eight metre wide stope). The hangingwall is allowed to deform under the influence of gravity. The zone of support influence at each different position is then measured as a function of the area of rock that does not fall out (due to gravitational acceleration). This is presented as the percentage instability of the hangingwall beam and is considered as a hazard indicator. The zone of support influence for a 30°/60° joint combination is shown in Figure 3.1.1.

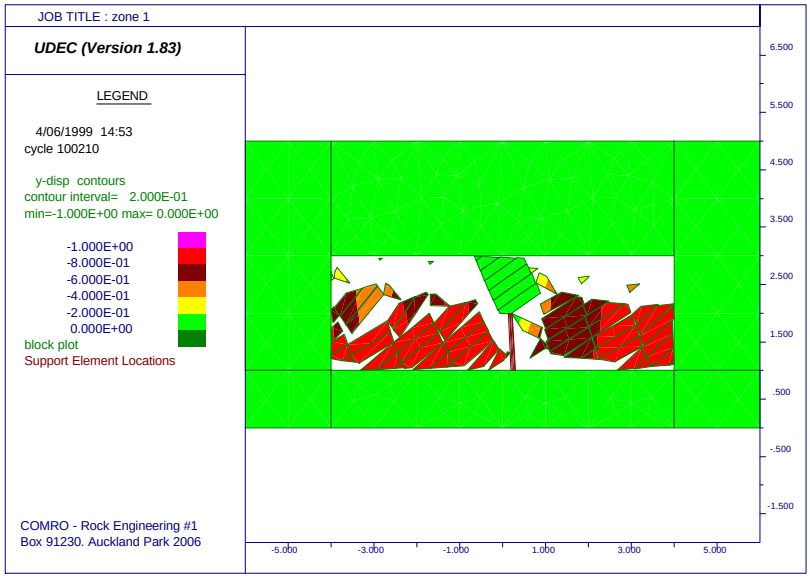

Figure 3.1.1 Zone of support influence for 30°/60° joint combination.

The zone of support influence can take on one of three shapes, and can be expressed as the total area, which is supported by the support unit. The three possibilities are shown in Figure 3.1.2. The areas of the three shapes are given by:

$$1)\ A = h\,b + (^1/_2)\,h^2\,(\cot a + \cot b) \qquad (3.1.1)$$

$$2)\ A = h\,b \qquad (3.1.2)$$

$$3)\ A = h\,b - (^1/_2)\,d^2\,\sin^2 a\,\tan b \qquad (3.1.3)$$

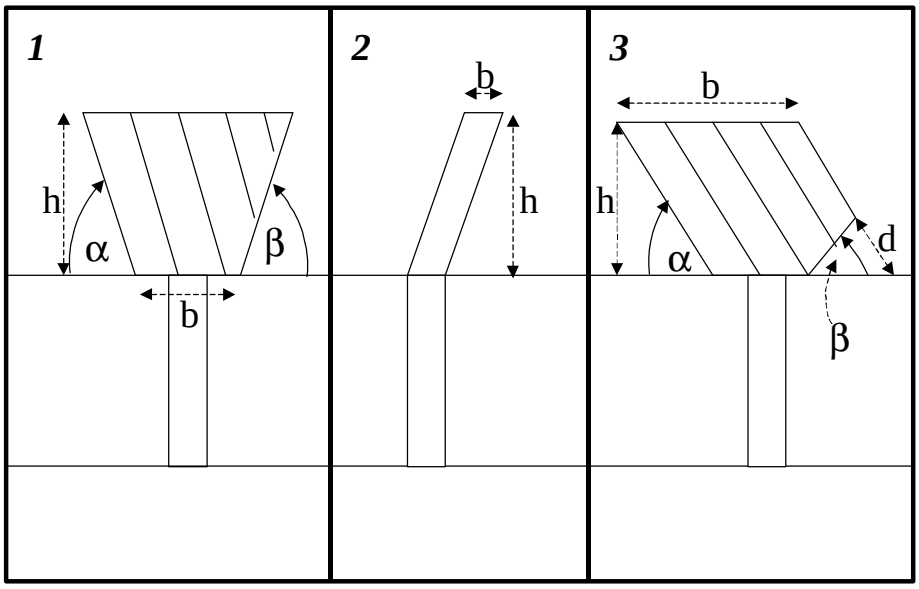

Figure 3.1.2 Three possible shapes of zone of support influence.

In the second approach the interaction between the support units is analysed. Thus, for the same rock mass conditions, the combined effect of the different support units in stabilising the stope hangingwall is quantified (see Figure 3.1.3).

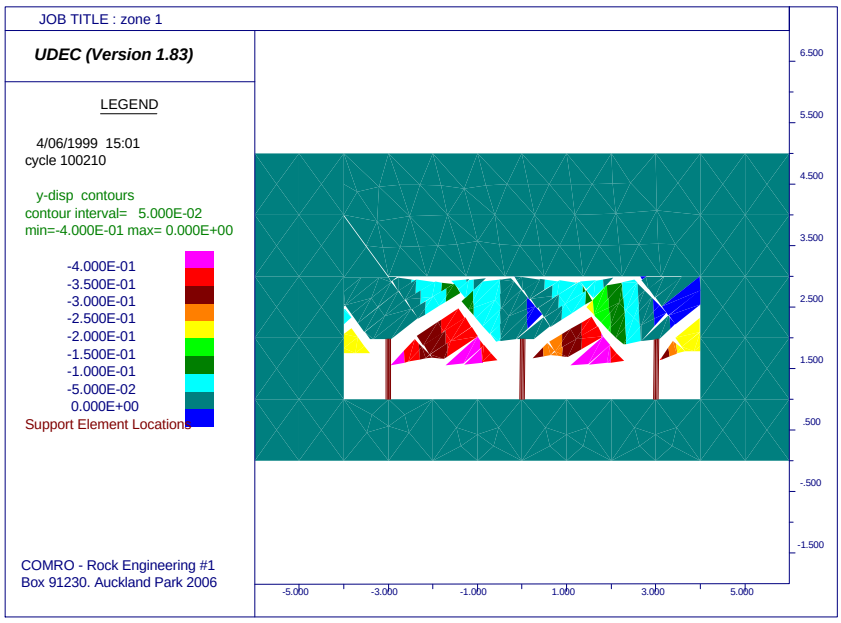

Figure 3.1.3 Support interaction for $30^0/60^0$ joint combination.

The exact zone of support influence was investigated for different combinations of joint orientations. This is, however, a function of the position of the support unit with respect to the joints. For the 30°/60° joint combination, repeated analyses were conducted with the support unit installed at 0,25 m intervals over a distance of 2 m. This gave all the possible zones of influence of the support unit. The influence of the support unit outside the boundaries of the 2 m area of interest would be similar to a position within the 2 m window, since the joints are repetitive and the same block sizes and shapes would be formed.

The results indicate that the position of the support relative to the shear fracture is very important. The maximum zone of influence is shown in Figure 3.1.2, part 1. If the shear fractures dip away from the stope face, the support unit must be placed on the footwall side of the fracture, as shown in Figure 3.1.4. If the support is installed on the down-dip side of the shear fracture, the support has less stabilising influence on the hangingwall beam and rock mass instabilities are more likely.

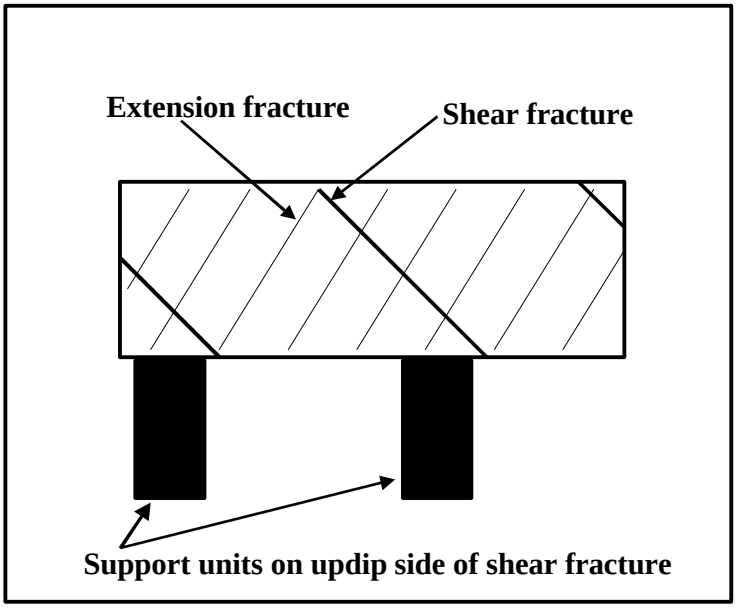

Figure 3.1.4 Support units installed on the footwall side of shear fractures.

3.2 Results of numerical modelling

The influence of support interaction on the stability of the hangingwall beam was analysed. The effects of joint orientation, horizontal clamping stress, beam thickness and support spacing are addressed in this section. The influence of joint friction angle and joint spacing on the stability of the hangingwall was investigated as part of GAP 334 and a summary is given in Chapter 2.

3.2.1 Influence of horizontal clamping stress on hangingwall stability

In this analysis, the orientation of the extension fractures is kept constant and the shear fractures' angles are varied between 30° and 90°.

3.2.1.1 Extension fracture orientation: a = 30°

The results for the fracture combinations of a = 30° with b = 90°, b = 60° and b = 30° are given in Figures 3.2.1, 3.2.2 and 3.2.3 respectively.

From Figure 3.2.1, it can be seen that the horizontal clamping stress has very little influence on the stability of the hangingwall. However, it is clear that the hangingwall can be stabilised by reducing the support spacing. For a support spacing of 1 m, a small percentage instability occurs. For this combination, the support spacing should be very small since the hangingwall is inherently unstable when intersected by these sets of fractures.

For the 30°/60° and 30°/30° combinations, the horizontal clamping stress also has little or no influence. The support spacing should be small to prevent any falls of ground from the hangingwall.

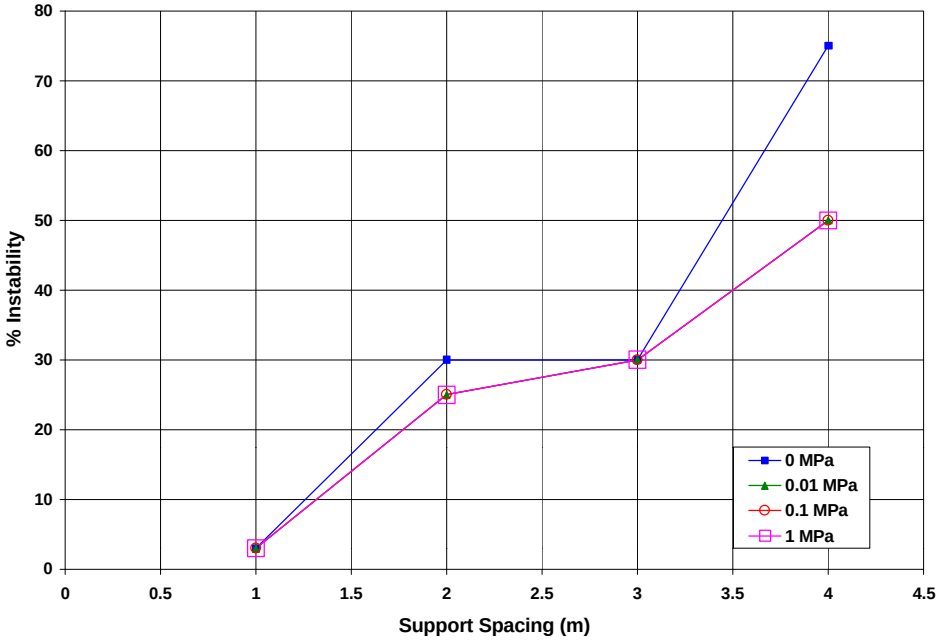

Figure 3.2.1 Influence of horizontal clamping stress and support spacing on stability of hangingwall for the 30°/90° combination.

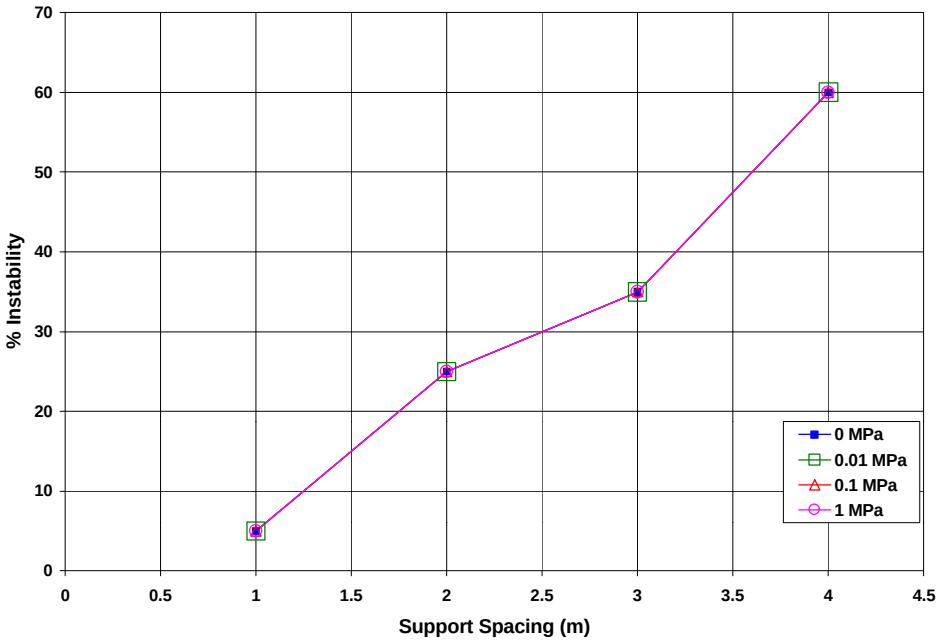

Figure 3.2.2 Influence of horizontal clamping stress and support spacing on stability of hangingwall for the 30°/60° combination.

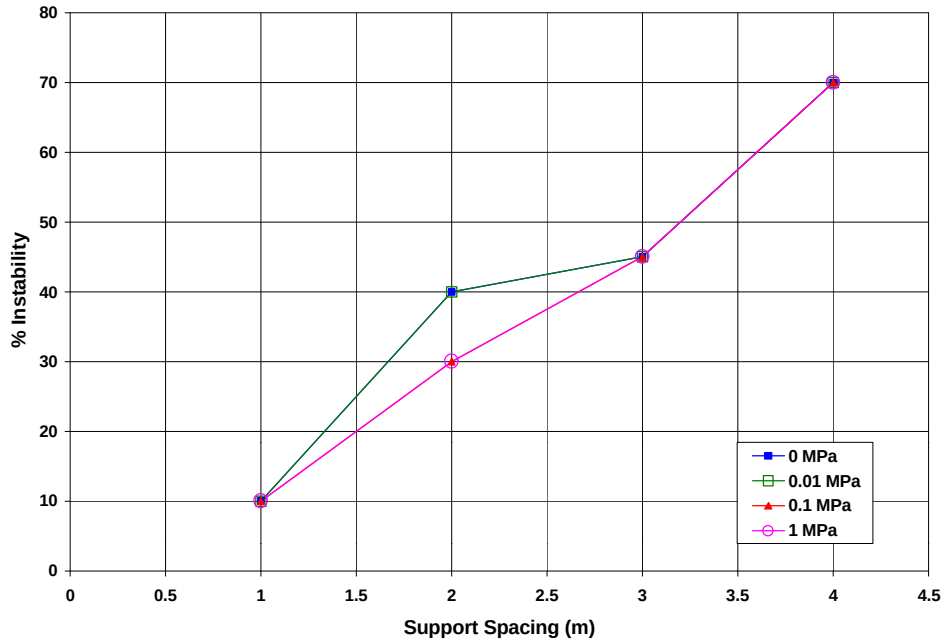

Figure 3.2.3 Influence of horizontal clamping stress and support spacing on stability of hangingwall for the 30°/30° combination.

3.2.1.2 Extension fracture orientation: a = 60°

The results for the 60°/90°, 60°/60° and 60°/30° combinations are shown in Figures 3.2.4, 3.2.5 and 3.2.6 respectively.

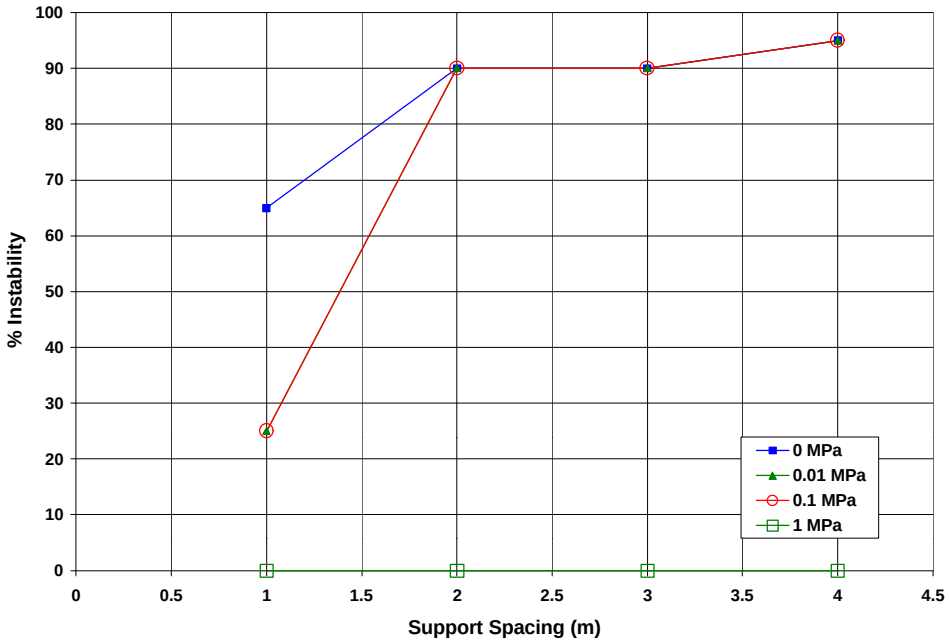

Figure 3.2.4 Influence of horizontal clamping stress and support spacing on stability of hangingwall for the 60°/90° combination.

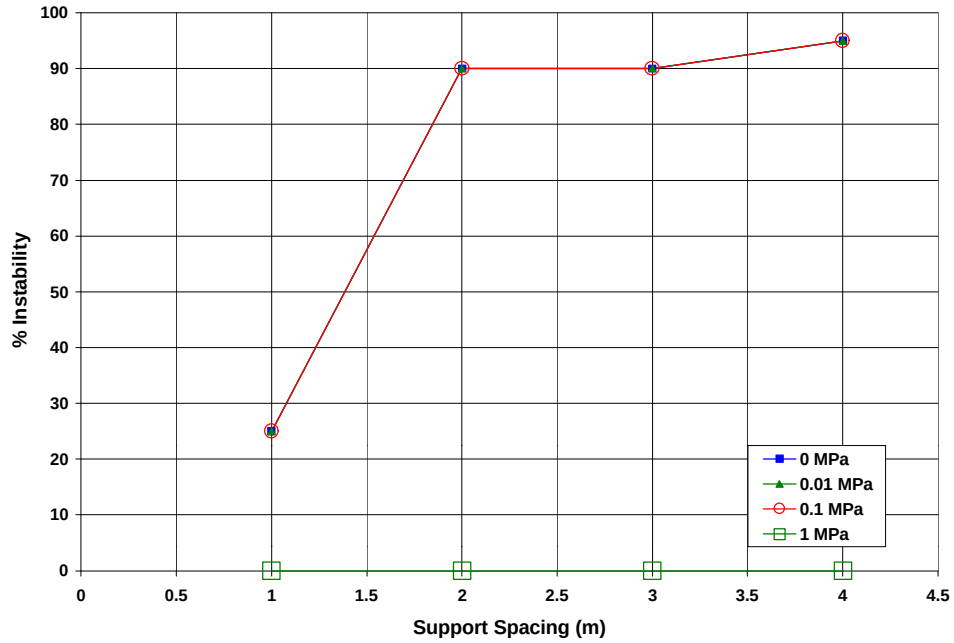

Figure 3.2.5 Influence of horizontal clamping stress and support spacing on stability of hangingwall for the 60°/60° combination.

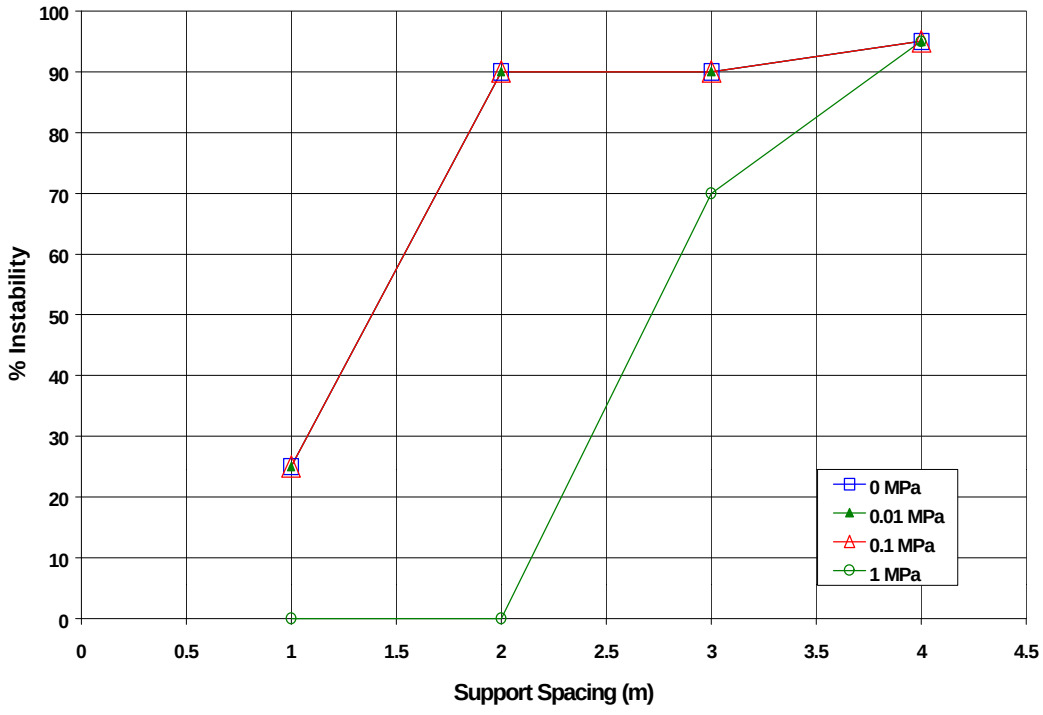

Figure 3.2.6 Influence of horizontal clamping stress and support spacing on stability of hangingwall for the 60°/30° combination.

For the 60°/90° and 60°/60° combinations, a horizontal clamping stress of 1 MPa reduces the percentage instability to zero. This occurs even at a support spacing of 4 m.

From Figure 3.2.6, it can be seen that for a clamping stress of 1 MPa, the hangingwall, containing extension fractures dipping at 60° and shear fractures dipping at 30°, is completely

stable for support spacings less than or equal to 2 m. Support spacings greater than 2 m result in unstable hangingwall conditions.

Thus, to achieve hangingwall stability in rock masses, which contain a combination of extension fractures that dip at 60° and shear fractures that dip at 30°, 60° or 90°, and where a horizontal stress of approximately 1 MPa is acting, a support spacing of 2 m is indicated for rockfall conditions.

If the horizontal clamping stress is closer to zero, a support spacing of no greater than 1 m is indicated for rockfall conditions.

From Figures 3.2.4, 3.2.5 and 3.2.6, it can be seen that when the horizontal clamping stress is smaller or equal to 0,1 MPa and the support spacing is equal to or greater than 2 m, the hangingwall is completely unstable.

From these results it is evident that the horizontal clamping stress plays a major role in the stability of the hangingwall.

3.2.1.3 Extension fracture orientation: a = 75°

The results for the combinations 75°/90°, 75°/60° and 75°/30° are shown in Figures 3.2.7, 3.2.8 and 3.2.9, respectively.

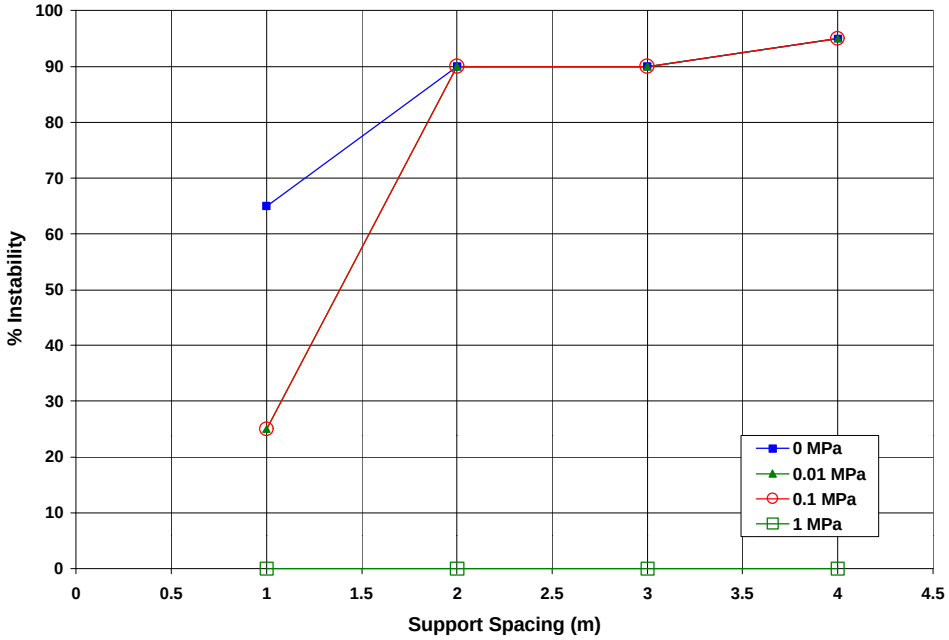

Figure 3.2.7 Influence of horizontal clamping stress and support spacing on stability of hangingwall for the 75°/90° combination.

The relationships that are obtained for these combinations are similar to those that were obtained for the combinations that involved the 60° extension fractures.

As is the case for the 60° extension fracture, a horizontal clamping stress of 1 MPa reduces the percentage instability to zero for the 75°/90° and 75°/60° combinations. The hangingwall, intersected by extension fractures dipping at 75° and shear fractures dipping at 30°, is completely stable for support spacings less than or equal to 2 m and when the horizontal clamping stress is 1 MPa.

From Figures 3.2.7, 3.2.8 and 3.2.9, it can be seen that if the horizontal clamping stress is less than or equal to 0,1 MPa and the support spacing is equal to or greater than 2 m, the hangingwall is unstable.

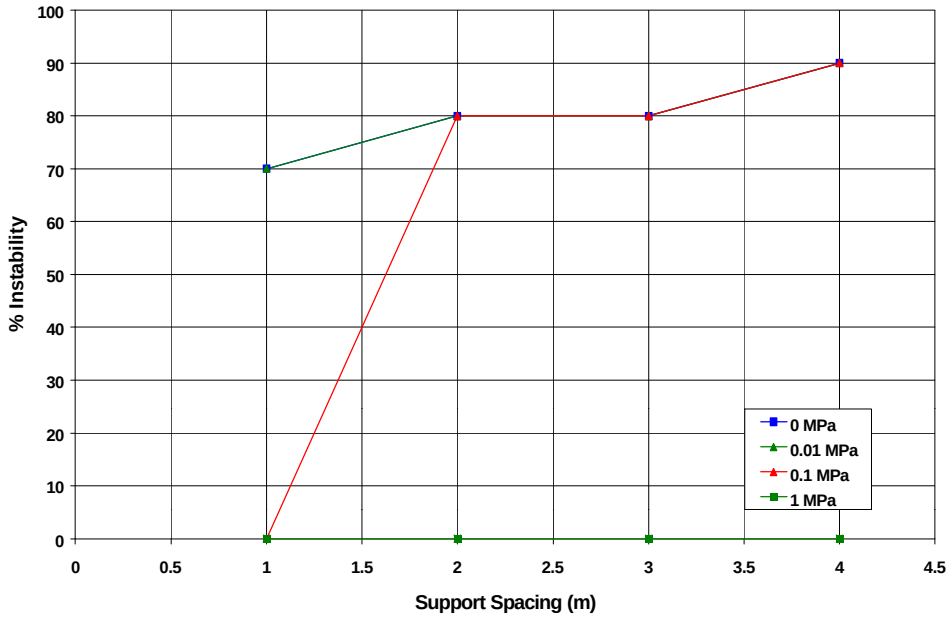

Figure 3.2.8 ***Influence of horizontal clamping stress and support spacing on stability of hangingwall for the 75°/60° combination.***

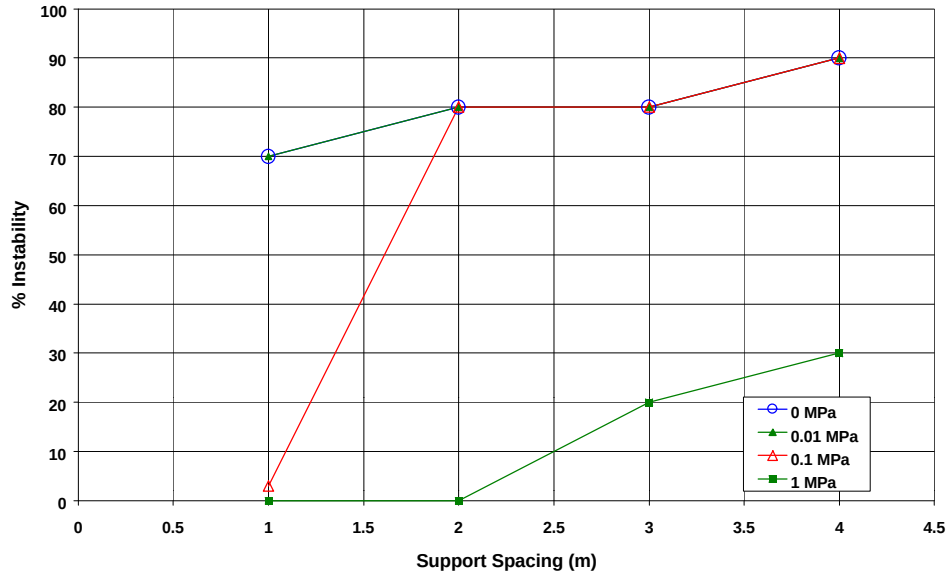

Figure 3.2.9 ***Influence of horizontal clamping stress and support spacing on stability of hangingwall for the 75°/30° combination.***

3.2.1.4 Extension fracture orientation: a = 90°

The results for the 90°/75°, 90°/60° and 90°/30° combinations are shown in Figures 3.2.10, 3.2.11 and 3.2.12, respectively.

From these figures, it can be seen that the combinations of shear fractures with extension fractures dipping at 90° are the most stable of all the combinations that were considered in this analysis. The combination of 90°/75° is stable at a support spacing of 4 m and a 0,1 MPa horizontal stress. The 90°/60° combination is stable up to a support spacing of 3 m with a horizontal stress of 0,1 MPa. The 90°/30° combination is stable at 2 m support spacing with a horizontal stress of 1 MPa.

The results show that the shallow fracture orientations tend to be less stable than the steeper orientations. This is as a result of the angle between the horizontal stress and the fracture orientation. If this angle is closer to 90°, the normal stress on the fracture is increased and the fracture interface more effectively clamped.

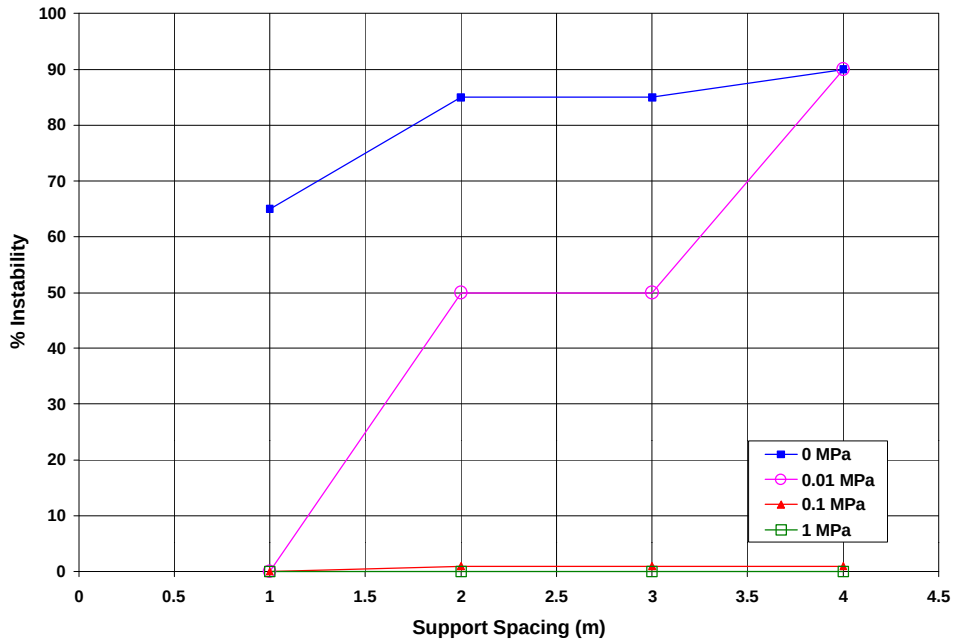

Figure 3.2.10 ***Influence of horizontal clamping stress and support spacing on stability of hangingwall for the 90°/75° combination.***

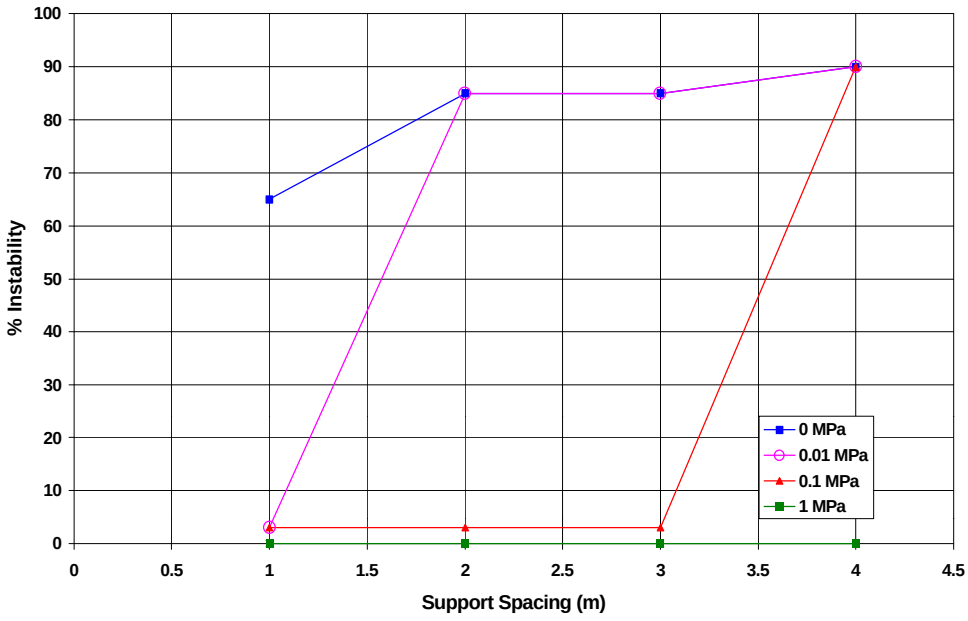

Figure 3.2.11 ***Influence of horizontal clamping stress and support spacing on stability of hangingwall for the 90°/60° combination.***

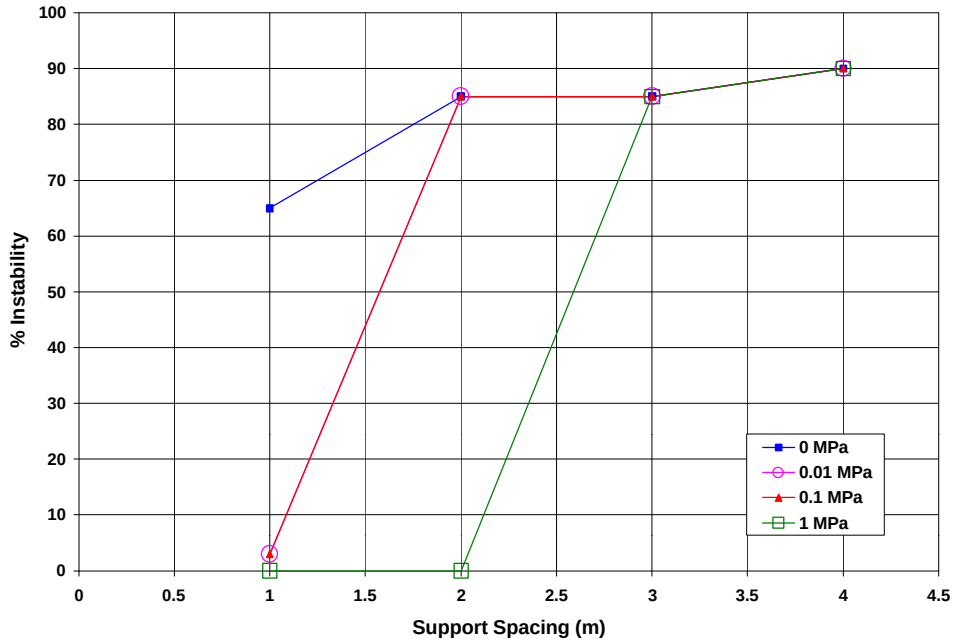

Figure 3.2.12 ***Influence of horizontal clamping stress and support spacing on stability of hangingwall for the 90°/30° combination.***

3.2.2 Influence of beam thickness on hangingwall stability

The influence of beam thickness and support spacing on the hangingwall stability, for different fracture orientations, is investigated in this section. A horizontal clamping stress of 1 MPa was applied to the model for all the combinations considered in this analysis.

3.2.2.1 Extension fracture orientation: a = 30°

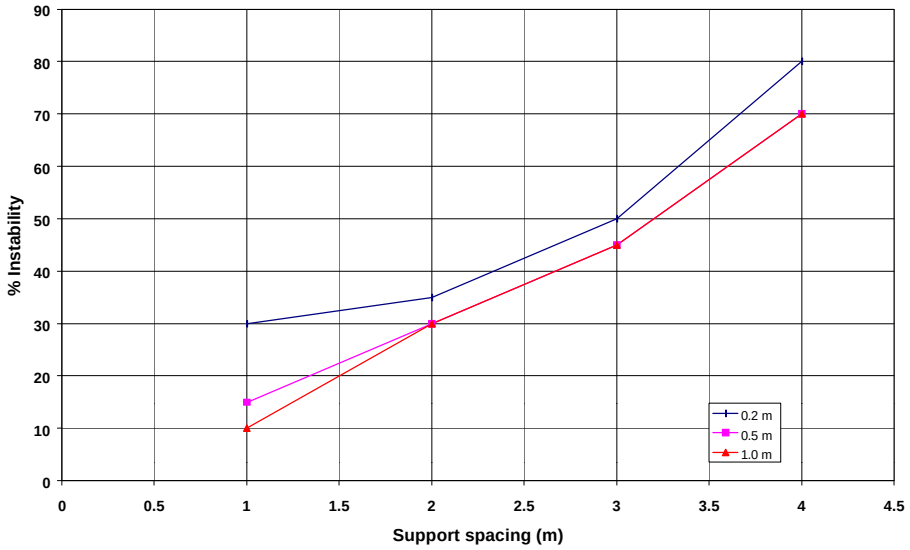

Figure 3.2.13 ***Influence of beam thickness and support spacing on stability of hangingwall for the 30°/60° combination.***

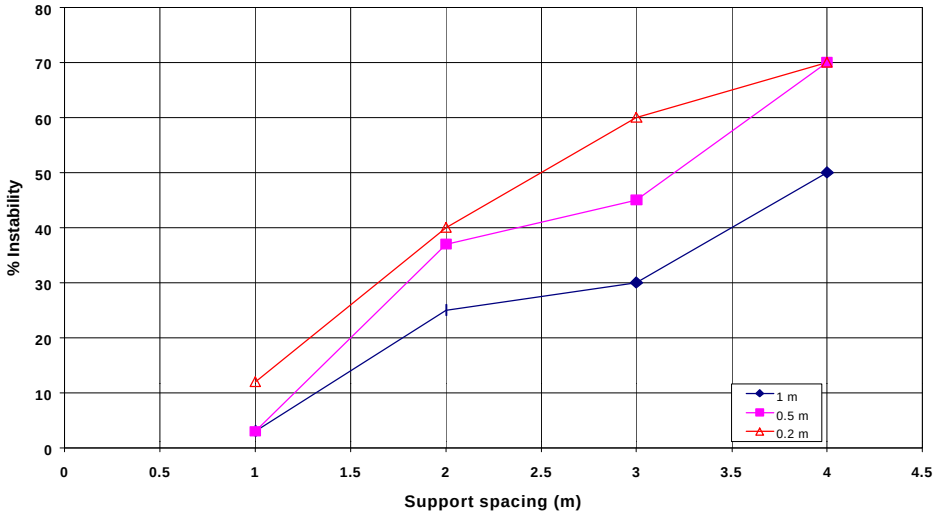

Figure 3.2.14 ***Influence of beam thickness and support spacing on stability of hangingwall for the 30°/90° combination.***

An almost linear relationship is obtained for the combinations in Figures 3.2.13 and 3.2.14. It is clear that thinner beams are less stable.

Failure of the hangingwall beam can occur due to two mechanisms, the first being shear failure on the fractures. This kind of failure can occur at any beam thickness. The second failure mechanism is beam buckling and occurs more readily when the beams are very thin. For a 0,2 m thin beam, even a 1 m support spacing does not guarantee total rock mass stability.

3.2.2.2 Extension fracture orientation: a = 90°

For the 90°/60° and 90°/75° combination, the hangingwall is stable, even at a beam thickness of 0,2 m and a support spacing of 4 m. This shows that if the horizontal clamping stress is 1 MPa, the hangingwall of the stope should be stable. It was seen previously that for a horizontal stress of 0,1 MPa and a beam thickness of 1 m, the hangingwall is stable at a support spacing of 3 m. Thus, this is a combination that results in stable conditions requiring less support. It must, however, still be supported. The results for the 90°/30° combination are shown in Figure 3.2.15.

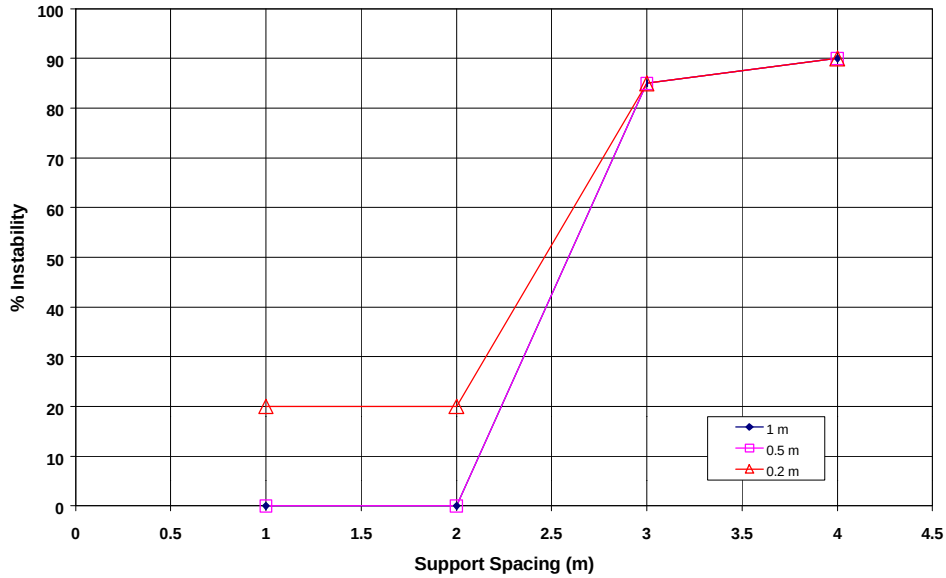

Figure 3.2.15 ***Influence of beam thickness and support spacing on stability of hangingwall for the 90°/30° combination.***

For the 90°/30° combination, the 0,2 m beam is slightly less stable than the 0,5 m and 1,0 m thick beams. This is an important finding since the support spacing should be decreased to below 1 m to ensure complete stability of the hangingwall if the beam thickness is equal to or less than 0,2 m.

3.2.2.3 Extension fracture orientation: a = 75°

The results for the 75°/30° combination is shown in Figure 3.2.16.

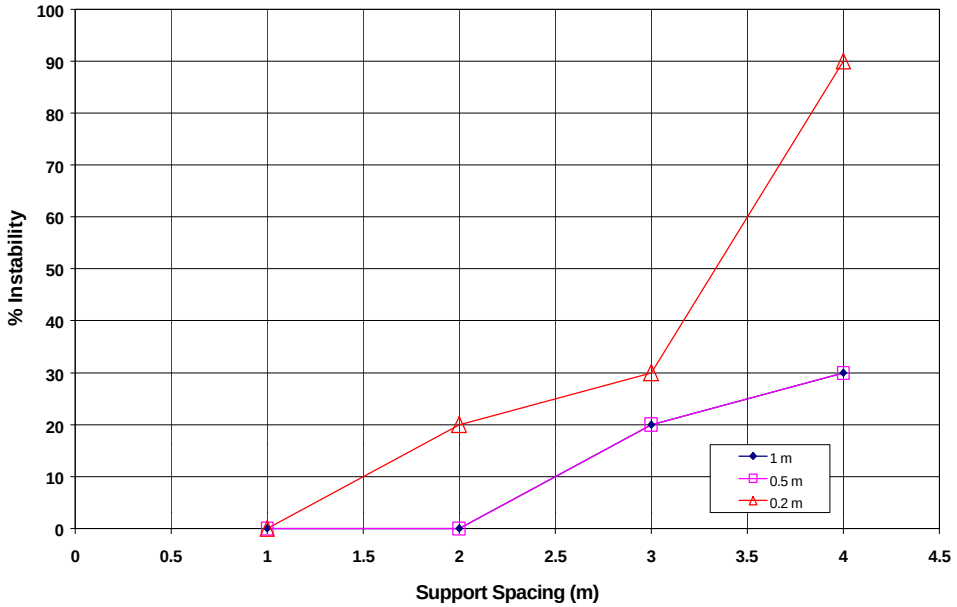

Figure 3.2.16 Influence of beam thickness and support spacing on stability of hangingwall for the 75°/30° combination.

The 0,2 m beam results in more instability than the 0,5 m and 1 m beams. The 75°/60° and 75°/90° combinations were all stable at 0,2 m beam thickness.

3.2.2.4 Extension fracture orientation: α = 60°

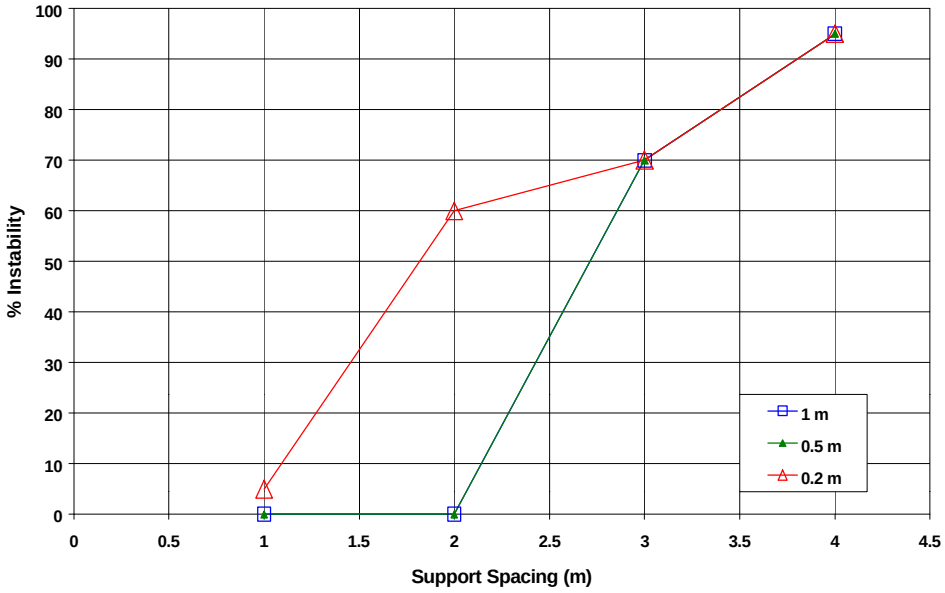

Figure 3.2.17 Influence of beam thickness and support spacing on stability of hangingwall for the 60°/30° combination.

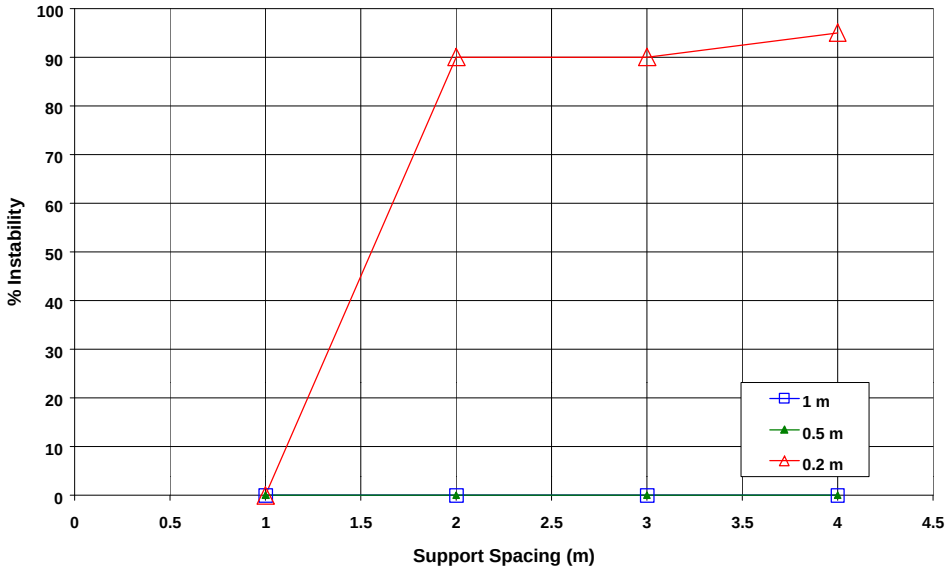

Figure 3.2.18 ***Influence of beam thickness and support spacing on stability of hangingwall for the 60°/60° combination.***

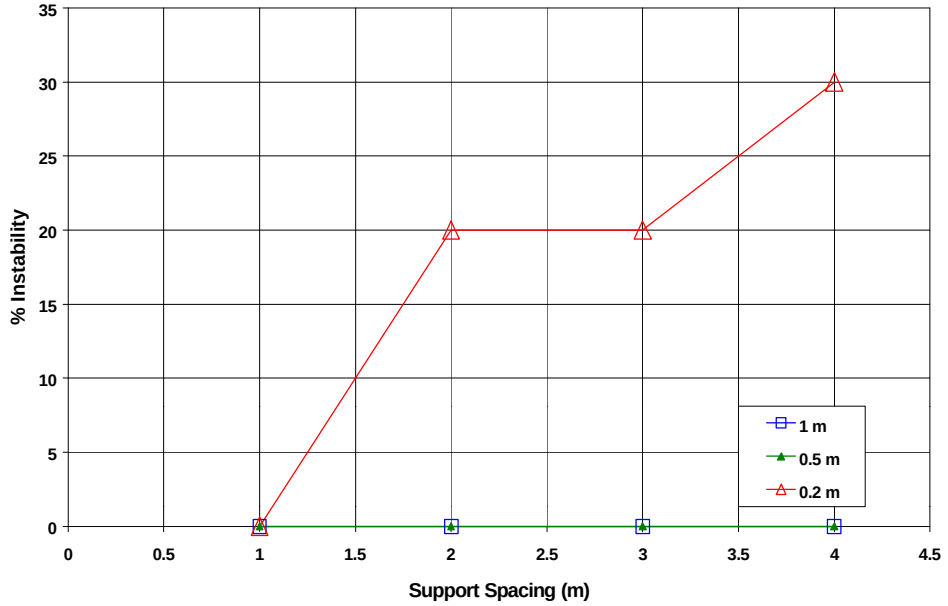

Figure 3.2.19 ***Influence of beam thickness and support spacing on stability of hangingwall for the 60°/90° combination.***

There is little difference between the 0,5 m and 1 m beam thickness, especially at small support spacings.

The steep fracture orientations are more stable than the shallow orientations at small (0,2 m) as well as large (1 m) beam thickness. For a beam thickness of 0,2 m, the optimum support spacing for most combinations is 1 m. Only the combinations of extension fractures of 90° and 75° with other steep shear fracture orientations are stable at larger support spacings.

3.3 Conclusions

The analyses reported in this chapter indicate that fracture orientation, beam thickness and horizontal clamping stresses all influence hangingwall stability significantly.

When the hangingwall beam is intersected by shallow dipping extension fractures, it is inherently unstable, and even relatively large horizontal clamping stresses do not increase the rock mass stability. This situation usually necessitates close support unit spacing and extensive areal coverage.

However, should the extension fractures be fairly steep dipping, and the shear fractures shallow, the presence of significant horizontal clamping stresses can have a marked effect on the stability of the hangingwall.

The numerical modelling results show that shallow fracture orientations are generally less stable than steeper orientations. This is because the normal stress on the fracture decreases with shallower dipping discontinuities. The shallower the fracture, the greater the component of the disturbing force, and the more likely it is that sliding will occur along the fracture.

Beam thickness affects the stability of the hangingwall, with thinner beams usually being less stable than thicker beams. Hangingwall beam thickness can, however, not be viewed in isolation, as the fracture orientation will also play a role in the stability of these beams. For steeply dipping fractures, even thin beams were found to be stable, where the horizontal clamping stress was high enough.

In light of the above, it is clear that none of the parameters that influence hangingwall stability should be studied independently, but the specific combination should be investigated when designing a support layout system.

These general trends are reflected by the mathematical models (developed in Chapter 4) describing the zone of influence of support units.

4 Quantifying zones of support influence in a discontinuous rock mass

4.1 Introduction

The numerical modelling results in Chapter 3 showed that fracture orientation, beam thickness and horizontal clamping stresses all affect hangingwall stability significantly. These influences need to be reflected by the proposed analytical model.

Recently Daehnke *et al.* (1999a,b) used numerical and analytical models to quantify maximum stable hangingwall spans between adjacent support units. Three failure mechanisms were modelled, namely (i) beam buckling, (ii) block rotation, and (iii) shear failure due to slip at the abutments.

A review of the current understanding of zones of influence is given in this chapter. The insights obtained from the numerical modelling exercises are incorporated into an analytical model describing the zone of support influence. The two-dimensional case is considered first, and this concept is then extended to a three-dimensional formulation of the zone of support influence.

4.2 Zone of support influence models

4.2.1 Zone of support influence definition

The zone of support influence is defined as the lateral extent of the vertical stress profile, induced in the hangingwall by a loaded support unit. The zone of influence can extend some distance away from the immediate support - hangingwall contact, and hence can contribute towards rock mass stability between adjacent support units. Zones of influence have some spatial distribution about the support unit, which describe the stress profile induced into the hangingwall by the support unit.

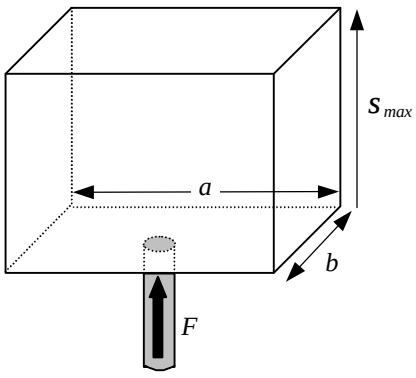

$$s_{\max} = \frac{F}{a\,b} \tag{4.2.1}$$

Figure 4.2.1 Rectangular parallelepiped zone of support influence and associated stress magnitude (s_{max}).

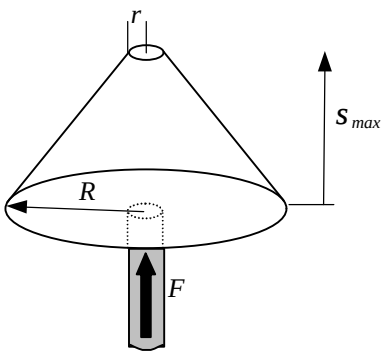

$$s_{max} = \frac{3F}{p\,(R^2 + Rr + r^2)} \qquad (4.2.2)$$

Figure 4.2.2 Frustum of right cone zone of support influence and associated stress magnitude (s_{max}).

The simplest spatial description of a zone of influence is in the form of a rectangular parallelepiped (i.e. rectangular box). The associated stress profile and magnitude are shown in Figure 4.2.1. This spatial description of the zone of influence has been used in the past (Roberts, 1999), where the parameters *a* and *b* were typically taken as 1,0 to 1,5 m.

A more complicated zone of influence stress profile in the shape of a frustum of a right cone was implemented in the support design analysis program (SDA II) developed by CSIR: Division of Mining Technology (1999). Figure 4.2.2 shows the stress profile. The radius of the support unit corresponds to *r* and the extent of the zone of influence from the support unit edge (*R* - *r*) is typically set between 1,0 and 1,5 m.

4.2.2 Classification of rock mass discontinuities

Mining induced and geological discontinuities govern the behaviour and deformation of the rock mass surrounding stopes. The discontinuities affect the zones of influence, and hence the following prevalent discontinuity types are considered in this study (Adams *et al.*, 1981):

- *Shear Fractures:*
  These fractures are associated with highly stressed rock, and are thus found in intermediate- and deep-level mines. It is estimated that the fractures initiate 6 to 8 m ahead of the advancing stope face and separate the rock into blocks of relatively intact material. They are oriented approximately parallel to the stope face and can be regularly spaced at intervals of 1 to 3 m. Shear fractures usually occur in conjugate pairs in the hangingwall and footwall, and typically reveal distinct signs of shear movement. Their dip in the hangingwall is generally towards the back area at angles of 60 to 70 degrees (Jager, 1998; Esterhuizen, 1998).

- *Extension Fractures*:
  These fractures initiate ahead of the stope face and are smaller than shear fractures. They form after shear fractures have propagated and generally terminate at parting planes. Extension fractures do not normally exhibit relative movement parallel to the fracture surface and are typically oriented parallel to the stope face. They are commonly spaced at intervals of 10 cm, with lower and upper limits of 5 and 50 cm, respectively. The strike length is typically 3 m, where lower and upper limits of 0,4 and 6 m have been observed (Esterhuizen, 1998). Extension fractures normally dip between 60 and 90 degrees, where

the direction of dip (i.e. towards or away from the stope face) can be influenced by the hanging- and footwall rock types (Roberts, 1995).

- *Bedding Planes:*
  Most reef extraction takes place in bedded quartzites. Bedding planes, which are parallel with the reef, often represent weak interfaces between adjacent strata and provide little cohesion (Jager, 1998). Bedding planes are generally spaced at 0,2 to 2,0 m intervals. The rock fall-out height is commonly governed by the position of bedding planes.

- *Joints:*
  Apart from stress-induced fractures and bedding planes, other types of geological weaknesses transect the rock mass. The most prevalent of these are geological joints, steep-dipping faults and dyke contacts. The spacing of the geological joints generally exceeds 1 m.

In intermediate- and deep-level mines, the three most prevalent discontinuity types are extension fractures, shear fractures and bedding planes (Figure 4.2.3). In shallow mines, less stress-induced fracturing occurs, and the rock mass is generally discretised by bedding planes and joint sets.

The work presented here is applicable to both intermediate- and deep-level mines, as well as to shallow mines. Sections 4.6 and 4.7 give a summary of the zones of influence for intermediate- and deep-level mines, and shallow mines, respectively.

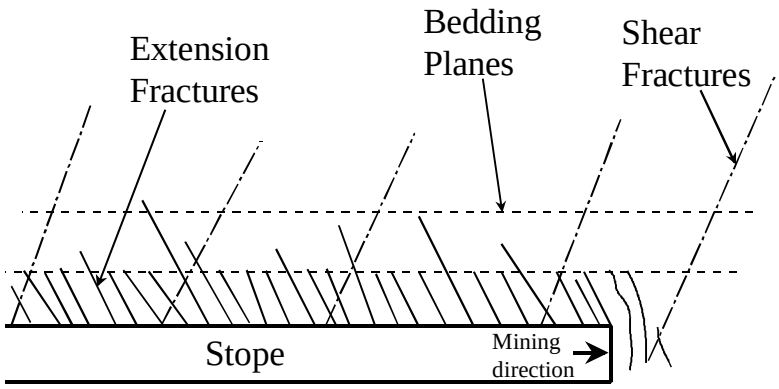

Figure 4.2.3 Simplified schematic illustrating the three most prevalent discontinuity types in intermediate- and deep-level mines.

4.2.3 Parameter definitions

The following naming conventions are adopted to describe the basic parameters governing the zones of support influence:

Rock mass parameters:

b	=	height of bedding plane above hangingwall skin
j	=	friction angle of bedding plane interface
f	=	friction angle of extension and shear fracture interface
a	=	angle of extension fracture (measured from h/wall skin)
b	=	angle of shear fracture (measured from h/wall skin)
f	=	spacing of discontinuities such as shear fractures & joints

Support parameters:

F	=	support load
r	=	radius of cylindrical support unit (e.g. elongate, prop)
w	=	width of rectangular support unit (e.g. pack) = 2 r

Zone of influence parameters:

$s\ (x)$	=	zone of influence profile in two dimensions
$s\ (x,y)$	=	zone of influence profile in three dimensions
x	=	co-ordinate perpendicular to stope face
y	=	co-ordinate parallel to stope face
z	=	extent of zone of influence from support unit edge
z_x	=	zone of influence extent extending in the x-direction from the support unit edge (3D case)
z_y	=	zone of influence extent extending in the y-direction from the support unit edge (3D case)

Figure 4.2.4 shows a schematic indicating some of the zone of influence parameters.

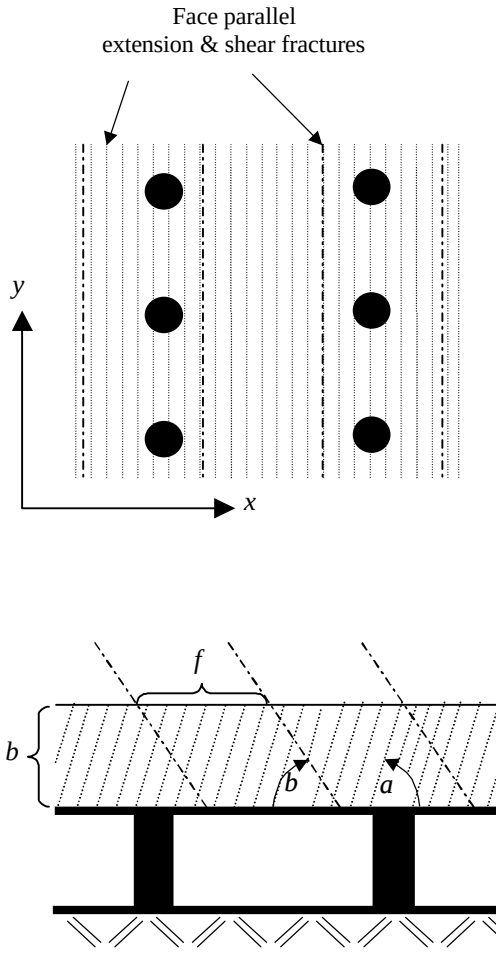

Figure 4.2.4 Naming conventions of rock mass parameters governing the zones of support influence.

4.3 Two-dimensional, plane strain formulation

4.3.1 Homogeneous hangingwall beam

The simplest zone of influence model is associated with a homogeneous hangingwall beam, i.e. a continuous hangingwall beam not discretised by any discontinuities. The boundary element program UDEC (ITASCA, 1992) is used to model the interaction of a single support unit with a homogeneous hangingwall beam (Figure 4.3.1).

For the purposes of this study, it will be shown that the maximum extent of the zone of support influence, *z*, is governed by the friction angle, j, at the bedding plane interface and the bedding plane height, *b*. This concept is schematically illustrated in Figure 4.3.2.

When the stress trajectories intercept the bedding plane at an angle exceeding the friction angle, it is assumed that slip occurs at the bedding plane. This is independent of the force generated by the support unit. Slip at the lowest significant bedding plane results in discontinuities (in the hangingwall beam and in the rock mass above the beam) opening, and comparatively little stress can be transferred across the bedding plane interface. This is a conservative assumption, as in reality bedding plane slip might be prevented due to compressive hangingwall stresses and the presence of comparatively large blocks of intact rock situated immediately above the bedding plane. The conservative engineering approach is, however, appropriate, as generally the presence and nature of discontinuities in the rock above the bedding plane are not well known. Hence, in all cases, support design and the interaction of adjacent support units should be based upon the *minimum* potential zone of influence.

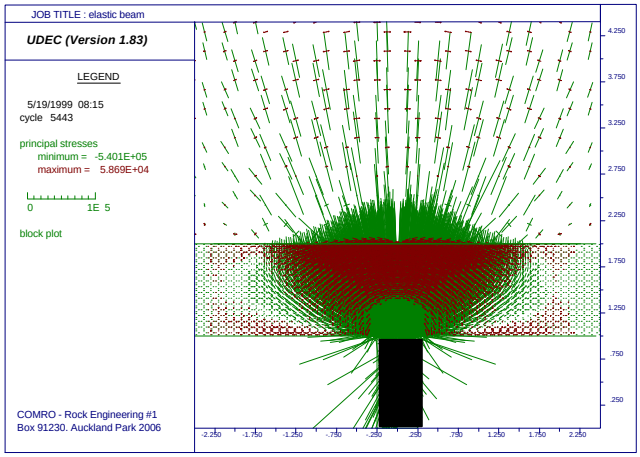

Figure 4.3.1 Principal stress trajectories through a homogeneous hangingwall beam loaded by a single support unit (b = 1,0 m, j = 40°, F = 200 kN, w = 0,5 m).

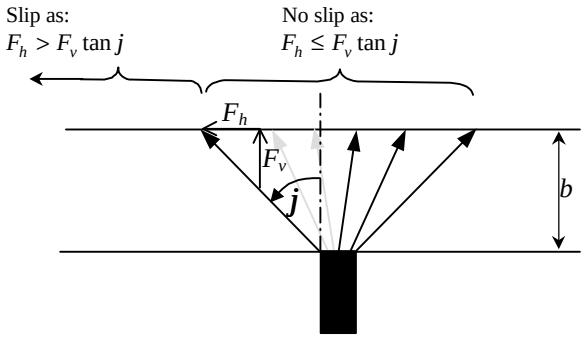

Figure 4.3.2 Maximum extent of the zone of support influence governed by bedding plane friction angle, j, and bedding plane height, b.

Using the simplified model proposed in Figure 4.3.2, it is evident that the zone of support influence extends for a distance of:

$$z = b \tan j \ . \tag{4.3.1}$$

The homogeneous beam model is applicable to shallow mines with comparatively competent and homogeneous hangingwall beams.

In intermediate- and deep level mines, however, extensive face-parallel mining-induced fractures discretise the hangingwall beam. As a consequence, zones of influence, in the direction normal to the discontinuities, can be of reduced extent. The homogeneous beam model can, however, approximate the zones of influence in the direction parallel to the discontinuities.

Numerical models of the homogeneous hangingwall beam are used to quantify the vertical stress profile (induced by the support unit) at the bedding plane interface. Figure 4.3.3 shows the numerically calculated vertical stress distribution at the interface, based on a two-dimensional plane strain model. The normalised support resistance is calculated as the ratio of the vertical stress induced in the hangingwall and the stress transmitted by the support unit. The support resistance is calculated for a support unit w = 0,5 m wide and carrying a load of F = 200 kN. The friction angle at the interface is assumed to be j = 40°. Also shown is a mathematical approximation of the numerically determined profile.

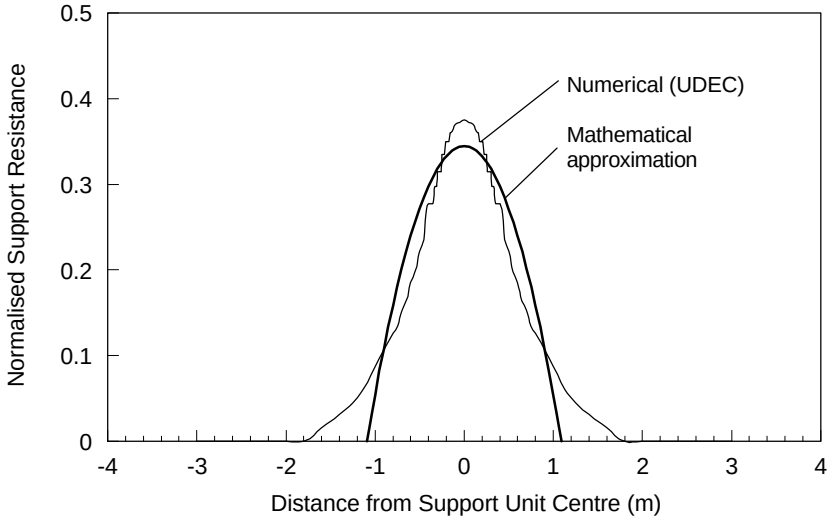

Figure 4.3.3 Numerical versus analytical support resistance profile.

The mathematical function describing the zone of influence stress distribution is in the form of a parabola. The suitability of numerous functions (conical, hyperbolic, Gaussian distribution) was evaluated, and the parabolic distribution was ultimately deemed to be the most appropriate and convenient function to describe stress profiles associated with zones of influence. In two dimensions the stress profile is mathematically described by:

$$s(x) = \begin{cases} 0 \ , & |x| > z \\ \dfrac{3F}{4z}\left[1 - \left(\dfrac{x}{z}\right)^2\right] \ , & |x| \le z \end{cases} \tag{4.3.2}$$

where: z = $z + r$ for cylindrical support units,
z = $z + 0{,}5w$ for rectangular support units,

and, as defined before,

$$z = b \tan j \ . \tag{4.3.3}$$

It is important to ensure that, for all stress profiles,

$$\int_{-z}^{z} s\,(x)\,dx = F\ , \tag{4.3.4}$$

i.e. the induced stress at the support-hangingwall contact is equal to the total stress within the zone of influence stress profile.

4.3.2 Hangingwall beam discretised by discontinuities

Numerical UDEC models are used to investigate zone of influence profiles in a hangingwall discretised by discontinuities. In intermediate- and deep-level mines, the hangingwall is typically discretised by closely spaced extension fractures. These generally terminate at parting planes and are typically oriented parallel to the stope face.

Figure 4.3.4 shows principal stress vectors as calculated by UDEC for a hangingwall discretised by fractures oriented between 30° and 90° to the hangingwall skin. In these models, no horizontal clamping stresses are applied to the hangingwall beam.

a = 90°

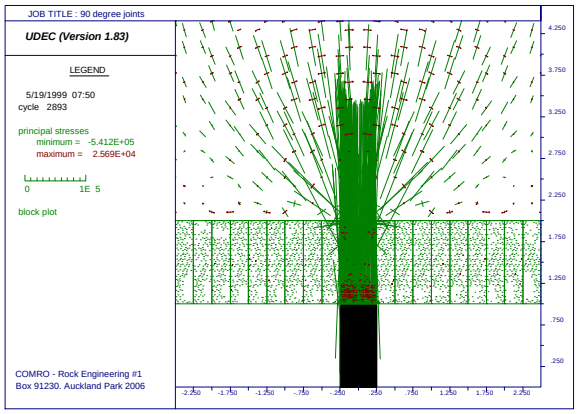

a = 75°

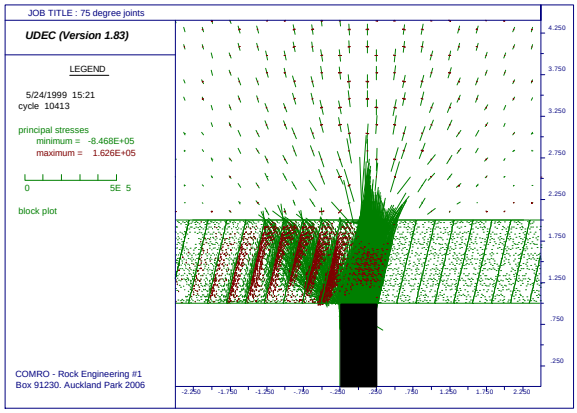

$a = 60^o$

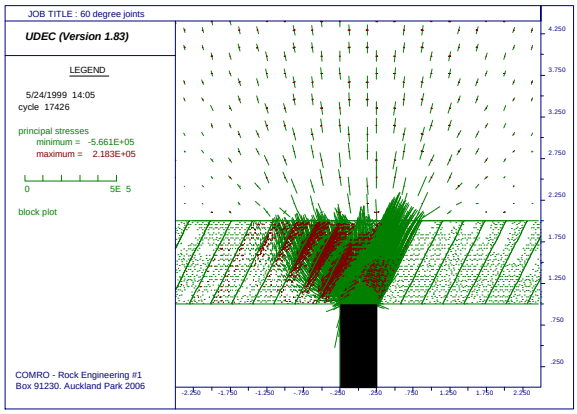

$a = 45^o$

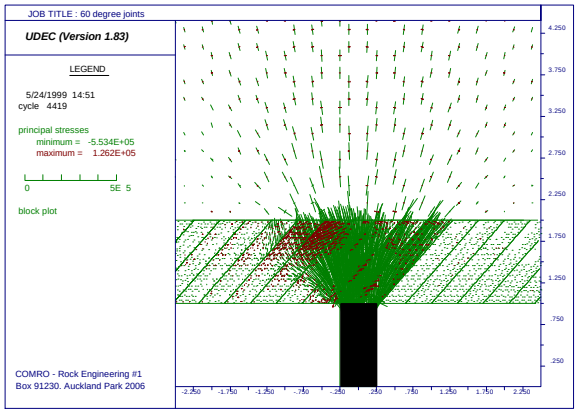

$a = 30^o$

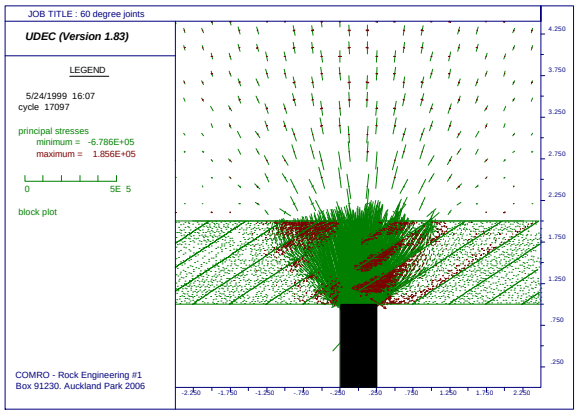

Figure 4.3.4 Principal stress trajectories through a hangingwall beam discretised by 90, 75, 60, 45 and 30 degree extension fractures (UDEC modelling results).

It is apparent that the stress trajectories follow two principal paths, i.e. (i) parallel to the discontinuities, and (ii) perpendicular to the discontinuities. Figure 4.3.5 shows a schematic illustrating the two principal stress paths.

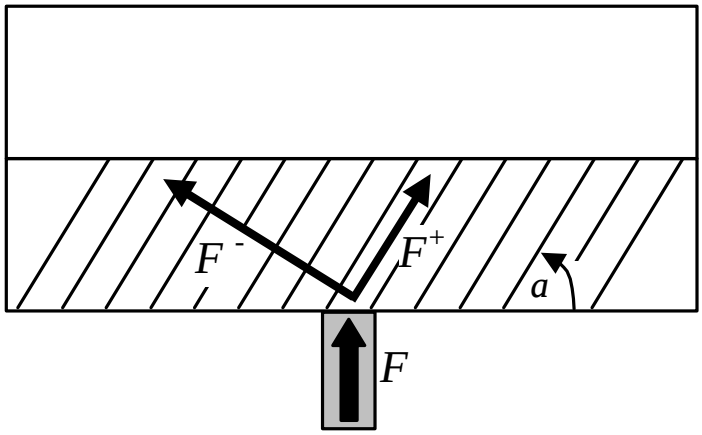

Figure 4.3.5. Stress trajectories through a hangingwall beam discretised by obliquely dipping extension fractures.

The zones on either side of the support unit differ. In an unclamped hangingwall beam, the zones of influence associated with F^+ and F^- are, respectively:

$$z^+ = \frac{b}{\tan a} \quad \text{and} \quad z^- = b \tan j \ . \tag{4.3.5}$$

The value of z^+ cannot exceed z^- and, if $90^o - a > j$, then $z^+ = z^-$.

Solving for the force vectors, it can be shown that,

$$F^+ = F \sin a \ \text{ and } \ F^- = F \cos a \ . \tag{4.3.6}$$

The vertical components of forces F^+ and F^- are

$$F_v^+ = F \sin^2 a \ \text{ and } \ F_v^- = F \cos^2 a \ . \tag{4.3.7}$$

Thus the ratio of F_v^+ versus F_v^- is equal to $\tan^2 a$. As the fracture angle, a, tends to 90^o, F_v^- reduces to zero. The corresponding zone of influence, z^-, needs to be modified accordingly, and when $a = 90^o$, $z^- = 0$. In this study, the following correction function is applied to z^-:

$$z^- = b \tan j \ \frac{100}{(100 + \tan^2 a)} \tag{4.3.8}$$

Figure 4.3.6 shows zone of influence stress profiles for $a = 90^o$, 60^o and 30^o.

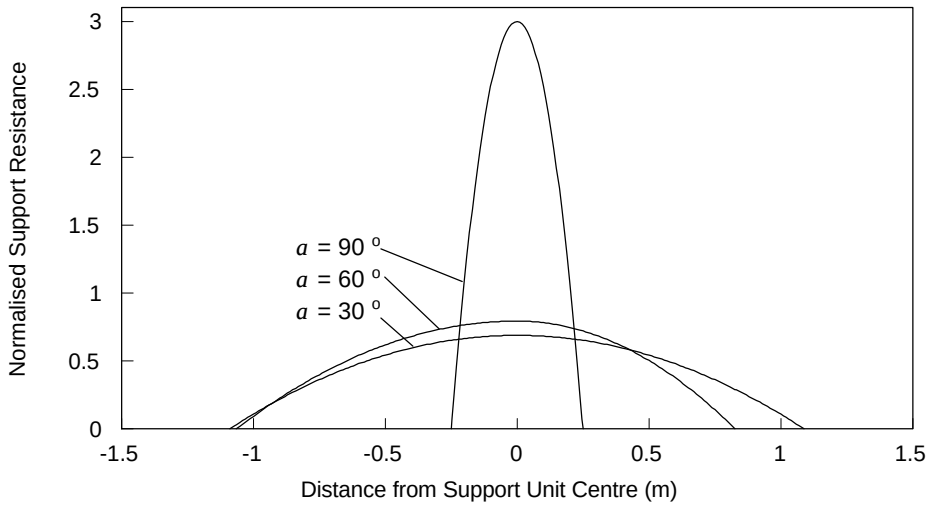

Figure 4.3.6 Zone of influence profiles for $a = 90^o$, 60^o and 30^o.

4.3.3 Clamped hangingwall beam discretised by discontinuities

In intermediate- and deep-level mines, fracturing ahead of the stope face induces rock dilation, leading to compressive hangingwall stresses parallel to the skin of the excavation (Jager and Roberts, 1986). Compressive hangingwall stresses usually contribute significantly to the rock mass stability. Squelch (1994) measured maximum compressive hangingwall stresses of 1 to 10 MPa at depths between 0,7 and 2,2 m into the hangingwall. These horizontal stresses clamp the fractured rock together and – depending on the orientation of the fractures – can significantly improve the structural integrity and stability of the hangingwall (Jager and Roberts, 1986).

Herrmann (1987) found that in stopes with back area caving, stress relaxation occurred in the lower layers of the hangingwall, and noted the importance of rock confinement to maintain compressive hangingwall stresses. Rockfalls and caving in the back area generally lead to reduced hangingwall confinement. However, compressive hangingwall stresses can still be maintained when frictional resistance, generated at bedding planes, restricts the lateral hangingwall movement. Such frictional resistance can be induced by appropriate support forces generated under the hangingwall beam (Daehnke *et al.*, 1999b).

Compressive hangingwall stresses affect the zone of influence by clamping hangingwall discontinuities together. As a consequence, stresses can be transmitted obliquely across discontinuities, and the zone of influence is extended to either side of the support unit. To quantify the stress profile and extent of the zone of influence associated with a clamped hangingwall beam, the simplified analytical model shown in Figure 4.3.7 is considered.

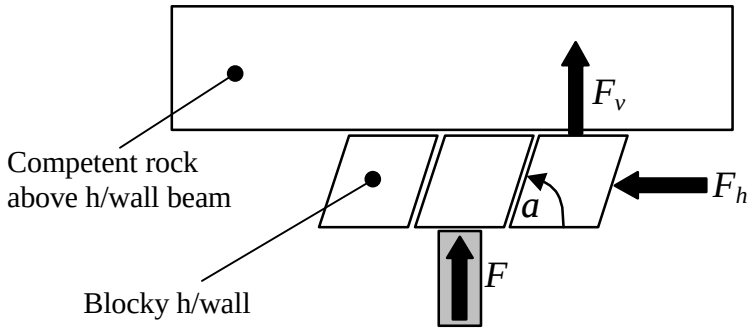

Figure 4.3.7 Simplified model used to quantify the zone of support influence in a clamped, discontinuous hangingwall beam.

By resolving the forces F_h and F_v normal and parallel to the inclined fracture, it can be shown that the maximum vertical force, F_v, that can be transmitted by a hangingwall block, adjacent to the block supported directly by the support unit, is:

$$F_v = F_h \frac{m - \cot a}{1 + m \cot a} \ , \qquad [4.3.9]$$

where m = tan f, and f is the friction angle of the inclined fracture interface. Note that, due to the interlocking nature of *in situ* mining induced fractures, the associated effective friction angle is typically comparatively high, and values of $f = 50^o$ to $f = 60^o$ are considered realistic. For the two-dimensional plane strain case $F_h = b\ s_h$. The minimum stress, s_h^{crit}, that is required to clamp the hangingwall discontinuities, is calculated by setting $F_v = F \sin^2 a$ (from Equation 4.3.7), i.e.

$$s_h^{crit} = \frac{F}{b} \quad c \quad \text{and} \quad c = \frac{\sin^2 a \quad (1 + m \cot a)}{m - \cot a} . \qquad [4.3.10]$$

The function c is graphically illustrated in Figure 4.3.8 for interface friction angles of $f = 50^o$ and $f = 60^o$. If, for example, b = 1,0 m, $f = 50^o$ and $a = 60^o$, then $s_h^{crit} = 2{,}1\,F$. For a typical elongate load of F = 200 kN, this implies that the horizontal compressive stresses should be at least s_h = 0,42 MPa for the discontinuities to be sufficiently clamped that the zones of influence correspond to the zones in a homogeneous hangingwall beam. This is an important and positive insight, as it implies that in intermediate- and deep-level mines, where typically s_h > 1,0 MPa, the zones of influence in a hangingwall discretised by moderately to steeply dipping fractures can generally be accurately approximated by the corresponding zones in homogeneous beams.

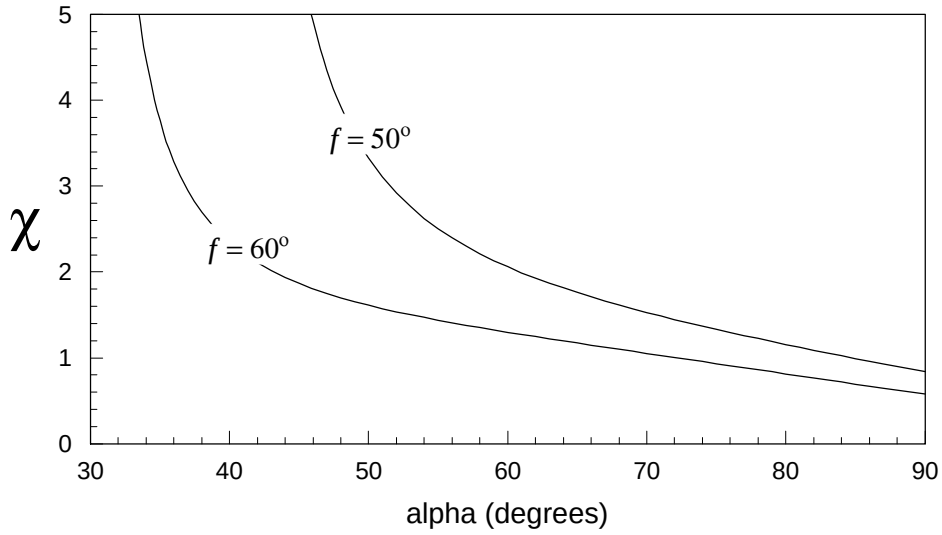

Figure 4.3.8 Graphical illustration of function c for $f = 50^o$ and $f = 60^o$.

4.4 Three-dimensional formulation

4.4.1 Homogeneous hangingwall beam

The three-dimensional formulation of the zone of influence in a homogeneous hangingwall beam follows analogous to the two-dimensional formulation. The zone of influence stress distribution in a homogeneous hangingwall beam is described by a circular paraboloid, i.e.

$$s(x,y) = \begin{cases} 0\,, & \left(\frac{x}{z}\right)^2 + \left(\frac{y}{z}\right)^2 > 1 \\ \frac{2F}{p\,z^2}\left[1 - \left(\frac{x}{z}\right)^2 - \left(\frac{y}{z}\right)^2\right], & \left(\frac{x}{z}\right)^2 + \left(\frac{y}{z}\right)^2 \le 1 \end{cases} \qquad (4.4.1)$$

Figure 4.4.1 shows a three-dimensional carpet plot of $s(x,y)$, where $z = r + b\tan j$.

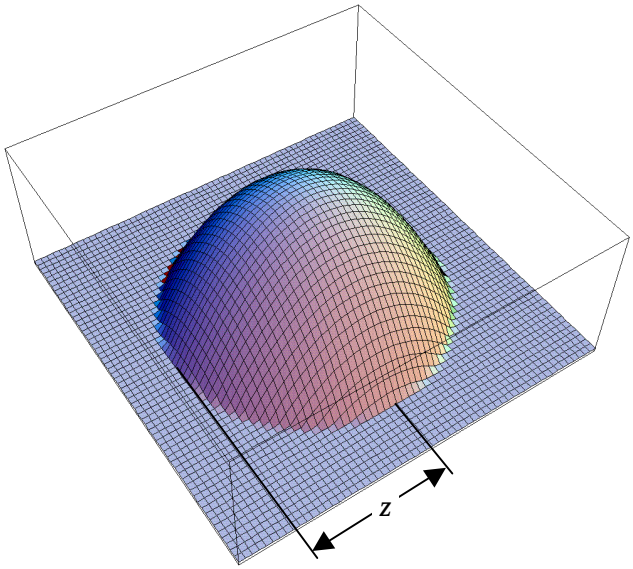

Figure 4.4.1 Zone of influence within a homogeneous beam in the shape of a circular paraboloid.

4.4.2 Hangingwall beam discretised by discontinuities

In the two-dimensional formulation it was shown that the zones of influence on either side of the support unit differ when the hangingwall is discretised by discontinuities. Figure 4.4.2 shows the zone of influence profile for a hangingwall beam transected by vertical discontinuities (a = 90^o),

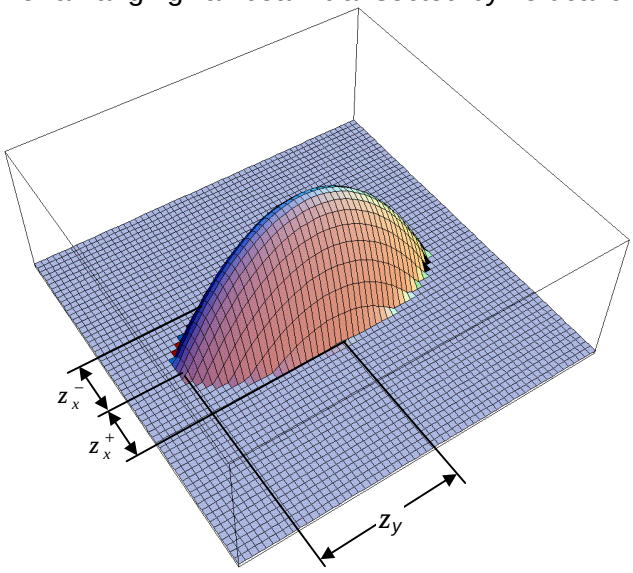

Figure 4.4.2 Zone of influence profile within an unclamped hangingwall discretised by vertical discontinuities.

where:

$$z_y = r + b\tan j \ , \tag{4.4.2}$$

$$z_x^+ = z_x^- = r \ . \tag{4.4.3}$$

Figure 4.4.3 shows a three-dimensional view of the zone of influence in a hangingwall discretised by oblique discontinuities ($0 < a < 90$). The hangingwall is assumed to be unclamped.

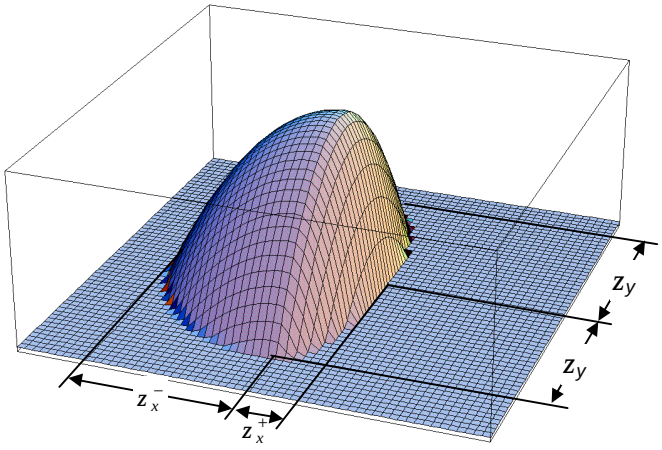

Figure 4.4.3 Zone of influence profile within an unclamped hangingwall discretised by oblique discontinuities.

The general stress profile, describing the zone of influence within an unclamped hangingwall beam, is given by Equation 4.4.4.

$$s(x,y) = \begin{cases} 0\,, & \left(\frac{x}{z_x^-}\right)^2 + \left(\frac{y}{z_y}\right)^2 > 1 \quad \& \quad x \le 0 \\ \Omega\left[1 - \left(\frac{x}{z_x^-}\right)^2 - \left(\frac{y}{z_y}\right)^2\right], & \left(\frac{x}{z_x^-}\right)^2 + \left(\frac{y}{z_y}\right)^2 \le 1 \;\&\; x \le 0 \\ \Omega\left[1 - \left(\frac{x}{z_x^+}\right)^2 - \left(\frac{y}{z_y}\right)^2\right], & \left(\frac{x}{z_x^+}\right)^2 + \left(\frac{y}{z_y}\right)^2 \le 1 \;\&\; x \ge 0 \\ 0\,, & \left(\frac{x}{z_x^+}\right)^2 + \left(\frac{y}{z_y}\right)^2 > 1 \quad \& \quad x \ge 0 \end{cases} \tag{4.4.4}$$

where:

$$\Omega = \frac{4F}{p\, z_y (z_x^+ + z_x^-)}, \text{ and} \tag{4.4.5}$$

$$z_y = r + b\tan j \;, \tag{4.4.6}$$

$$z_x^+ = r + \frac{b}{\tan a} \;, \tag{4.4.7}$$

$$z_x^- = r + b\tan j \;\frac{100}{100 + \tan^2 a} \;. \tag{4.4.8}$$

The scaling parameter Ω is determined by ensuring that:

$$\int_{-z_x}^{z_x} \int_{c_1(x)}^{c_2(x)} s\,(x, y)\, dy\, dx = F \quad , \tag{4.4.9}$$

where:

$$c_1(x) = -z_y \sqrt{1-\left(\frac{x}{z_x^-}\right)^2} \quad , \qquad c_2(x) = z_y \sqrt{1-\left(\frac{x}{z_x^+}\right)^2} \quad . \tag{4.4.10}$$

4.4.3 Clamped hangingwall beam discretised by discontinuities

In the two-dimensional case it was shown that compressive hangingwall stresses affect the zone of influence. The compressive stresses clamp discontinuities together and stresses induced by the support unit can be transmitted obliquely across discontinuities. Using an analogous approach to the two-dimensional case, it can be shown that in three dimensions, considering that

$$F_h = \tfrac{4}{3} z_y b s_h \quad , \tag{4.4.11}$$

the minimum stress, s_h^{crit}, that is required to clamp the hangingwall discontinuities, is:

$$s_h^{crit} = \frac{3F}{4bz_y}\ c \quad \text{and, as before,} \quad c = \frac{\sin^2 a\ \ (1 + m\cot a)}{m - \cot a}. \tag{4.4.12}$$

As noted before, it is evident from Equation 4.4.12 that comparatively low hangingwall clamping stresses are required, such that the zones of influence in a discontinuous hangingwall beam correspond to the zones of influence within a homogeneous hangingwall beam.

4.5 Effect of shear fractures on the zone of support influence

A probabilistic approach is used to quantify the effect of shear fractures on the zone of support influence. Consider a hangingwall beam discretised by shear fractures, oriented at an angle, *b*, as shown in Figure 4.5.1.

The parameters that are considered in the probabilistic formulation are:

w = support width (rectangular support units, e.g. packs)
r = radius of support (cylindrical support units, e.g. props)
d = distance from the edge of the support to the fracture
f = fracture spacing (constant)

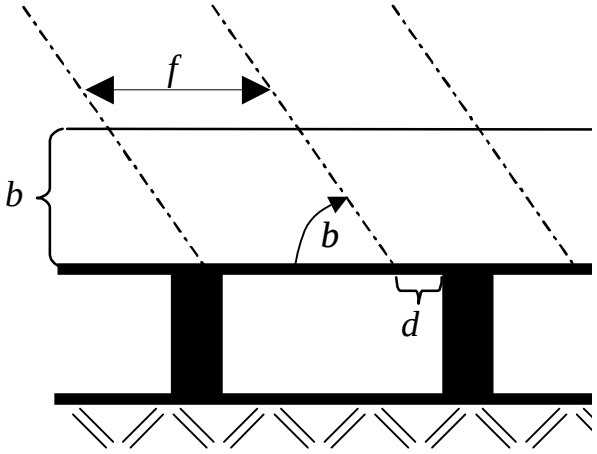

Figure 4.5.1 Hangingwall beam discretised by shear fractures

The shear fractures are randomly distributed in relation to the support units, i.e. the distance, *d*, is not constant. The minimum value of *d* is 0, when the fracture coincides with the support edge. This is considered the worst case as, with no clamping stresses, the zone of support influence could be limited by the shear fracture. Conversely, the best case is assumed to occur when $d = f - r$, which is taken as the maximum value of *d* (i.e. when the centre of the adjacent fracture is situated immediately above the support unit centre). At $d > f - r$, the effective stress transfer from the support unit to the hangingwall is assumed to be compromised by the adjacent shear fracture, and the zone of influence is potentially once again limited by the shear fracture.

The probability that *d* will lie between 0 and *x*, where $0 \le x \le (f - r)$, is given by

$$P = \frac{x}{f - r}. \tag{4.5.1}$$

The probability that *d* will exceed *x*, is given by

$$1 - P = 1 - \left(\frac{x}{f - r} \right). \tag{4.5.2}$$

It is thus possible to determine *d* probabilistically:

$$d = (1 - P)(f - r) \tag{4.5.3}$$

For example, if P = 0,8 (i.e. the probability is 80 per cent that the fracture is not within a distance, d, of the support edge), then

$$d = (1 - 0{,}8)(f - r) = 0{,}2(f - r).$$

If no horizontal compressive stress acts on the beam, i.e. $s_h = 0$, then the extent of the zone of influence, on the left hand side of the support, z_x^-, is given by:

$$z_x^- = \begin{cases} \dfrac{b}{\tan b} + d\ , & b > \frac{p}{2} - j \\ \\ b \tan j\ , & b \le \frac{p}{2} - j \end{cases} . \qquad (4.5.4)$$

Substituting equation (4.5.3) in (4.5.4) gives:

$$z_x^- = \begin{cases} \dfrac{b}{\tan b} + (1 - P)(f - r)\ , & b > \frac{p}{2} - j \\ \\ b \tan j\ , & b \le \frac{p}{2} - j \end{cases} . \qquad (4.5.5)$$

To avoid being too conservative in the design of support spacing, it may be beneficial to assume that 90 % of all the zones of support influence will be free of shear fractures. This gives $d = (1 - 0{,}9)(f - r) = 0{,}1(f - r)$.

If the horizontal compressive stress, s_h, is high enough to ensure that the beam is clamped, the extent of the zone of influence on the left-hand side of the support, z_x^-, is given by $z_x^- = b \tan j$ as before.

4.6 Quantifying zones of influence in intermediate- and deep-level mines

The aim of this section is to briefly review the zones of influence applicable to intermediate- and deep-level mines. The typical hangingwall of mines at these depths is characterised by face parallel, ubiquitous and closely spaced extension fractures, with face parallel conjugate shear fractures spaced between 1 and 3 m.

Table 4.6.1 is given to summarise the principal results and facilitate the convenient quantification of zones of support influence.

Assuming an elliptic parabolic stress distribution (Equation 4.4.4) about the support, the maximum stress can be calculated using the following equation:

$$s_{\max} = \frac{4F}{p\ z_y (z_x^+ + z_x^-)}\ , \qquad (4.6.1)$$

where:

$$z_{x,y}^{+,-} = z_{x,y}^{+,-} + r \qquad (4.6.2)$$

Table 4.6.1 Zones of influence in intermediate- and deep-level mines.

Is $s_h > s_h^{crit}$? (Eq. 4.4.12)

YES NO

	Clamped	Unclamped	
z_x^+	$b \tan j$	$a > \frac{p}{2} - j$	$\frac{b}{\tan a}$
		$a \le \frac{p}{2} - j$	$b \tan j$
z_x^-	$b \tan j$	$b > \frac{p}{2} - j$	$\frac{b}{\tan b} + (1-P)(f-r)$
		$b \le \frac{p}{2} - j$	$b \tan j \frac{100}{100 + \tan^2 a}$
z_y	$b \tan j$		$b \tan j$

Note that the maximum value of z_x^- cannot exceed $b \tan j$, even if b is greater than $p/2 - j$.

4.7 Quantifying zones of influence in shallow mines

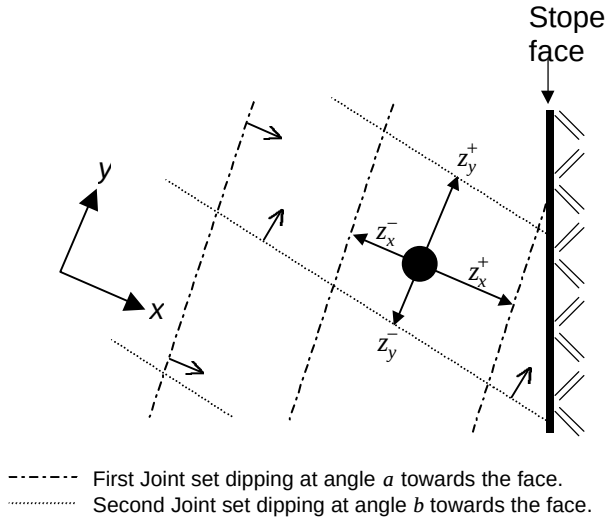

Figure 4.7.1 Zones of influence associated with a stope in a shallow mining environment.

The methodology to quantify zones of support influence can also be applied to shallow mines. In general, the hangingwall in shallow mines is characterised by zero or low clamping stresses and conjugate joint sets, which discretise the hangingwall beam into blocks of relatively intact rock. It is important to adopt a probabilistic approach when quantifying the zones of influence in

shallow mines. Failing to do so results in comparatively small zones of influence, and too conservative support design in terms of support spacing.

A brief overview of an approximate solution for zones of influence in a shallow mining environment follows. Consider a stope as shown in Figure 4.7.1. The hangingwall is discretised by two joint sets oriented at two different angles with respect to the stope face. The dip direction of the joint sets, as well as the zones of influence in the four relevant directions, are indicated in Figure 4.7.1.

The zones of influence are as follows:

$$z_x^+ = \begin{cases} \dfrac{b}{\tan a} + d\ , & a > \frac{p}{2} - j \\ \\ b \tan j\ , & a \le \frac{p}{2} - j \end{cases}, \tag{4.7.1}$$

$$z_x^- = b \tan j\ \frac{100}{100 + \tan^2 a} + d\left(1 - \frac{100}{100 + \tan^2 a}\right), \tag{4.7.2}$$

$$z_y^+ = \begin{cases} \dfrac{b}{\tan b} + d\ , & b > \frac{p}{2} - j \\ \\ b \tan j\ , & b \le \frac{p}{2} - j \end{cases}, \tag{4.7.3}$$

$$z_y^- = b \tan j\ \frac{100}{100 + \tan^2 b} + d\left(1 - \frac{100}{100 + \tan^2 b}\right), \tag{4.7.4}$$

where *d* is calculated using Equation 4.5.3.

A further improved probabilistic support design methodology for shallow mines is discussed in Chapter 9.

4.8 Conclusions

This chapter gives a new and improved formulation of zones of support influence in a discontinuous rock mass. Numerical models are used to gain qualitative insights into stress trajectories through fractured hangingwall beams and facilitate the formulation of mathematical models approximating the zone of influence stress profiles.

As mentioned in Chapter 3, the analytical model describing the zone of influence needs to cater for beam thickness, fracture orientation and horizontal clamping stresses. Beam thickness is accounted for by *b* in all the equations describing the extent of the zone of influence. Fracture orientation (a, b) is also taken into consideration by these equations. By checking if the hangingwall beam is clamped or not, the influence of horizontal clamping stress is taken into account. Thus, the model complies with the criteria set in the previous chapter.

Elliptic paraboloids are chosen to conveniently describe three-dimensional zones of influence in a hangingwall beam arbitrarily discretised by two discontinuity sets.

The mathematical formulation of the zone of influence stress profiles is straightforward and can easily be incorporated into a support design computer program.

An important finding is that in intermediate- and deep-level mines, where the hangingwall is generally compressed by clamping stresses in excess of 0,5 MPa, the zones of influence correspond to those in homogeneous beams.

A novel probabilistic methodology is developed to quantify the zones of influence associated with hangingwall beams discretised by comparatively widely spaced discontinuities.

It is emphasised that zones of support influence are not the sole mechanism contributing towards the rock mass stability between adjacent support units. For example, consider the cross-section of the support layout given in Figure 4.8.1. The props are assumed to exert a load of F = 200 kN and the pack a load of F = 150 kN. The bedding plane height is assumed as b = 1,0 m, the bedding plane friction angle is $j = 40^{o}$, and the beam is fully clamped, i.e. the zones of influence corresponding to a homogeneous beam apply. The cross-section shown in Figure 4.8.1 is along the centre of the support units, i.e., when considering the support layout in three dimensions, the cross-section shown represents the highest possible support resistance in the strike direction.

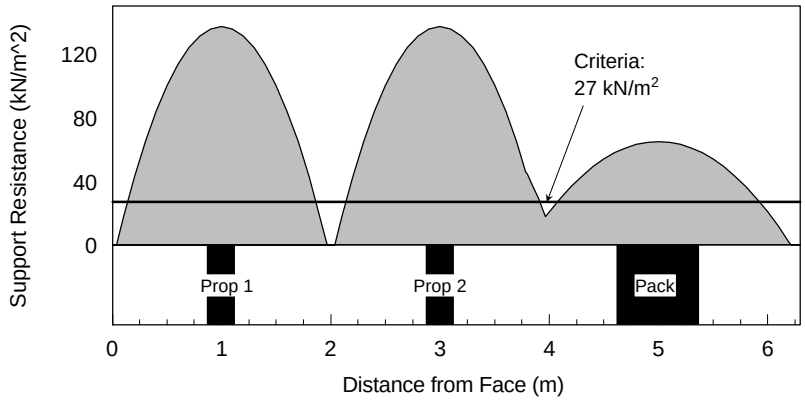

Figure 4.8.1 Cross-section of support resistance profiles induced by two props (F = 200 kN, r = 0,125 m) and a pack (F = 150 kN, w = 0,75 m).

As is evident from Figure 4.8.1, a deficit in support resistance occurs whenever the shaded stress profile is less than the rock fall criterion ($r\ g\ b$ = 27 kN/m^2).

A support resistance deficit does not necessarily imply that the rock mass is unstable in these areas. The possibilities of failure mechanisms, such as beam buckling, block rotation and shear failure (Daehnke *et al.*, 1999b), need to be investigated. The likelihood of such failure mechanisms *and* the zones of influence need to be considered in order to assess the rock mass stability between adjacent support units. Chapter 8 gives a proposed design methodology which combines both the zones of influence and keyblock buckling, rotation and shear mechanisms.

To continue mining at ever-increasing depths with reduced rock-related risk and optimum productivity, support system design needs to be based upon sound engineering principles. Various tools have been developed to address support performance in quasi-static and dynamic conditions, support interaction with the hangingwall, and maximum stable spans between adjacent support units. The various design criteria and engineering principles need to be incorporated into a unified design methodology. A computer program in the form of SDA II is required to engage the methodology and enable the rock engineer to conveniently optimise geotechnical area specific support systems.

5 Quantifying the zone of influence of the stope face

5.1 Introduction

A preliminary investigation into the zone of influence of the stope face is carried out in this chapter. The influence of the stope face is modelled using UDEC and these results are used to facilitate the formulation of analytical models.

The results of the numerical modelling are given in Chapter 6, as the modelling of the stope face and backfill zones of influence are done simultaneously. (These results are referred to in this chapter, but are not repeated here.)

5.2 Quantifying zone of stope face influence in intermediate- and deep-level mines

Consider a hangingwall discretised by extension fractures oriented at an angle, a, and shear fractures at an angle, b, as shown in Figure 5.2.1.

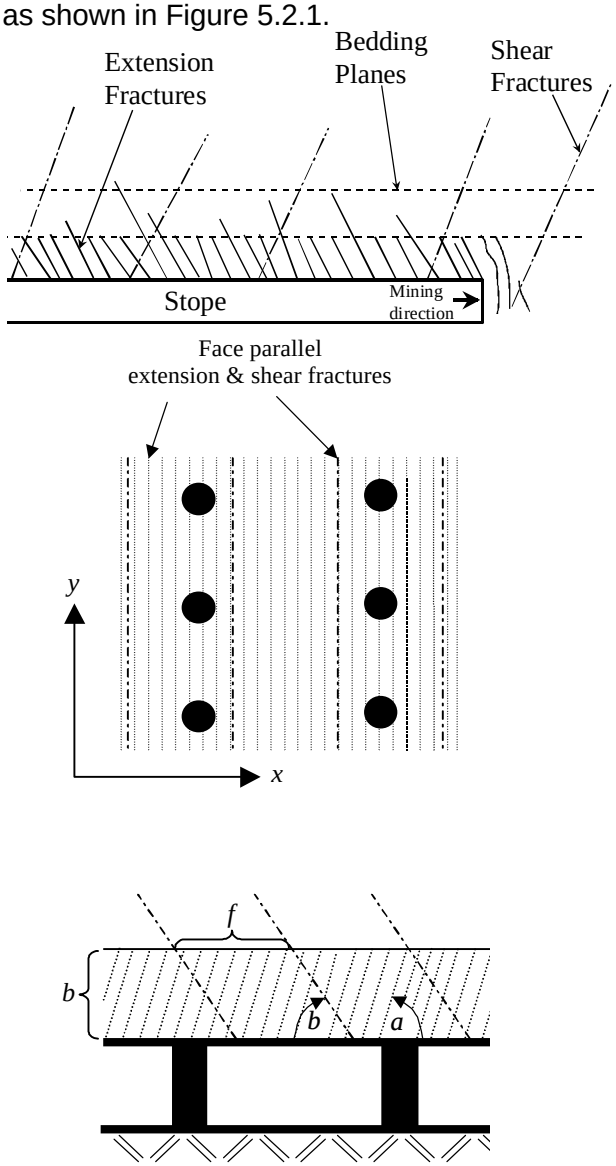

Figure 5.2.1 Schematic showing hangingwall discretised by extension and shear fractures.

From the numerical modelling results (Section 6.3), it is clear that the orientation of the extension fractures have a pronounced influence on the stress path at the stope face. However, investigations into the zones of *support* influence (Chapter 4), showed that in most intermediate- and deep-level mines, the horizontal stresses are high enough to clamp the discretised hangingwall beam. For the purposes of this study, the horizontal stress is assumed to be sufficient to clamp the hangingwall beam, and thus

$$z = b \tan j \qquad (5.2.1)$$

Assuming a linear decline in stress with distance from the face, the zone of influence stress distribution in a hangingwall beam is described by:

$$s(x,y) = \begin{cases} r\,g\,H\,(1 - x/z) & ; \quad 0 \le x \le z \qquad (5.2.2) \\ 0 & ; \quad x \ge z \qquad (5.2.3) \end{cases}$$

where r is the density of the rock,
H is the depth of mining,
x is measured from the edge of the face, and
z is the extent of the zone of influence from the edge of the face.

The maximum stress at the stope face is taken as the virgin stress, i.e. $r\,g\,H$. This is a conservative assumption, as in practice the stress concentration in the immediate vicinity of the stope face results in vertical stresses exceeding the virgin stress by, typically, a factor of 2 – 3.

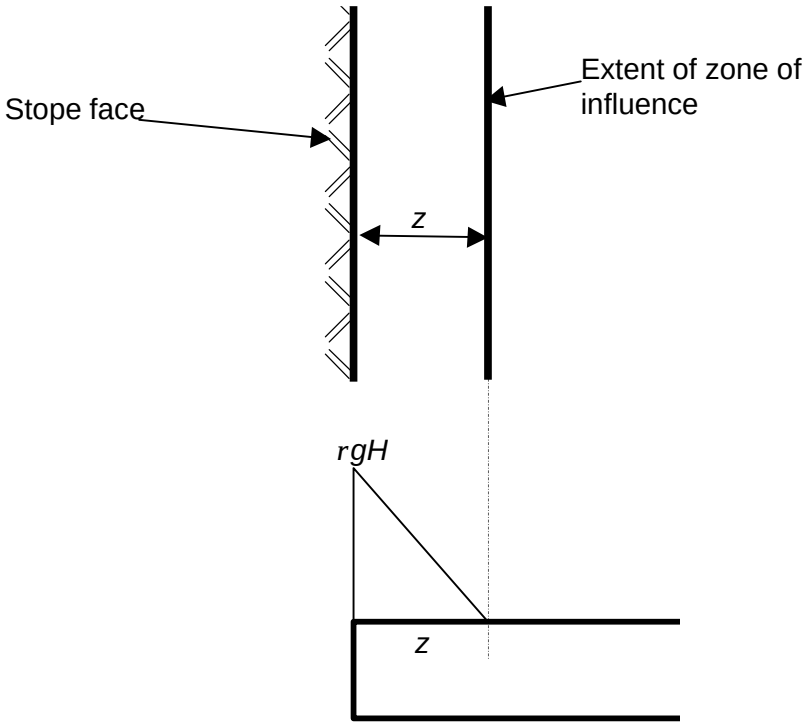

Figure 5.2.2 Zone of stope face influence and associated stress distribution.

5.3 Quantifying zone of stope face influence in shallow mines

In shallow mines, the hangingwall is generally characterised by little or no clamping stresses and discretised by conjugate joint sets.

Consider a stope as shown in Figure 5.3.1. The hangingwall is discretised by two joint sets oriented at two different angles with respect to the stope face. The dip direction of the joint sets, as well as the zones of influence in the four relevant directions, are indicated in Figure 5.3.1.

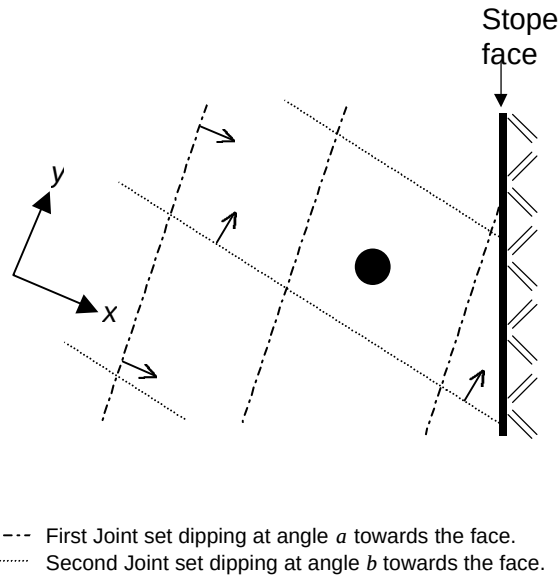

Figure 5.3.1 Zone of influence associated with a stope face in a shallow mining environment.

As can be seen from Figure 5.3.1, the joints intersect the stope face. Because of the absence of horizontal clamping stresses in shallow mines, the zone of influence of the stope face will be limited to the block delineated by these joints. Thus the zone of influence will not have a simple shape.

The determination of the exact shape of the zone of influence and the associated stress distribution is a complex problem, and falls outside the scope of this study. It is, however, recommended that further work concerning the quantification of these zones of influence should be undertaken.

5.4 Conclusions

In intermediate- and deep-level mines, the hangingwall is assumed to be clamped by the horizontal stress, and the zone of influence of the stope face is simple to establish. The stress distribution associated with the zone of stope face influence is assumed to be linear, with a maximum value equal to the virgin stress situated at the stope face.

Due to the nature of the discontinuities which discretise the hangingwall beam in shallow mines, the determination of the zone of stope face influence is complicated, and falls beyond the scope of this investigation. In the interim, the zone of influence of the stope face in shallow mines should conservatively be assumed to be zero.

6 Zone of influence of backfill

6.1 Introduction

A preliminary study to investigate the zone of influence of backfill is undertaken in this chapter.

The numerical code, UDEC, was used to investigate the zone of influence of backfill and the stope face. The results obtained in the numerical exercise are compared to the underground study of the zone of influence of backfill. The underground study was done on two different reef types where backfill is being used.

6.2 In situ evaluation of zone of influence of backfill

A number of underground visits were conducted to backfill stopes in order to investigate the effectiveness of the placed backfill. In these stopes the zone of backfill influence was estimated by pushing, as deeply as possible, an inclino-rule between the backfill and the hangingwall of the stope. This gives an approximation of the point at which the backfill and the hangingwall comes into contact. The readings are shown in Figure 6.2.1 (the point of contact between the backfill and the hangingwall is measured from the face of the backfill). The panels in which the readings were taken are approximately 2200 m below surface.

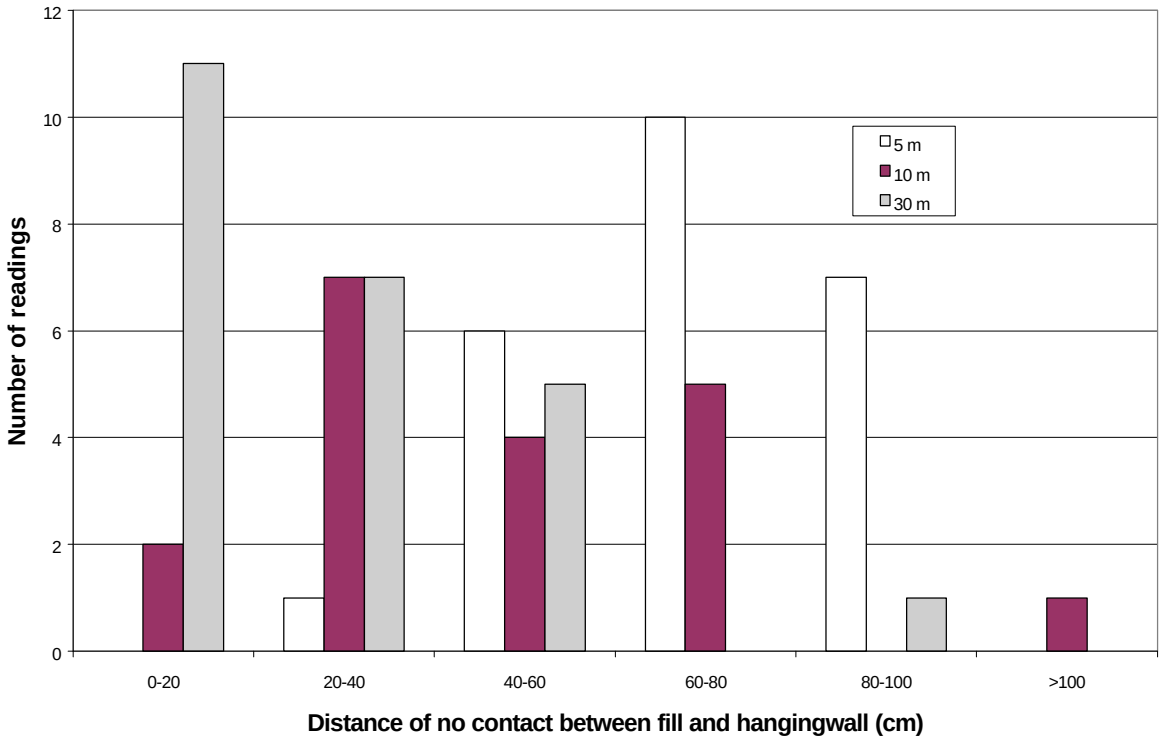

Figure 6.2.1 In situ data of the point of backfill – hangingwall contact with respect to the side of the backfill, measured along dip for different stopes.

The zone of influence of backfill is assumed to be zero if it does not take any load, i.e. immediately after installation of the backfill. It is understood that if the backfill is very compressed, it will exert more pressure on the hangingwall and thus its zone of influence will increase.

The parameter *c* is defined as the average distance between the edge of the backfill and the point of contact between the hangingwall and backfill.

The averages of the readings, *c*, taken for the panels in which the backfill is 30 m, 10 m, and 5 m from the face, are 25 cm, 50 cm and 70 cm respectively (Figure 6.2.1). Thus, it can be said that the point of contact between the backfill and the hangingwall is behind the face of the backfill for all cases.

A graphical representation of the zone of backfill influence is given in Figure 6.2.2.

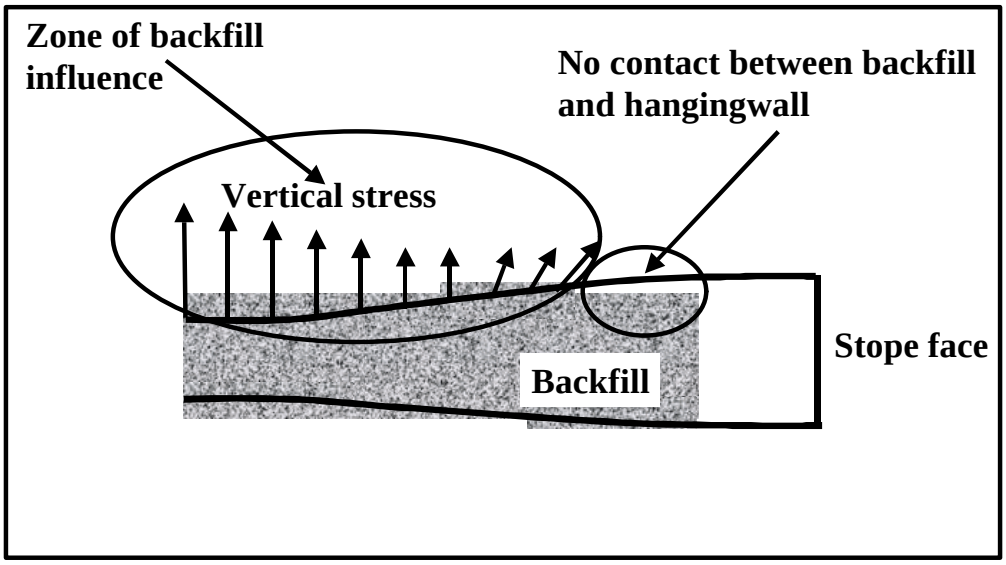

Figure 6.2.2 Graphical representation of the zone of backfill influence at the stope face (section on strike).

Assuming the backfill is in contact with the hangingwall at the edge of the backfill, the zone of backfill influence can be expressed as:

$$z = b \tan j\,, \tag{6.2.1}$$

where *b* is the bedding thickness, and j is the friction angle of the bedding plane contact Thus, using the notation as in Chapter 4, the effective zone of influence of the backfill, z_b, is the difference between *z* and *c* (as defined earlier).

$$z_b = z - c, \tag{6.2.2}$$

$$z_b = b \tan j - c. \tag{6.2.3}$$

For example, consider a 1 m thick bedding plane with an interface friction angle of 45°. The value of *c* for the panel in which the backfill is 10 m from the face is 50 cm (Figure 6.2.1). The effective zone of influence of the backfill is:

$$z_b = 1 \text{ m} - 0{,}5 \text{ m} = 0{,}5 \text{ m}$$

Thus, the zone of influence of the backfill would extend approximately 50 cm ahead of the backfill face.

Western Area Gold Mine (WAGM) installs cemented backfill in the stopes. This is a stiff backfill and is usually installed such that the hangingwall and the backfill are in contact throughout the panel. Although this is the case for most of the panel, at the up-dip and down-dip side of the panel the backfill and hangingwall are not in contact. This is shown in Figure 6.2.3.

The numerical analyses (Section 6.3) indicate that the zone of backfill influence does extend ahead of the position of the backfill face. It is shown that the backfill exerts pressure on the rock immediately above it and slightly ahead of the point of backfill-hangingwall contact. If the backfill is extremely stiff or taking very large stresses, i.e. large deformation of the backfill has occurred, the zone of influence of backfill extends further ahead of the contact.

Evaluation of the data obtained from WAGM (see Figure 6.2.4) indicated that the point of backfill-hangingwall contact on the up-dip side of the panel was up to approximately 2,3 m behind the actual face of the backfill. If the zone of backfill influence extends only 1 m ahead of the point of contact, there is at least another metre that is not supported.

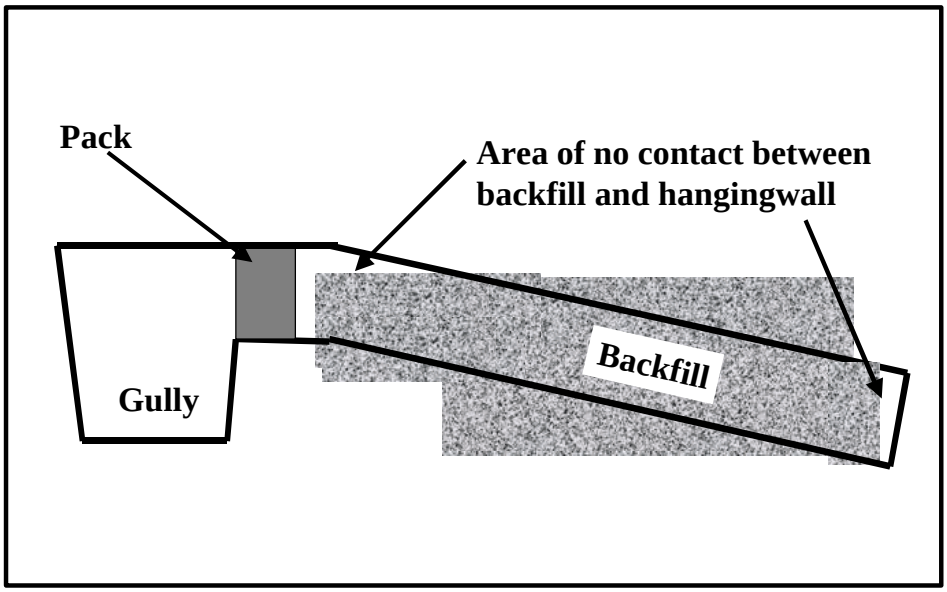

Figure 6.2.3 Section view of stope showing the lack of contact at up-dip and down-dip sides of panel between the backfill and the hangingwall.

The measurements taken on the down-dip side of the panel (Figure 6.2.4) show that the point backfill-hangingwall contact starts at a point approximately 2,2 m behind the face of the backfill. Thus, although at first glance the up-dip side of the panel appears to be more problematic, the down-dip side also results in a substantial distance of hangingwall that is under very little or no influence of the backfill. This could, however, be due to poor installation, using incorrect density, i.e. too much water, which results in high shrinkage of the backfill, or the reef dipping at a low angle to the horizontal. If the dip of the reef is near horizontal, the correct installation of the backfill is problematic since the backfill flow is dependent on gravity.

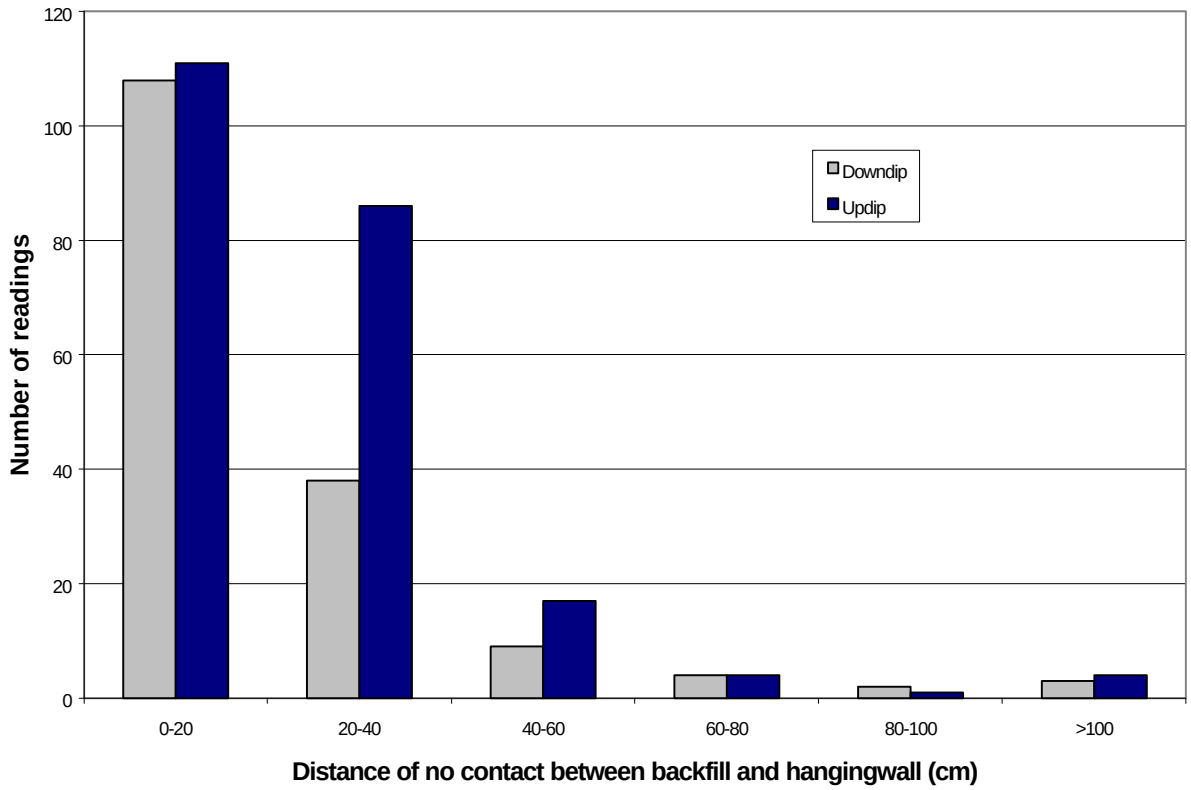

Figure 6.2.4 Measurements of distance between side of backfill and point of first contact with hangingwall on the up-dip and down-dip side of the panel.

6.3 Numerical modelling results

As was the case for the zone of influence of conventional supports, a model was created in UDEC to investigate the influence of the stope face and the backfill on the stability of the hangingwall.

The backfill used in the numerical exercise has a- and b-values of 3 MPa and 20%, respectively (Squelch, 1994). A typical backfill graph highlighting the a- and b-values is shown in Figure 6.3.1.

The backfill models include horizontal bedding planes, extension fractures (the orientation of these are denoted by angle a) and shear fractures (the orientation of these are denoted by angle b). No fractures were present ahead of the stope face. The properties are the same as those assumed in Section 3.1. A vertical stress of 81 MPa is applied to the top of the model.

In establishing the zone of influence of the stope face and the backfill, the stabilising effects that these supports have on the hangingwall within the different rock mass environments are considered.

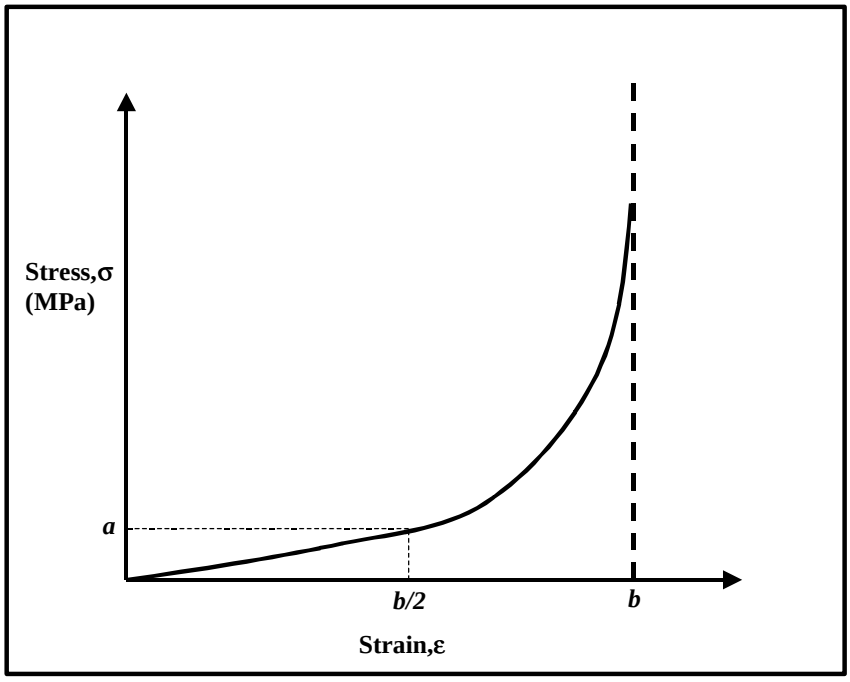

Figure 6.3.1 Typical backfill graph showing a- and b-values.

The horizontal clamping stresses have a major influence on the stability of the hangingwall beam (Chapter 2 and 3). For this specific study, the horizontal clamping stress that results from the dilation ahead of the stope face, and possibly the backfill, is considered as the most important parameter. Thus, the magnitude and orientation of the stresses in the hangingwall beam is used to describe the influence of the backfill and the stope face for the different rock masses.

Figure 6.3.2 shows the stress vectors for the 30°/90° combination. From Figure 6.3.2, it is clear that the orientations of the extension fractures have a major influence on the stress path at the stope face. The two arrows that originate at the stope face show the fracture orientations. Due to the influence of the fracture orientation, very little horizontal stress (with respect to the magnitude of stress ahead of the stope face) acts on the unsupported immediate hangingwall beam (closer to the backfill than the stope face).

A much higher horizontal stress acts on the second layer in the hangingwall. In this layer, the absence of extension fractures could be the reason for the higher horizontal stress. The shallow dipping extension fractures at the face are also subjected to very high shear stresses. This can result in extensive fallout of rock at the stope face if this area is not properly supported.

The 90° shear fractures at the stope face are, however, clamped by the horizontal stresses (Figure 6.3.2). The steep 90° fractures do not influence the stress path in the same way that the shallow 30° fractures do. The highest horizontal clamping stresses are concentrated in the immediate hangingwall beam.

The hangingwall in Figure 6.3.3, where fracture orientation is $90^o/60^o$, is much more stable than the hangingwall in Figure 6.3.2. It can be seen from Figure 6.3.2 that the horizontal clamping stresses are mostly a result of the dilation that occurs ahead of the stope face. The backfill has little influence on the horizontal stress in the unsupported hangingwall beam.

In this section the influence of backfill to face distances and stope width on the stability of the hangingwall is analysed and quantified in terms of the horizontal stress measured in the immediate hangingwall.

The influence of backfill-to-face distance was determined by keeping all parameters constant and varying the distance of the backfill to the face from 5 m to 7 m. The results for the 60°/30° are shown in Figures 6.3.4 (A) and (B). Figure 6.3.5 shows the backfill-induced zone of influence ahead of the backfill edge.

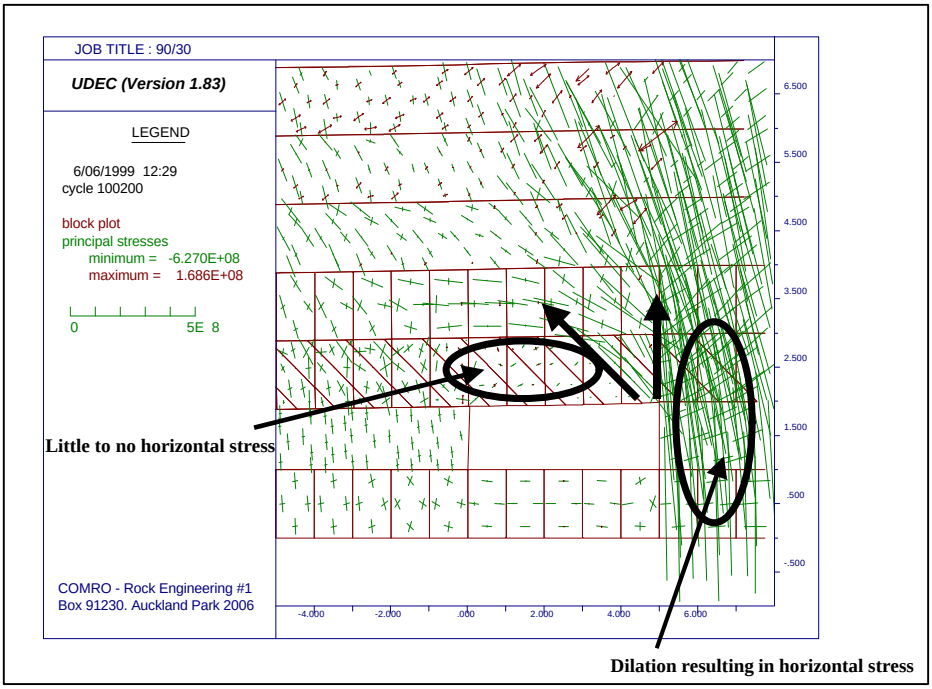

Figure 6.3.2 Influence of backfill, stope face and fracture orientation on stability of hangingwall for the 30°/90° combination. The backfill is installed 5 m from the face.

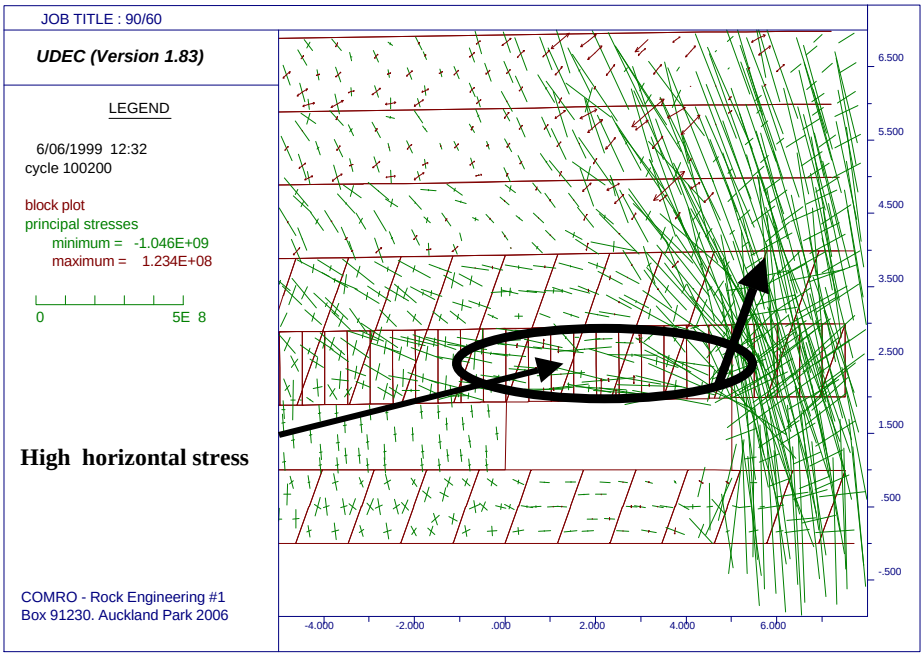

Figure 6.3.3 Influence of backfill, stope face and fracture orientation on stability of hangingwall for the 90°/60° combination. The backfill is installed 5 m from the face.

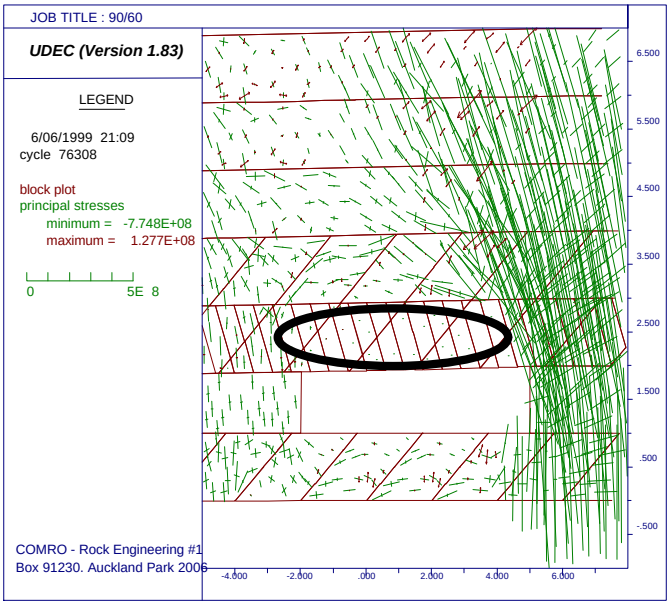

Figure 6.3.4 (A)

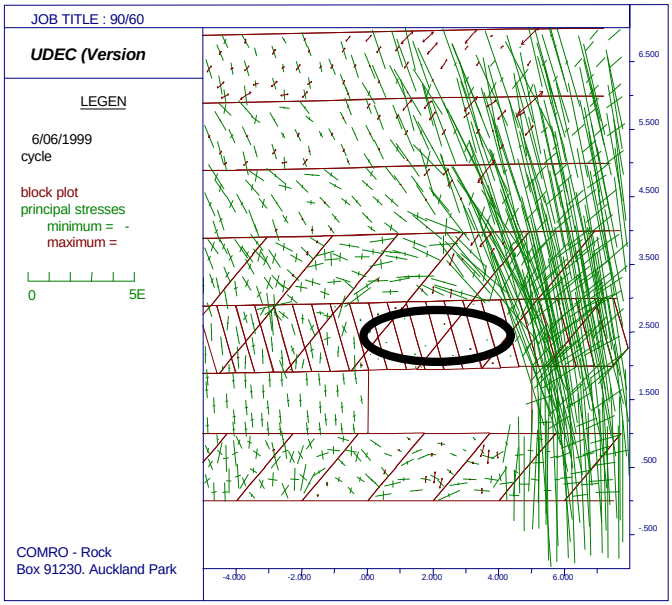

Figure 6.3.4 (B)

Figure 6.3.4 Influence of backfill, stope face and fracture orientation on stability of hangingwall for the 60°/30° combination. The backfill is installed 7 m from the face in (A) and 5 m from the face in (B).

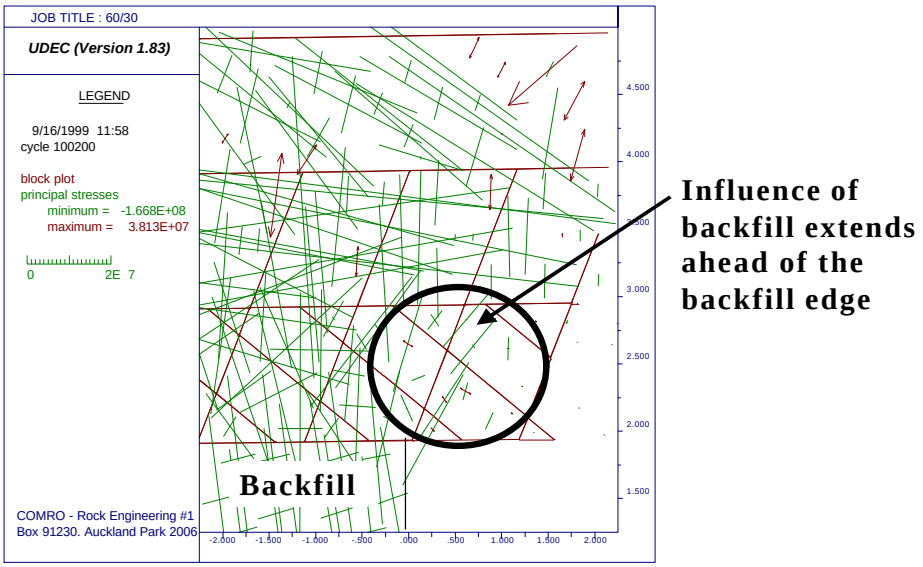

Figure 6.3.5 Influence of backfill extends ahead of the backfill side for the 60°/30° combination. The backfill is installed 5 m from the face. The area at the backfill side was enlarged to show the stresses ahead of the backfill side.

From Figure 6.3.4, it is apparent that when the backfill is placed 7 m from the face, a larger unsupported area in the immediate stope hangingwall is not influenced by the horizontal clamping stresses. The stresses in the second layer above the stope appear to be higher when the backfill is placed 5 m from the stope face. This is, however, not quantified.

To analyse the influence of backfill at 3 m, 5 m and 7 m from the stope face, the modelled horizontal stresses were extracted for points 1 m into the hangingwall at 1 m, 1,5 m, 2 m and 2,5 m from the position of the stope face.

From Figure 6.3.6 it can be seen that the clamping stress in the unsupported hangingwall increases with a decrease in the backfill-to-face distance for the fracture combination of 90°/30°. This is, however, not the case for the 90°/60° fracture combination, in which the horizontal clamping stress is not influenced by the backfill-to-face distance (Figure 6.3.7). This is because the stress path is governed by the orientation of the extension fracture. The 30° fracture is very shallow and comparatively little stress is transferred across this fracture. The steeper 60° fracture allows the stress to be transferred across it, and thus increases the horizontal clamping stress in the immediate hangingwall. The backfill-to-face distance also has an influence on the horizontal clamping stresses in the immediate hangingwall for the 30°/30° fracture combination (Figure 6.3.8). This is particularly evident when the backfill-to-face distance is 3 m. Thus, the fracture orientation together with the backfill-to-face distance controls the stability of the unsupported hangingwall.

This work should be viewed qualitatively, rather than quantitatively. For Figures 6.3.6 to 6.3.13, the values of the horizontal stress in the hangingwall are normalised with respect to the vertical stress ahead of the face.

The graphs for other fracture combinations are shown in Figures 6.3.9 to 6.3.14. From these graphs it is seen that the general trend is that the closer the backfill is installed to the stope face, the higher the horizontal clamping stress in the hangingwall. Thus, if the backfill is close to the stope face, the face area is likely to be more stable.

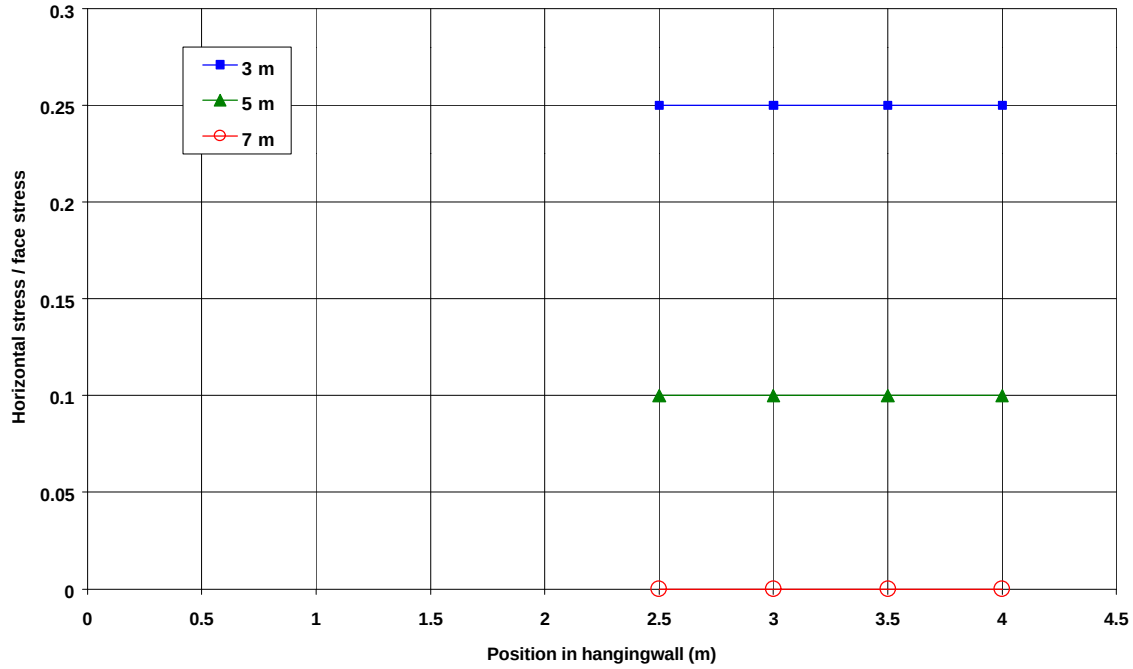

Figure 6.3.6 Influence of backfill to face distance for fracture combination 90°/30°.

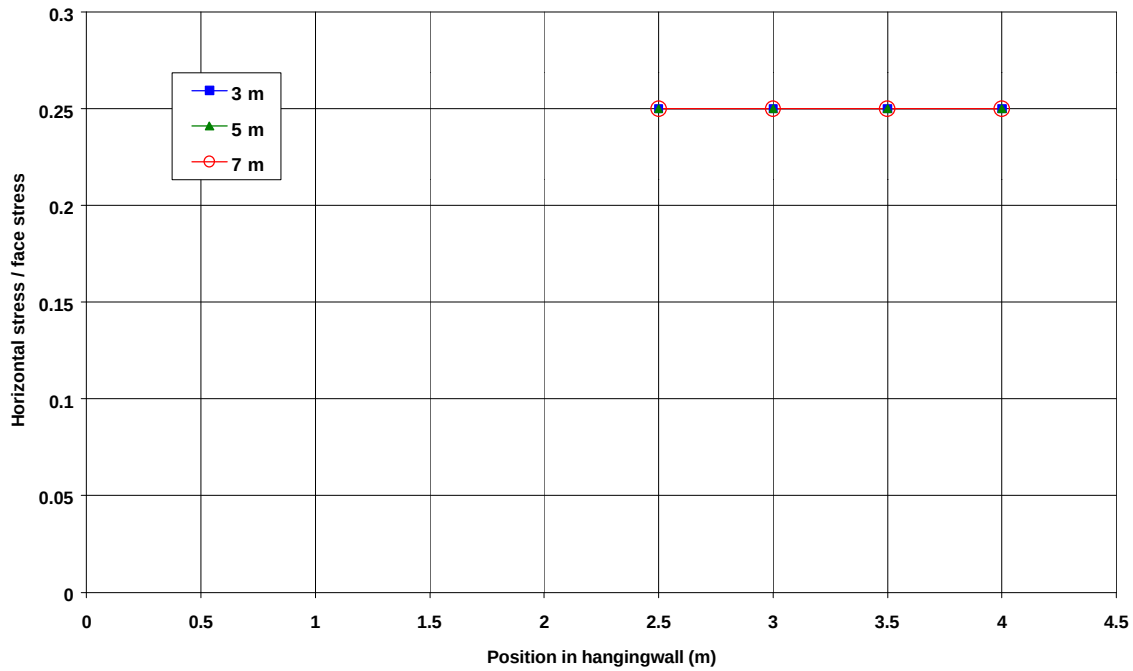

Figure 6.3.7 Influence of backfill to face distance for fracture combination 90°/60°.

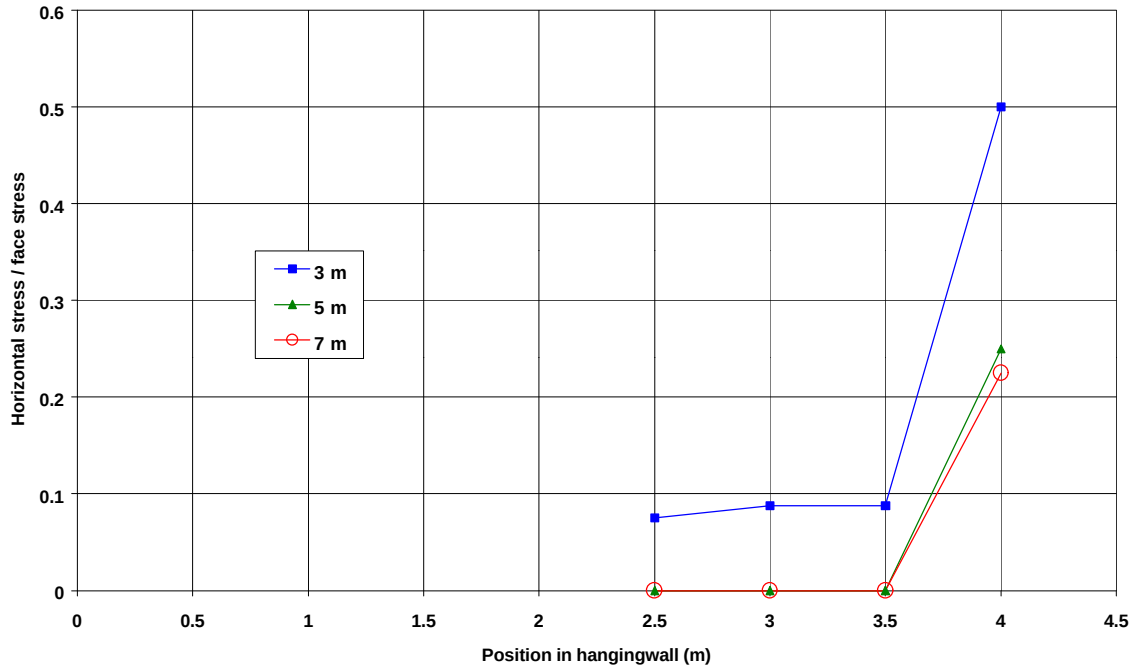

Figure 6.3.8 Influence of backfill to face distance for fracture combination 30°/30°.

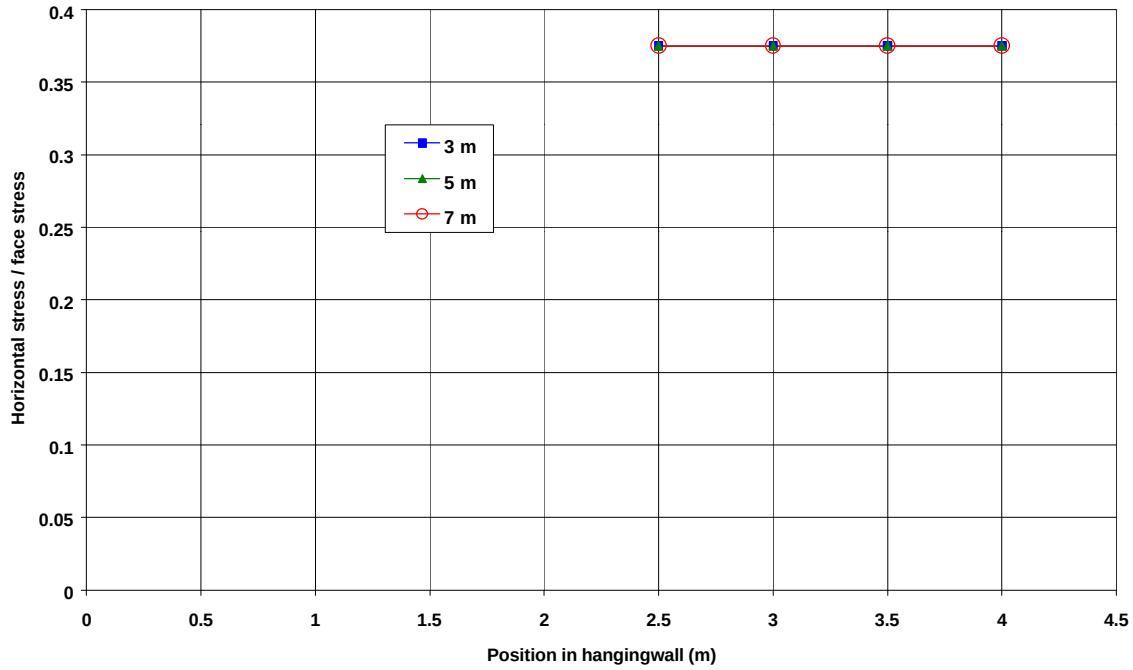

Figure 6.3.9 Influence of backfill to face distance for fracture combination 75°/90°.

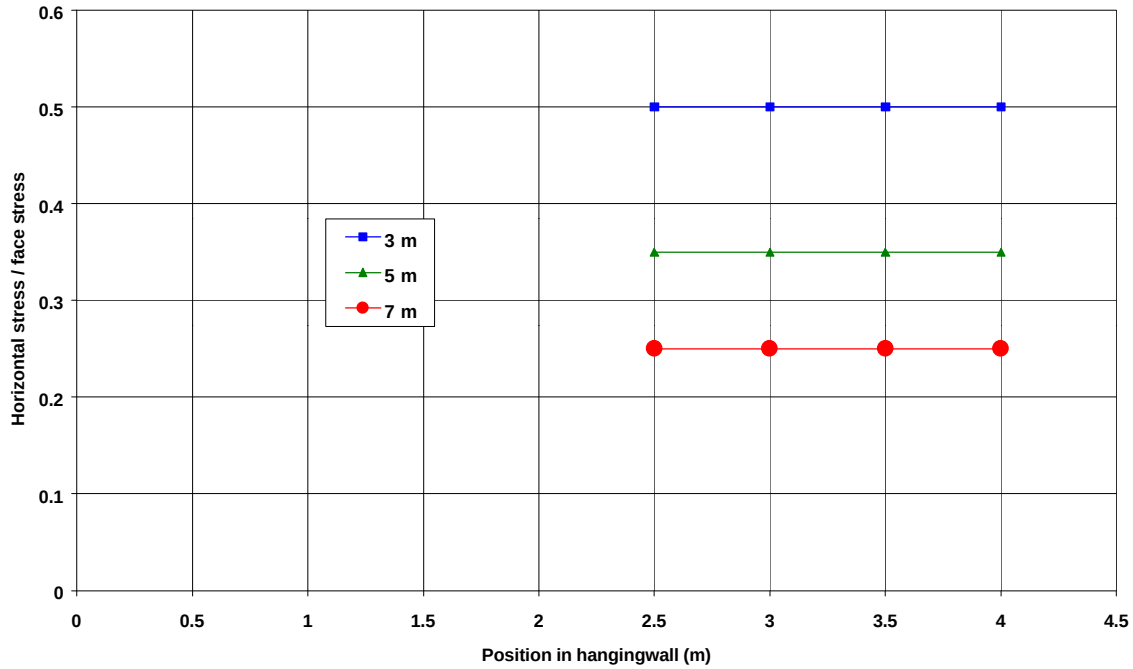

Figure 6.3.10 ***Influence of backfill to face distance for fracture combination 60°/90°.***

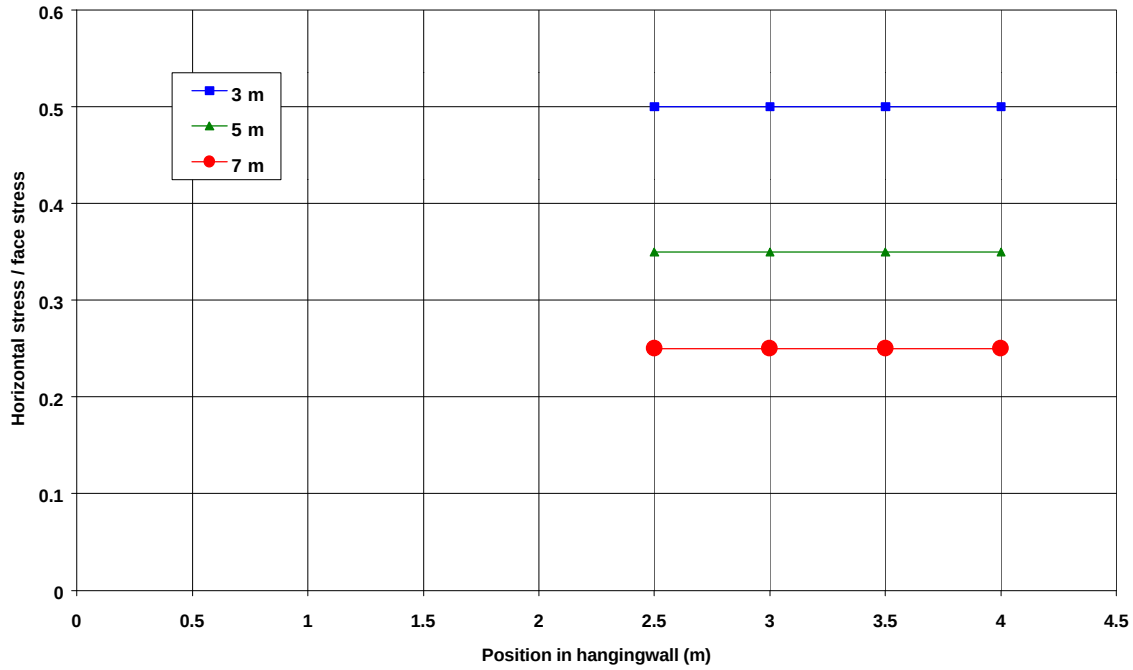

Figure 6.3.11 ***Influence of backfill to face distance for fracture combination 60°/60°.***

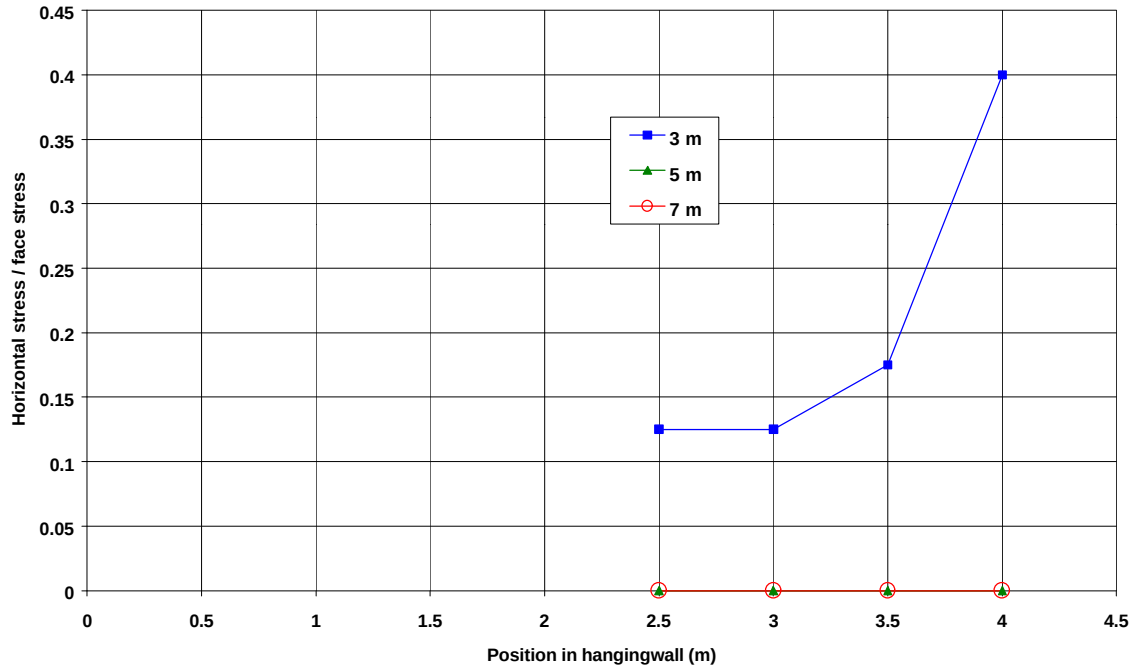

Figure 6.3.12 ***Influence of backfill to face distance for fracture combination 60°/30°.***

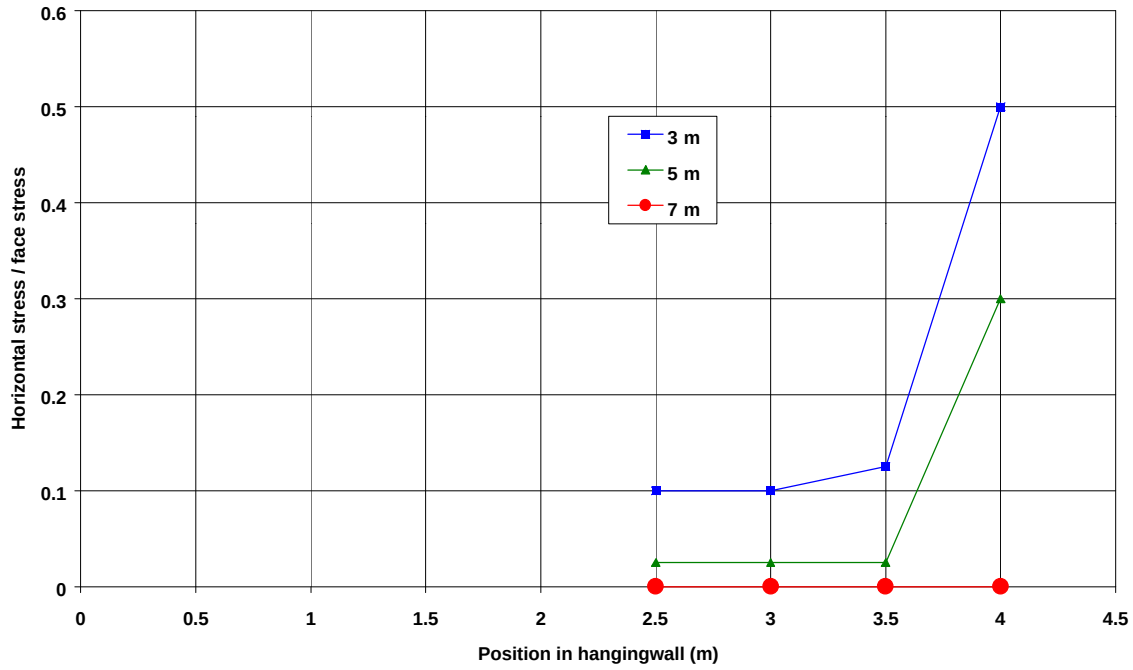

Figure 6.3.13 ***Influence of backfill to face distance for fracture combination 30°/90°.***

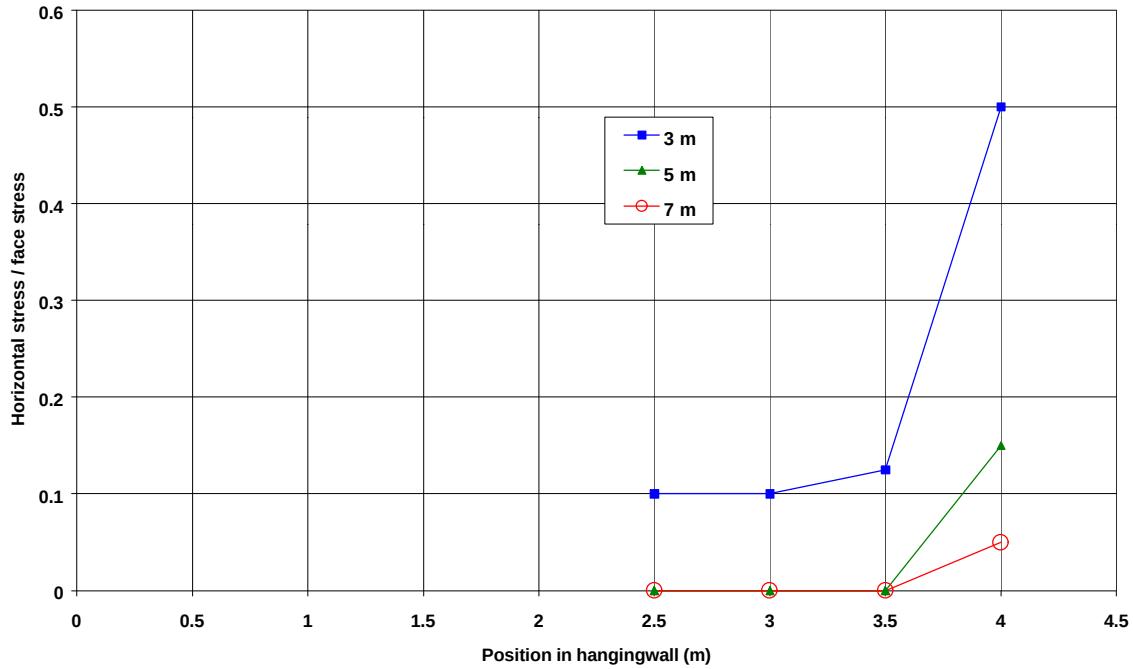

Figure 6.3.14 ***Influence of backfill to face distance for fracture combination 30°/60°.***

6.4 Conclusions

By comparing the underground results with numerical modelling results, it is apparent that the numerical modelling does not account for the initial gap between the backfill and the hangingwall. The two dimensional code, UDEC, also cannot address the problem at the up-dip and down-dip sides of the stope. The underground results give a realistic view of the problems of backfill placement and the lack of initial stiffness of backfill. The numerical modelling gives a more theoretical view of the zone of influence of backfill. It shows that the influence of backfill extends slightly ahead of the point of contact between the backfill and the hangingwall. Combining the two approaches, the zone influence of the backfill can be estimated (see the example in section 6.2).

It is further evident that the zone of influence of backfill is dependent on the stiffness of the backfill. Placement of backfill as close as possible to the stope face results in higher compressive hangingwall stresses and, consequently, increased rock mass stability.

7 Calibration and verification of theoretical models describing the zone of influence

7.1 Introduction

For an analytical model to be useful in the industry, it needs to be verified by comparing the predicted results to actual cases, so that the model can be used with confidence in the design of support systems. This chapter investigates means of calibrating the theoretical models introduced earlier.

The various methods, which can be used to estimate the *in situ* hangingwall strength in various geotechnical areas, are discussed in this chapter.

Preliminary back-analyses of rockburst and rockfall accidents, using the CSIR accident database, were carried out in order to determine a statistical distribution of unstable hangingwall spans for various geotechnical areas.

Finally, this data was applied to establish a procedure to verify and calibrate theoretical models describing the zones of influence.

7.2 Quantification of in situ hangingwall strength in various geotechnical areas

A proposed method to quantify the *in situ* hangingwall strength is by means of pull-out tests and recording the load at failure of the rock. Pull tests were done in tunnels to quantify the strength of different rock types (Haile *et al*., 1998). This was assessed by evaluation of the pull out strength of the rock mass by attaching a point anchor at a specified depth. An example of the load and deformation characteristic of the unreinforced skin rock mass and a diagrammatic representation of the pull test set-up are shown in Figure 7.2.1.

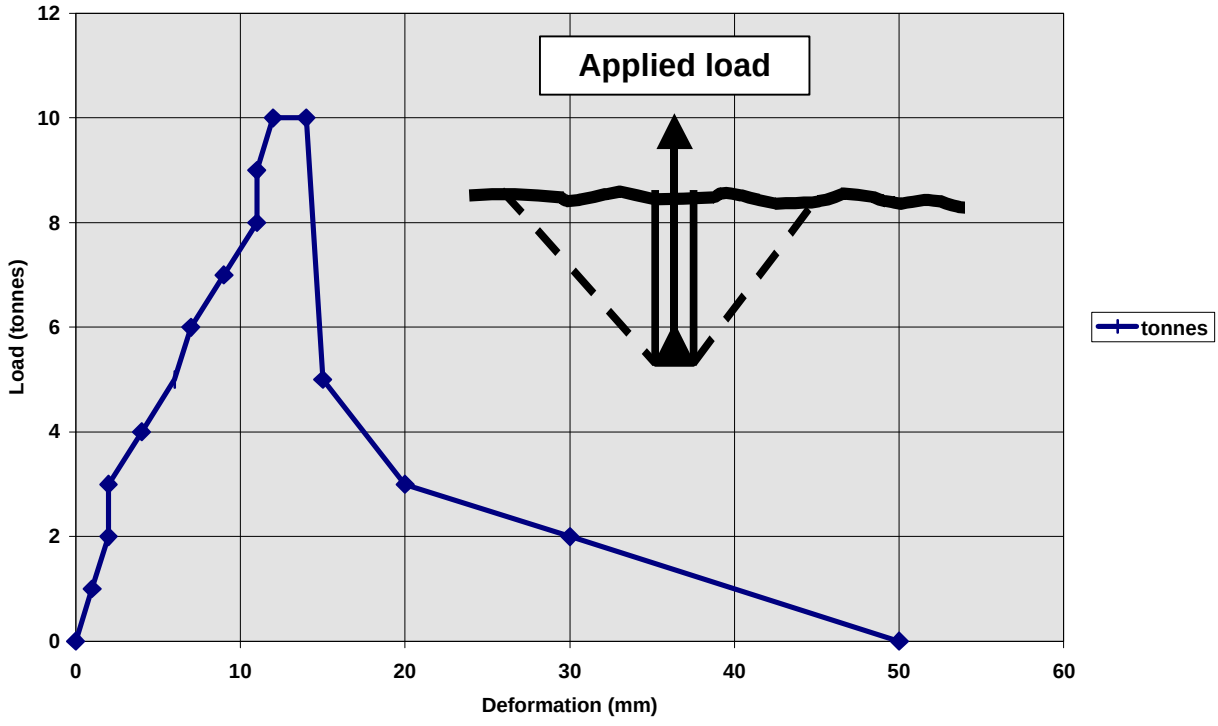

Figure 7.2.1 Load and deformation characteristic for 0,5 m anchor in shale rock type (after Haile et al., 1998).

It was found that the more discontinuous the rock mass structure, the lower the inherent strength of the sidewall rock mass. This is derived from the direct value of the load at sidewall failure for a specific rock mass type. A summary of the average pull out loads for the rock mass types as tested is shown in Figure 7.2.2.

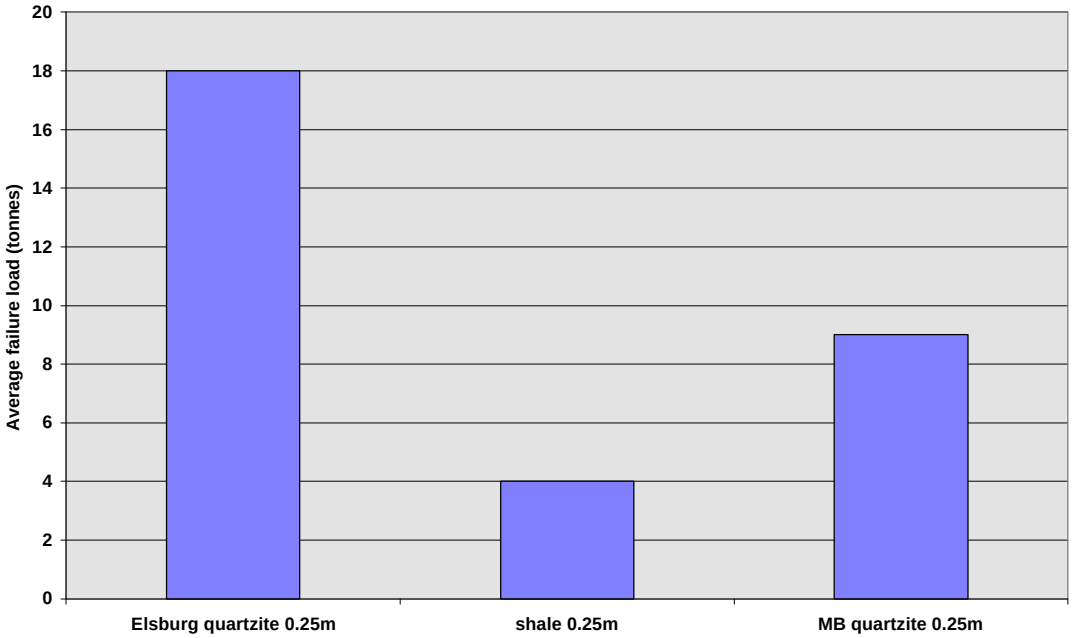

Figure 7.2.2 Summaries of peak pull out loads for rock mass type and anchor depth (after Haile et al., 1998).

In stopes the experiment is more dangerous since the pull test can result in a large fall of ground. Thus, the area where the tests are done must be thoroughly supported to ensure the safety of the person conducting the tests.

Although the rock mass structure can be highly complex, a reasonable number of tests in a specific geotechnical area can give a good indication of the in situ failure loads of the different rock types.

Another method is to test the rock mass resistance to failure under dynamic loading. The strength of the rock is determined by setting off explosives in the stope hangingwall and counting the number of blocks that fall out, or calculating the volume of rock that has fallen. Using geophones, the critical velocity, at which rock failure occurs, can be established for a particular area.

A third method is to use an instrumented pinch bar to dislodge rocks in the hangingwall. From this, the load at rock failure can be obtained for different rocks. This was done in SIMRAC project GAP 330 (Daehnke *et al.*, 1998). This is, however, not a true reflection of the three dimensional nature of the in situ environment, i.e. barring of a rock on the weak side will result in a lower load than if it is barred on the side where the cohesion is higher.

7.3 Determination of statistical distribution of unstable hangingwall spans for various geotechnical areas

Using CSIR's accident database, preliminary back-analyses of rockburst and rockfall accidents were carried out to determine a statistical distribution of unstable hangingwall spans for various geotechnical areas.

Analyses of the rockfall and rockburst statistics were done to investigate whether the zone of support influence could be derived from this data. This was done for different reefs mined by the South African mining industry. The data was normalised with respect to the number of panels per reef that contained a certain number of support units per square metre. This data was obtained from discussions with mine personnel and standards that are used on these mines.

7.3.1 VCR

The result for the VCR is shown in Figure 7.3.1.

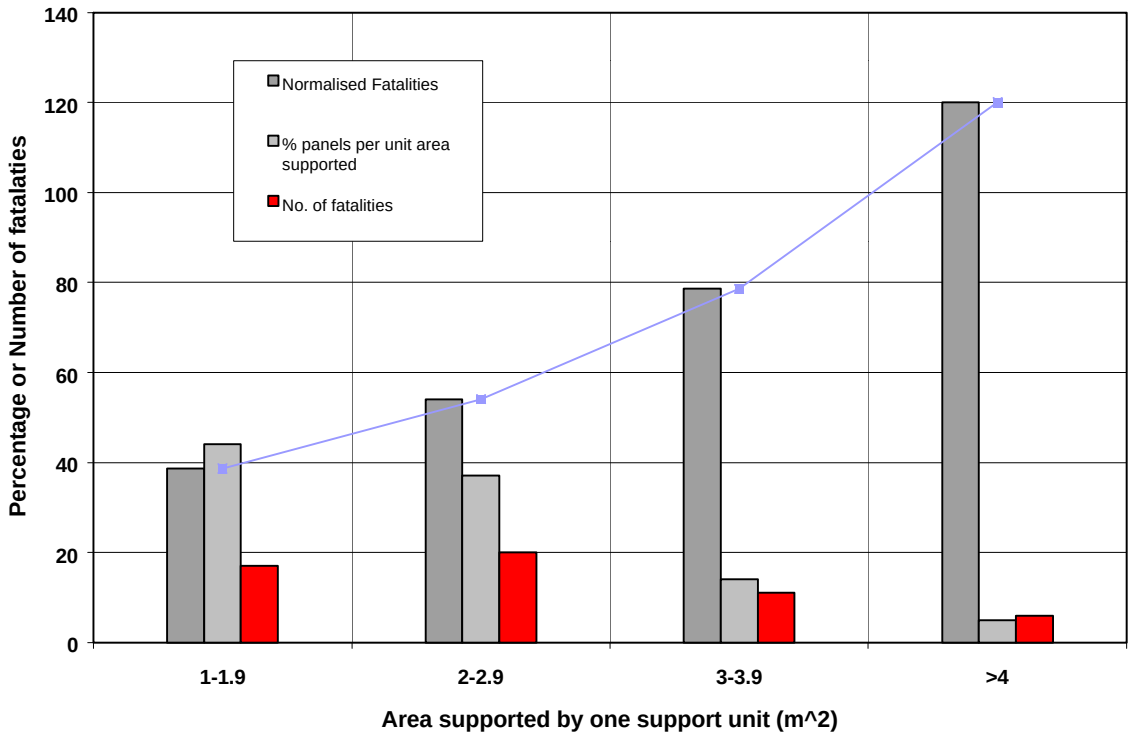

Figure 7.3.1 Influence of support spacing on the number of fatalities for the VCR.

There is an almost linear increase in the number of fatalities, as the number of support units per square metre decreases. Although the data does not give a clear answer to the question of the zone of support influence, it does show that the smaller the support spacing (i.e. the higher the number of support units per unit area), the lower the probability of a fatal accident occurring. The same relationship was obtained between the strike spacing of support and the number of fatalities (see Figure 7.3.2).

From the VCR data, the influence of fracture orientation on the number of fatalities was evaluated. This is shown in Figure 7.3.3.

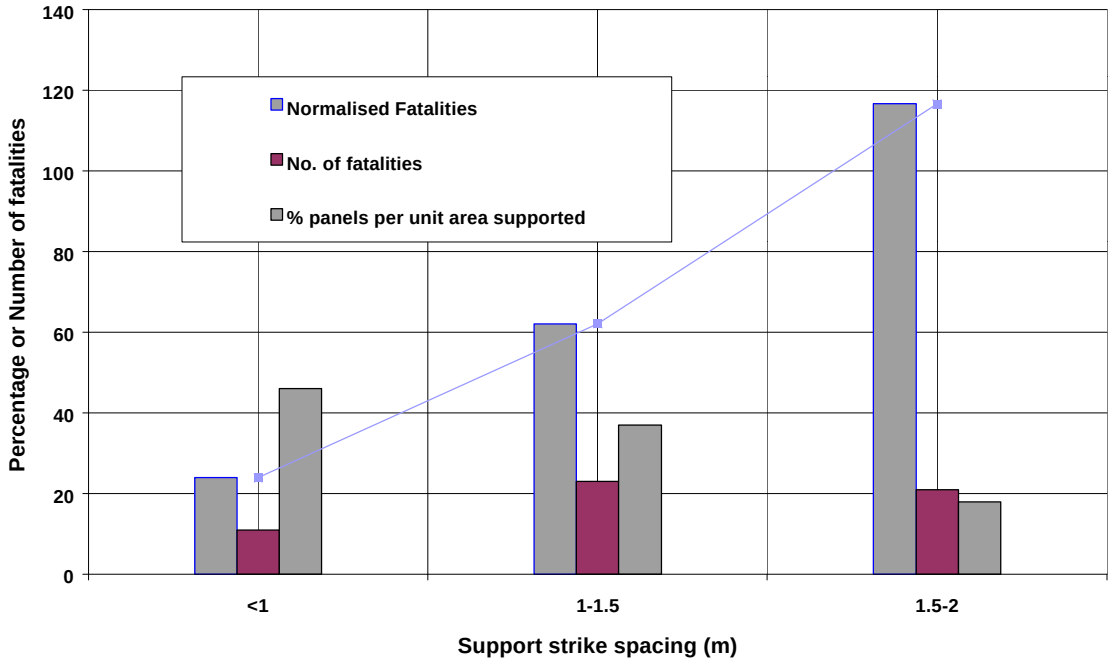

Figure 7.3.2 Influence of support strike spacing on the number of fatalities for the VCR.

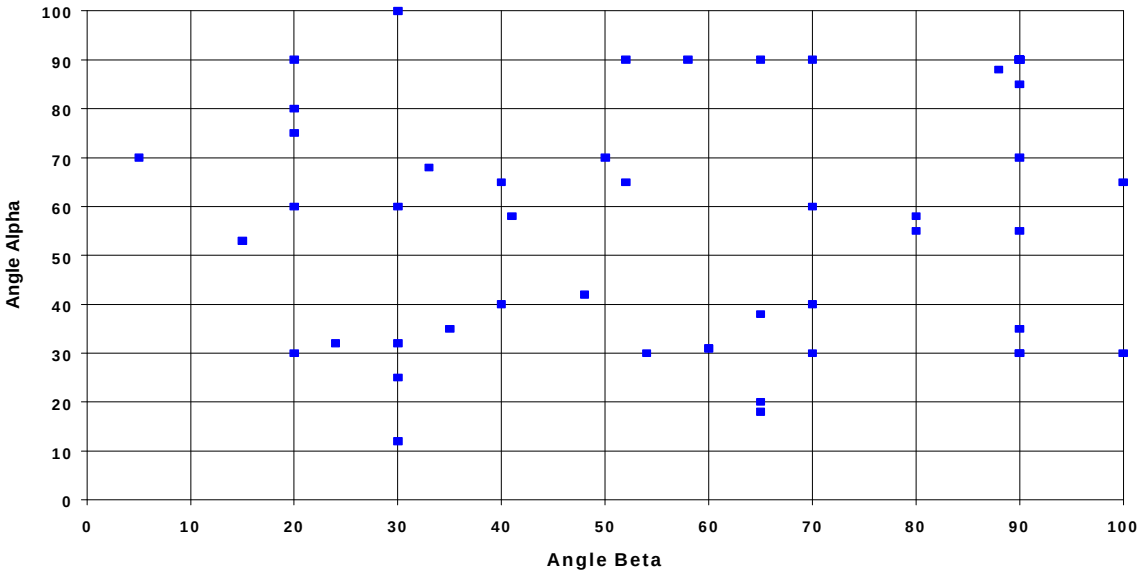

Figure 7.3.3 Influence of fracture orientation on the occurrence of fatalities for the VCR (each marker is associated with a fatal occurrence).

Although the data is not normalised with respect to the number of panels that are intersected by either steep or shallow dipping fracture orientations, this gives a good indication of the influence of fracture orientation. Observations show that most shear fractures have a steep dip angle with respect to the horizontal, and that extension fractures are usually steep at the stope face. The shallow fractures occur mostly around the stope corners and during the ledging phase. Thus, according to Figure 7.3.3, any combination of fracture orientations can be obtained in the hangingwall of this reef.

7.3.2 Carbon Leader

The influence of support unit per square metre on the number of fatalities is shown in Figure 7.3.4.

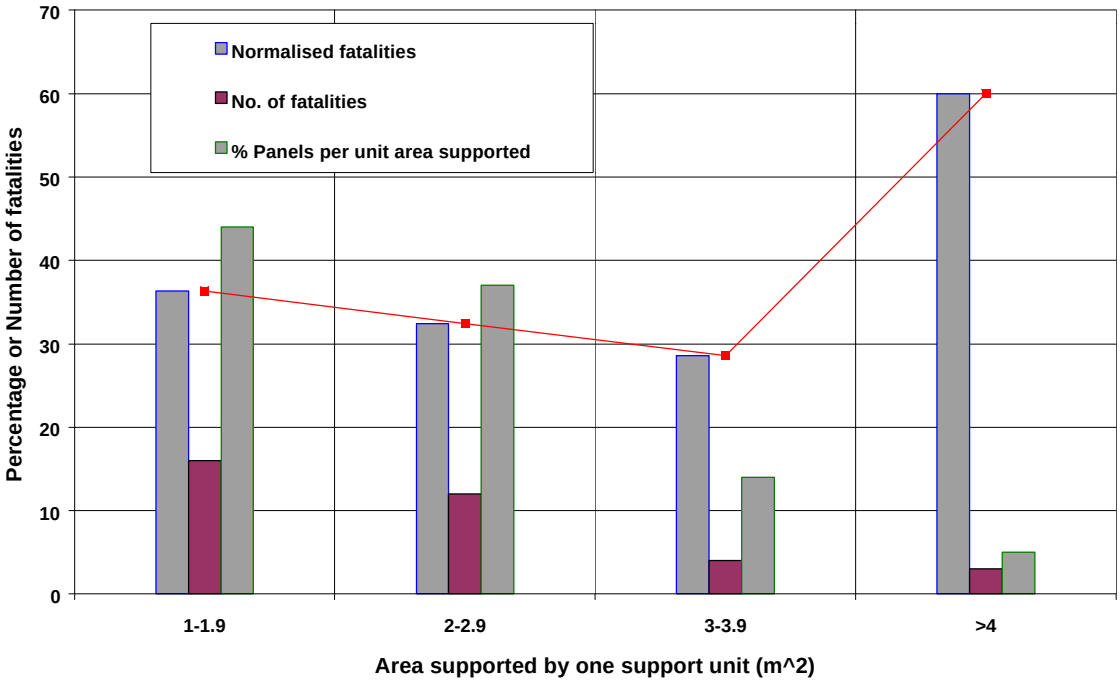

Figure 7.3.4 Influence of support spacing on the number of fatalities for the Carbon Leader.

From Figure 7.3.4, we see that there is a slight decrease in the number of fatalities, as the area per support unit increases from 1 m^2 to 4 m^2. The decrease is, however, very small and can be considered to be constant. At an area of 4 m^2 per support unit, there is a steep increase in the number of fatalities (normalised to support spacing). This sudden increase indicates that the particular support spacing is not recommended.

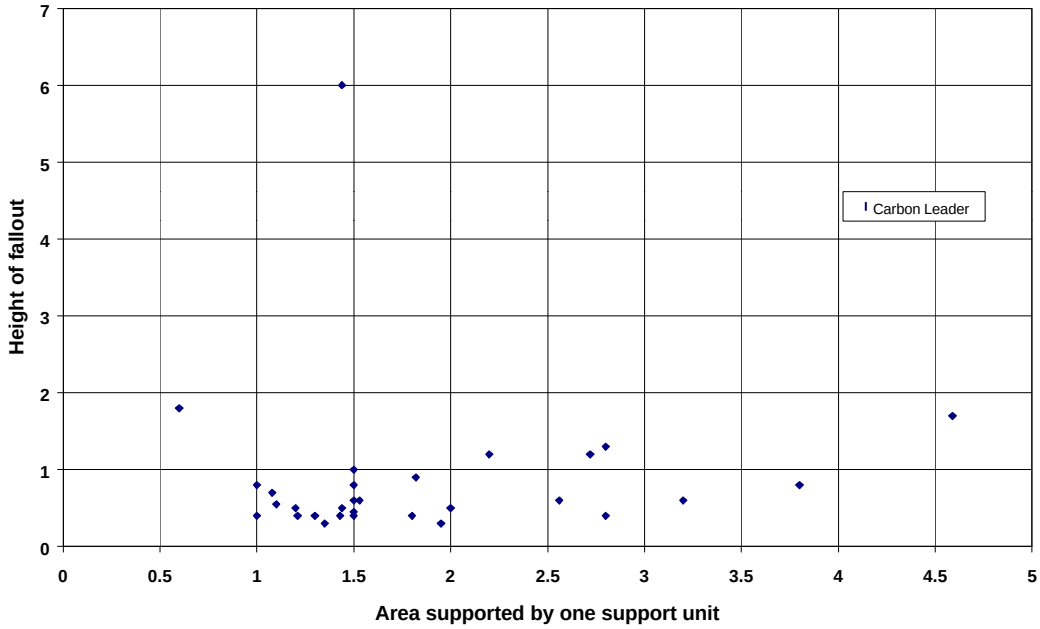

Figure 7.3.5 Influence of the area supported by one support unit (m^2) versus height of fallout (m).

From Figure 7.3.5, it can be seen that the average fallout height between the support units for the Carbon Leader is mostly less than 1 m. Few falls of ground were measured to be greater than 1 m in thickness.

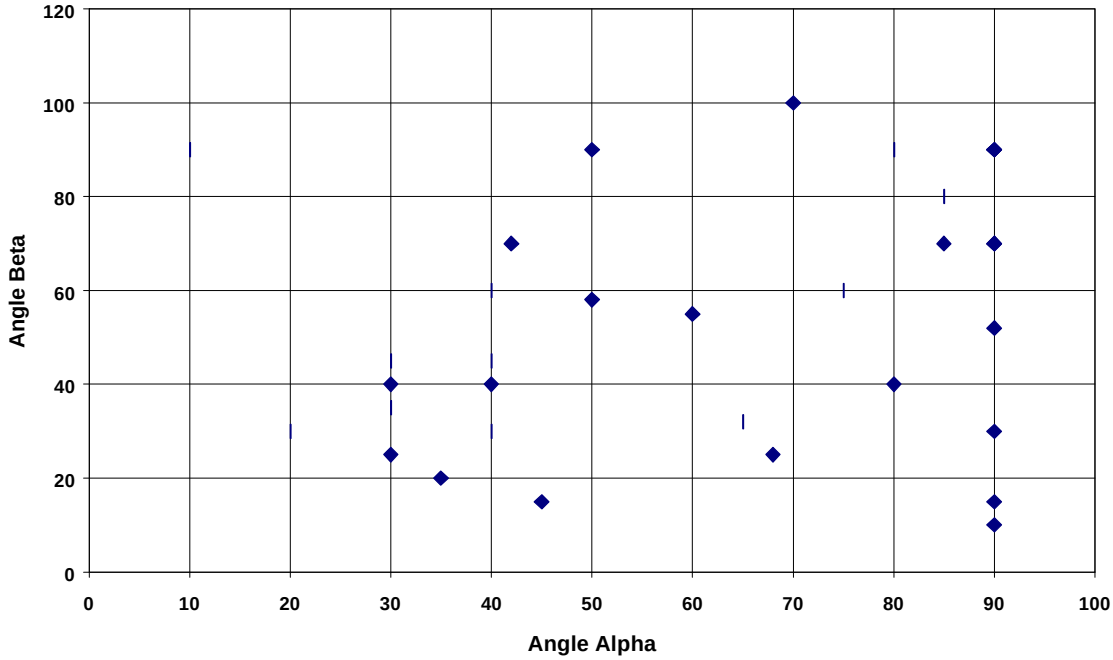

Figure 7.3.6 Influence of fracture orientation on the occurrence of fatalities.

Figure 7.3.6 shows that both shallow and steep dipping extension and shear fractures are present in the hangingwall of the Carbon Leader. Thus, support systems should be designed to account for any joint orientation.

7.3.3 Vaal Reef

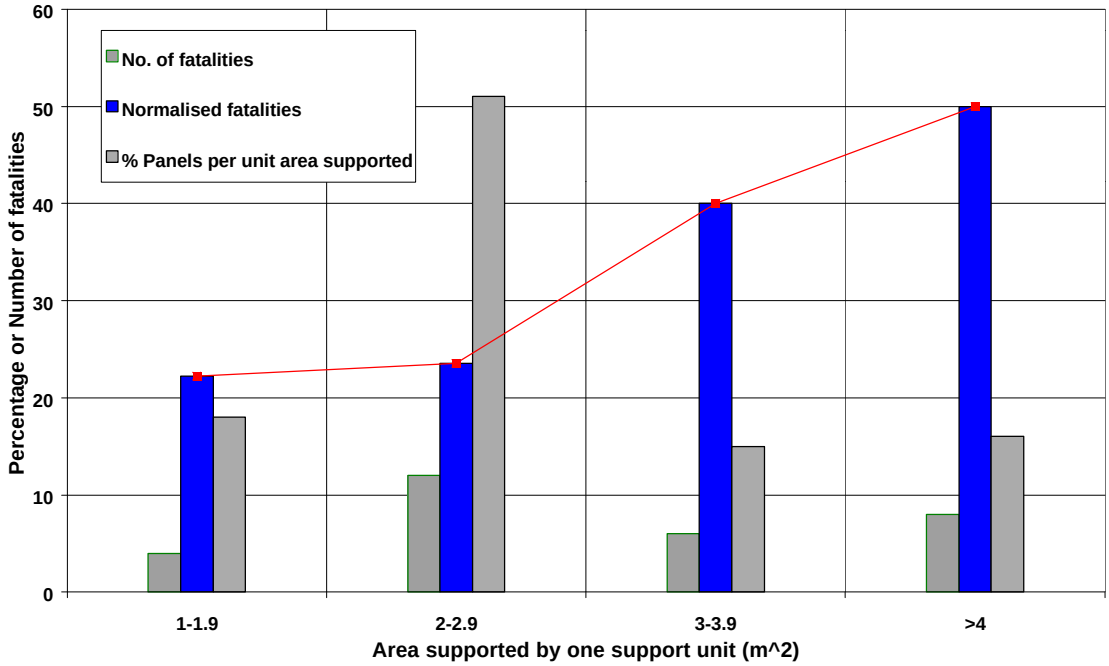

Figure 7.3.7 Influence of support spacing on the number of fatalities for the Vaal Reef.

There is a steep increase in the number of fatalities, as the area supported by one support unit increases from between 2 m^2 and 2,9 m^2 to between 3 m^2 and 3,9 m^2 (Figure 7.3.7). Thus, if the support spacing increases for the same conditions, the number of falls of ground will also increase.

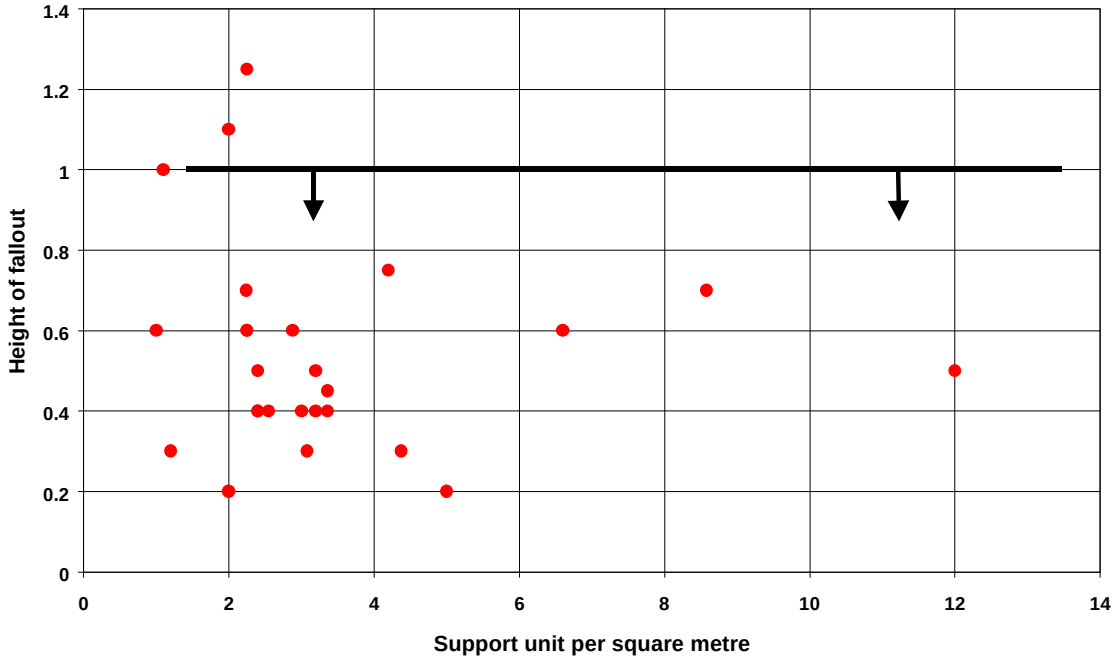

Figure 7.3.8 Influence of support spacing on height of fallout (VR).

This is only a statistical estimation of the critical support spacing per square metre. It must be remembered that these conclusions were reached from limited data, and thus the results should be interpreted with care.

Although the results were not normalised with respect to different geotechnical areas within the Vaal Reef, they were normalised with respect to the number of panels supported at particular support spacings. The fatalities that occurred on the VCR in the Klerksdorp district were not taken into account in the analysis.

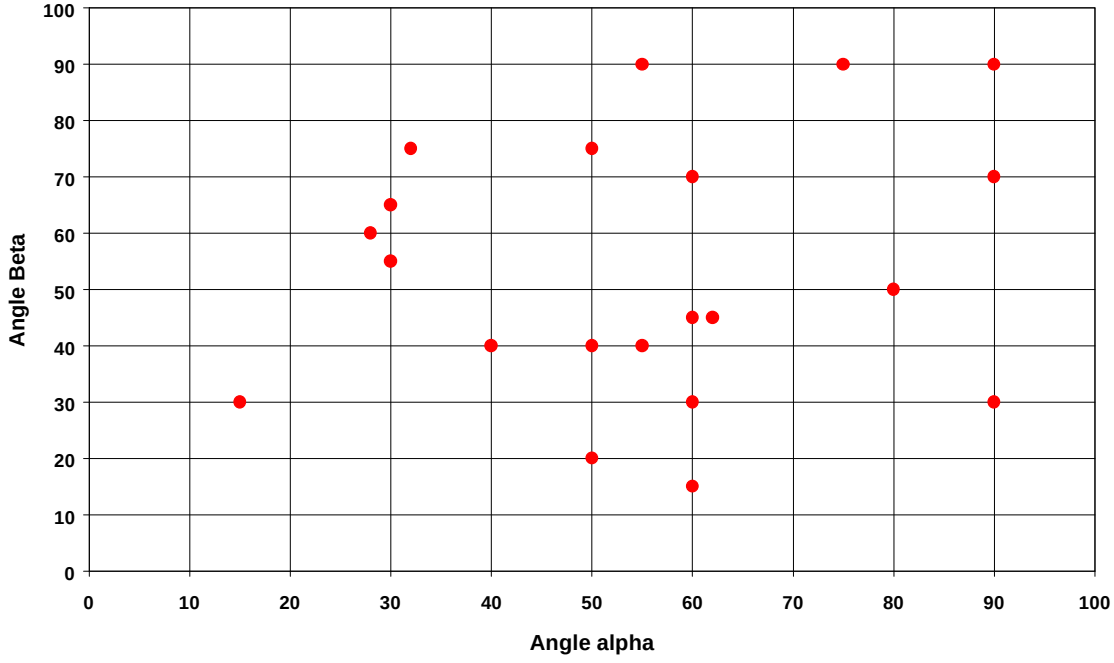

Figure 7.3.9 Influence of fracture orientation on the occurrence of fatalities (VR).

Most of the fall of ground accidents that caused fatalities were less than 1 m in thickness (Figure 7.3.8). Most of the combinations of extension and shear fracture orientations range anywhere between 30° and 90° (Figure 7.3.9). Thus, from the data, we can assume that the all fracture orientations can result in a fall of ground.

7.3.4 B - Reef

There is an almost linear increase in the number of fatalities, as the support spacing increases. From Figure 7.3.10, it can be seen that the smaller the support spacing, the lower the probability of a fatal accident occurring.

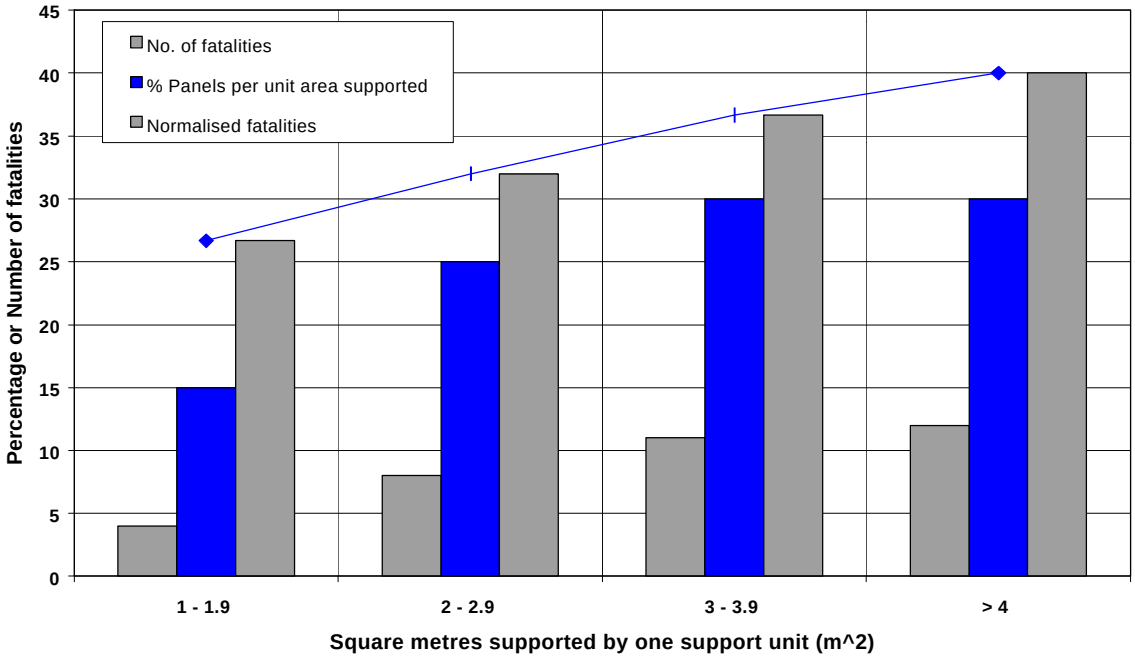

Figure 7.3.10 ***Influence of support spacing on the number of fatalities for the B - Reef.***

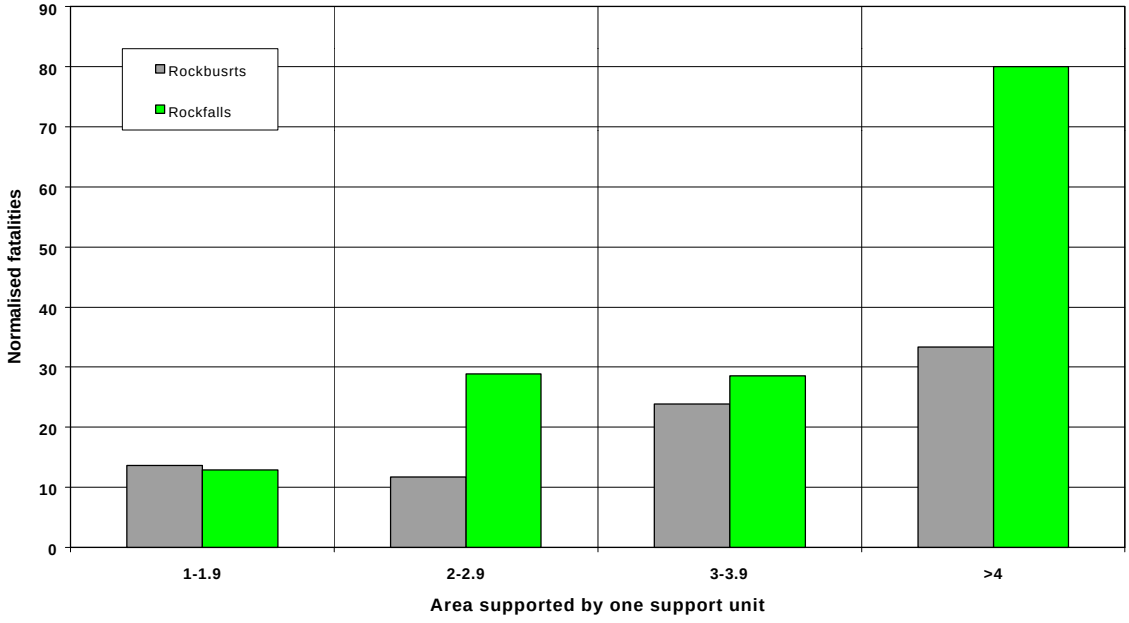

Figure 7.3.11 ***Influence of support spacing on the number of fatalities caused by rockfalls and rockbursts for the four reefs discussed previously.***

7.3.5 Combining different reefs

There is a sharp increase in the number of rockfall related fatalities when the area supported by one support unit increases to 4 m^2 per support. The gradient of the curve for the rockburst-related fatalities seems to be less steep. There is no sudden increase in the number of rockburst fatalities. This is a surprising result, and further work is required to explain this outcome. The fatality data was normalised with respect to the number of panels supported at specific support spacings. An important conclusion from Figure 7.3.11 is that, if more support units are installed per square metre, the probability of rock related fatalities occurring decreases.

7.4 Calibration and verification procedure

A flow diagram is designed to combine the theoretical models and the *in situ* data. The theoretical design charts and the fatality data per reef can both be applied to determine the optimum support design. The relation between support design and the effective hangingwall strength is more complex, but a combination of the two parameters is included in the flow diagram shown below.

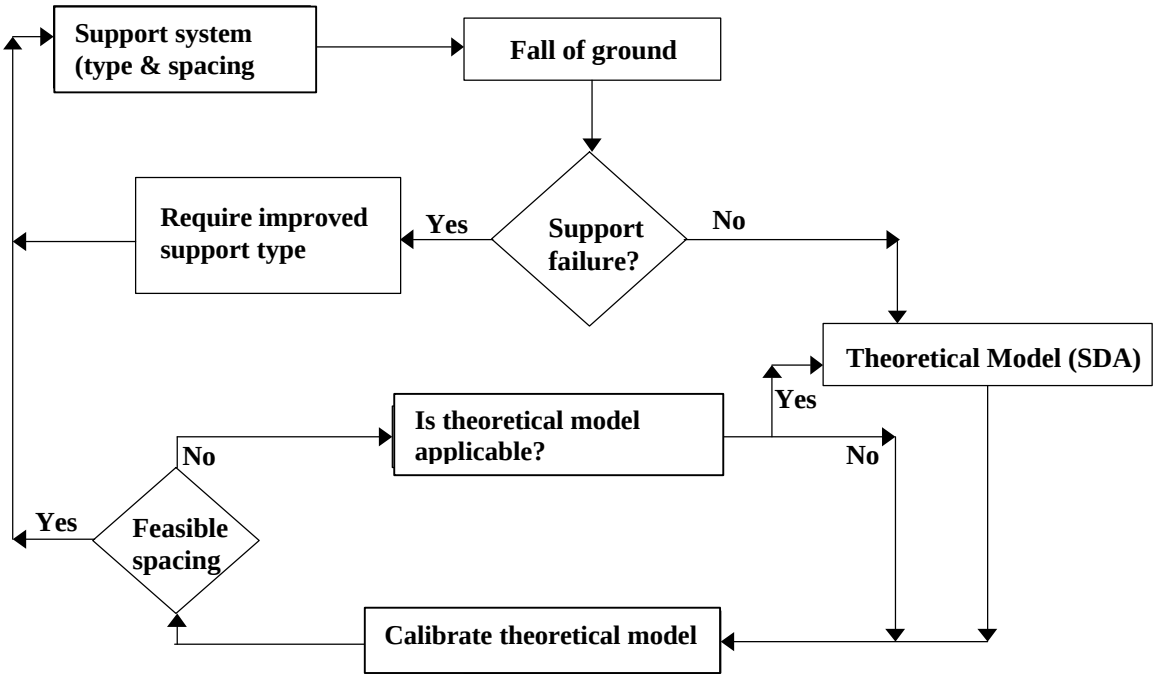

Figure 7.4.1 Flow chart for using theoretical models in design of support system.

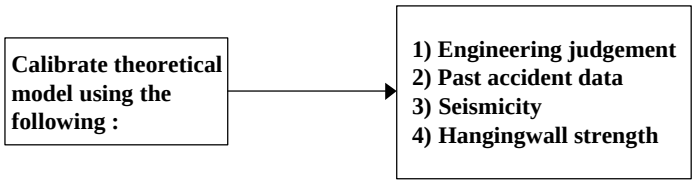

Figure 7.4.2 Method of calibration of the theoretical model.

The fatality data used to give a practical view of the support spacing per reef is very limited and probably not very accurate. In addition to the fatality data, any fall of ground that occurs should be measured and included in the database. Different geotechnical areas within a specific reef should, if possible, be addressed separately. More data is needed for this and thus continuous

monitoring of falls of ground should be done. The calibration of theoretical models is discussed below.

7.4.1 Engineering judgement

A support system must be engineered to counter rockfalls and reduce the damage caused by rockbursts (in seismically active areas). It must, however, also be economically viable for the mine. The engineer must combine the requirements for safety and cost to design the optimum cost effective support system for the specific conditions. Cost effectiveness can be considered as the economic value of the benefits, e.g. reduction in dilation, reduction in accident costs, increase in face advance rate etc., minus the cost of the installed support.

7.4.2 Past accident data

All data must be stored in a database and analysed for calibration purposes. Support design should take into account the following points: *i)* analyses of *in situ* data (geotechnical data, accident data, fall of ground measurements, etc.) and, *ii)* theoretical analysis (determination of zone of support influence and support spacing). Combining the *in situ* data with the theoretical data will add a practical view to the design process and will determine whether the support system is realistic in terms of cost and safety aspects.

7.4.3 Seismicity

The influence of seismicity should be taken into account when designing a support system. Some areas are more seismically active than other areas. Using experience and engineering judgement, the engineer can give each area that exhibits different rock mass behaviour a rating as a function of the number of damaging events and actual damage experienced. If the rating is very high, the support system for the specific area should be altered to reduce the damage (i.e. decrease support spacing or change support types, etc.).

7.4.4 Hangingwall strength

The hangingwall strength can give an indication of the stability of the rock mass. If the tensile strength and height of potential instability of the hangingwall is known, the support types, capacity and spacing can be determined.

7.5 Conclusions

The fatality data has shown that for all reefs discussed above there is an increase in the fatality rate, as the support spacing increases. It is also indicated that the same trend is observed if the support strike spacing is plotted against the number of fatalities. The data that was used in the analyses is very limited and is not sufficient to produce any conclusive results for the optimum support spacing. This exercise should however be done for each mine to get an indication of what the optimum support spacing is for that mine.

The flow chart shown in Figure 7.4.1 gives a procedure for support design. This flow chart can be used for any single stope panel in which a fall of ground has taken place, or for designing a support system for a particular ground control district. Engineers should view this as a guide only when designing a support system.

8 Design methodology

8.1 Introduction

In this chapter, the zones of influence and the key-block approaches are combined to formulate a unified design methodology for stope support systems in intermediate- and deep-level mines.

8.2 Summary of zones of influence approach

A summary of the design procedure, using the zone of influence approach, is given below.

$$s_h^{crit} = \frac{3F}{4bz_y}\ c \quad \text{where} \quad c = \frac{\sin^2 a\ \ (1+m\cot a)}{m-\cot a} \tag{8.2.1}$$

Table 8.2.1 Zones of influence in intermediate- and deep-level mines.

Is $s_h > s_h^{crit}$? (Eq. 8.2.1)

YES NO

	Clamped	Unclamped	
z_x^+	$b\tan j$	$a > \frac{p}{2} - j$	$\frac{b}{\tan a}$
		$a \le \frac{p}{2} - j$	$b\tan j$
z_x^-	$b\tan j$	$b > \frac{p}{2} - j$	$\frac{b}{\tan b} + (1-P)(f-r)$
		$b \le \frac{p}{2} - j$	$b\tan j\ \frac{100}{100+\tan^2 a}$
z_y	$b\tan j$		$b\tan j$

Note that the maximum value of z_x^- cannot exceed $b\tan j$, even if b is greater than $p/2 - j$.

Equations for determination of stress profiles:
Note that in the following equations:

$$z = r + z \tag{8.2.2}$$

Clamped:

$$s(x,y) = \begin{cases} 0\,, & \left(\frac{x}{z}\right)^2 + \left(\frac{y}{z}\right)^2 > 1 \\ \frac{2F}{p\,z^2}\left[1 - \left(\frac{x}{z}\right)^2 - \left(\frac{y}{z}\right)^2\right], & \left(\frac{x}{z}\right)^2 + \left(\frac{y}{z}\right)^2 \le 1 \end{cases} \tag{8.2.3}$$

Unclamped:

$$s(x,y)=\begin{cases} 0, \quad \left(\frac{x}{z_x^-}\right)^2+\left(\frac{y}{z_y}\right)^2>1 \quad \& \quad x\le 0 \\ \Omega\left[1-\left(\frac{x}{z_x^-}\right)^2-\left(\frac{y}{z_y}\right)^2\right], \left(\frac{x}{z_x^-}\right)^2+\left(\frac{y}{z_y}\right)^2\le 1 \& \; x\le 0 \\ \Omega\left[1-\left(\frac{x}{z_x^+}\right)^2-\left(\frac{y}{z_y}\right)^2\right], \left(\frac{x}{z_x^+}\right)^2+\left(\frac{y}{z_y}\right)^2\le 1 \& \; x\ge 0 \\ 0, \quad \left(\frac{x}{z_x^+}\right)^2+\left(\frac{y}{z_y}\right)^2>1 \quad \& \quad x\ge 0 \end{cases} \tag{8.2.4}$$

where:

$$\Omega=\frac{4F}{p\; z_y (z_x^+ + z_x^-)}, \text{ and} \tag{8.2.5}$$

(The derivation of the above equations can be found in Chapter 4).

8.3 Summary of keyblock approach

A summary of the keyblock approach is given below.

Two failure mechanisms are considered, namely instabilities due to (i) beam buckling and (ii) shear failure due to slip at the abutments.

8.3.1 Introduction

The present objective is to propose more advanced support mechanisms, specifically, to gain a deeper insight into the influence of rock discontinuities such as joints, fractures and bedding planes on ‘safe’ or ‘stable’ spans. Instabilities generally initiate at discontinuities in the hangingwall. These planes of weakness are shown to be of prime importance when spacing support units. An attempt is made to evaluate the interaction of the support with a discontinuous rock mass. The aim is to develop a more appropriate support design methodology. This approach to design should, within its own limitations, maximise support spacing, whilst maintaining a stable hangingwall span between support units. The methodology addresses hangingwall stability problems due to both quasi-static (rockfalls) and dynamic (rockbursts) failures. Due to widely varying rock mass conditions and behaviour of the reefs extracted by the gold and platinum mines, the methodology takes into account local geological conditions. During the design stage, local rock and discontinuity types, as well as their spacing and orientation, need to be available.

The final outcome of this work is a proposed design tool for the gold and platinum mining industry to assist the rock mechanics engineer to improve support design. Emphasis is placed on the estimation of optimised support spacing and support performance requirements for static and dynamic conditions. These proposals are untried in practice. Thus they will have to be

assessed and calibrated under real conditions. It is hoped that the rock engineers in the industry will produce sufficient feedback to facilitate the next advance towards an even better support system design method.

8.3.2 Classification of rock mass discontinuities

Mining induced and geological discontinuities influence the behaviour and deformation of the rock mass surrounding stopes. Hence, in order to gain an insight into the support – rock mass interaction, a better understanding of typical rock mass discontinuities is required. Investigations into fractures in intermediate and deep level gold mine stopes have revealed that two main types of mining induced stress fractures are present in the hangingwall (Adams *et al*., 1981):

Shear Fractures: These fractures are associated with highly stressed rock, and thus are found in intermediate and deep level mines. It is estimated that the fractures initiate 6 to 8 m ahead of the advancing stope face and separate the rock into blocks of relatively intact material. They are oriented approximately parallel to the stope face and are regularly spaced at intervals of 1 to 3 m. Shear fractures usually occur in conjugate pairs in the hangingwall and footwall, and typically reveal distinct signs of shear movement. Their dip in the hangingwall is generally towards the back area at angles of 60 to 70 degrees (Jager, 1998; Esterhuizen, 1998).

Extension Fractures: These fractures initiate ahead of the stope face and are smaller than shear fractures. They form after shear fractures have propagated and generally terminate at parting planes. Extension fractures normally do not exhibit relative movement parallel to the fracture surface and are typically oriented parallel to the stope face. They are commonly spaced at intervals of 10 cm with lower and upper limits of 5 to 50 cm, respectively. The strike length is typically 3 to 5 m, where lower and upper limits of 0,4 and 8 m have been observed (Esterhuizen, 1998). Extension fractures normally dip between 60 and 90 degrees, where the direction of dip (i.e. towards or away from the stope face) can be influenced by the hanging- and footwall rock types (Roberts, 1995)

Most gold reef extraction takes place in bedded quartzites. Bedding planes, which are parallel with the reef, often represent weak interfaces between adjacent strata, and provide little cohesion and low frictional resistance (Jager, 1998). Bedding planes are generally spaced at 0,2 to 2,0 m intervals. The rock fall-out height is commonly governed by the position of bedding planes.

The three most prevalent discontinuity types, extension fractures, shear fractures and bedding planes, are illustrated in Figure 8.3.1. Their influence on the rock mass behaviour and stability is considered in this study. An attempt is also made to quantify their effect on support spacing and rock mass stability in static and dynamic conditions.

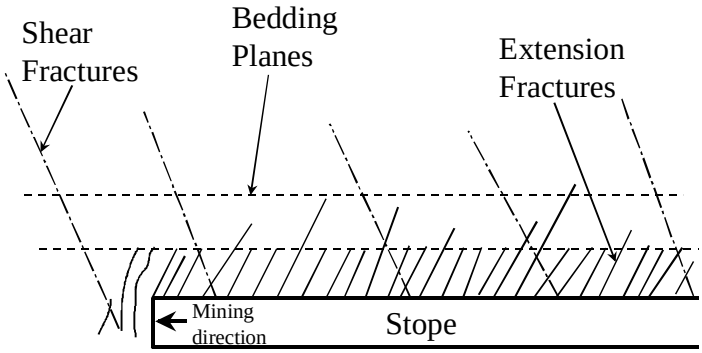

Figure 8.3.1 Simplified schematic illustrating the three most prevalent discontinuity types in intermediate and deep level mines.

8.3.3 Numerical simulations of support interaction with a discontinuous rock mass

The finite-discrete element program ELFEN (Rockfield, 1996) was used as a tool to investigate the interaction of support units with a discontinuous rock mass. Various ELFEN models were constructed, incorporating several discontinuity types. The aim of the numerical models was to gain a qualitative insight into the development of stress trajectories that arise from the load transmission between the support elements and the discontinuous hangingwall rock.

In the ELFEN models a beam, which was discretised by closely spaced extension fractures, simulated the fractured hangingwall. In intermediate and deep level mines, the extension fractures are typically oriented face parallel, where the fracture length in the dip direction is generally much longer than the fracture spacing in the strike direction. Hence, it is considered reasonable to model a section of the hangingwall along the strike direction in two dimensions, and assume plane strain conditions in the out-of-plane (dip) direction. The fracture surfaces were modelled with no cohesion and a friction angle of 40 degrees.

Along the top of the numerical models a uniformly distributed load was applied. In reality the hangingwall beam is probably not loaded uniformly. Local bed separations, as well as the influence of the unmined face and the extracted back area, can lead to irregular hangingwall loading. However, the aim of these simulations is to gain a qualitative view of the stress distribution within a discontinuous hangingwall beam. In these circumstances a simplification of the applied boundary conditions seems permissible.

The hangingwall is assumed to be confined at both ends, i.e. at both the face and back area. Furthermore, the presence of a compressive horizontal stress is postulated in the beam. The effects of hangingwall confinement and of the compressive hangingwall stresses are significant and will be further discussed in Section 8.3.4.

Figure 8.3.2 depicts the principal stress distribution induced by two prop like support elements, when loaded by a hangingwall slab discretised into blocks by closely spaced vertical fractures. It is evident that the stresses are transmitted from the support units, through the long axis of the blocks defined by the vertical discontinuities, into the more competent (in this case not fractured) rock above the bedding plane.

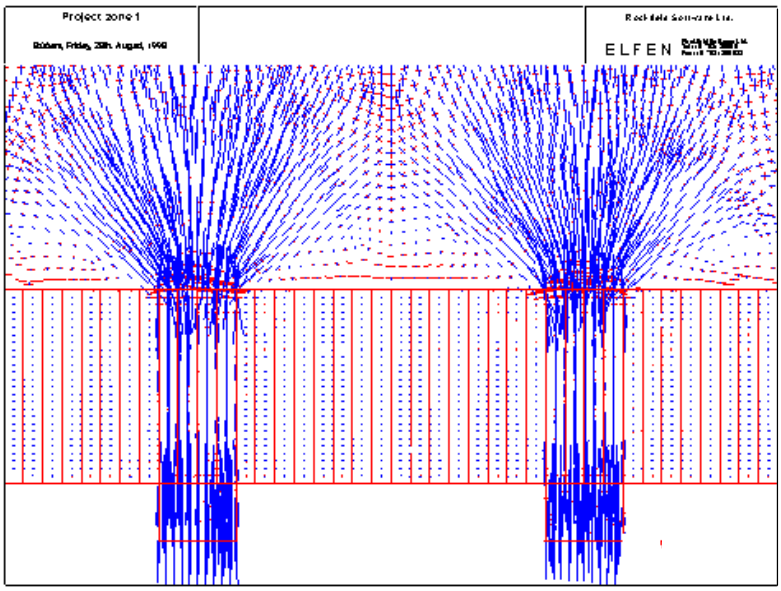

Figure 8.3.2 Stress distribution associated with a discontinuous hangingwall interacting with two support units.

In the case of a hangingwall beam discretised by dipping extension fractures and in the presence of a discontinuity modelling a shear fracture, the stress trajectories follow the paths shown in Figure 8.3.3. The stresses seem to be transmitted again mainly parallel to the discontinuities, through the fractured layer into the competent layer above the bedding plane.

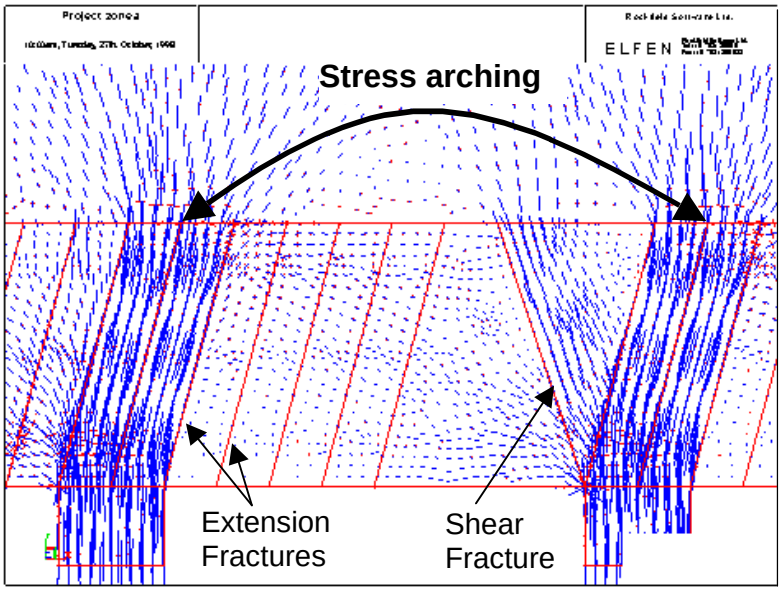

Figure 8.3.3 Stress transfer through a hangingwall beam discretised by discontinuities modelling extension and shear fractures.

It is important to note that in Figures 8.3.2 and 8.3.3 those blocks of the discretised beam that are not directly supported are kept in position by friction. Furthermore, friction will be sustained only in the presence of horizontal normal stress. Thus, it is important to understand how the horizontal normal stress is induced and maintained in the hangingwall. In intermediate and deep mines, fracturing ahead of the stope face induces rock dilation, leading to compressive hangingwall stresses parallel to the skin of the excavation (Jager and Roberts, 1986). The compressive stresses can be maintained only if the hangingwall beam is prevented from freely moving in the horizontal direction. The face obviously provides such a restraint. The situation at the end towards the mined-out area, however, requires further attention and is dealt with in Section 8.3.4.

Compressive hangingwall stresses usually contribute significantly to the rock mass stability. Figure 8.3.4 shows the stress distribution associated with a model loaded in the vertical and horizontal direction. The magnitude of the horizontal stress is 1 MPa, whilst the total load carried by each support unit is 200 kN. These magnitudes are typical of values measured underground (Squelch, 1994; Herrmann, 1987).

The stress distribution is complicated further by the addition of the horizontal stresses. It should be remembered, however, that the resultant stress field arises from the superposition of components due to the vertical and horizontal loads. Stress arching can be discerned in the competent layer (see Figure 8.3.4), leading to the conclusion that most of the forces transmitted by the support units follow a path parallel to the discontinuities, as observed in Figure 8.3.3.

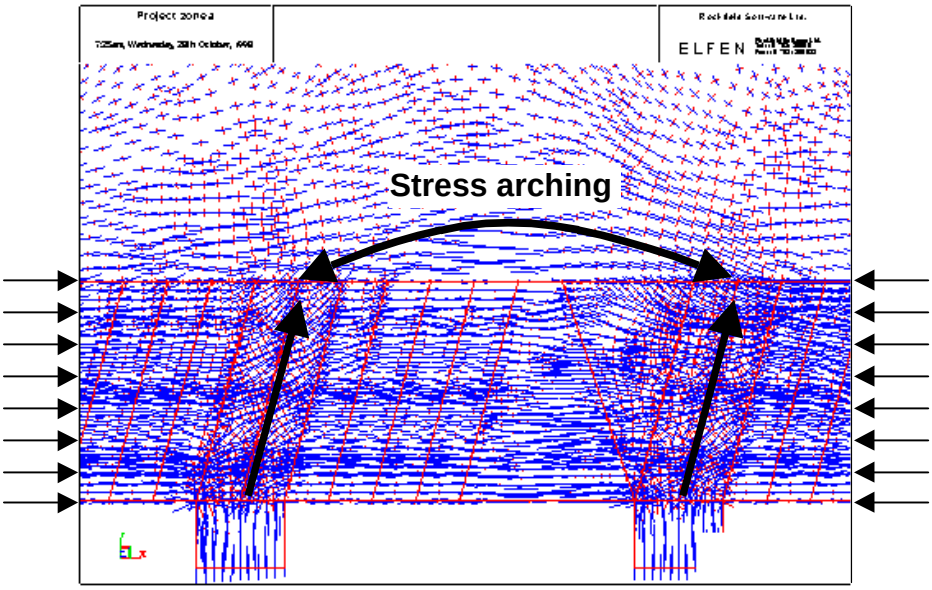

Figure 8.3.4 Vertical and horizontal loading of a discontinuous hangingwall beam.

To summarise, simplified numerical models representing a discontinuous hangingwall beam, discretised by extension fractures, a shear fracture and a bedding plane, have shown that the load carried by support units is generally transmitted in a direction parallel to the fracture orientations. Comparatively little stress is transmitted across the fractures, and the hangingwall rock between adjacent support units is essentially unstressed. When the hangingwall is clamped by compressive stresses acting parallel to the excavation surface, the resulting stress field can be approximated by the superposition of stresses due to horizontal and vertical loads. The majority of the stress induced by the support units continues to be transmitted parallel to the fracture surfaces.

Hence, in results given in the following sections, the compressive stresses induced by support units are assumed to be transmitted parallel to the fracture surfaces. Support units do not directly stress the hangingwall rock between adjacent support units. Hangingwall stability in this region is governed by compressive stresses due to dilation and the buckling potential of the hangingwall beam.

8.3.4 Hangingwall confinement

An assumption implicit in this work is that the hangingwall rock is confined. Squelch (1994) measured maximum compressive hangingwall stresses of 1 to 10 MPa at depths between 0,7 to 2,2 m into the hangingwall. These horizontal stresses clamp the fractured rock together and, depending on the orientation of the fractures, can significantly improve the structural integrity and stability of the hangingwall (Jager and Roberts, 1986).

Herrmann (1987) found that in stopes with back area caving, stress relaxation occurred in the lower layers of the hangingwall, and noted the importance of rock confinement to maintain compressive hangingwall stresses. Rockfalls and caving in the back area generally lead to reduced hangingwall confinement. However, compressive hangingwall stresses can still be maintained when frictional resistance generated at bedding planes restricts the lateral hangingwall movement. Such frictional resistance can be induced by appropriate support forces generated under the hangingwall beam, at or near to its end closest to the extracted area.

As an example of this mechanism, consider the stope shown in Figure 8.3.5. The elongates and packs shown here are assumed to be carrying a load of 200 kN and 400 kN, respectively. Thus, in order to estimate the horizontal compressive stress which can be maintained between the face and the two rows of elongates, the total load carried by the second elongate and the two

packs is determined as 200 kN + 400 kN + 400 kN = 1000 kN. The self-weight of the rock between the second elongate and the packs is 160 kN (assuming a centre to centre support spacing of 3 m and a bedding height of 1 m). Thus the effective clamping force pinning the hangingwall to the bedding plane is 1000 kN – 160 kN = 840 kN. If the bedding plane has an apparent friction angle of 40°, the maximum horizontal force which can be maintained is: (tan 40°) x 840 kN ≈ 700 kN, or, converting to stress, 0,7 MPa. Thus it is shown that, even with caving and rockfalls in the back area, reasonably high compressive hangingwall stresses can be maintained.

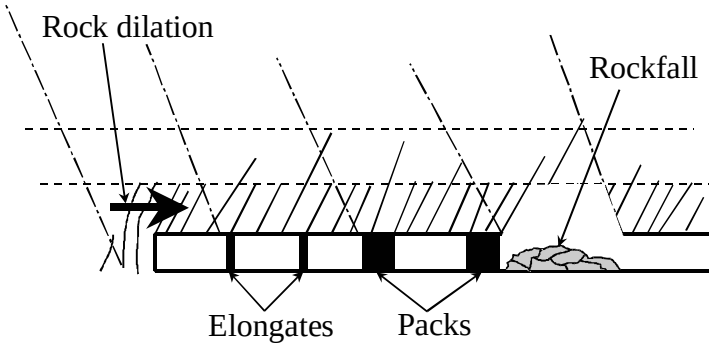

Figure 8.3.5 Stope with a back area rockfall leading to reduced hangingwall confinement.

8.3.5 Quantifying stable hangingwall spans between support units

The qualitative insights gained from the numerical simulations are used to develop a simplified conceptual model describing the rock mass stability and quantifying stable spans between adjacent support units. It is believed that the model is suitable to incorporate into a support design procedure, which intends to optimise support spacing, while maintaining an acceptable level of safety.

8.3.5.1 Hangingwall beam buckling

The design procedure followed here is based on that developed by Evans (1941), and subsequently modified and extended by Beer and Meek (1982), Brady and Brown (1985), and Hutchinson and Diederichs (1996). The solution technique, which is based on the voussoir beam, follows the intuitive idea that, in a discontinuous hangingwall beam, the central transverse crack determines the deformational behaviour (Figure 8.3.6). In the buckling mode the beam becomes unstable to form a 'snap-through' mechanism.

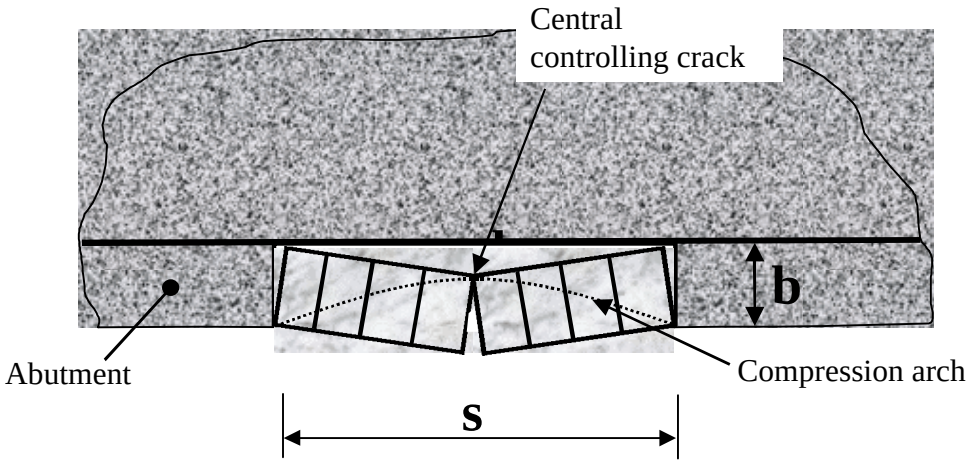

Figure 8.3.6 Voussoir beam geometry for hangingwall beam analysis.

In analysing the stability of the voussoir beam the following assumptions are made:

- As the beam deflects, a parabolic compression arch develops in the beam.

- Deflection of the beam occurs before slippage at the abutments. Stability against slippage (see Section 5.2) is determined after the compression arch develops.

- The abutments are stiff, i.e. they do not deform under the arching stress. Each abutment is subjected to the same distributed load as the ends of the beam, however the loaded area is small compared with the beam span. Therefore, elastic compression of the abutments will be small compared with the beam compression, and may be neglected (Brady and Brown, 1985).

The voussoir beam problem is statically indeterminate, i.e. no explicit solution is available and an iterative process is followed to determine the beam equilibrium position. The solution procedure is given in texts such as Brady and Brown (1985), and Hutchinson and Diederichs (1996), and is not repeated here.

Previously documented results of this solution have used an absolute snap-through limit, which is the limit of stable deflection according to the mathematical formulation. This limit is extremely sensitive to beam thickness, a difficult parameter to estimate accurately and reliably. Hutchinson and Diederichs (1996) recommend a design snap-through limit which is reached when the mid-span deflections reach 10 per cent of the beam thickness. Beyond this deflection, small differences in thickness have an unacceptably large influence on stability, and the beam's stability becomes uncertain.

Using the design snap-through limit of Hutchinson and Diederichs (1996), the span versus minimum beam thickness is given in Figure 8.3.7. The snap-through limits are given for various values of *in situ* rock mass elasticity modulus (E`) parallel to the excavation surface. The *in situ* rock mass modulus is predominantly governed by the stiffness of the rock mass discontinuities, and is lower than the stiffness of solid rock, which is characterised by the Young's modulus. It is apparent from Figure 8.3.7 that the relationship between span and beam thickness is highly dependent on the *in situ* rock mass modulus measured in a direction parallel to the excavation surface.

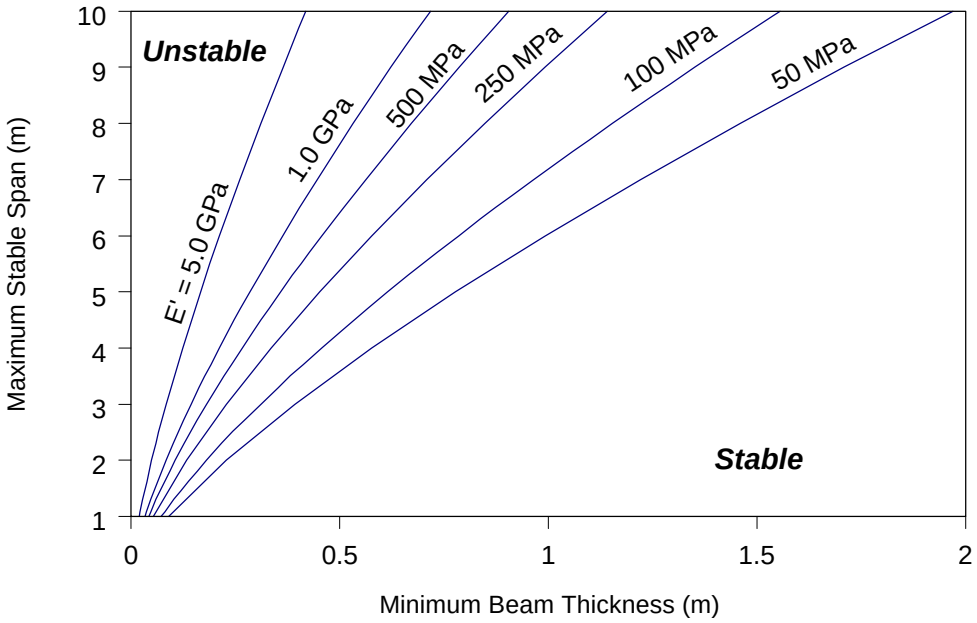

Figure 8.3.7 Span versus minimum beam thickness at 10 % beam deflection for various values of in situ rock mass modulus (E`).

Bandis *et al*. (1983) made use of experimental data to establish a relationship between normal joint stiffness and normal stress for well interlocked joints in various rock types (Figure 8.3.8). The joint stiffness is found to increase with increasing normal stress. For rock mass discontinuities in a typical gold or platinum hangingwall, where the compressive hangingwall stresses are generally less than 5 MPa, a discontinuity stiffness of 40 MPa/mm is assumed for the purposes of this study. It is recognised, however, that further *in situ* discontinuity stiffness measurements are required to obtain more accurate and representative stiffness data.

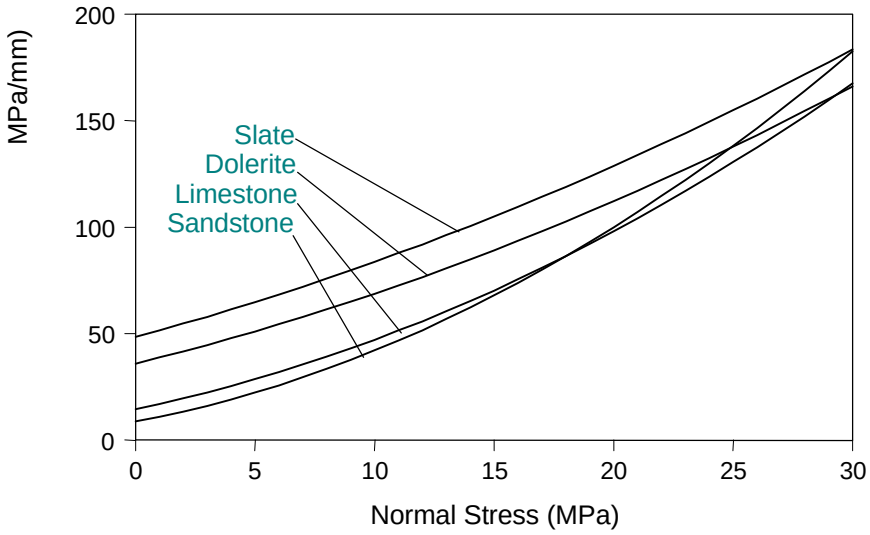

Figure 8.3.8 Normal joint stiffness for well interlocked joint examples in various rock types (after Bandis et al., 1983).

The joint stiffness is incorporated in the buckling analysis procedure. To simplify the analysis, and in view of the comparatively minor variations in stiffness for normal stresses ranging from 0 to 5 MPa, the stiffness is assumed to be constant. The value selected was 40 MPa/mm, irrespective of the compressive stresses acting within the hangingwall beam.

The effective rock modulus (E`) is calculated by multiplying the normal joint stiffness by the lateral deformation (arch shortening) during beam deflection. It is thus assumed that lateral hangingwall deformation occurs at the discontinuities only, and the rock between adjacent discontinuities does not deform. This is a realistic assumption as the Young's modulus of the intact rock is much higher than the effective joint modulus.

Multiple discontinuities act as springs in series, and each discontinuity is compressed equally. Span versus thickness relations shown in Figure 8.3.9 give the stability envelopes of hangingwall beams with three joints, as well as one, three, five and ten joints per metre of hangingwall length.

As shown in Figure 8.3.6, the unsupported hangingwall span needs to be discretised by at least three joints to allow deformation in the buckling mode. Hence, the line shown in the graph of Figure 8.3.9 indicating the stability envelope of a hangingwall discretised by one joint per metre is only shown for maximum stable spans exceeding 3 m. At spans below 3 m the beam would be discretised by less than three joints, and thus no deformation in the buckling mode would be possible.

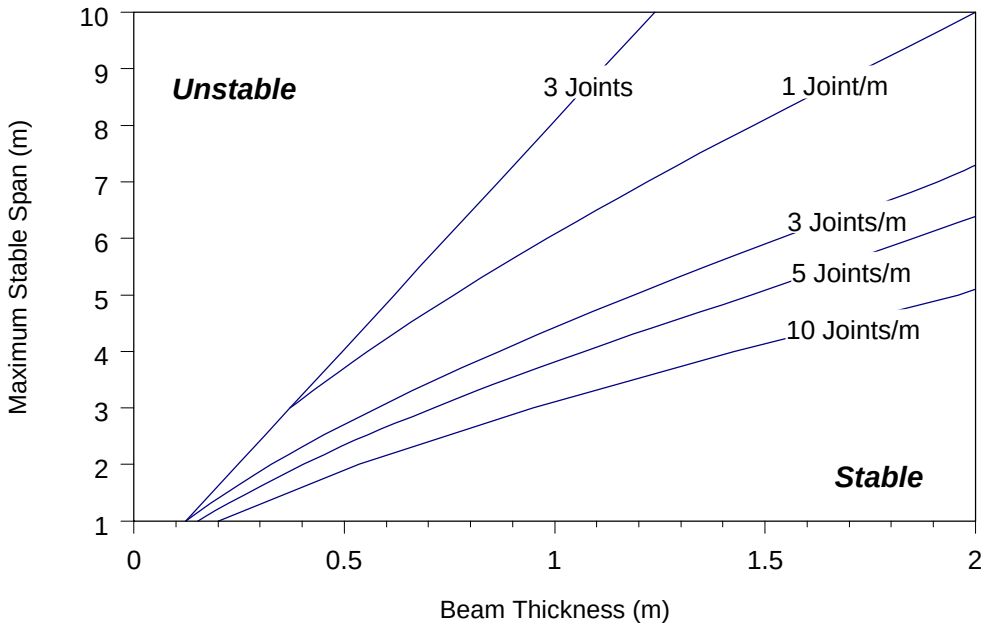

Figure 8.3.9 Buckling stability envelopes of a discontinuous hangingwall beam.

As the beam deflects, the arch stresses are transmitted through the beam edges to the abutments. The maximum abutment stresses for various beam thicknesses are plotted in Figure 8.3.10 as a function of span (postulating five joints per metre).

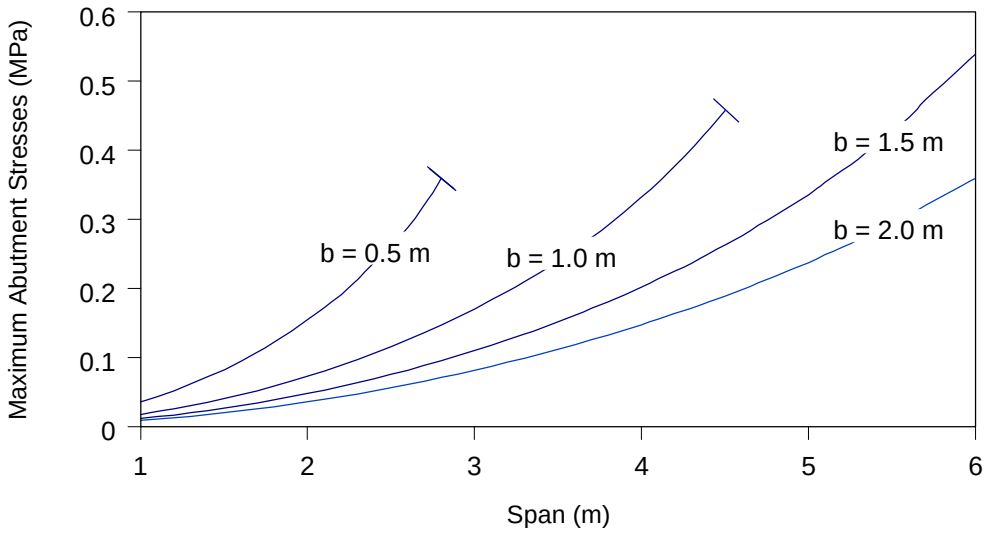

Figure 8.3.10 Maximum abutment stresses versus span for various beam thicknesses.

It is evident that the maximum abutment stress for typical beam thicknesses encountered in South African mines is approximately 0,4 – 0,5 MPa for spans ranging from 2,5 to 6 m. However, these are localised stresses induced by block rotation. If these stresses are averaged across the full thickness, the mean compressive stress in the buckling mode is considerably lower than the earlier calculated magnitude.

8.3.5.2 Shear and rotational failure by slip at the abutments

The second failure mechanism considered in this study is shear and rotational failure by slip at the abutments. In Figure 8.3.11 a schematic diagram is depicted of the geometry governing the stability of a hangingwall keyblock. Here shear forces prevent the fall of the block. To analyse

this situation in some detail, the following notations are introduced. The weight of the block is denoted by *W*, the beam thickness by *b*, the span between adjacent support units by *s* and s_x is the magnitude of compressive horizontal stress in the hangingwall. Finally, a and b are the angles that define the orientation of the extension and shear fractures. The hangingwall stress may be generated by two mechanisms, namely:

- In intermediate and deep level mines, the rock dilation associated with fracturing immediately ahead of the stope face may induce compressive stresses parallel to the excavation surface.

- The block rotation associated with the 'snap-though' failure mechanisms described in Section 8.3.5.1 may also generate compressive stresses in the hangingwall.

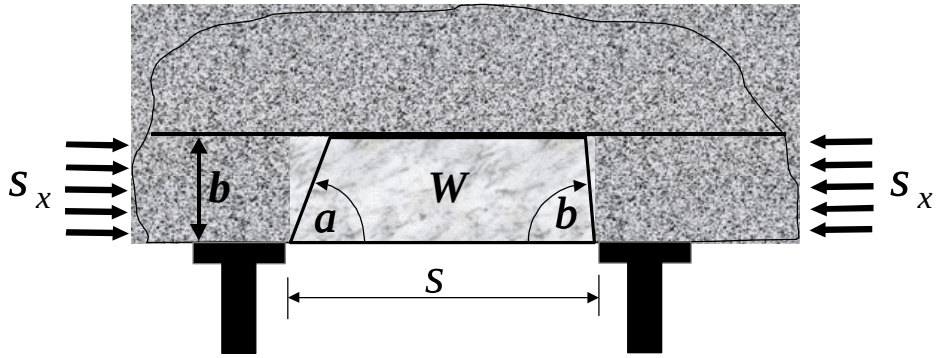

Figure 8.3.11 Potential keyblock instability due to shear failure at the abutments.

The discontinuities, which represent mining induced fractures, are assumed to have zero cohesion on the inclined contact surfaces. Hence, for the keyblock to be stable, the lateral thrust at the abutments due to *in situ* compressive hangingwall stresses must mobilise a frictional resistance sufficient to provide the abutment shear force. The frictional resistance for either side of the keyblock can be calculated using the following expressions:

$$V_I = -s_x b \cot(a + j) \quad \text{and} \quad V_{II} = -s_x b \cot(b + j) \tag{8.3.1}$$

The coefficient of friction, m, is an important parameter governing the resistance to shear and it defines the angle of friction $j = \arctan(m)$. Typically, underground discontinuities have closely matched surfaces, especially in the case of mining induced fractures. Hence, the apparent friction angle can be relatively high; a range of 30 to 50 degrees is considered realistic.

Stability or instability of the keyblock depends on various factors. The criteria for stability are summarised as follows:

- *Unconditional stability.* The keyblock is unconditionally stable (Figure 8.3.12a) if the forces and moments are both in equilibrium. The forces will not induce the fall of the block if $V_I + V_{II} > W$. Similarly, the moments will not cause dislodging movements (rotation) if the supporting forces satisfy the following inequalities: $V_I > \frac{1}{2}W$ and $V_{II} > \frac{1}{2}W$. Obviously, if the two conditions concerning moments are satisfied, the first criterion will also be fulfilled. A set of necessary and sufficient criteria for unconditional stability can be found from the relationships in Equation 8.3.1 in terms of the angles. The conditions for unconditional stability can now be expressed as follows:

$$a > \tfrac{1}{2}p - j \quad \text{and} \quad b > \tfrac{1}{2}p - j \tag{8.3.2}$$

- *Conditional stability.* If only the criterion concerning forces and *one* of those arising from moments are satisfied, then the block may or may not be stable. To illustrate such a situation, postulate the following:

$$V_I + V_{II} > W; \qquad V_I < \tfrac{1}{2}W; \qquad V_{II} > \tfrac{1}{2}W \tag{8.3.3}$$

  Clearly this block is not unconditionally stable, but it may *not* get dislodged if its rotation is *kinematically impossible*. Such a case is illustrated in Figure 8.3.12c. If, however, rotation is possible, failure will occur and the block will fall (Figure 8.3.12d).

The next task is to determine the criteria that prevent rotation. As an example, postulate that the block, if it moves, will pivot around its furthermost hangingwall point on the left (see Figure 8.3.13). Let this point of fulcrum be A. Denote by r the distance between the fulcrum and point B, the furthest point on the right of the top plane of the block. Rotation can occur only if point B can move past the next block to the right.

Let C be the point where the fracture at the right end of the block intersects the hangingwall. Clearly, the limiting geometry is when the block can start to pivot around its fulcrum, that is, around point A. This can occur when the line $\overline{BC}$ (in section) is tangent to the circle of radius r with its centre at point A. If we denote the angle enclosed by lines $\overline{AC}$ and $\overline{AB}$ by e, then this criterion is satisfied if $e + b = ½\ p$. Thus if $e + b \leq ½\ p$, the keyblock can rotate around its fulcrum and, if $e + b > ½\ p$, keyblock rotation is kinematically impossible.

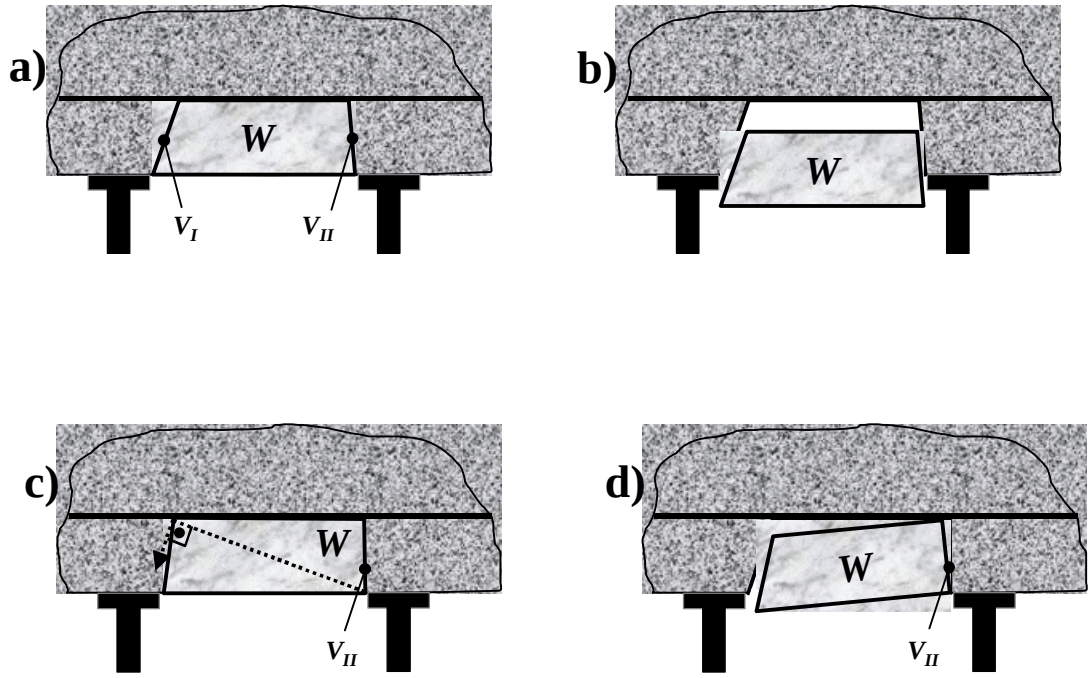

Figure 8.3.12 Schematic diagrams showing possible failure modes due to shear at discontinuity interfaces:

a) Keyblock is stable as $V_I > ½\ W$ and $V_{II} > ½\ W$.

b) Keyblock shear failure as $V_I < ½\ W$ and $V_{II} < ½\ W$.

c) Although $V_I < ½\ W$, the keyblock is stable as $V_{II} > ½\ W$ and no block rotation is possible.

d) Keyblock is unstable as $V_I < ½\ W$ and block rotation is kinematically possible ($V_{II} > ½\ W$).

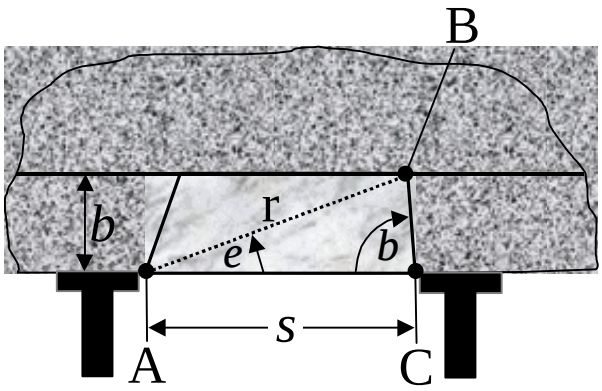

Figure 8.3.13 ***Geometry parameters governing the rotational stability of hangingwall blocks.***

Now introduce the ratio $k = b/s$. It is simple to show that

$$e = \arctan\left(\frac{k}{1 - k\cot(b)}\right). \tag{8.3.4}$$

These two relationships are sufficient to obtain the following results:

$$k(b) = \frac{1}{2}\sin(2b) \quad \text{or alternatively} \quad b(k) = \frac{1}{2}\arcsin(2k). \tag{8.3.5}$$

The first of these relationships is depicted graphically in Figure 8.3.14. In this illustration, rotation is prevented for cases that fall above the curve, therefore, the block is *stable*. In instances that plot on or under the curve rotation can occur, and hence the block is *unstable.* Since the value of the sine function does not exceed unity, it is obvious from the first of these expressions that instability cannot occur when $k > ½$ or $b > ½\, s$.

It is evident from Figure 8.3.14 that $k(b)$ is a double valued function. If we denote the two solutions by b_1 and b_2 ($0 < b_1 \le \frac{1}{4}p$ and $\frac{1}{4}p \le b_2 \le \frac{1}{2}p$), the stability conditions concerning the block can be summarised as follows:

Stable:
a) If $k \le \frac{1}{2}$ and $b < b_1$ or $b > b_2$
b) If $k > \frac{1}{2}$

Unstable: If $k \le \frac{1}{2}$ and $b_1 \le b \le b_2$

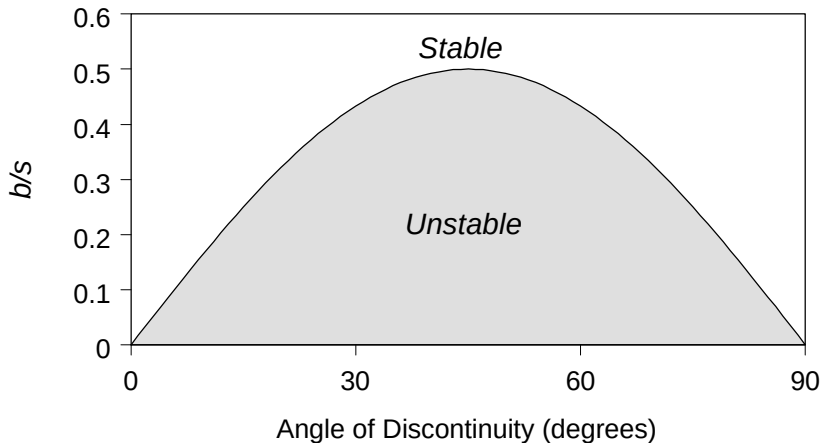

Figure 8.3.14 ***Stability envelopes characterised by the ratio of b over s versus discontinuity angle.***

It is obvious from Figure 8.3.15 that the upper bound of the span that will not rotate increases (for a fixed beam thickness) as the value of angle b (or a) departs, up or down, from 45 degrees. It is also noteworthy that for situations where b is greater than 2 m, rotation is unlikely to limit the stability of the hangingwall.

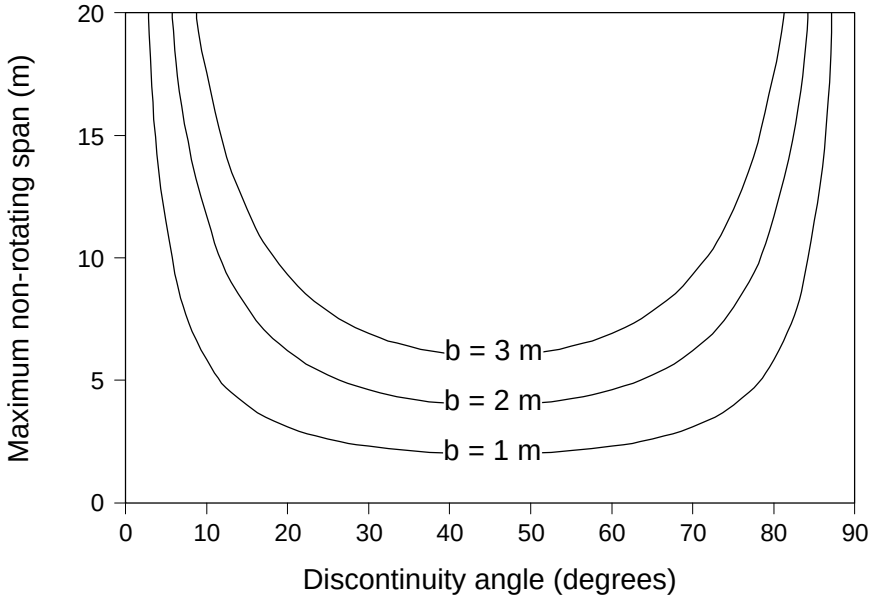

Figure 8.3.15 Upper limit of stable spans.

The above discussion is valid for keyblocks having a geometry as shown in Figure 8.3.13. For certain keyblocks delineated by shallow dipping discontinuities and/or small spans, however, the geometry could be of the form shown in Figure 8.3.16.

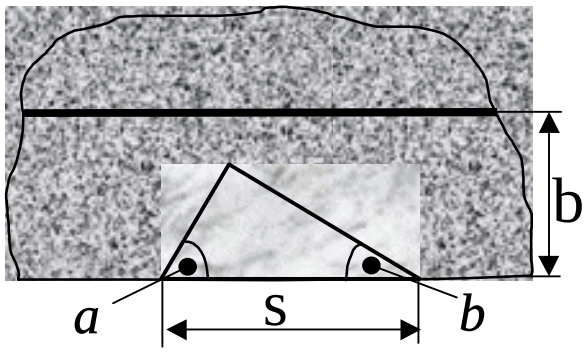

Figure 8.3.16 Keyblock geometry delineated by shallow dipping discontinuities and/or small spans.

In this case keyblock rotation is kinematically impossible if $a + b > ½\ p$.

An interesting particular case occurs when all fractures are parallel. Postulate that the face is on the left-hand side. In this case $a = p - b$ and the expression for the vertical component of the shear resistance on the left becomes:

$$V_I = s_x b \cot(b - j) \tag{8.3.6}$$

(note the change in sign) and the formula for V_{II} remains unaltered. This expression remains positive as long as

$$j < b < \tfrac{1}{2}p + j \tag{8.3.7}$$

It is obvious from these expressions that $V_I > V_{II}$ as long as $b > j$. Since this criterion is almost always satisfied in practice, it can be concluded that this block is unconditionally stable in most cases, provided $V_{II} > \frac{1}{2}W$.

The parameters governing the maximum stable hangingwall span are the discontinuity angles (a and b), the fall-out height (b), the friction coefficient (m), and the hangingwall clamping stress (s_x). The influence of these parameters on the stable span is investigated next.

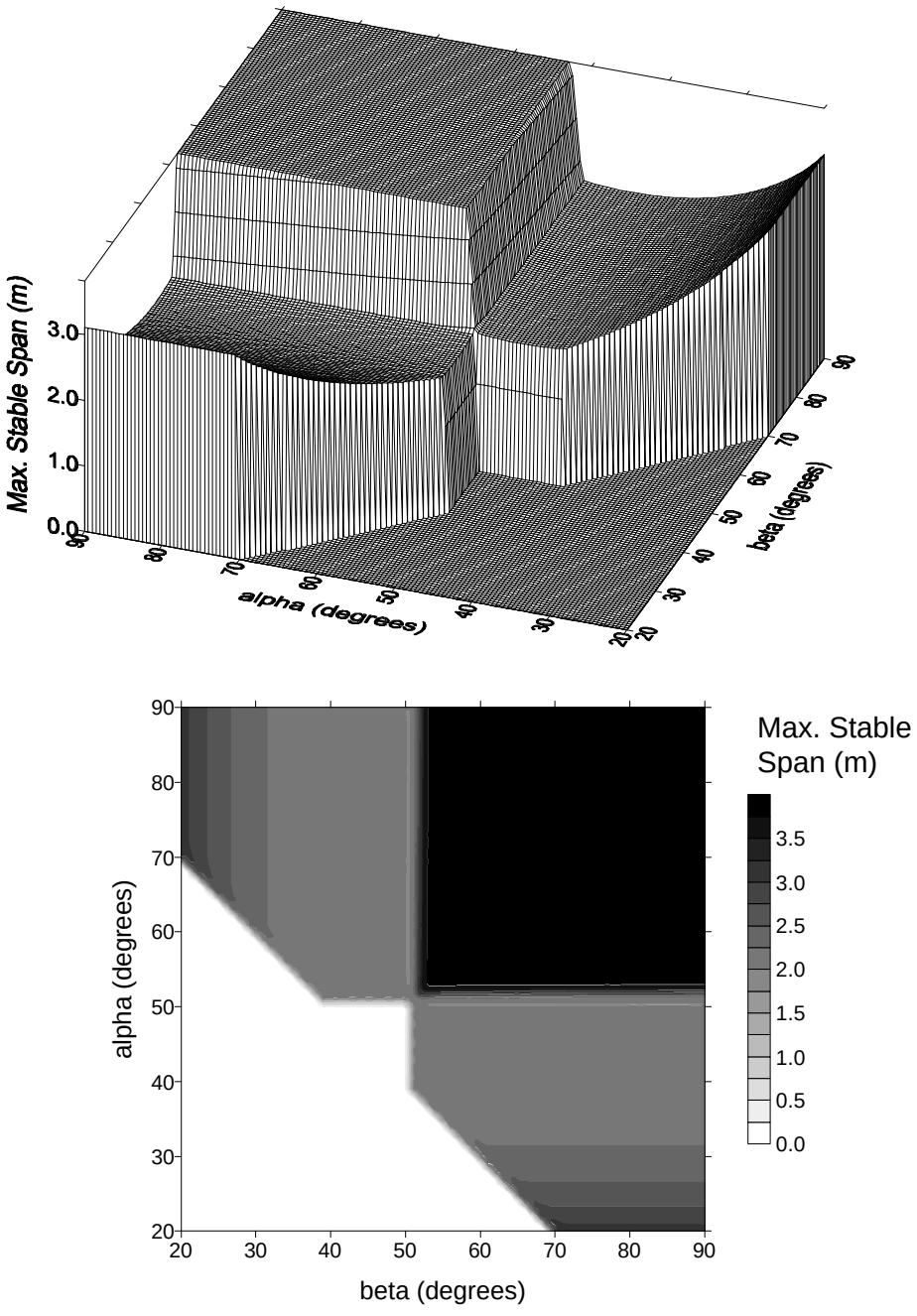

Figure 8.3.17 ***Maximum stable span versus discontinuity angles for s_x = 1.0 MPa, b = 1.0 m and m = tan 40^o. Both carpet (top) and contour (bottom) plots are given to facilitate convenient data interpretation.***

The maximum span was determined using the proposed rockfall design methodology for a mine in intermediate depth with five fractures per metre in the hangingwall. Possible failures due to buckling and slip at the discontinuities are analysed. The limiting equilibrium of the keyblock is governed by one of two failure mechanisms: (i) shear failure due to slip at the abutments and/or block rotation, and (ii) buckling failure. Figure 8.3.17 gives stability envelopes for the hangingwall at limiting equilibrium for s_x = 1,0 MPa, b = 1,0 m and m = tan 40°.

As is evident from Figure 8.3.17, the maximum stable span for the case study investigated here varies from zero to 3,8 m. The maximum span is governed by three types of failure mechanisms, which depend on the combinations of discontinuity angles (a and b). A set of stability definitions in the various parts of the a, b plane are illustrated in Figure 8.3.19. The plane is subdivided into four regions and these regions are delineated by inequalities.

Region A: This region is defined by $0 < a \le a_{\min}$ and $0 < b \le b_{\min}$, where $a_{min} = b_{min} = ½\ p - j$, as defined previously in Equation 2. Hence, for the example given here ($j = 40^o$), $a_{\min} = b_{\min} = 50^o$. At angles $0 < a \le a_{\min}$ and $0 < b \le b_{\min}$ the supporting forces V_I and V_{II} are negative, and hence all keyblocks, irrespective of size, are *unstable*. This is evident from Figure 8.3.17, and for $0 < a \le a_{\min}$ and $0 < b \le b_{\min}$ the maximum stable span is zero.

Region B: Here the limits are defined by $a_{min} < a \le ½\ p$ and $0 < b \le b_{\min}$. Thus $V_I \ge 0$, $V_{II} < 0$ and the keyblock is conditionally stable, depending on whether keyblock rotation is kinematically possible. In Section 8.3.5.2 it was shown that it is kinematically impossible for a keyblock to rotate if $b/s \ge 1/2\sin(2b)$. This condition holds for keyblocks having the shape shown in Figure 8.3.18a. For keyblocks with a short span (Figure 8.3.18b) the stability condition to prevent rotation becomes $a + b > ½\ p$. Hence, in Region B, keyblocks rotate and are unstable if $a + b \le ½\ p$ (see Figures 8.3.17 and 8.3.19). The maximum stable span at $a + b = ½\ p$ corresponds to a keyblock having the shape shown in Figure 8.3.18c.

Region C: Here the boundaries are given by the following inequalities $0 < a \le a_{\min}$ and $b_{min} < b \le ½\ p$. For these angles $V_I < 0$, $V_{II} \ge 0$ and the keyblock is conditionally stable, depending on whether rotation is kinematically possible. The conditions outlined for Region B are also applicable to Region C, and are thus not repeated here.

Region D: This region is delineated by $a_{min} < a \le ½\ p$ and $b_{min} < b \le ½\ p$. Here $V_I \ge 0$, $V_{II} \ge 0$ and comparatively large spans are stable. The upper limit of the stable spans are governed by the buckling potential of the beam. Figure 8.3.9 gives the maximum stable spans versus beam thickness for a hangingwall discretised by various numbers of joints. For the case study shown in Figure 8.3.19 (b = 1 m, 5 Joints/m), the maximum stable span governed by the buckling potential is 3,8 m.

Figure 8.3.20 shows the influence of hangingwall beam thickness (b) on the maximum stable span at limiting equilibrium for various angles of discontinuities. It is apparent that the maximum stable span decreases with decreasing beam thickness.

The effect of compressive hangingwall stresses on the maximum stable span is given in Figure 8.3.21. It is evident that reduced compressive stresses decrease the stability and associated stable span lengths between adjacent support units. In particular, as the compressive stresses are reduced from s_x = 0,1 MPa to 0,01 MPa, the stable hangingwall span is considerably reduced from a maximum of 4 m (s_x = 0,1 MPa) to 1 m (s_x = 0,01 MPa). This stress is clearly a critical component and it requires further study.

Figure 8.3.22 gives the effect of various coefficients of friction (m) on maximum stable spans. As the coefficient of friction is decreased, the size of Region A is increased. This results in an increased possibility of shear failure and consequently, for smooth rock mass discontinuities, greater areal coverage requirements are necessary.

The methodology proposed here is likely to be better suited for comparatively densely fractured hangingwall, consisting of hard rock, as typically encountered in intermediate and deep level gold and platinum mines. The method is unlikely to be applicable to shallow mines, such as collieries, where the surrounding rocks are relatively soft. In these mines, due to sedimentation, often intensively laminated roof strata is encountered. The failure of such laminated roof is controlled by mechanisms not discussed in this paper.

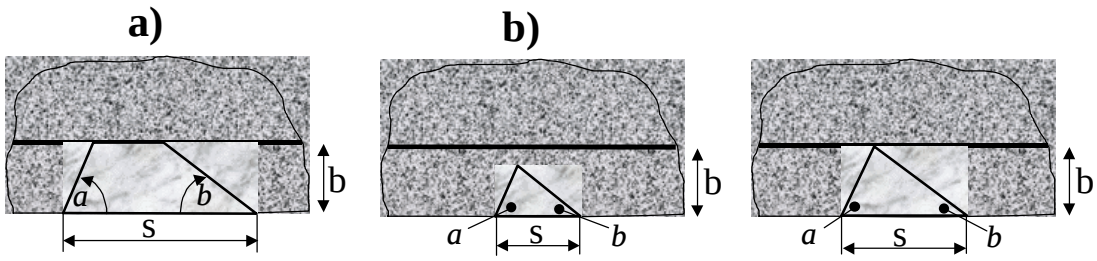

Figure 8.3.18 ***Various keyblock shapes associated with different rotational stability conditions.***

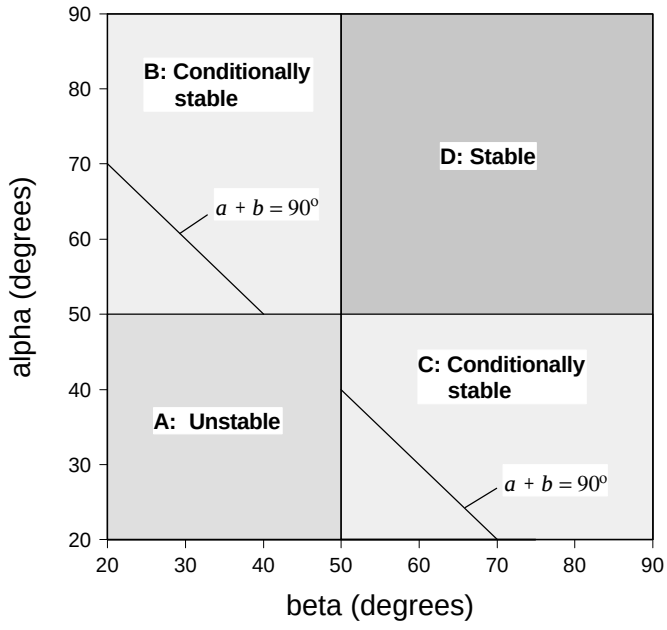

Figure 8.3.19 ***Stability definitions in the various parts of the a, b plane.***

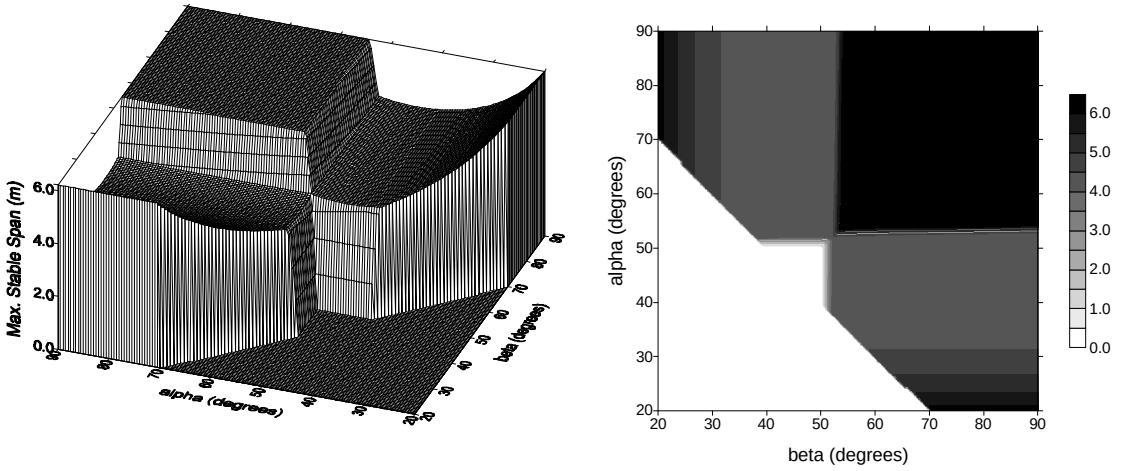

s_x = 1,0 MPa, b = 2,0 m and m = tan 40°

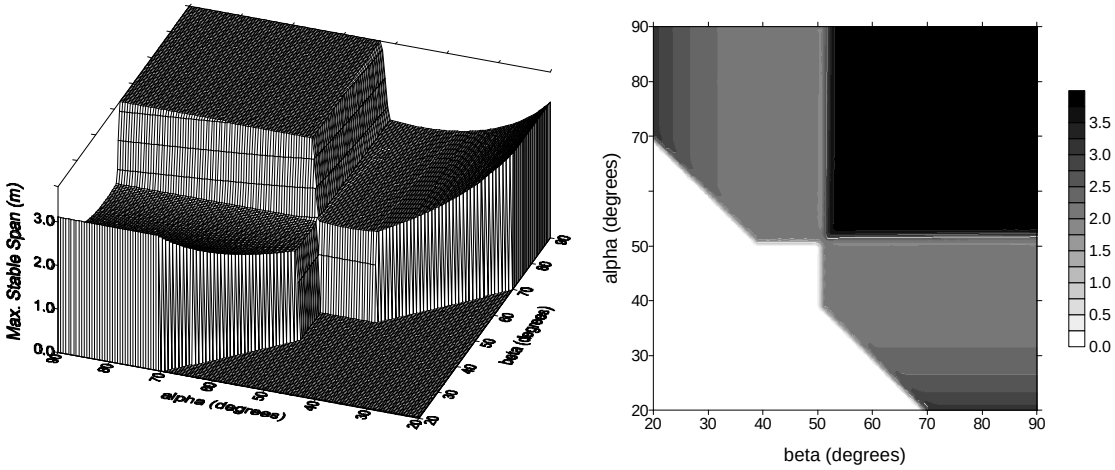

s_x = 1,0 MPa, b = 1,0 m and m = tan 40°

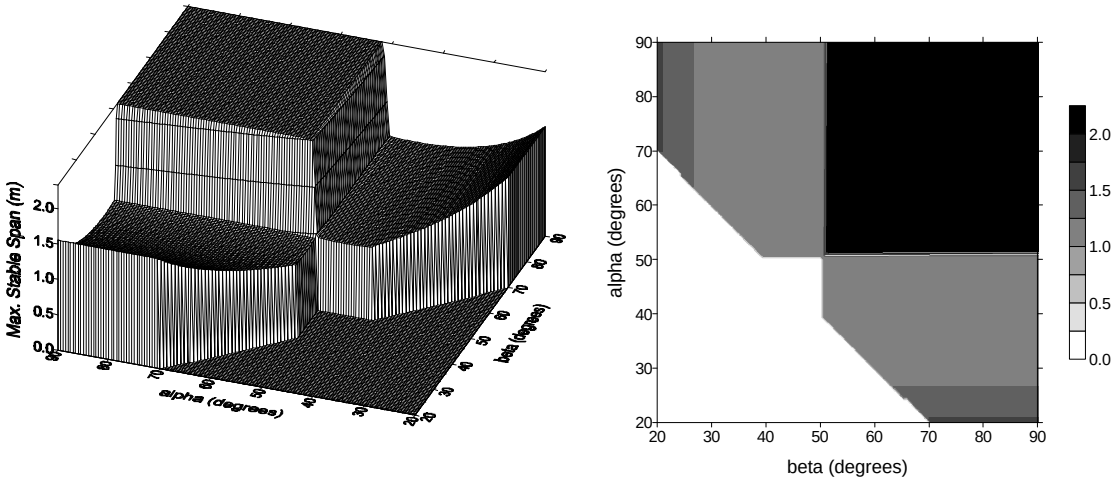

s_x = 1,0 MPa, b = 0,5 m and m = tan 40°

Figure 8.3.20 Effect of reduced hangingwall beam thickness (b).

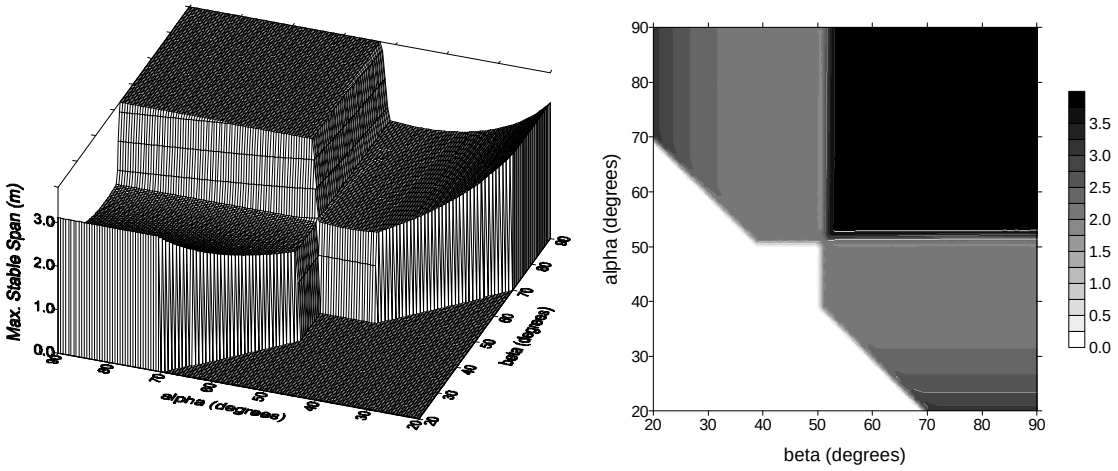

s_x = 1,0 MPa, b = 1,0 m and m = tan 40°

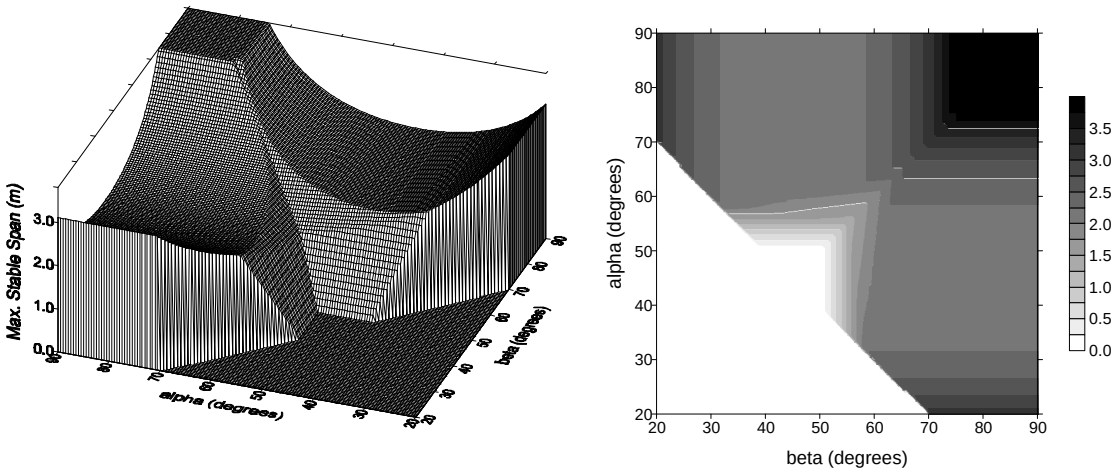

s_x = 0,1 MPa, b = 1,0 m and m = tan 40°

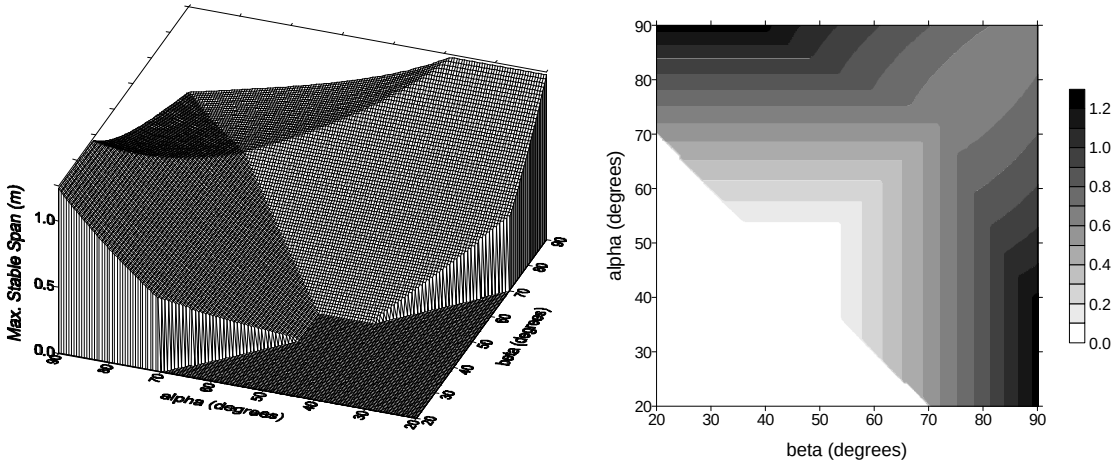

s_x = 0,01 MPa, b = 1,0 m and m = tan 40°

Figure 8.3.21 Effect of reduced hangingwall compressive stresses (s_x).

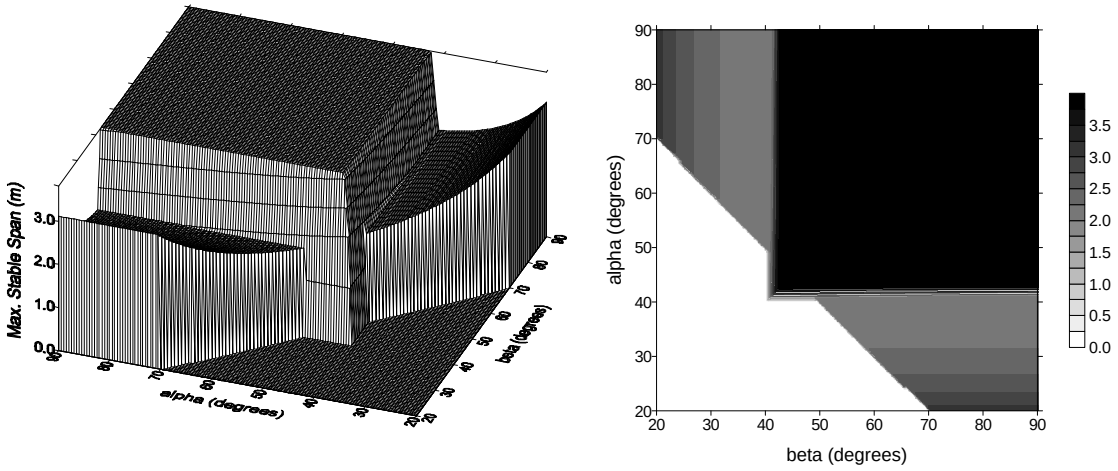

s_x = 1,0 MPa, b = 1,0 m and m = tan 50°

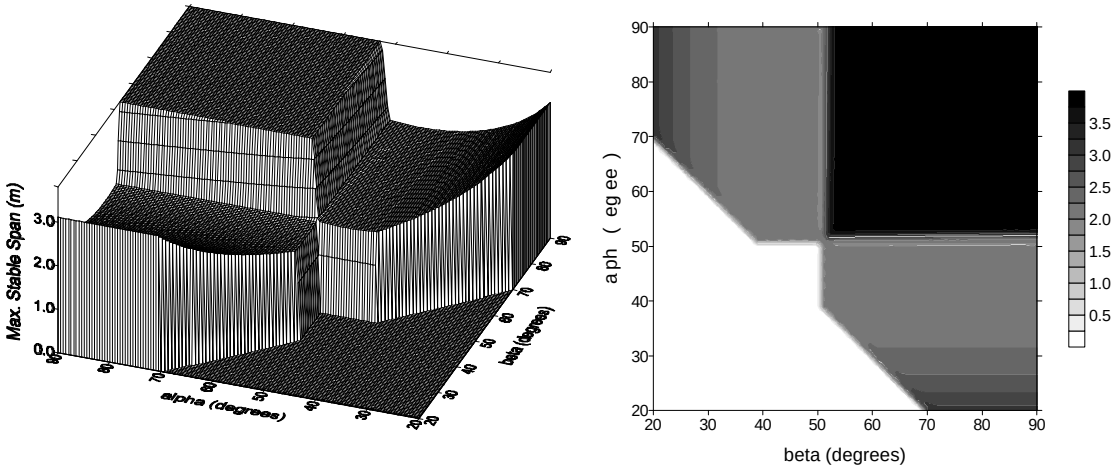

s_x = 1,0 MPa, b = 1,0 m and m = tan 40°

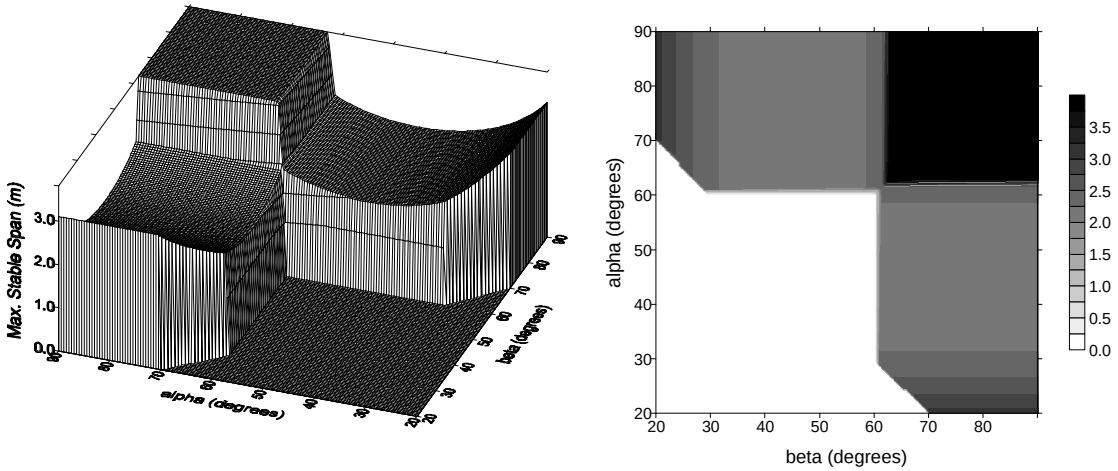

s_x = 1,0 MPa, b = 1,0 m and m = tan 30°

Figure 8.3.22 Effect of coefficient of friction (m).

8.3.6

In seismic and rockburst prone mines, sudden fault rupture or the explosive failure of highly strained rock leads to energy being radiated in the form of stress waves. The stress waves

and wave focussing (Daehnke, 1997). The rock is subjected to rapid accelerations, resulting in rock fabric failure, keyblock ejection and stope closure. The most widely used support design

account the kinetic and potential energy of the keyblocks. Underground observations, rockburst back analyses and numerical simulations have indicated that hangingwall blocks can be m/s. The criteria for effective support systems are thus to

velocity of 3 m/s. Roberts (1995) assumed that during a rockburst the hangingwall must be m of downward movement, i.e. the total energy which had to be

$$E = \tfrac{1}{2}mv^2 + mgh \ , \qquad (8.3.8)$$

where *E* is the total energy to be absorbed by the support system, *m* is the mass of the hangingwall (dependent on fall-out height), *v* is the initial hangingwall velocity (taken as 3 m/s) and *h* is the downward hangingwall displacement (taken as 0,2 m).

In the design methodology proposed here, the hangingwall is also assumed to have an initial velocity of 3 m/s, however the downward displacement (*h*) is determined from the energy absorption capabilities of the support units as was originally proposed by Wagner (1984) (Figure 8.3.23 and Equation 8.3.12). Thus the total hangingwall displacement up to the point in time when motion ceases is greater for a support system providing less support resistance, while a high resistance support will arrest the hangingwall within a shorter distance. In the first case the hangingwall deceleration is reduced, however, the potential energy component, which needs to be absorbed by the support system, is increased. In the second case the hangingwall deceleration is higher and the potential energy component is decreased.

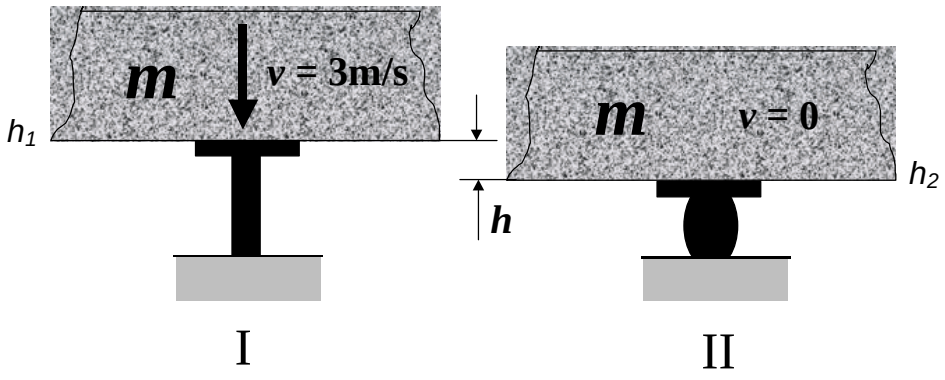

$$\int_{h_1}^{h_2} F(x)dx = \frac{1}{2}mv^2 + mgh, \text{ where } h = h_2 - h_1 \qquad (8.3.9)$$

Figure 8.3.23 ***Conceptual model of dynamic hangingwall displacement and associated energy absorption requirements of the support system, where h_1 and h_2 is the closure acting on the support unit before and after the dynamic event, respectively.***

To illustrate the load bearing requirements of a support unit during a dynamic event, assume a support unit with force deformation characteristics shown in Figure 8.3.24 is installed underground. Due to pre-stressing and stope convergence, the unit is quasi statically deformed up to point h_1; thereafter a rockburst occurs and the unit is rapidly compressed to point h_2. The hashed area of the graph in Figure 8.3.24 defines the total energy, which is required to arrest

the hangingwall. For the support system to meet the rockburst loading requirements, the following criteria apply.

The average dynamic hangingwall displacement (*h*) in the stope should not exceed 0,3 m. If the mean displacement would exceed this value, differential downward movements between the face and the support units, as well as between different supports of varying stiffness, could compromise the post-rockburst hangingwall integrity. This would lead to a heavily fractured hangingwall with low structural strength. Further work needs to be done to provide a more appropriate estimate of *h*. However, in this preliminary study, a maximum value of *h* = 0,3 m is considered realistic and suitable for initial support design trials.

To ensure post-rockburst stability, the load borne by each support unit after the rockburst, that is $F(h_2)$, should exceed the corresponding tributary load.

The stoping width minus h_2 should exceed 0,6 m to ensure a sufficient post-rockburst stoping width to prevent injury to and allow movement of mine personnel.

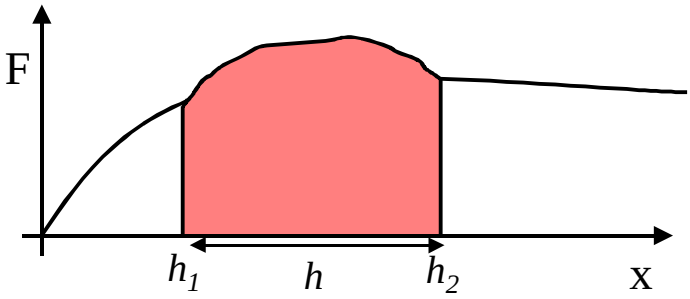

Figure 8.3.24 ***Quasi-static and dynamic force-deformation behaviour of a support unit prior and during a rockburst.***

Having calculated *h* using Eq. 8.3.9, the local hangingwall deceleration can be determined from the equations of motions (assuming linear deceleration from *v* = 3 m/s).

$$a = \frac{v^2}{2h} \tag{8.3.10}$$

Taking the acceleration due to gravity into account, the *effective* hangingwall weight is calculated from the following relationship:

$$W_{eff} = m\left(g + \frac{v^2}{2h}\right) \tag{8.3.11}$$

The procedure of designing rockburst resistant support follows similar lines to those presented as part of the methodology of evaluating stope support for the purposes of combating rockfalls. The assumptions made in the rockfall related case also hold in rockburst prone mines. The main difference between the two procedures is that, in the rockburst related case, the effective hangingwall weight in Eq. 8.3.11 replaces the static weight of $W = m\,g$.

The effect of dynamic hangingwall displacement (*h*) is shown in Figure 8.3.25. Reduced displacement implies higher hangingwall deceleration and associated higher effective weight. This affects the hangingwall stability primarily in the buckling mode, and reduced stable spans are evident.

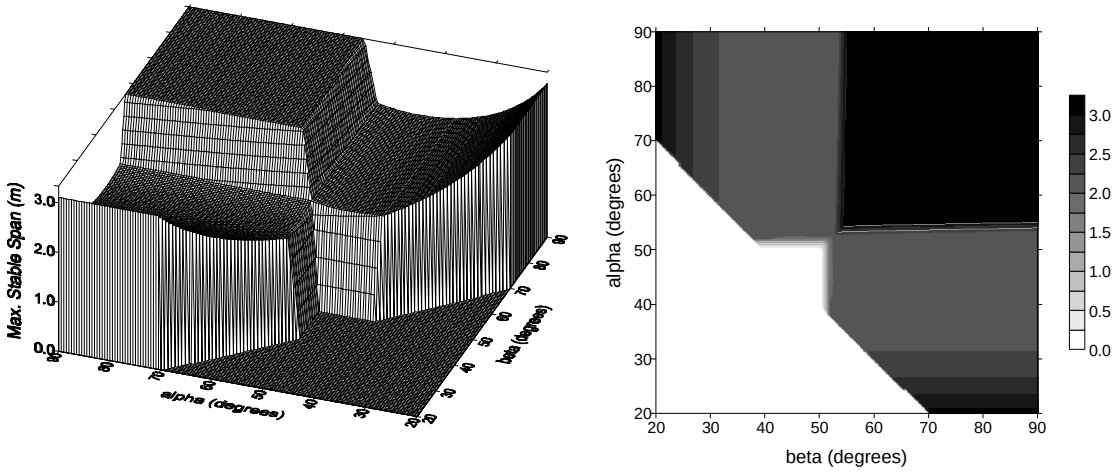

h = 0,3 m, s_x = 1,0 MPa, b = 1,0 m and m = tan 40°

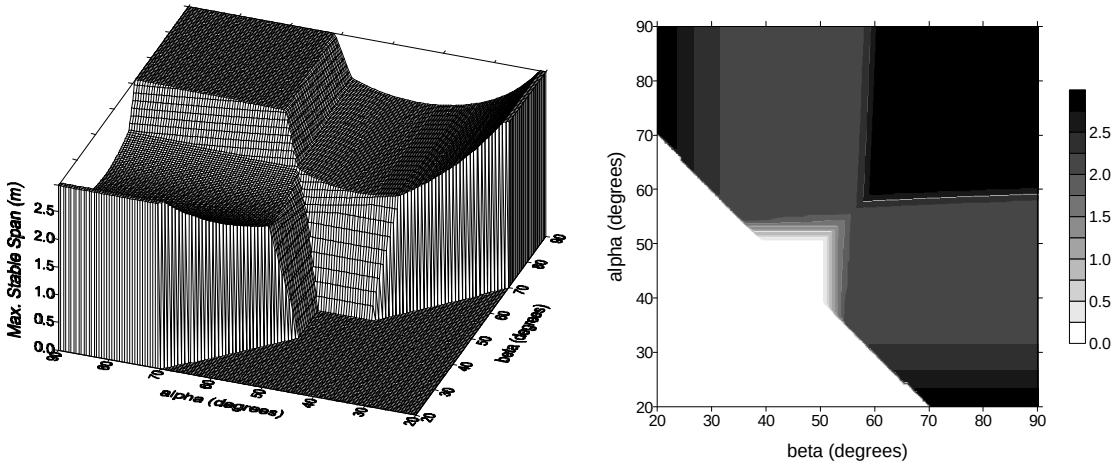

h = 0,1 m, s_x = 1,0 MPa, b = 1,0 m and m = tan 40°

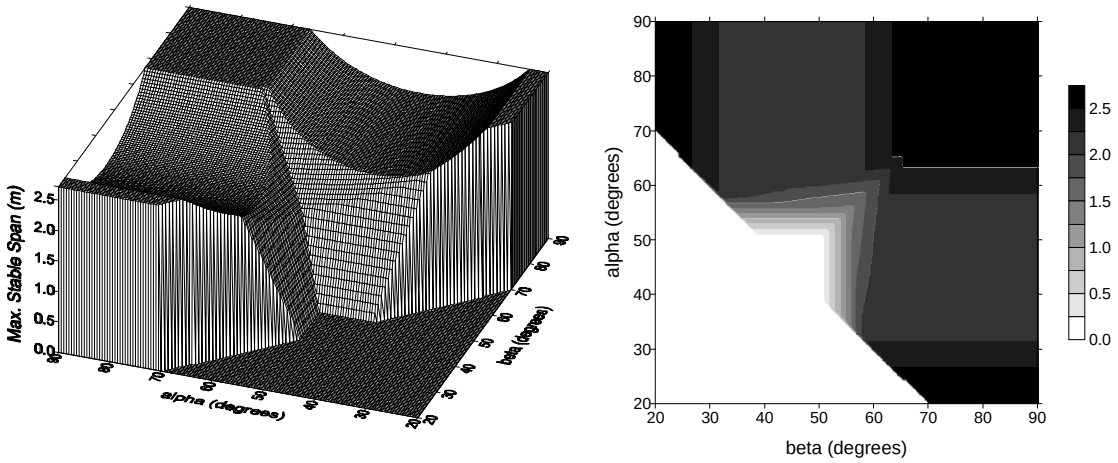

h = 0,05 m, s_x = 1,0 MPa, b = 1,0 m and m = tan 40°

Figure 8.3.25 Output of the rockburst support design methodology; effect of various hangingwall arrest distances (h).

8.4 Design procedure

This section summarises the existing design procedure and describes a new design methodology, which is based on the determination of zones of influence and keyblock stability analyses. Design charts for both the rockfall and the rockburst cases are given at the end of this section.

8.4.1 Existing design procedure

In the present version of SDA, there are two separate processes, namely the continuous and discontinuous analyses. Furthermore, in the current SDA version the two processes are completely independent of each other.

In the continuous analysis, a fixed zone of influence in the shape of a frustum of right cone (Figure 8.4.1) is assumed, with (R – r) typically between 1 and 1,5 m. The program works on the principle that all areas, where the zones of influence of adjacent support units do not overlap, are unstable.

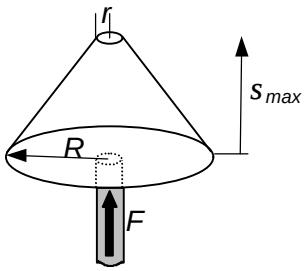

$$s_{max} = \frac{3F}{p\,(R^2 + Rr + r^2)}$$

Figure 8.4.1 Frustum of right cone zone of support influence and associated stress magnitude (s_{max}).

The discontinuous analysis checks for the stability of the hangingwall with respect to buckling, shear and rotational failure. The length of the unsupported beam is taken as the skin to skin distance between adjacent support units. The skin to skin support unit spacing under consideration here is taken in the strike direction and is denoted by *s* in this discussion. The spacing in the dip direction will be referred to as *d*. (Figures 8.4.2 and 8.4.3)

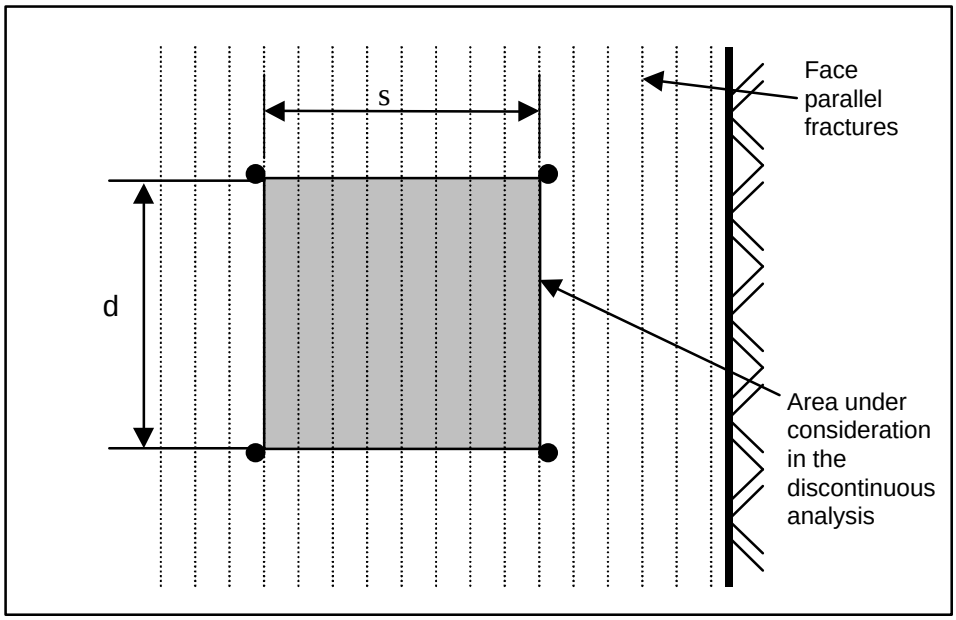

Figure 8.4.2 Schematic showing hangingwall discretised by face-parallel fractures and area used in the discontinuous analysis of the current design methodology.

The keyblock analysis determines if the hangingwall is stable for the strike spacing (*s*). An assumption of the program is that the hangingwall will be stable if $d \leq 1{,}5s$ (Daehnke *et al.*, 1998).

8.4.2 Proposed design methodology

A proposed design method, which incorporates both the zone of influence and the keyblock theories, is described below.

A programme such as SDA can easily be modified to incorporate the discussed design procedure.

The first step in the design procedure is the definition of the following rock mass parameters:

i) Angle of extension (a) and shear fractures (b)
ii) Friction coefficient (m)
iii) *In situ* compressive hangingwall stress (s_x)
iv) Extent of fracturing (discontinuities per metre of hangingwall)

Next, the above information is used to determine the extent of the zones of influence and the associated stress profile. This must be done for both the stope face and the support units (and backfill, where applicable). A spatial distribution of the zones of influence of the support units and stope face is established.

It is now necessary to set the support resistance criteria:

i) Fallout thickness (*b*) to prominent bedding plane (from rockfall back-analyses), or
ii) 95 % cumulative fallout thickness (*b*) from fatality database (Roberts, 1995).

A cross-section of support resistance profiles is taken, also showing the support resistance criteria. Where the support resistance profile falls beneath the support resistance criteria, the effect of the zone of influence is ignored (a conservative assumption). The length of this distance is denoted by *s*. This unsupported section must now be analysed further to check for keyblock stability. (Figures 8.4.3 and 8.4.4).

The support design method gives insights into spacing and associated stable hangingwall spans in the strike direction only. Due to the face parallel mining induced fracture orientation in intermediate and deep level mines, the hangingwall rock is generally less prone to failure between two support units in the dip direction, compared to failure between units in the strike direction.

As discussed earlier, the current design method considers the shaded area indicated in Figure 8.4.2 in the discontinuous analysis. In the design procedure proposed here, the shaded area shown in Figure 8.4.4 must be considered for the keyblock analysis.

Probabilistic keyblock analyses (Daehnke *et al*., 1998) have shown that, for a typical discontinuity spacing and attitude as encountered in intermediate depth and deep gold mines, the support spacing in the dip direction can be increased by a factor of $\pm$ 1,5 compared with the strike spacing, while maintaining an equal probability of keyblock failure in the dip versus strike direction. Hence, the support spacing in the dip direction can be up to, but should not exceed, 1,5 times the spacing in the strike direction.

In the new design procedure, *s* is defined as the distance, in the strike direction, where the stress profiles of adjacent supports fall below the support resistance criteria. Similarly, *d* is defined as this distance in the dip direction. Thus, *s* and *d* no longer refer to the skin-to-skin support spacing. However, the assumption is made that if the area considered in the

discontinuous analysis is stable in the strike direction, then the area in the dip direction will also be stable, as long as $d \leq 1{,}5s$.

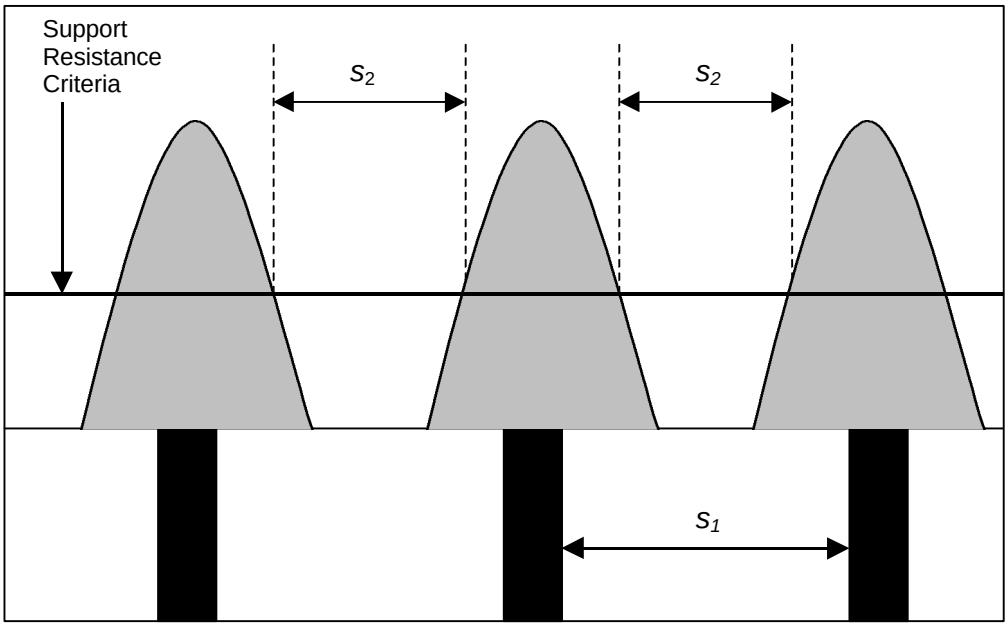

Figure 8.4.3 Cross-section of support resistance profiles, illustrating the unsupported sections, which have to be checked for keyblock stability, where s_1 is the spacing used in the current SDA version, and s_2 is the length to be used in the proposed design method.

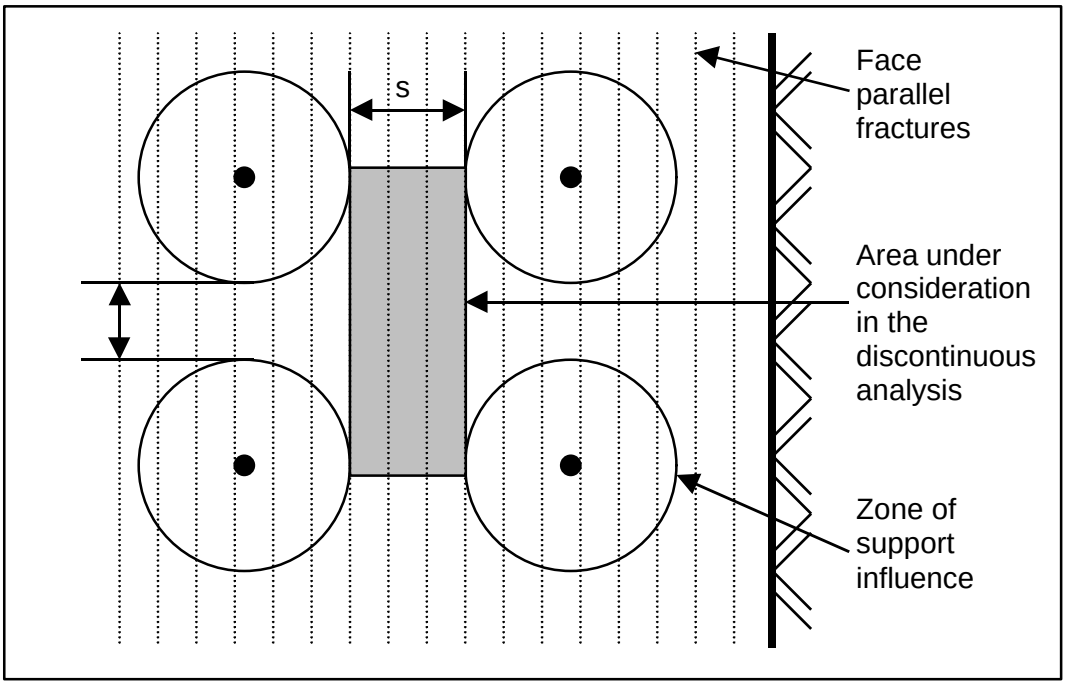

Figure 8.4.4 Schematic showing clamped hangingwall discretised by face-parallel fractures, zones of support influence and area to be considered in the discontinuous analysis of the new design methodology.

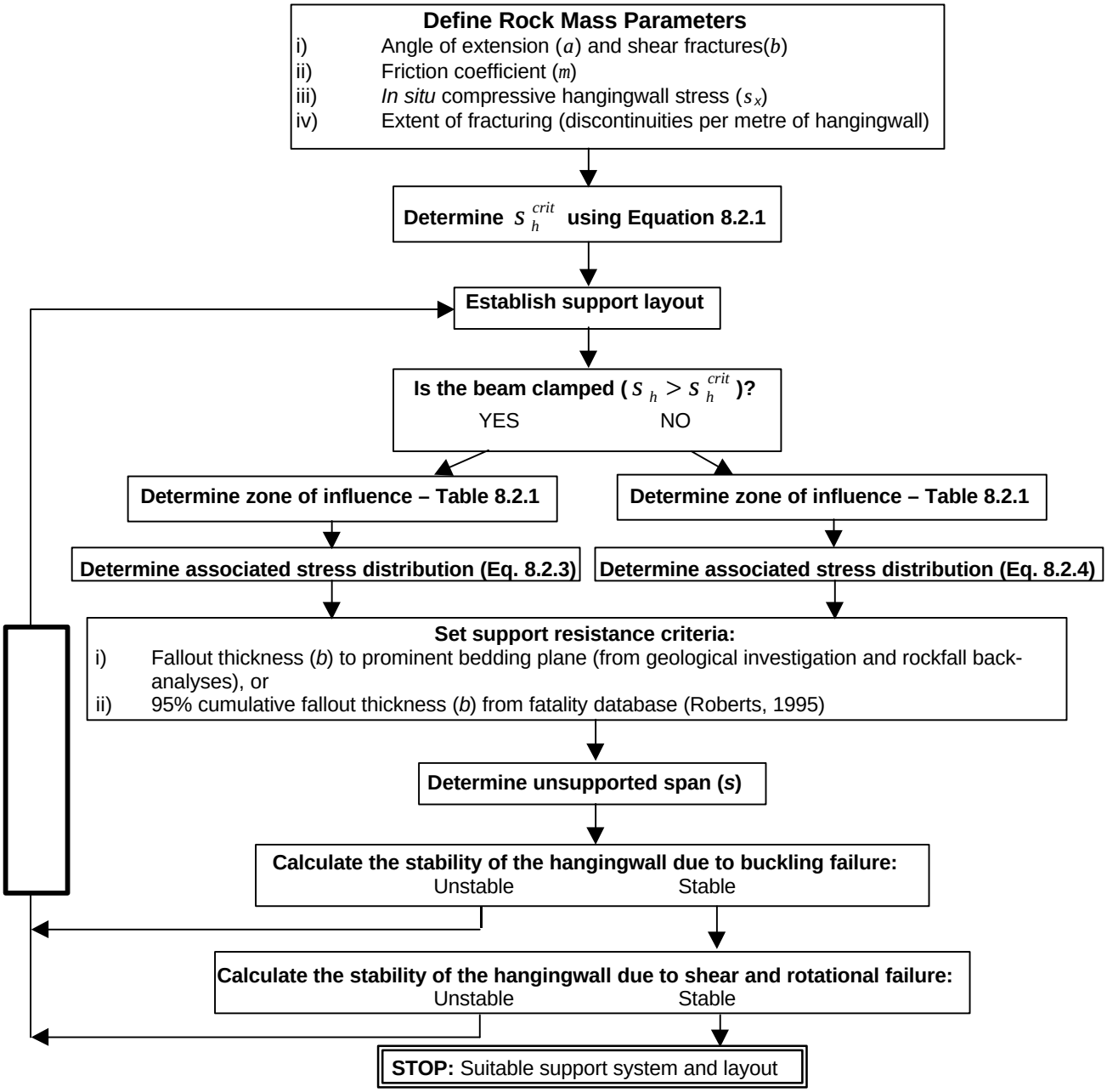

Figure 8.4.5 Proposed design flow chart for the rockfall case.

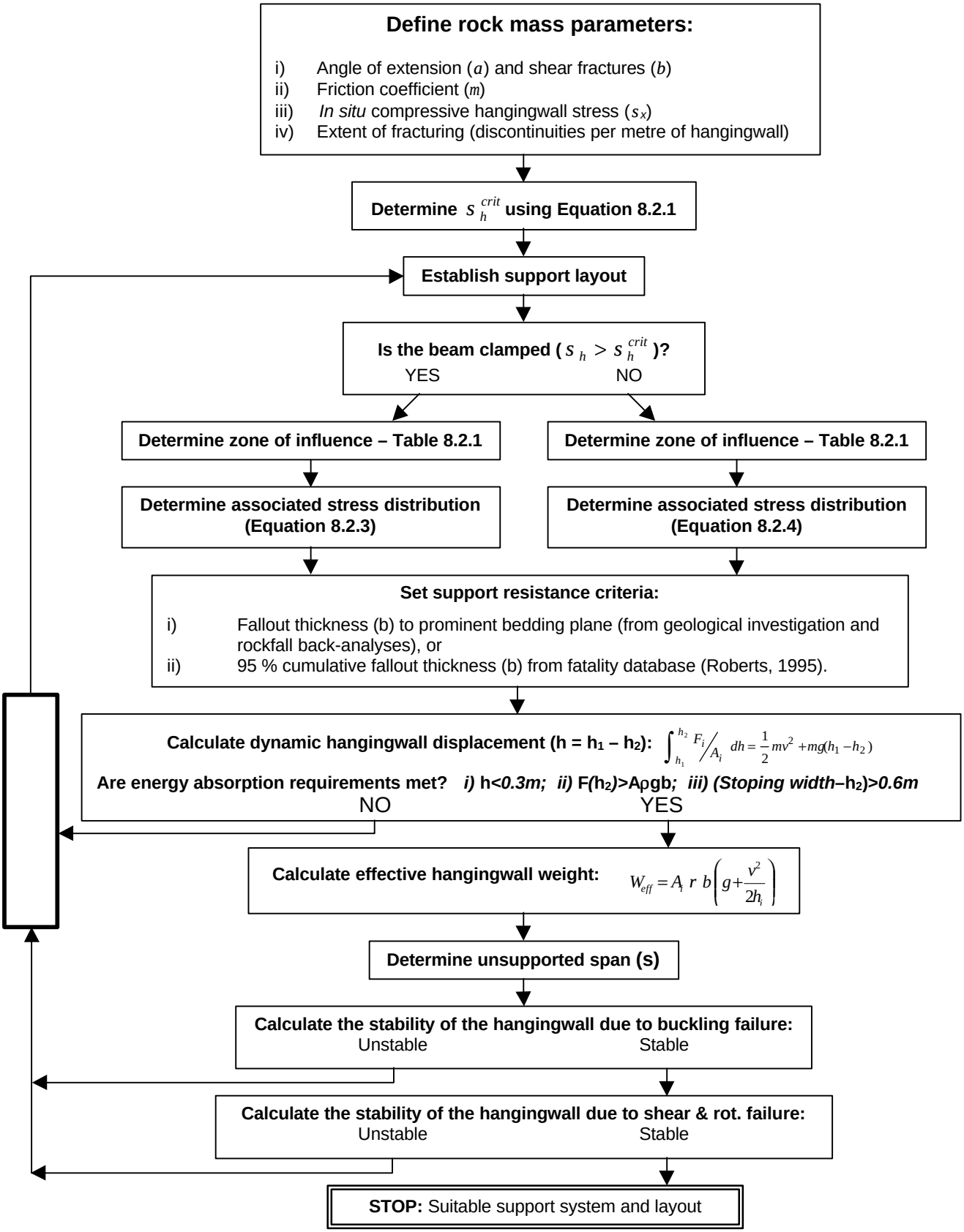

Figure 8.4.6 Proposed design flowchart for the rockburst case.

8.5 Support design example

Support design example

To illustrate the calculation procedure using the equations derived in Chapter 4, the following example is given.

1. Calculate the maximum support spacing for rockfall conditions for the given rock mass parameters,
(i) using the current SDA II design methodology, and
(ii) using the proposed design methodology

b = 1,0 m	(beam thickness)
j = 20^o	(bedding plane friction angle)
f = 60^o	(friction angle between fracture surfaces)
r = 2700 kg/m^3	(density of hangingwall beam)
F = 200 kN	(support force)
r = 0,08 m	(support radius)
s_h = 1,0 MPa	(horizontal clamping stress)
a = 45^o	(extension fracture orientation)
b = 65^o	(shear fracture orientation)

Note:
For the beam to be stable, the actual unsupported span of the hangingwall beam, L, must be less than or equal to the maximum stable span, L_s:

$$L \leq L_s \qquad (8.5.1)$$

The limiting equilibrium of the keyblock is governed by one of two failure mechanisms: (i) shear failure due to slip at the abutments and/or block rotation, and (ii) buckling failure. Figure 8.5.1 gives stability envelopes for the hangingwall at limiting equilibrium for s_x = 1,0 MPa, b = 1,0 m and m = tan 40^o.

1(i) ***Approach 1: Considering only keyblock analysis (current SDA II methodology)***

From Figure 8.5.1, the maximum stable span (L_s) can be read off as L_s = 2,0 m for the given combination.

The maximum support spacing (centre to centre) is given by

$L_{max} = L_s + 2r = 2{,}0 + 2(0{,}08) = 2{,}16$ m.

1 (ii) ***Approach 2: Considering keyblock and zones of influence analyses (proposed methodology)***

Using the new methodology, involving zones of support influence:

$z_y = z_y + r = b \tan j + r = 0{,}36 + 0{,}08 = 0{,}44$ m

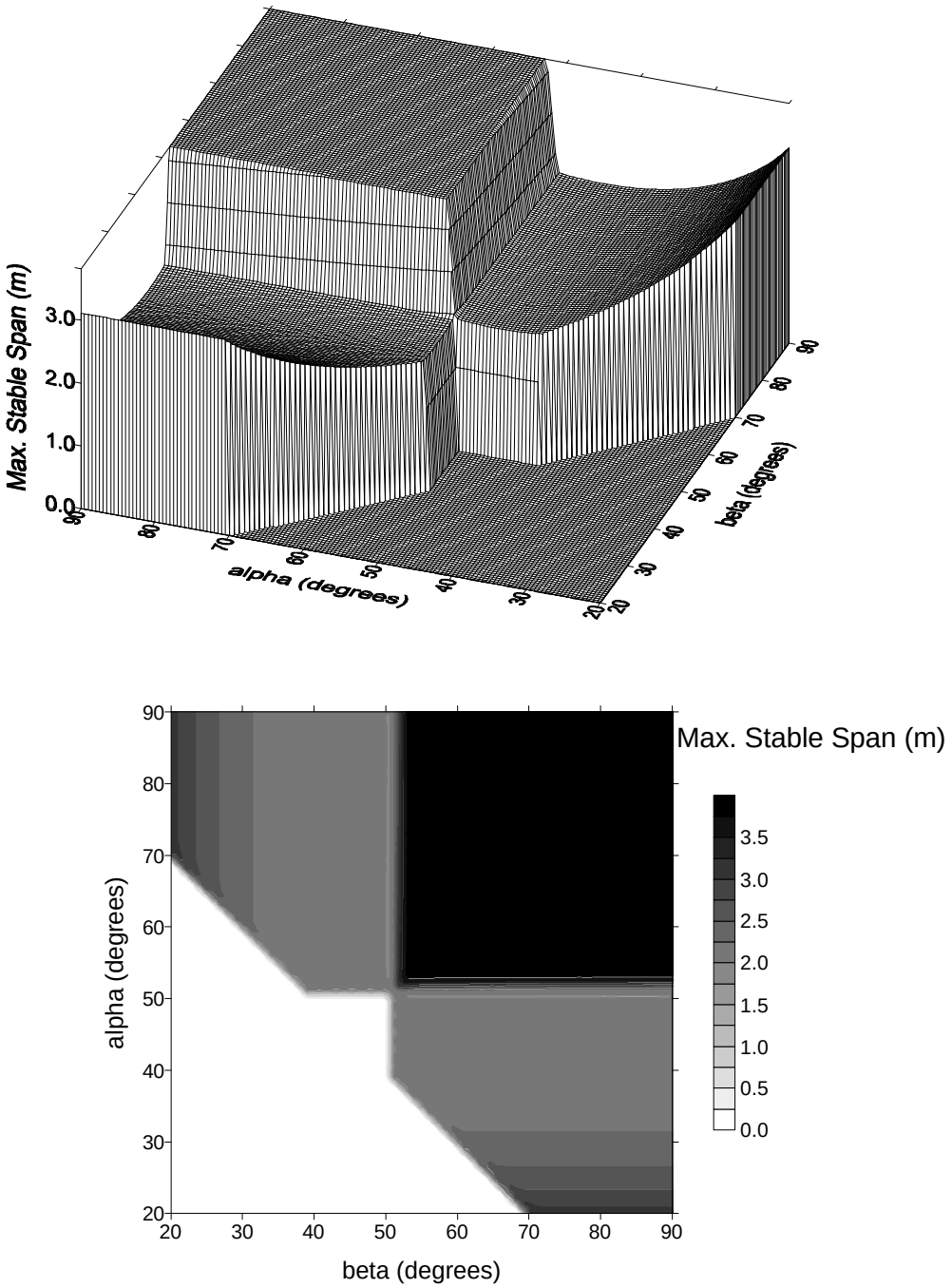

Figure 8.5.1 ***Maximum stable span versus discontinuity angles for s_x = 1.0 MPa, b = 1.0 m and m = tan 40^o. Both carpet (top) and contour (bottom) plots are given to facilitate convenient data interpretation.***

By substituting the above values into Equation 8.2.1, the critical horizontal stress is calculated as 636 kPa, thus $s_h > s_h^{crit}$, and the equation for determining the stress profile for a homogenous beam can be used (Equation 8.2.3).

$z = b \tan j = (1{,}0) \tan 20^o = (1{,}0)\ (0{,}36) = 0{,}36$ m

$z = z + r = 0{,}36 + 0{,}08 = 0{,}44$ m

The maximum stress (above the centre of the support, where $x = 0$ and $y = 0$) can be calculated (using Equation 8.2.3), as:

$s_{max} = (2F) / (\pi z^2) = (2)(200) / (\pi)(0{,}44)^2 = 657{,}7$ kN/m^2

The support resistance criterion:

$s_{req} = r\ g\ b = 27\ kN/m^2$

The length of the hangingwall beam is calculated as the distance between the two points where $s(x,y) = s_{req}$. Re-writing Equation 8.2.3, and substituting $s_{req} = 27\ kN/m^2$, $F = 200$ kN, $z = 0{,}44$ m and $y = 0$ into the equation, gives $x_{req} = 0{,}43$ m (Figure 8.5.2).

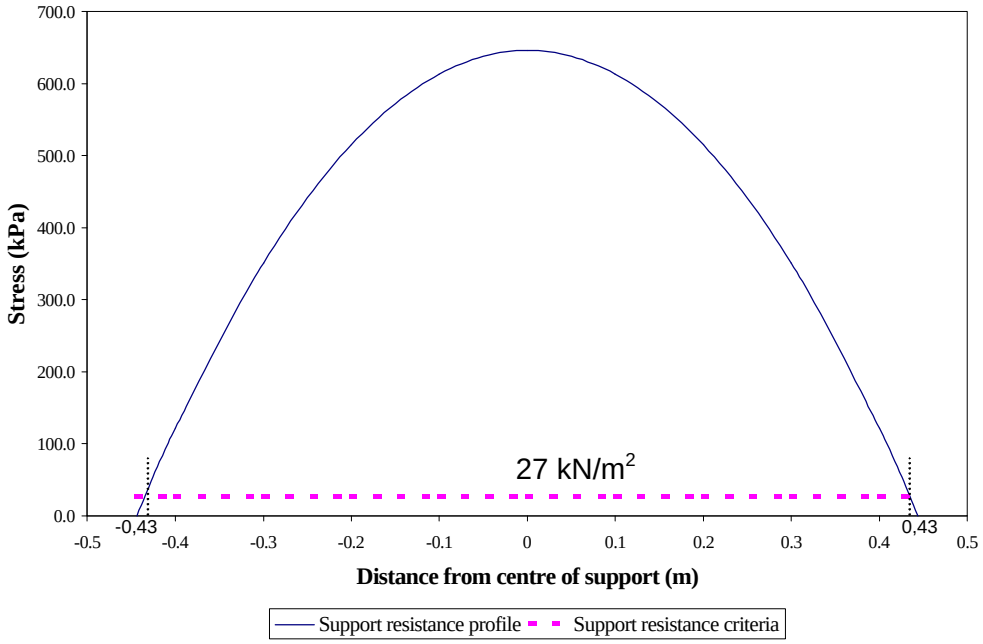

Figure 8.5.2 Stress profile of a support unit and the required support resistance

As mentioned before, the maximum stable hangingwall beam span (from Figure 8.5.1) is $L_s = 2{,}0$ m.

The maximum support spacing (centre to centre) for the case under consideration is given by $L_{max} = L_s + 2x_{req} = 2{,}0 + 2(0{,}43) = 2{,}86$ m.

Using the proposed design methodology, a maximum support spacing of 2,86 m can be used, whereas the current methodology does not allow for a spacing of greater than 2,16 m for this specific case. Thus, if proven to be applicable underground, this design method will provide a more optimal support design tool than is presently the case.

> *It is estimated that, for the total gold and platinum mining industry, every increase of 10 cm in support unit spacing results in an annual saving of R 70m (6%) in support costs (Hagan, 1997). Hence, by optimising support design, the potential for significant cost savings exists.*

The following table shows the influence of various bedding plane heights and bedding plane friction angles on the maximum supportable span. The following maximum centre-to-centre spacings were calculated for the $45^o/65^o$ fracture combination for supports with $r = 80$ mm, where $s_h = 1{,}0$ MPa and $f = 40^o$.

Table 8.5.1 Maximum centre-to-centre spacing for various bedding plane height and friction angle combinations.

Bedding plane friction angle (j)	Fallout height (b)	L_{max} *(Approach 1)*	L_{max} *(Approach 2)*
20^o	0,5 m	1,41 m	1,77 m
20^o	1,0 m	2,16 m	2,86 m
30^o	0,5 m	1,41m	1,98m
30^o	1,0 m	2,16 m	3,26 m
40^o	0,5 m	1,41 m	2,24 m
40^o	1,0 m	2,16 m	3,67 m

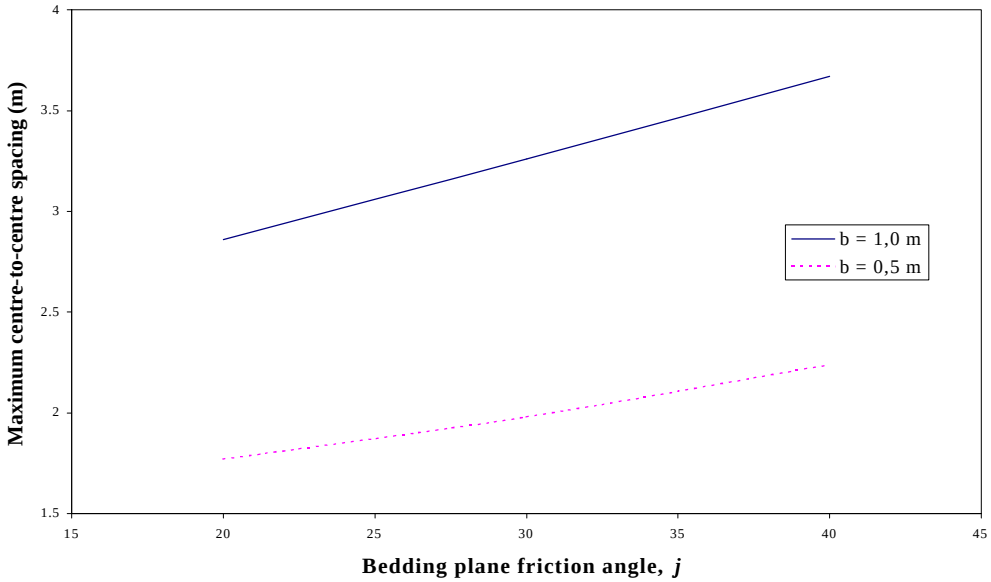

Figure 8.5.3 Maximum centre-to-centre spacing for various bedding plane height and friction angle combinations (using Approach 2).

Note that in this example, the calculated support spacing is for rockfall conditions. A similar design procedure (see Figure 8.4.6) can be followed to determine optimum support spacing for rockburst conditions. In all cases, the maximum stable support spacing for rockburst conditions is less than for rockfall conditions.

8.6 An engineering approach to the design of support systems in tabular stopes

8.6.1 Introduction

An engineering approach to the design of support systems, in particular the support strength, energy absorption and spacing requirements, is proposed. The approach makes use of models and support design methodologies developed as part of SIMRAC projects GAP032 'Stope and Gully Support' (Roberts, 1995), GAP330 'Stope Face Support Systems' (Daehnke *et al.*, 1998), GAP335 'Strata Control in Tunnels' (Haile *et al.*, 1998), and this project. The findings of these projects culminate in comparatively complex theoretical models describing the rock mass interaction with support units and support requirements during quasi-static and dynamic loading conditions.

The design method proposed here combines the salient findings of the above-mentioned projects to provide a unified support design methodology for rockfall and rockburst conditions in different geotechnical areas. This design tool is of practical value and enables the rock engineer to make initial designs of appropriate support systems by using a few comparatively straightforward graphs.

It is emphasised, however, that certain assumptions are made during the design process. To ensure rock mass stability and reduce rock-related hazards, these assumptions are generally conservative, i.e. the resulting support system is marginally over-designed. To fully optimise the support system, it is recommended that the complete models developed by, specifically, SIMRAC projects GAP330, GAP335 and this project be applied. It is further recommended that appropriate software, such as SDA II (Daehnke *et al.*, 1999), be used to expedite the more accurate evaluation of support systems.

The core of the design methodology proposed here is a set of seven graphs, which facilitate the design of support systems under various loading and geotechnical conditions. These graphs are given below, and their associated assumptions and design implications are discussed. For convenience, design flowcharts leading to the correct application of the graphs, as well as the graphs themselves, are given in Section 8.6.3. Finally, support design examples for rockfall and rockburst conditions are also given in Section 8.6.3.

8.6.2 Support design graphs

8.6.2.1 Fundamental tributary area requirements for rockfall conditions

Figure 8.6.1 gives the maximum tributary area (A_T) that can be supported by a single support unit for rockfall conditions. The tributary area is given as a function of the height of potential rock mass instability and support force. The height of instability (b) is commonly governed by the position of bedding planes, and should be determined from previous rock mass instabilities and FOGs.

The basic tributary area relationship, $F = r\ g\ b\ A_T$, can be re-written as:

$$A_T = \frac{F}{r\ g\ b}\ , \tag{8.6.1}$$

where: A_T = maximum tributary area (m^2),
F = support unit load (N),
r = rock density (2700 kg/m^3),
g = acceleration due to gravity (10 m/s^2), and
b = height of instability (m).

Figure 8.6.1 shows the relationship given by Equation 8.6.1 graphically.

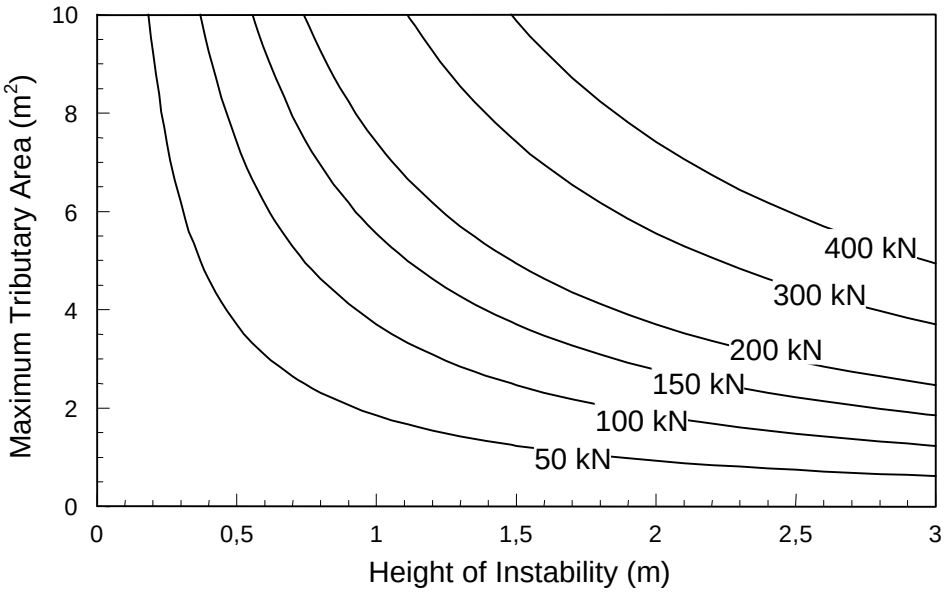

Figure 8.6.1 Tributary area requirements for rockfall conditions.

Assume that a support unit with the force versus deformation characteristics shown in Figure 8.6.2 is used. It is further assumed that the closure rate, as measured in the stope, is 20 mm per metre of face advance, and the support unit should maintain rock mass stability if the face is advanced a further 10 m. This implies that for at least 200 mm of closure the support unit needs to carry sufficient load to meet the tributary area requirements.

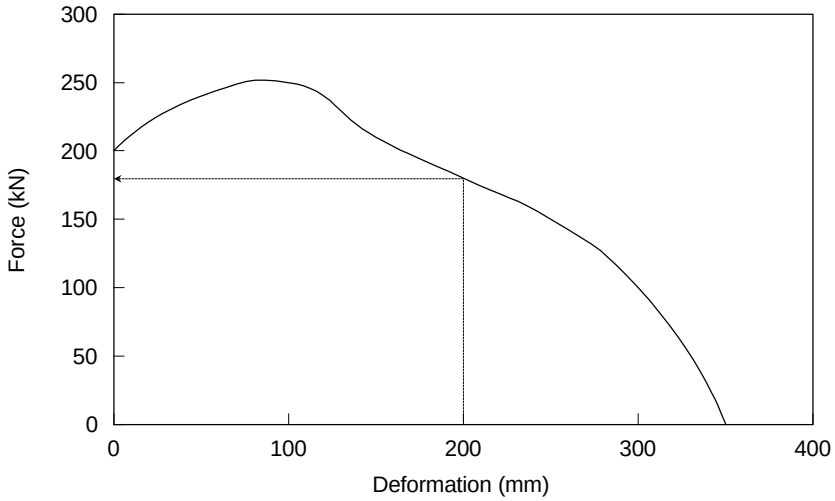

Figure 8.6.2 Design force versus deformation curve of hypothetical support unit (in this example the support unit was initially pre-stressed to 200 kN).

At 200 mm deformation the support unit carries a load of 180 kN. For the rock mass to be stable over this deformation range (based on the tributary area criterion), the maximum tributary area should not exceed 4,5 m^2 (determined from Figure 8.6.1, assuming F = 180 kN and b = 1,5 m).

8.6.2.2 Fundamental tributary area requirements for rockburst conditions

Energy absorption (rockburst) requirements based on the tributary area criterion follow analogously to the support resistance (rockfall) case. Figure 8.6.3 gives the maximum tributary area as a function of the height of instability and the energy absorption capacity of the support unit. The relationship is based on the well-known kinetic and potential energy absorption criteria (Wagner, 1984), i.e. $E_a = 0{,}5\ m\ v^2 + m\ g\ h$, where $m = r\ b\ A_T$. The relationship is re-written as:

$$A_T = \frac{E_a}{r\, b\,(0{,}5v^2 + gh)} \quad , \tag{8.6.2}$$

where: A_T = maximum tributary area (m^2),
E_a = energy absorption capacity of the support unit (J),
r = rock mass density (2700 kg/m^3),
b = height of instability (m),
v = rock ejection velocity (3 m/s),
g = acceleration due to gravity (10 m/s^2), and
h = hangingwall displacement during dynamic event (0,2 m).

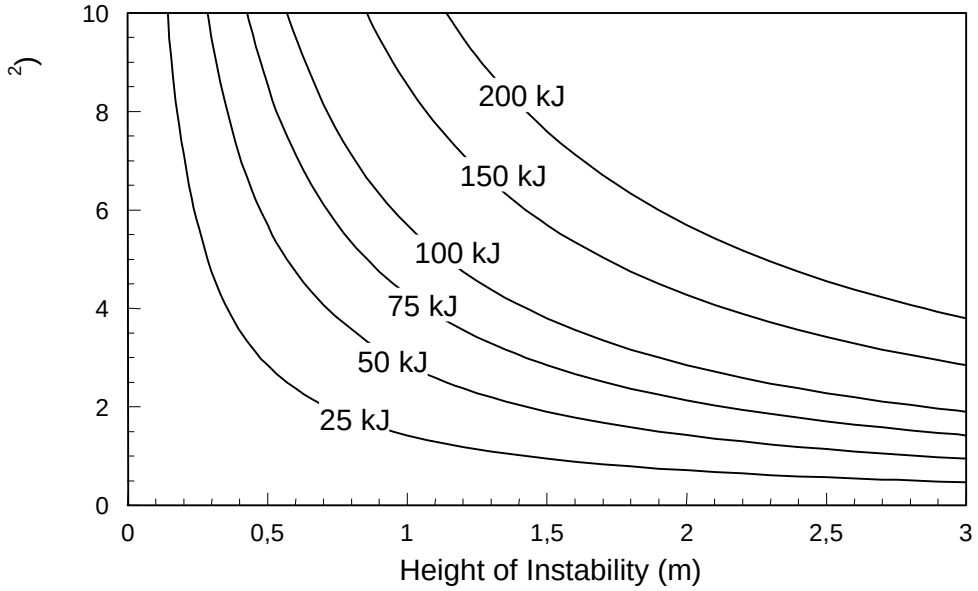

Figure 8.6.3 Tributary area requirements for rockburst conditions.

The use of Figure 8.6.3 is illustrated by means of an example. Assume that a support unit is used with a force versus deformation curve as shown in Figure 8.6.2. The design requirements are that as the face is advanced a further 5 m, the support unit must maintain rock mass stability during a rockburst and retain a support resistance after dynamic deformation of mg. Stope closure is 20 mm per metre of face advance, i.e. the support unit needs to maintain rockburst stability after having been compressed by up to 100 mm of quasi-static closure. Figure 8.6.4 graphically illustrates the remaining energy absorption capacity of the support unit (calculated by the area under the force versus deformation curve).

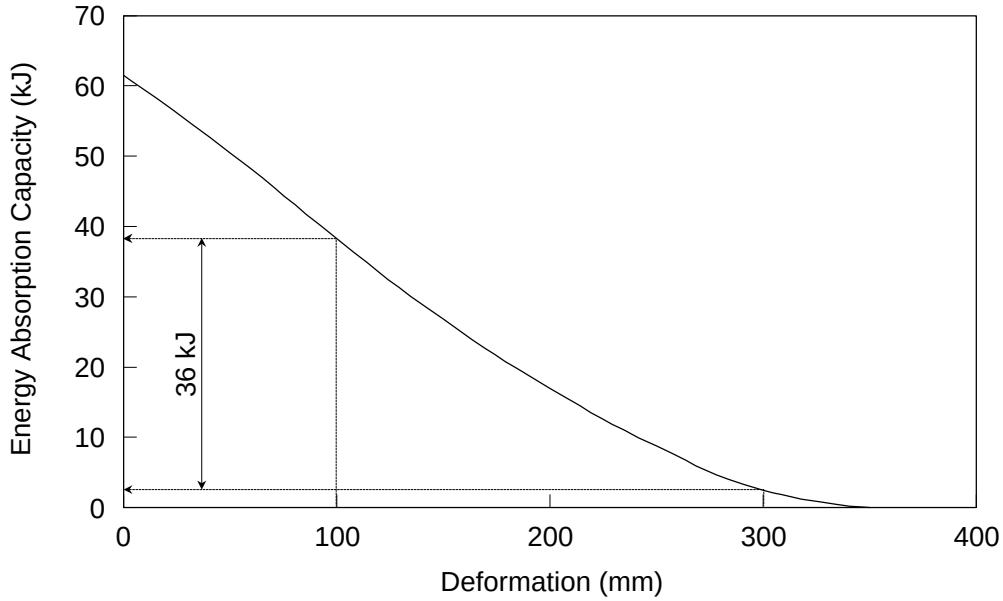

Figure 8.6.4 Remaining energy absorption capacity of the hypothetical support unit.

From Figure 8.6.4 it is apparent that after 100 mm of deformation 38 kJ of energy absorption capacity remains available. The hangingwall is assumed to displace dynamically over a distance of 0,2 m, i.e. up to 300 mm deformation. At this point only 2 kJ energy absorption capacity remains. The change in energy absorption capacity, i.e. $\Delta E_a = E_a(100 \text{ mm}) - E_a(300 \text{ mm}) = 36 \text{ kJ}$, is the amount of energy available. The tributary area criterion is based on this amount of energy, i.e. in this example 36 kJ. From Figure 8.6.3 it is apparent that the maximum tributary area should not exceed 1,5 m^2 (assuming E_a = 36 kJ and b = 1,5 m).

Two further criteria, which need to be considered when designing rockburst resistant support systems, are:

1. The load carried by the support unit after the rockburst must exceed the corresponding tributary area load. In this example F(300 mm) = 100 kN, which is adequate to support the tributary area load = $r\ g\ b\ T_A$ = 61 kN. (If the load carried by the support unit after the rockburst is less than the tributary area load, a different support unit should be chosen or the support spacing reduced.)

2. The stoping width minus the total closure after the rockburst should be adequate to prevent injury to, and allow movement of, mine personnel. A minimum post-rockburst stoping width of 0,6 m is recommended, i.e. in the example given here the initial stoping width should not be less than 0,9 m.

In the design method given here a dynamic hangingwall displacement of 0,2 m is assumed. In practice the downward movement of the hangingwall is dependent on the support reaction and, for example, a support system providing high support resistance will arrest the hangingwall within a shorter distance. In this case the potential energy component is decreased and hence the total energy absorption requirements are reduced. In practice most support systems will decelerate the hangingwall over a distance less than 0,2 m. The h = 0,2 m assumption made here is conservative. To fully optimise support systems the use of the SDA II software is recommended, where the value of h is explicitly calculated for each support unit.

8.6.2.3 Support spacing requirements for rockfall conditions and hangingwalls with face-parallel fractures (FPFs)

The tributary area requirements reviewed in Sections 8.6.2.1 and 8.6.2.2 are adequate to address general stability requirements of a continuous, unfractured hangingwall beam. In

practice, however, the hangingwall is discretised by joints and mining induced fractures. In a highly discontinuous hangingwall the tributary area criteria are not sufficient to ensure rock mass stability and, in addition, the rock mass stability between adjacent support units needs to be considered.

In this section the stability criteria of a hangingwall with FPFs are developed. The failure of hangingwalls with FPFs is generally characterised by keyblock failure (sliding and rotational failure) and beam buckling. An example of a hangingwall with FPFs is given in Figure 8.6.5.

Figure 8.6.5 Example of a hangingwall with FPFs.

The work conducted as part of SIMRAC project GAP330 (Daehnke *et al.*, 1998) and this project, quantified the rotational, sliding and buckling stability envelopes of hangingwall keyblocks. It was found that the stability is predominantly governed by the keyblock height (b) and the angles of the discontinuities discretising the keyblock, a and b (see Figure 8.6.6). In intermediate and deep level mines the angles a and b are normally defined by face parallel mining induced extension and shear fractures.

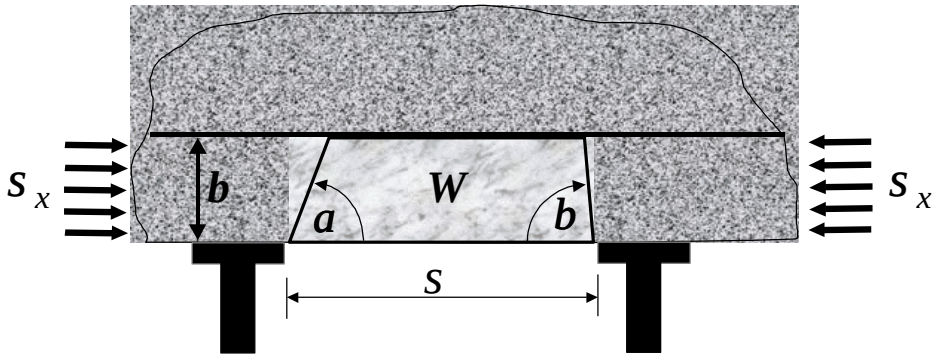

Figure 8.6.6 Critical keyblock parameters influencing the rock mass stability.

It was further found that the compressive hangingwall stresses contribute towards the hangingwall stability. In the design method proposed here, a compressive stress of s_x = 1 MPa is assumed. In deep level mines s_x might exceed 1 MPa, however, until further *in situ* measurements have been made, s_x = 1 MPa is considered an appropriately conservative assumption for the purposes of designing support systems.

Figure 8.6.7 gives stability envelopes of keyblocks based on instability height (b), support force (F), unsupported span (s), discontinuity angles (a and b), and g, where $g = 90^o - f$ and f is the apparent friction angle associated with the fracture surfaces. Due to the interlocking and matching surfaces of mining induced fractures, the apparent friction angle (f) is relatively high, and values of 40^o to 50^o are considered realistic.

Two main stability zones are given in Figure 8.6.7:

(i) **Dark grey zone:** Here the keyblocks are discretised by shallow dipping fractures and keyblock rotation and subsequent sliding is likely. In this zone the stability of keyblocks is governed by overlapping zones of support influence, and the work conducted as part of this project is applied to estimate maximum stable unsupported spans, whilst maintaining rock mass stability. In quantifying the extent of the zones of support influence, a bedding plane friction angle of 20^o is assumed.

(ii) **Light grey zone:** Relatively steeply dipping fractures reduce the possibility of block rotation and failure is generally governed by beam buckling. Note that in this case the zones of influence also contribute towards the hangingwall stability, and the maximum stable unsupported spans are consequently extended. The extent of this zone is dependent on the fractured hangingwall stiffness. Data from Bandis *et al.* (1983) was used to estimate the stiffness of the fractured hangingwall (for further details see Daehnke e*t al.*, 1998).

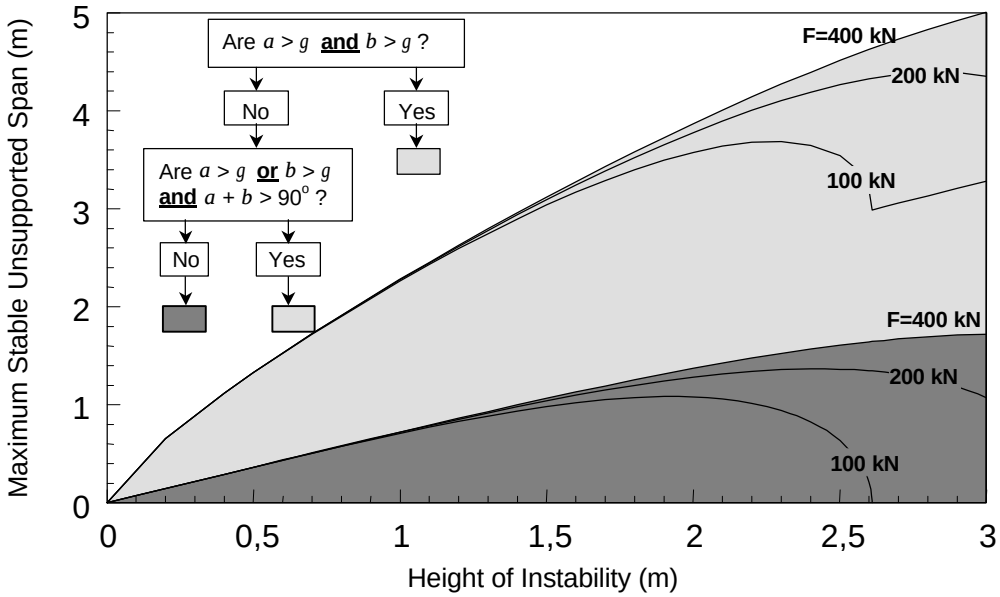

Figure 8.6.7 Rockfall stability envelopes for hangingwalls with FPFs as a function of instability height, unsupported span, support load and discontinuity orientation ($g = 90^o - f$, where f is the friction angle associated with the fracture surfaces).

As an example, consider the stability of a hangingwall discretised by face-parallel extension and shear fractures dipping at $a = 50^o$ and $b = 30^o$, respectively and $g = 40^o$.

Are $a > g$ and $b > g$? No.

Are $a > g$ or $b > g$ **and** $a + b > 90^o$? No

Since $a + b < 90^o$, the dark grey stability zone is applicable (using the flowchart in Figure 8.6.7). Assuming a support unit load of F = 200 kN and height of instability b = 1,5 m, the maximum stable unsupported span is determined from Figure 8.6.7 as 1,0 m. Note that, by installing props with headboards, the unsupported span remains the same, but the prop spacing can be increased by the length of the load spreader.

If $a = 60^o$ and $b = 80^o$ and the friction angle is assumed to be $f = 40^o$ (hence $g = 50^o$), the stability zone is determined by the light grey area. From Figure 8.6.7 the maximum unsupported span is given as 3,0 m (assuming F = 200 kN and b = 1,5 m).

It is emphasised that the above stability zones are simplified approximations of the stability envelopes developed as part of GAP330 (Daehnke *et al.*, 1998,) and this project. To fully

optimise the support systems, it is recommended that the SDA II software or the 3D stability plots given by Daehnke *et al.* (1998, 1999) are used.

8.6.2.4 Support spacing requirements for rockburst conditions and hangingwalls with face-parallel fractures (FPFs)

The stability requirements for rockburst conditions and hangingwalls with FPFs follow analogously to the rockfall case. The hangingwall is assumed to be accelerated to a velocity of 3 m/s, which is decelerated over a distance of 0,2 m. The extent of the zones of support influence is calculated for an effective hangingwall weight taking into account the rock mass deceleration (see Daehnke *et al.*, 1998, 1999 for a description of the effective hangingwall weight concept).

Figure 8.6.8 gives the stability envelopes for rockburst conditions of a hangingwall with FPFs. As in the rockfall case, two stability zones (light and dark grey) are shown. The appropriate stability zone is dependent on the discontinuity angles (a and b) and friction angle (f).

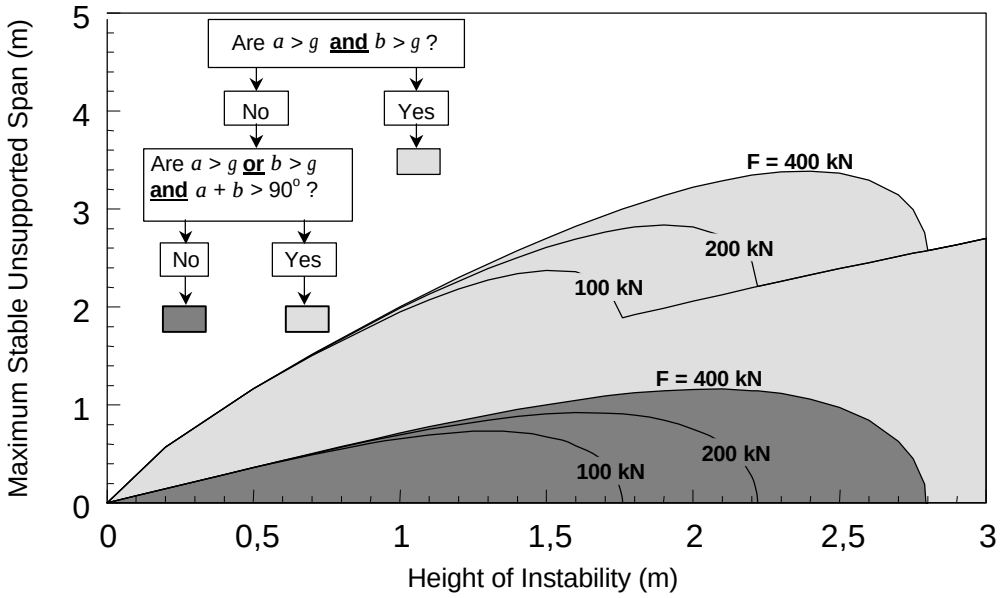

Figure 8.6.8 Rockburst stability envelopes for hangingwalls with FPFs as a function of instability height, unsupported span, support load and discontinuity orientation ($g = 90^o - f$, where f is the friction angle associated with the fracture surfaces).

As an example, consider the stability of the same hangingwall discretised by face-parallel extension and shear fractures dipping at $a = 50^o$ and $b = 30^o$, respectively and $g = 40^o$ used in the previous section.

Are $a > g$ and $b > g$? No.

Are $a > g$ or $b > g$ **and** $a + b > 90^o$? No

Since $a + b < 90^o$, the dark grey stability zone is applicable (using the flowchart in Figure 8.6.8). Assuming a support unit load of $F = 200$ kN and height of instability $b = 1,5$ m, the maximum stable unsupported span is determined from Figure 8.6.8 as 0,9 m. (This is slightly less than for the rockfall case.) Note that, by installing props with headboards, the unsupported span remains the same, but the prop spacing can be increased by the length of the load spreader.

8.6.2.5 Support spacing requirements for rockfall conditions and blocky hangingwalls

The support spacing requirements described in Sections 8.6.2.3 and 8.6.2.4 are only applicable if the hangingwall stability is controlled by sliding, rotating or buckling keyblocks. This section summarises a second approach to support spacing requirements, which is particularly applicable for blocky hangingwall conditions (see, for example, Figure 8.6.9). The design charts are based on work conducted as part of SIMRAC project GAP335 (Haile *et al.*, 1998), and can be used to design the spacing requirements of both prop and tendon support units. A fundamental assumption of the design procedure given here is that, when applied to tendon support, the tendons are anchored beyond the potentially unstable zone into the more competent overlying rock mass.

Figure 8.6.9 Example of a blocky hangingwall.

Haile *et al.* (1998) found that the critical rock mass parameters determining the stability of blocky rock mass structures are the aspect ratio and the volume of the blocks. Based on the findings of numerical models, these two parameters were found to satisfactorily express the variations in size and geometry of the blocks that make up the rock mass structure, and reflect their relative stability. This correlation is best expressed in the form of a log-log plot, where linear divisions between the rock mass classes, which are based on the relative stability with regard to rock mass unravelling potential, are made (Figure 8.6.10). Also indicated on this chart are equivalent RQD (Rock Quality Designation) values as derived from the work of Palmstrøm (1996).

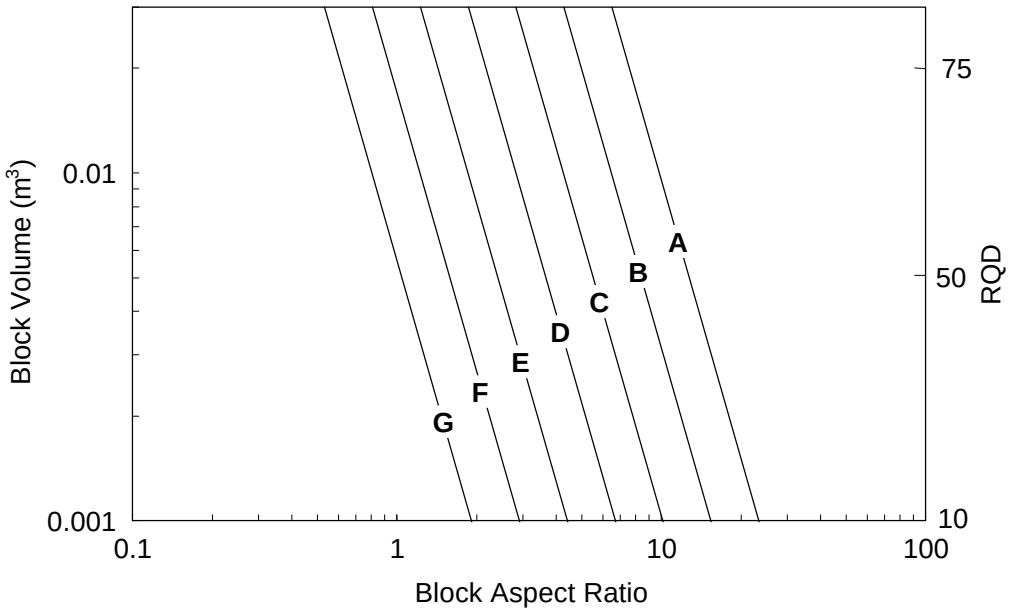

Figure 8.6.10 ***Classification of a rock mass on the basis of the aspect ratio parallel to the hangingwall skin and the volume of the blocks.***

Once the rock mass classification is established, the stability of the rock mass between adjacent support units can be determined. This relationship, as derived from numerical modelling (Haile *et al.*, 1998), is illustrated in Figure 8.6.11. The relationship is given as a function of depth of instability, from a completely stable span, to a 1,5 m depth of instability. In practice, it is desirable to ensure a completely stable span at all times. In certain situations, however, a limited amount of rock fallout between adjacent support units may occur. If the resulting arches are unstable areal support coverage is required to prevent rock hazard to the stope workers.

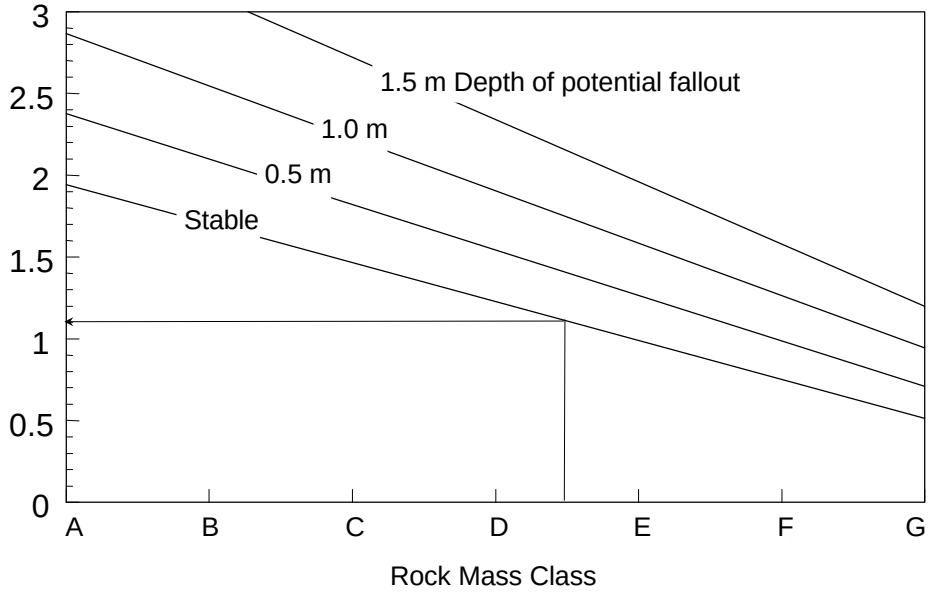

Figure 8.6.11 ***Maximum unsupported span for blocky rock mass structures as a function of rock mass class and depth of instability (rockfall conditions).***

An example is given to illustrate the application of Figures 8.6.10 and 8.6.11. Consider a blocky rock mass structure with blocks that are approximately 15 cm in length in the strike direction, 30 cm in the dip direction, with a thickness of 5 cm. This would give an average estimated block volume of 0,002 m^3 and an average aspect ratio in the strike direction of 3 and in the dip

direction of 6. For a simplified analysis the average aspect ratio (4,5) should be used. For a more detailed analysis the spacing in the strike and dip directions can be related to the aspect ratios in the corresponding directions, i.e. Figures 8.6.10 and 8.6.11 are used twice to determine the strike and dip spacing based on the respective aspect ratios.

From Figure 8.6.10, considering an aspect ratio of 4,5 and block volume of 0,002 m^2, a rock mass class of D/E is found. Using Figure 8.6.11, a rock mass class of D/E implies a maximum unsupported span of 1,1 m to ensure a stable hangingwall. The recommended support spacing is applicable for both prop and tendon support spacing, provided the tendons are long enough to be anchored in competent rock.

8.6.2.6 Support spacing requirements for rockburst conditions and blocky hangingwalls

For rockburst conditions Figure 8.6.10 is used to determine the appropriate rock mass class, based on the geometrical parameters of the blocks. Figure 8.6.12 is then applied to estimate maximum unsupported spans as a function of rock mass class and depth of instability. Figure 8.6.12 is based on dynamic correction factors established by Haile *et al.* (1998), where the block ejection velocity is assumed to be 3 m/s and the reduced support spacing for dynamic conditions is proportional to the anticipated increase in the depth of instability.

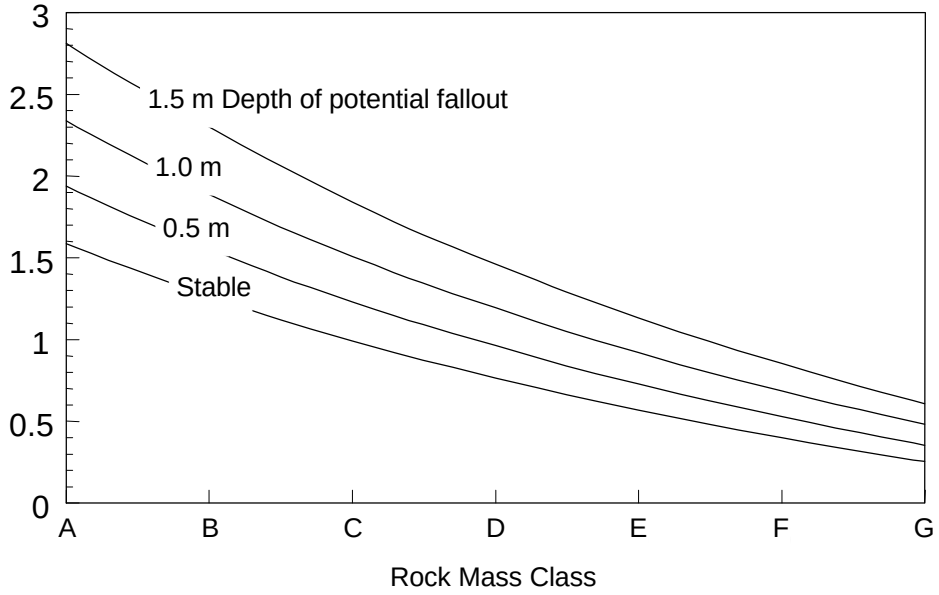

Figure 8.6.12 ***Maximum unsupported span for blocky rock mass structures as a function of rock mass class and depth of instability (rockburst conditions).***

8.6.2.7 Support spacing calculation procedure

Support spacing for hangingwalls with FPFs

The support design method gives insights into spacing and associated stable hangingwall spans in the strike direction only. Due to the face-parallel mining-induced fracture orientation in intermediate and deep level mines, the hangingwall rock is generally less prone to failure between two support units in the dip direction, compared to failure between units in the strike direction. Probabilistic keyblock analyses (Daehnke *et al*., 1998) have shown that, for a typical discontinuity spacing and attitude as encountered in intermediate depth and deep gold mines, the support spacing in the dip direction can be increased by a factor of ± 1,5 compared with the strike spacing, while maintaining an equal probability of keyblock failure in the dip versus strike

direction. Hence, to propose a prudent system, it is recommended that the support spacing in the dip direction can be up to but should not exceed 1,5 times the spacing in the strike direction. This simplifies the design procedure by eliminating the need for complicated three-dimensional analyses. Furthermore, this relationship has been found to be generally valid in practice, but, however, may not apply in blocky ground such as can be expected in sections of lagging panels which intersect siding parallel fractures.

In order to determine the strike and dip spacing of support units, the following calculation procedure is proposed:

Calculate s_{s1} from the tributary area spacing requirements using the following equation:

$$s_{s1} = \sqrt{\frac{T_A}{1{,}5}} \, . \tag{8.6.3}$$

Calculate s_{s2} from the hangingwalls with FPFs stability analyses (from Figures III and IV).

The centre-to-centre strike spacing (s_s) is calculated as:

$$s_s = \min \begin{cases} s_{s1} \\ s_{s2} + w \end{cases}, \tag{8.6.4}$$

where w = width of the support unit or headboard.

The unsupported span in the dip direction can be up to but must not exceed 1,5 times the unsupported span in the strike direction.

Support spacing for blocky hangingwalls

Calculate s_{s1} from the tributary area spacing requirements using the following equation:

$$s_{s1} = \sqrt{T_A} \, . \tag{8.6.6}$$

Calculate s_{s2} from the blocky hangingwalls stability analyses (from Figures V and VI).

The centre-to-centre strike spacing (s_s) is calculated as:

$$s_s = \min \begin{cases} s_{s1} \\ s_{s2} + w \end{cases}, \tag{8.6.7}$$

and the centre-to-centre dip spacing, s_d, as

$$s_d \approx s_s \, . \tag{8.6.8}$$

8.6.3 Support design procedures

In this section support design procedures, based on (i) shallow and intermediate/deep mines and (ii) hangingwalls with face-parallel fractures and blocky hangingwalls, are proposed. Design flowcharts are given to facilitate the convenient use of the appropriate design charts.

Shallow Mines

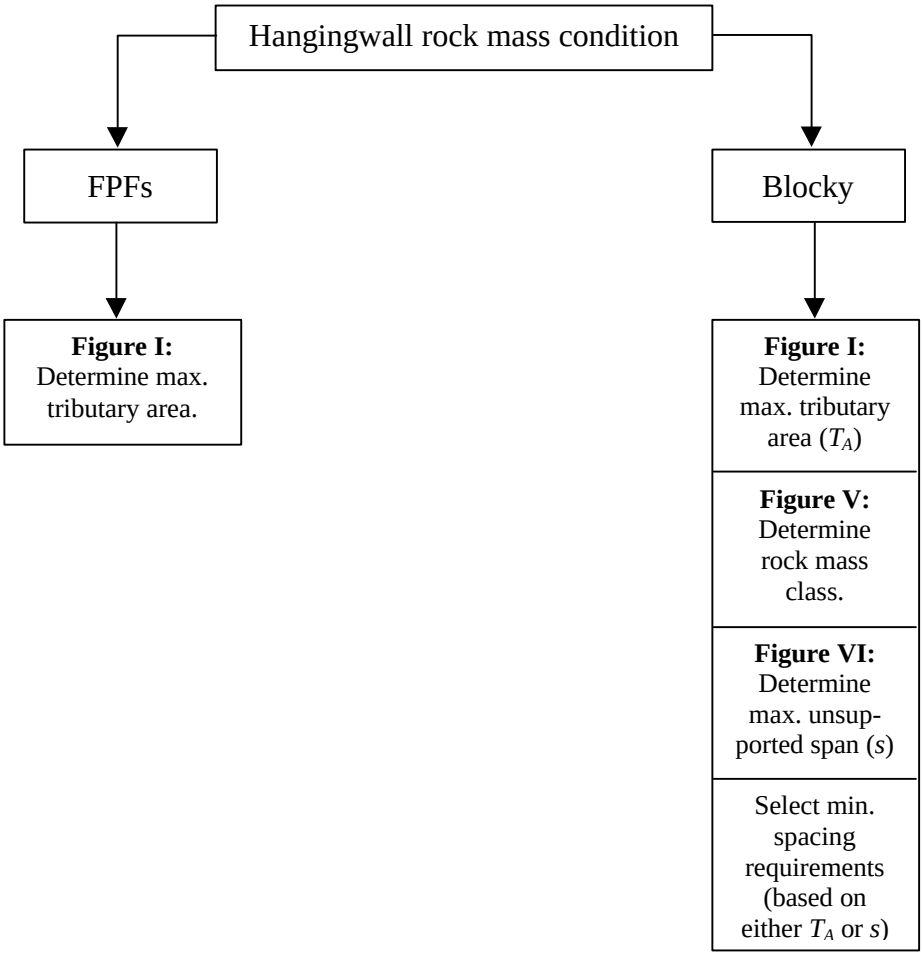

Figure 8.6.13 Design flowchart for shallow mines

Intermediate and Deep Level Mines

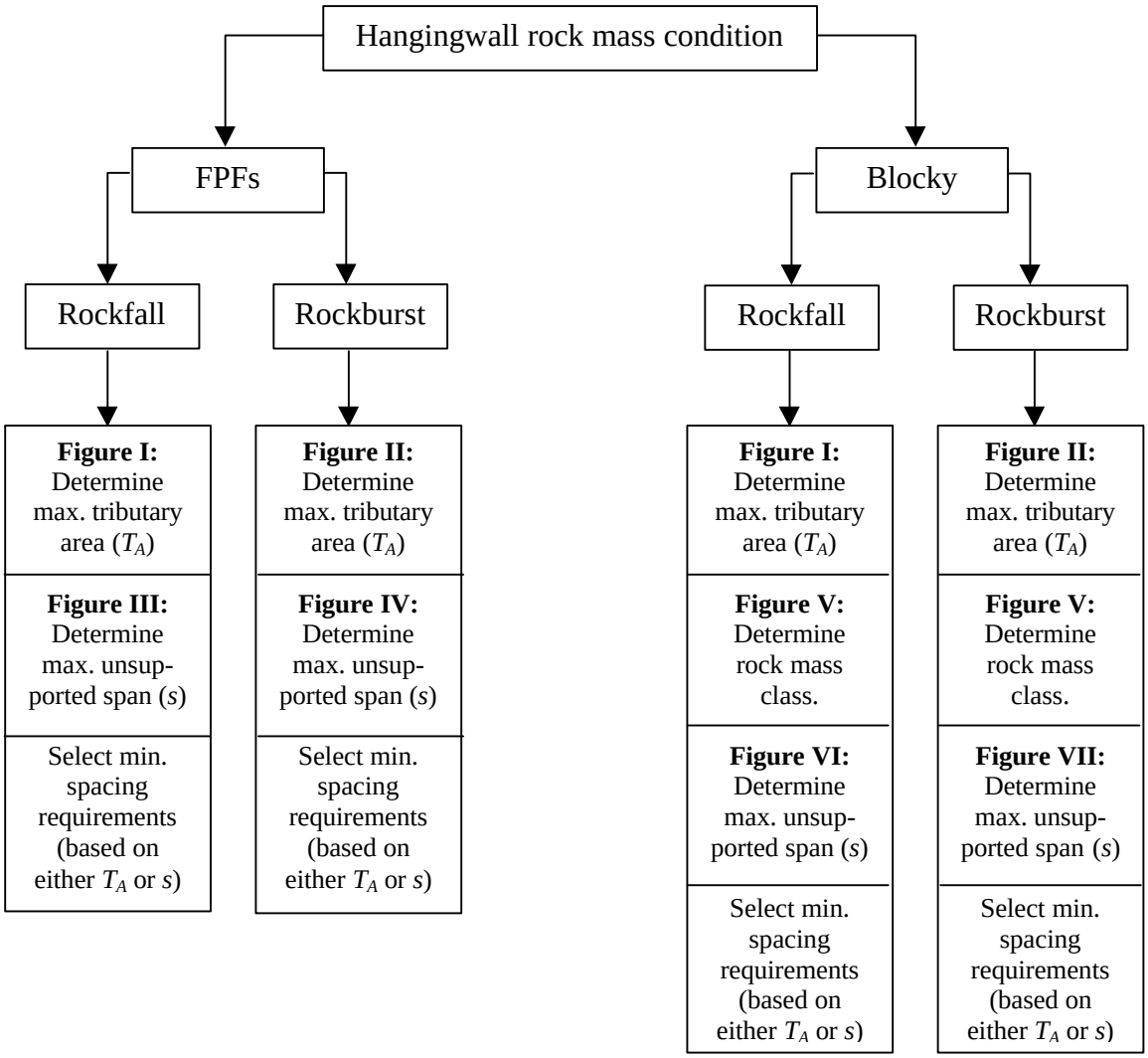

Figure 8.6.14 Design flowchart for intermediate- and deep-level mines

Tributary Area Analyses

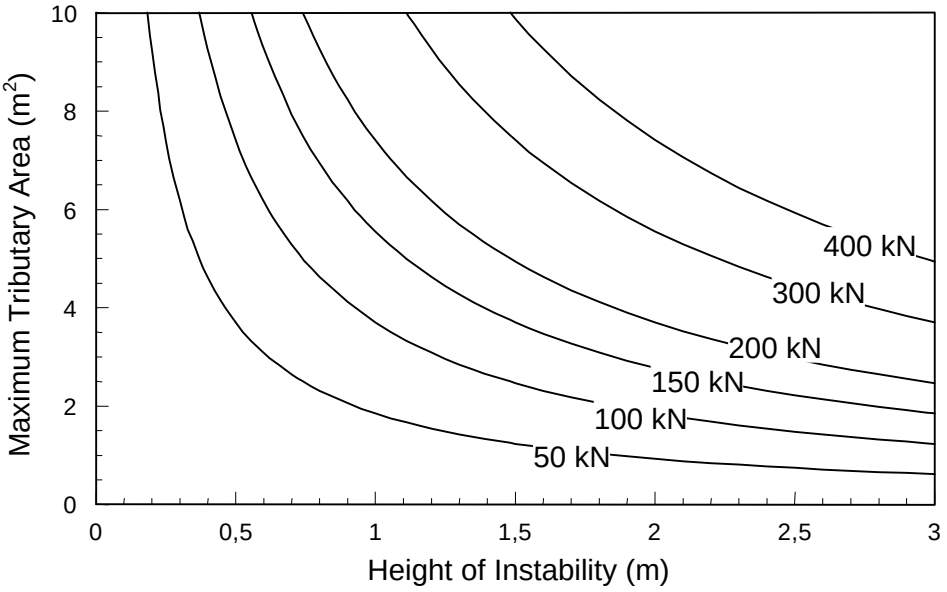

Figure I ***Tributary area requirements for rockfall conditions.***

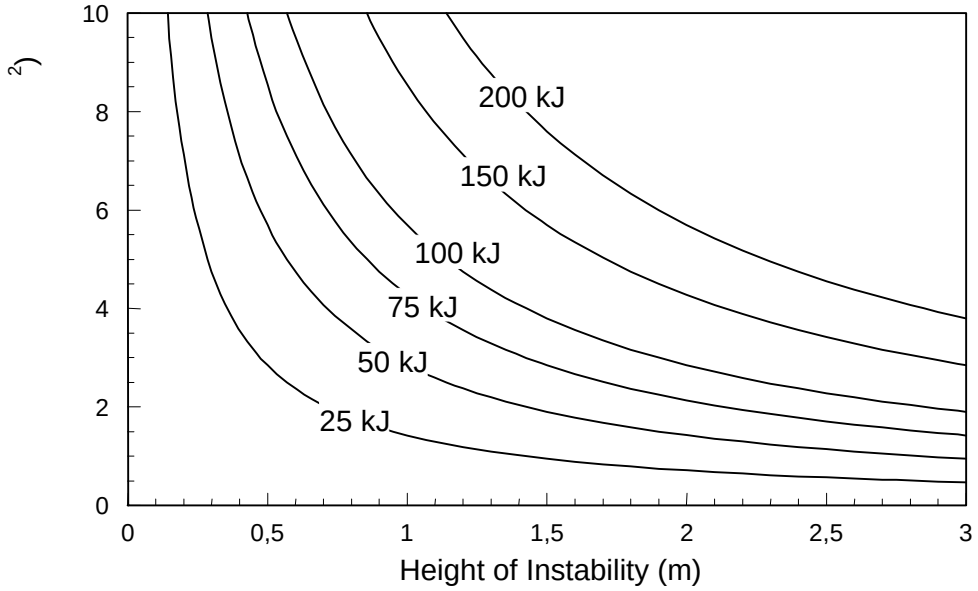

Figure II ***Tributary area requirements for rockburst conditions.***

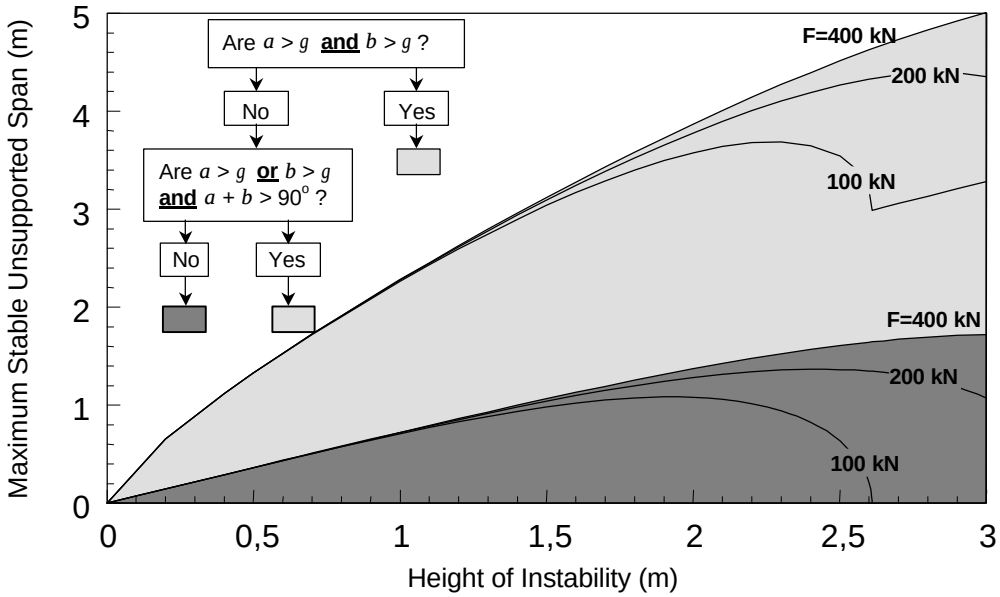

Figure III ***Rockfall stability envelopes for hangingwalls with FPFs ($g = 90^o - f$, where f is the friction angle associated with the fracture surfaces).***

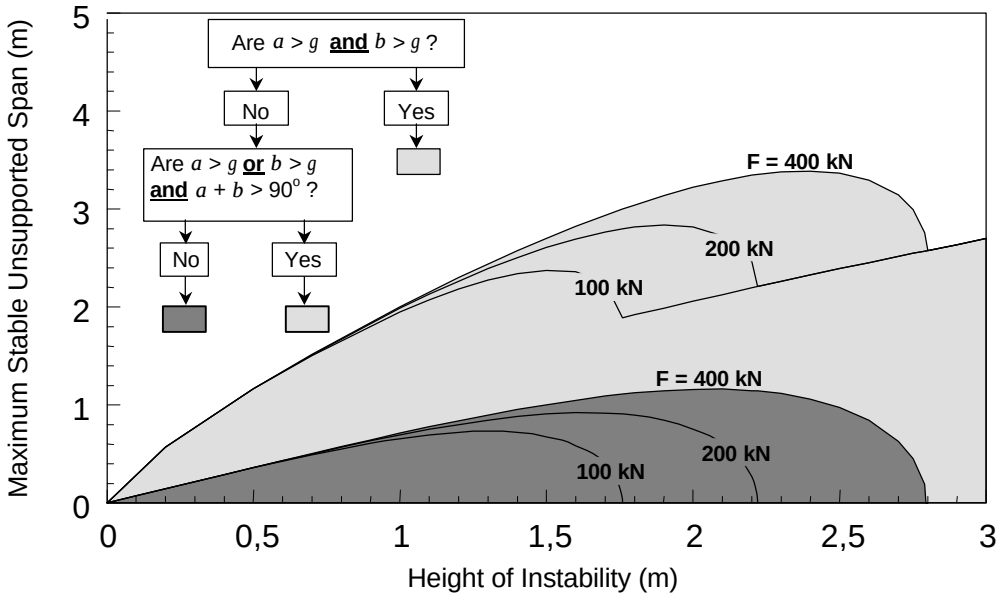

Figure IV ***Rockburst stability envelopes for hangingwalls with FPFs ($g = 90^o - f$, where f is the friction angle associated with the fracture surfaces).***

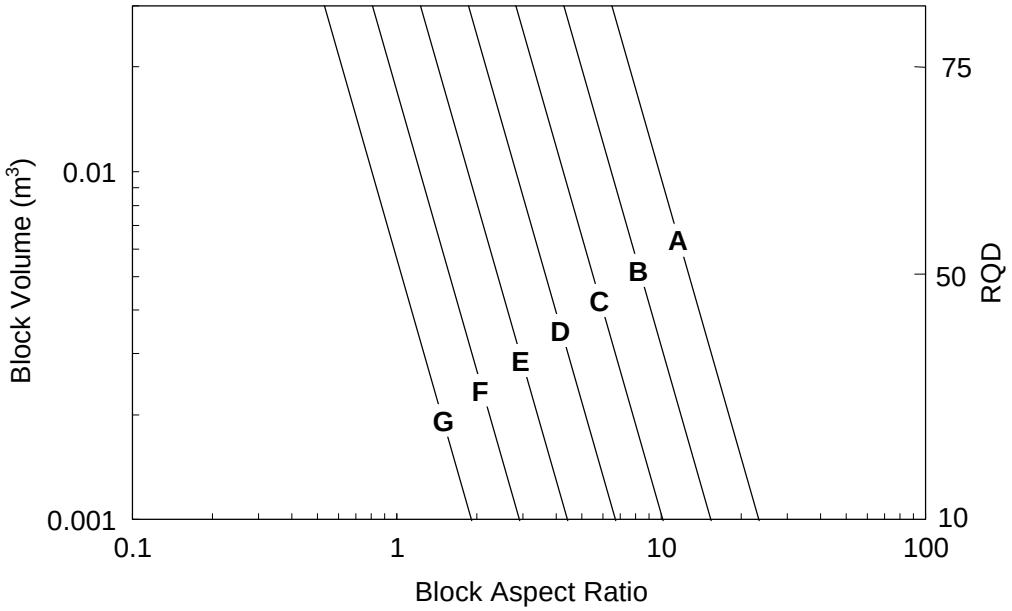

Figure V ***Classification of a rock mass on the basis of the aspect ratio parallel to the hangingwall skin and the volume of the blocks.***

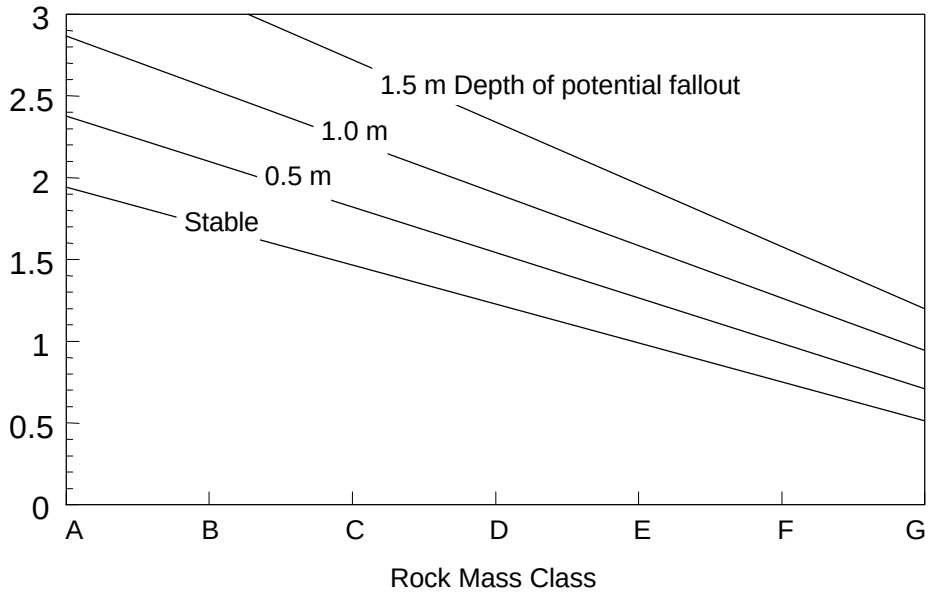

Figure VI ***Maximum unsupported span for blocky rock mass structures as a function of rock mass class and depth of instability (rockfall conditions).***

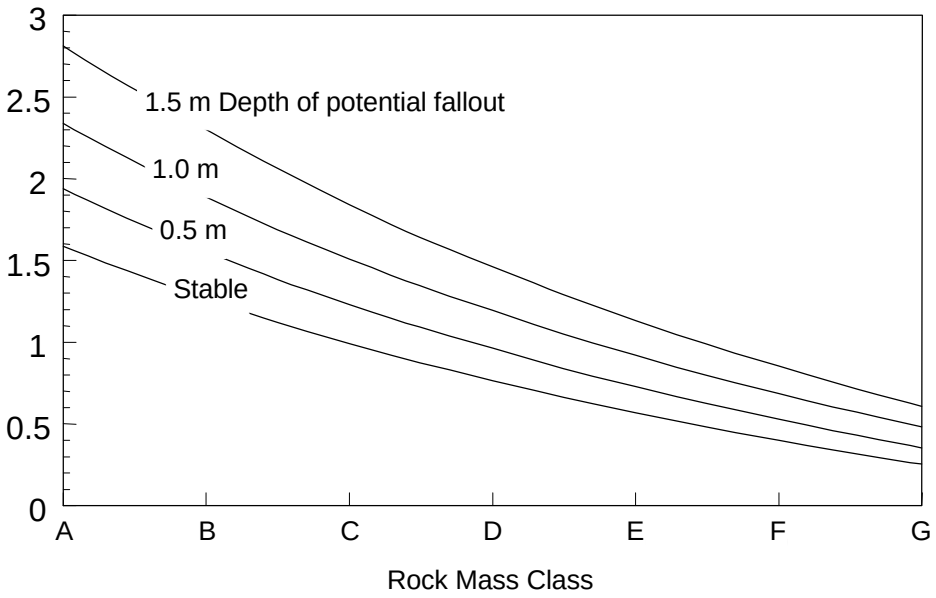

Figure VII ***Maximum unsupported span for blocky rock mass structures as a function of rock mass class and depth of instability (rockburst conditions).***

Support Design Example

To illustrate the support design procedure, the optimum spacing of Loadmaster props in an intermediate depth mine for rockfall and rockburst conditions is determined. The height of instability (hangingwall beam thickness) is 1,0 m, the closure rate is 20 mm per metre of face advance, the stoping width is 1,6 m, and the hangingwall is discretised by extension and shear fractures dipping at 80^o and 60^o, respectively. The hangingwall is smooth, and the sliding, rotational and buckling failure of keyblocks governs the hangingwall stability.

Rockfall Conditions:

1. *Determine force versus deformation characteristics of Loadmaster props:*
   By means of laboratory compression tests, the 1,6 m Loadmaster force versus deformation characteristics shown in Figure 8.6.15 were established (the characteristics of the most commonly used elongate types are given in Daehnke *et al.*, 1998). Ten laboratory compression tests were conducted and Figure 8.6.15 shows the mean of the ten tests, as well as the 90 % probability curve (further details of probability curves are given by Daehnke *et al.*, 1998). In this example, the 90 % probability curve is used as the reference force versus deformation curve of the Loadmaster prop.

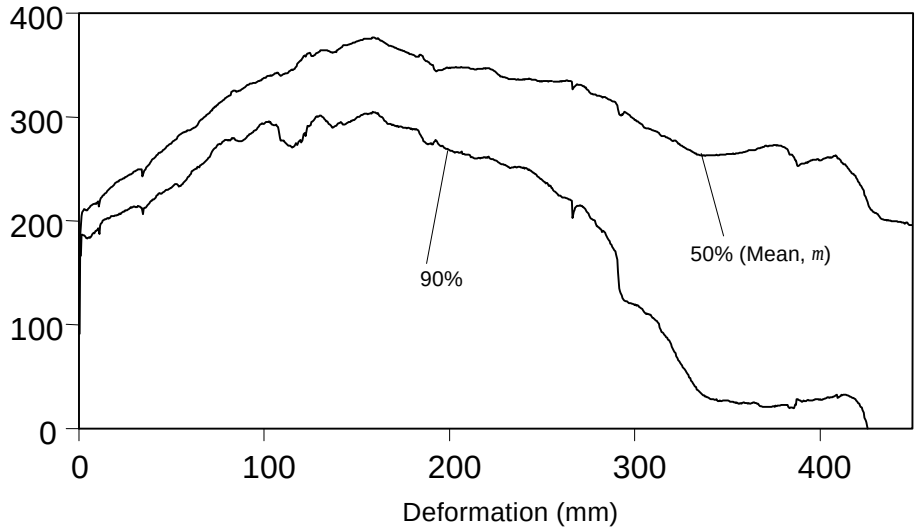

Figure 8.6.15 Force versus deformation characteristics of the Loadmaster prop.

The Loadmaster reference curve is downgraded for loading rate by the following equation (Roberts, 1995):

$$F_{u/g} = F_{lab}\left[m\log\left(\frac{v_{u/g}}{v_{lab}}\right)+1\right],$$

where:
- $F_{u/g}$ = adjusted force
- F_{lab} = original force as measured during laboratory test
- v_{lab} = laboratory test velocity
- $v_{u/g}$ = underground site velocity
- m = empirically determined correction factors,
  where: m = 0,123 for rockbursts, and
  m = 0,084 for rockfalls.

The corrected 90 % design curve is shown in Figure 8.6.16 (v_{lab} = 30 mm/min, $v_{u/g}$ = 20 mm/day assuming the face is advanced every day).

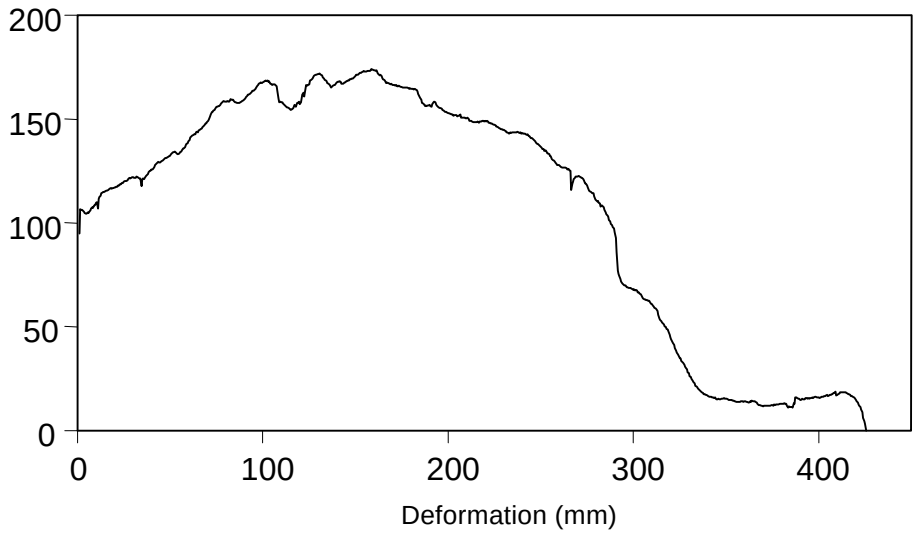

Figure 8.6.16 Corrected Loadmaster reference curve (90 % probability).

Correction factors for stoping width are given by Roberts (1995). Since the stoping width in this example is 1,6 m, and the length of the laboratory tested Loadmaster was 1,6 m, no correction for prop height is necessary.

2. *Tributary area spacing requirements:*
From Figure 8.6.16 it is apparent that the prop is initially set at a load of 100 kN. The yield load exceeds this value up to a total deformation of 290 mm. At a closure rate of 20 mm/m face advance, this implies that the prop will exceed 100 kN up to a distance of 14.5 m behind the stope face. This is considered a suitable working lifespan for the prop to ensure hangingwall stability in the working area, and hence the tributary area spacing requirements are based on a single support unit carrying 100 kN. From Figure I it is evident that, with F = 100 kN and height of instability b = 1,0 m, the maximum tributary area should not exceed 3,6 m^2.

3. *Hangingwall with FPFs stability analysis:*
For extension and shear fracture angles of $a = 80^o$ and $b = 60^o$, respectively, the light grey zone of Figure III is applicable (assuming the friction angle $f = 40^o$). The maximum unsupported span in the strike direction, at b = 1,0 m, is 2,2 m.

The recommended support spacing should be based on the minimum of the tributary area spacing and the maximum unsupported strike span requirements. When using props without headboards, the strike spacing (centre to centre) of the props is approximately equal to the unsupported span. Hence, $T_A = s_s \times s_d$, where T_A is the tributary area and s_s, s_d are the strike and dip spacing of support units and, in this example, $T_A \leq 3{,}6$ m^2. Using Equation 8.6.3, s_{s1} is calculated as

$$s_{s1} = \sqrt{\frac{T_A}{1{,}5}} = \sqrt{\frac{3{,}6}{1{,}5}} = \sqrt{2{,}4} = 1{,}5$$, and from the hangingwall with FPFs stability analysis, s_{s2} = 2,2 m.

Substituting these values into Equation 8.6.4, the strike spacing, s_s, can be calculated as

$$s_s = \min\begin{cases} s_{s1} \\ s_{s2} \end{cases} = \min\begin{cases} 1{,}5 \\ 2{,}2 \end{cases} = 1{,}5 .$$

The dip spacing can be up to, but must not exceed 1,5s_s = 2,25 m. Thus, a strike spacing of 1,5 m and dip spacing of 2,2 m is recommended.

<u>Rockburst Conditions:</u>

1. *Determine the energy absorption capacity of Loadmaster props:*
Figure 8.6.17 shows the force versus deformation characteristics of a Loadmaster prop loaded dynamically. The mean of ten laboratory compression tests, as well as the 90 % probability curve, is given. The prop was initially compressed at a slow rate over a distance of 80 mm. Thereafter

the prop was rapidly compressed at a rate of 3 m/s over a distance of 200 mm, followed once again by slow loading.

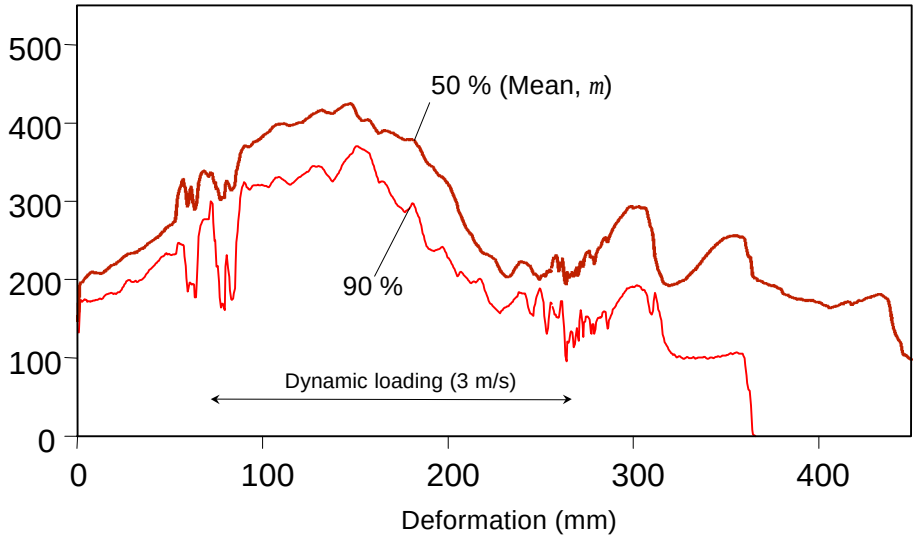

Figure 8.6.17 Dynamic force versus deformation characteristics of the Loadmaster prop.

Figure 8.6.18 gives the remaining energy absorption capacity of the Loadmaster prop. From the graph it is apparent that between 80 mm and 280 mm dynamic compression, 50,8 kJ of energy is absorbed.

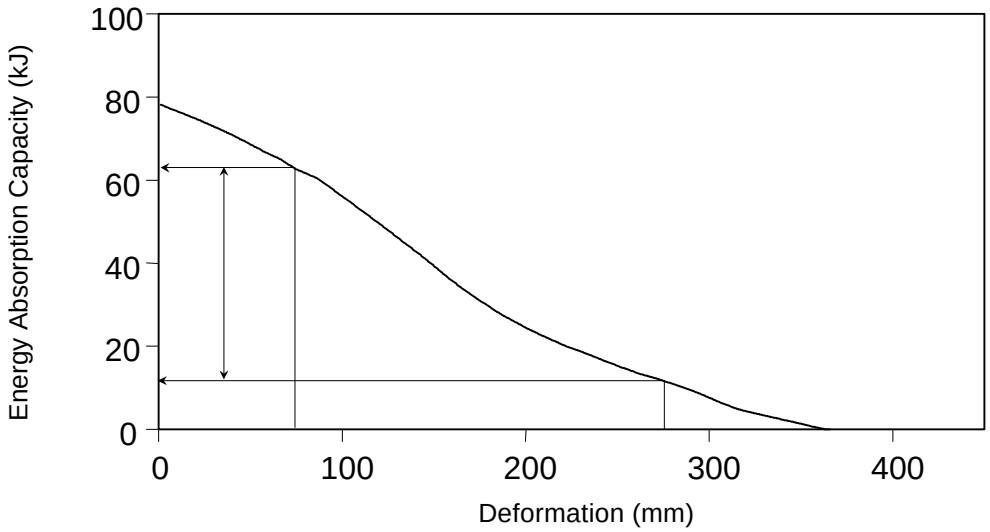

Figure 8.6.18 Energy absorption capacity of the Loadmaster prop.

2. *Tributary area spacing requirements:*
Assuming the prop is subjected to rockburst loading (3 m/s over 0,2 m) after 80 mm of quasi-static convergence, 50,8 kJ of energy can be absorbed. From Figure II, at a height of instability of 1,0 m and 50 kJ, the maximum tributary area for rockburst conditions is found to be 2,9 m^2.

Further rockburst support criteria that need to be satisfied are:

(i) The load carried by the support unit after the rockburst must exceed the corresponding tributary area load. In this example F(280 mm) = 110 kN (from Figure 8.6.16), which is adequate to support the tributary area load = $r\ g\ b\ T_A$ = 78 kN.

(ii) The stoping width minus the total closure after the rockburst should be adequate to prevent injury to and allow movement of mine personnel (> 0,6 m is recommended). In the example given here the initial stoping width is 1,6 m and thus the post-rockburst stoping width (1,6 m – 0,08 m – 0,2 m = 1,32 m) is adequate.

Note that by checking the energy absorption capacity of the prop after 80 mm of quasi-static convergence, it is implied that the prop will meet the rockburst criteria as the face is advaced a

further 4 m (80 mm / 20 mm/m face advance). At prop to face distances exceeding 4 m plus the installation distance from the face, the rockburst criteria are not necessarily met and the energy absorption capacity, post-rockburst support resistance or post-rockburst stoping width may be inadequate.

3. *Hangingwall with FPFs stability analysis:*
For extension and shear fracture angles of a = 80° and b = 60°, respectively, the light grey zone of Figure IV is applicable (assuming a friction angle of f = 40°). The maximum unsupported span in the strike direction, at b = 1,0 m, is 1,9 m.

To summarise, the maximum tributary area is 2,9 m^2 and the maximum strike spacing of the support units is 1,9 m.

From Equation 8.6.3,

$$s_{s1} = \sqrt{\frac{T_A}{1{,}5}} = \sqrt{\frac{2{,}9}{1{,}5}} = \sqrt{1{,}9} = 1{,}4 ,$$

and from the hangingwall with FPFs stability analysis, $s_{s2} = 1{,}9$. Thus, s_s = 1,4 m (from Equation 8.6.4).

The dip spacing can be up to, but must not exceed 1,5s_s = 2,1 m.

A strike spacing of 1,4 m and a dip spacing of 2,0 m is considered suitable.

Note that in the case of shallow dipping fractures (a < 50° and b < 50° if the fracture surface friction angle f = 40°) the maximum strike spacing is limited to 0,75 m and 0,65 m for rockfall and rockburst conditions, respectively (determined from Figures III and IV for b = 1,0 m). In this case considerably closer support spacing and/or the use of strike parallel headboards is recommended.

For hangingwall conditions in which both the stability of keyblocks, as well as the unravelling of a blocky rock mass structure governs the rock mass integrity, it is recommended to determine the maximum stable spans for both blocky hangingwalls and hangingwalls with FPFs. In this case, the ultimate support spacing to be used should be the minimum of the blocky hangingwall and hangingwall with FPFs analyses.

Finally, the rock engineer should at all times apply his/her engineering judgement to design support systems offering a high probability of rock mass stability. The work presented here considers only two fundamental failure mechanisms and may well be unsuitable for particular geotechnical areas. At all times a conservative approach should be taken to support system design. For particularly complex rock mass structures and/or poorly understood failure mechanisms, support spacing should be further reduced and support resistance and energy absorption capacities increased.

8.7 Conclusions

It is clear from the above discussion that the proposed design procedure provides a link between the continuous and discontinuous analyses. This is accomplished by making use of the zones of support influence to determine the length of the unsupported beam, s, and using this length in the discontinuous analysis. This method is not as conservative as the present design methodology, where the continuous and discontinuous analyses are independent of each other, and will thus allow for more optimal designs.

A unified methodology to evaluate support systems catering for rockfall and rockburst conditions is proposed. The method consists of two stages: (i) a tributary area analysis, and (ii) a zone of influence analysis, which determines the general support resistance and spacing requirements for the support system as a whole, and a stability analysis considering hangingwall failure due

to buckling, shear and block rotation, which gives maximum safe spacing of individual support units. The methodology is particularly suited to mines of intermediate and great depth, where, typically, the hangingwall consists of hard rock and is highly discontinuous due to face-parallel mining-induced fractures.

The new design methodology also combines both the zone of influence and keyblock stability theories, thus providing an improved support design tool. It is recommended that, following in situ evaluations of the support design methodology proposed here, the methodology be incorporated in a program such as SDA for use in the industry.

It is further recommended that additional work be conducted to quantify the effects of arbitrarily oriented discontinuities of geological origin on support spacing in the strike and particularly the dip directions. Further work could also re-address the influence of the modified hangingwall stress distribution and zones of influence due to loading by the stope face, support units and backfill. The horizontal clamping stress is a vital part of the design procedure. Further work needs to be done to clarify the magnitude and role of this important component.

It should be remembered that the method proposed is untried in the field and, before its full acceptance, it should undergo field trials. Parametric evaluations of the proposed support design methodology show that, for typical discontinuities observed underground (i.e. dipping between 50^{o} and 90^{o}), the design procedure provides realistic spans corresponding to typical spacing of support units in current gold and platinum mines.

9 Support design in shallow mines

9.1 Introduction

In general, the hangingwall in shallow mines is characterised by zero or low clamping stresses and conjugate joint sets, which discretise the hangingwall beam into blocks of relatively intact rock.

A brief overview of an approximate solution for zones of influence in a shallow mining environment follows.

9.2 Proposed design methodology

Consider a stope as shown in Figure 9.2.1. The hangingwall is discretised by two joint sets oriented at two different angles with respect to the stope face. The dip directions of the joint sets are indicated in Figure 9.2.1. The two most prominent joint sets should be taken into consideration when designing the layout of the support system.

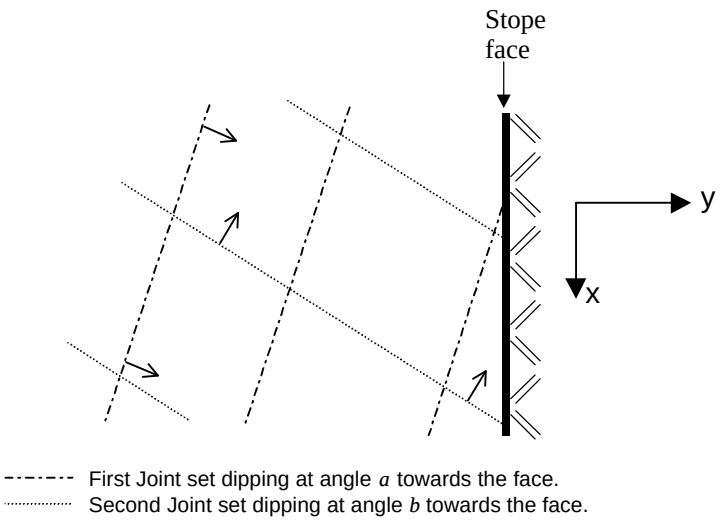

Figure 9.2.1 Hangingwall discretised by two joint sets in a shallow mining environment.

It is important that a probabilistic approach is followed when designing support layouts in shallow mines. The parameters which are considered in the probabilistic formulation are:

f = joint spacing
S = support unit spacing (centre to centre)

Joint set 1:
Spacing = f_1 metres

Joint set 2:
Spacing = f_2 metres

Consider the two dimensional case shown in Figure 9.2.2. The support units are spaced at a distance, S. Let M_x represent the mid-point of the support unit (Figure 9.2.2). A block is considered to be supported if M_x lies between A and B (where A and B represent the edges of the block).

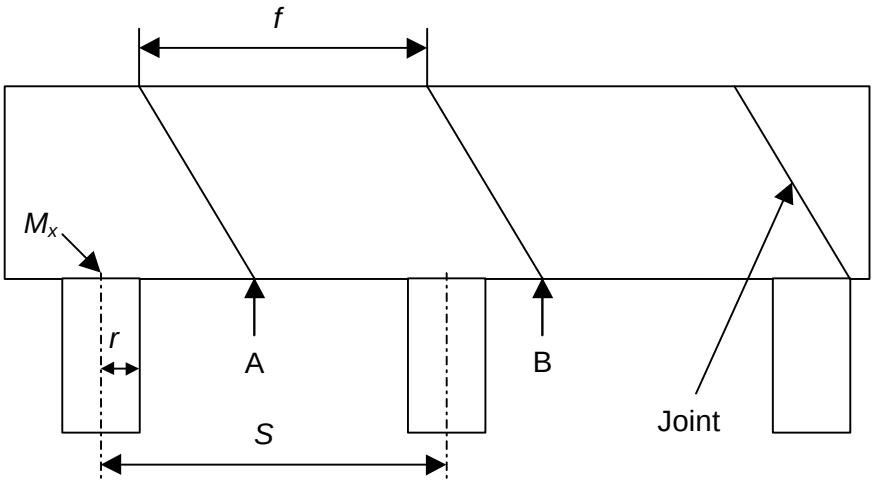

Figure 9.2.2 Hangingwall beam discretised by joints.

Consider a panel extending *m* metres in the x-direction and *n* metres in the y-direction. The area of the panel, A_p, is given by

$$A_p = m \times n. \tag{9.2.1}$$

The area of a block, A_b, is given by

$$A_b = f_x \times f_y. \tag{9.2.2}$$

Thus, the number of blocks in the panel, *N*, can be calculated as

$$N_b = A_p / A_b = (m \times n) / (f_x \times f_y). \tag{9.2.3}$$

where f_x = joint spacing in the x-direction,
f_y = joint spacing in the y-direction.

Now, if S_x = support spacing in the x-direction, and S_y = support spacing in the y-direction, the number of support units, N_s, is given by

$$N_s = (m / S_x) (n / S_y). \tag{9.2.4}$$

The probability, *P*, of a block being supported, i.e. the probability that a support unit is situated underneath a block, is given by the number of support units divided by the number of blocks in the panel under consideration:

$$P = N_s / N_b. \tag{9.2.5}$$

Consider a hangingwall beam discretised by face-parallel and -perpendicular joint sets. (Figure 9.2.3) If the probability that a block is supported is *P*,

$$S_x = f_x / (P)^{0,5} \quad \text{and} \quad S_y = f_y / (P)^{0,5} \tag{9.2.6}$$

where S_x = support spacing in the x-direction,
S_y = support spacing in the y-direction,
f_x = joint spacing in the x-direction, and
f_y = joint spacing in the y-direction.

In this case, $f_x = f_1$ and $f_y = f_2$ (Figure 9.2.4).

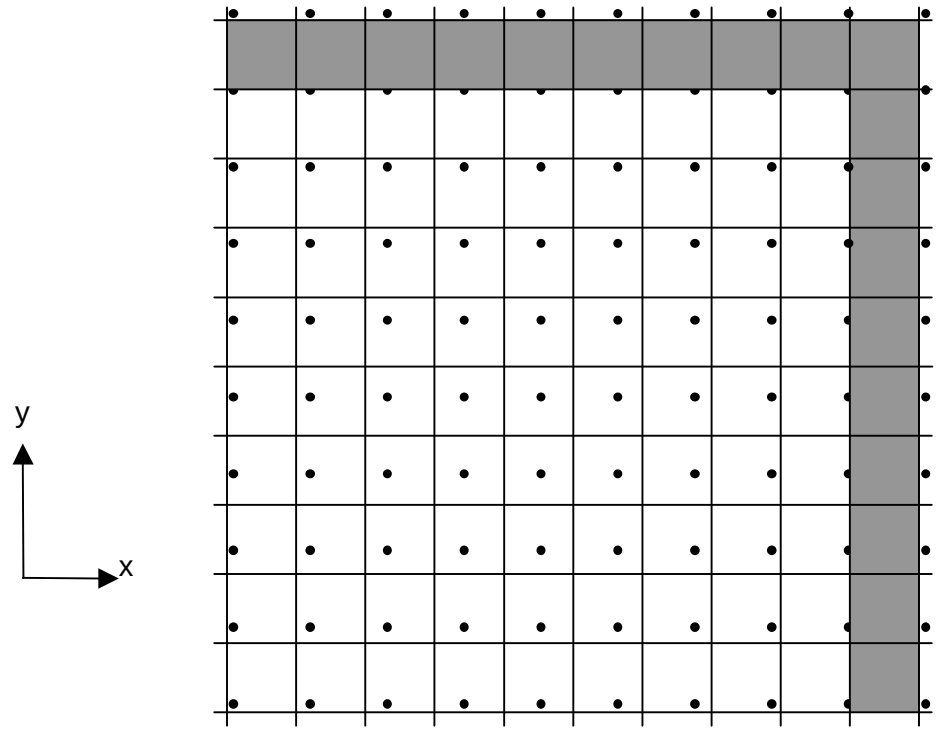

Figure 9.2.3 Support layout for situation where joint set 1 is perpendicular and set 2 is parallel to the face.

Thus, the percentage of blocks which will be supported (thus probability, P):

$$P = \frac{N_s}{N_b} = \frac{\dfrac{n}{f_x/\sqrt{P}}\ \dfrac{m}{f_y/\sqrt{P}}}{\dfrac{n}{f_x}\ \dfrac{m}{f_y}}. \qquad (9.2.7)$$

In Figure 9.2.3 the shaded blocks are those that will not be supported.

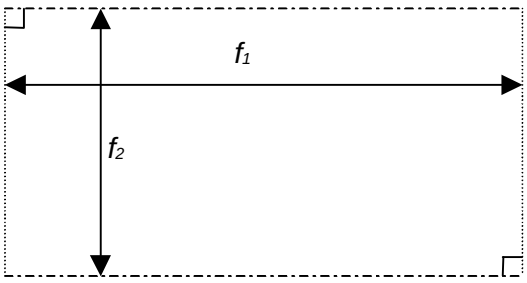

Figure 9.2.4 Perpendicular joint sets.

Now consider the layout shown in Figure 9.2.5. The panel area, A_p, is the same as in the previous scenario.

Let q denote the acute angle between joint set 1 and the x-axis (Figure 9.2.6).

$$f_x = f_1 / \sin q \qquad (9.2.8)$$

Thus:

$$S_x = f_x / (P)^{0,5} \quad \text{and} \quad S_y = f_y / (P)^{0,5} \ , \qquad (9.2.9)$$

as before.

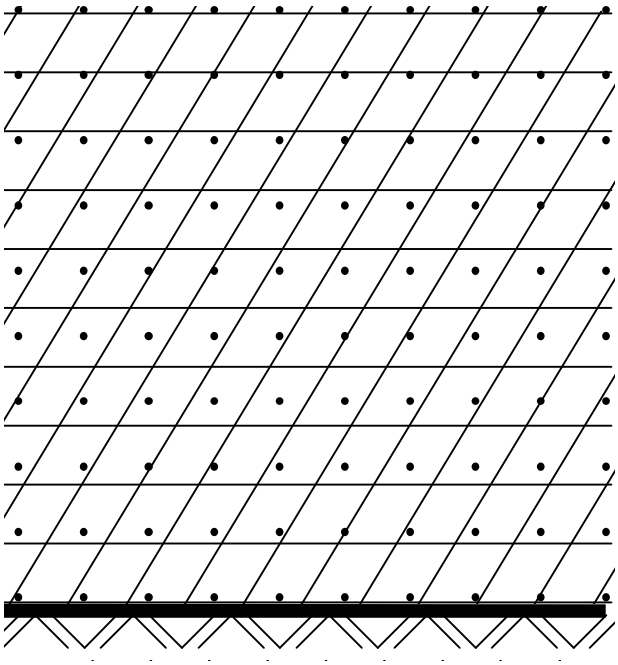

Figure 9.2.5 Support layout for situation where joint set 1 is oriented at an angle, q, and joint set 2 is parallel to the face.

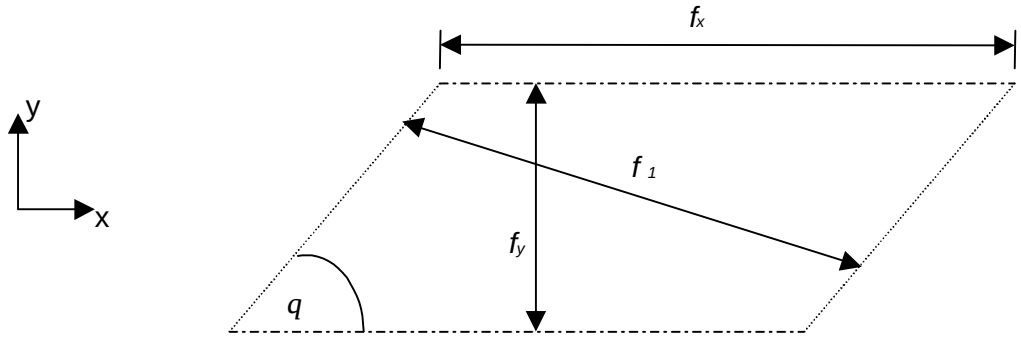

Figure 9.2.6 Block delineated by two joint sets, which are not perpendicular.

If neither of the joint sets is either parallel or perpendicular to the stope face (Figure 9.2.7), the support spacing cannot be designed using the above equations. This is a more complicated problem, which requires further investigation, and falls beyond the scope of this project.

Rotational failure is not considered in the above approach, as only approximately 3 per cent of all keyblock failures in the Bushveld mines are associated with rotational failure mechanisms (Esterhuizen, 1999).

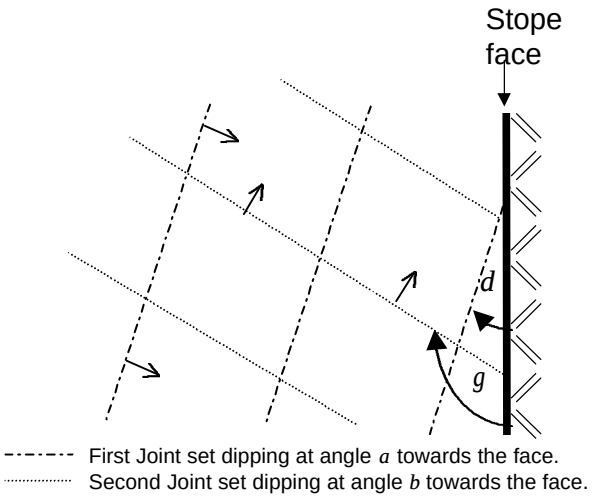

Figure 9.2.7 Hangingwall discretised by two joint sets, neither of which is parallel or perpendicular to the face.

9.3 Conclusions

In shallow mines the keyblocks delineated by geological joints are relatively large and generally intact (i.e. competent). It is recognised that the zone of influence approach is not suitable when designing support systems in shallow mining environments. Instead, the probability of a block being supported by an individual support unit is used to design the support layout and spacing.

It is important to adopt a probabilistic approach when dealing with support systems in shallow mines. Failing to do so results in comparatively conservative support design in terms of support spacing.

The design methodology presented here is simple and easy to use, but it is not applicable to all shallow mining situations, only the specific cases dealt with in this chapter.

This approach does not consider the possibility of rotational failure, as only about 3 per cent of all keyblock failures in the Bushveld mines are rotational (Esterhuizen, 1999).

It is recommended that the situation where there are three joint sets and the case where neither of the two joint sets is either parallel or perpendicular to the face, be further investigated and a support design methodology formulated for these circumstances.

10 Review of principal findings and recommendations for further work

Since the inception of large scale mining and associated rock mass stability problems, relatively little progress has been made in quantifying the effect of support spacing on the rock mass stability. At present, it is the responsibility of the rock engineer to estimate support spacing based upon past experience. In order to improve safety and continue mining at increasing depth, it is important to improve the understanding of the mechanisms involved in the support-rock interaction, the zones of support influence and the role of rock mass discontinuities.

The project work forms the basis of a stope support design methodology with the objective of quantifying optimised support spacing, whilst maintaining stable hangingwall spans between adjacent support units for rockfall and rockburst conditions.

Four enabling outputs were defined to reach this objective:

EO 1 Identify relevant rock mass parameters to characterise the hangingwall integrity in various geotechnical areas.

EO 2 Using analytical and numerical techniques, establish models to quantify the zone of support influence in a discontinuous rock mass.

EO 3 Establish a procedure to verify and calibrate theoretical models (describing the zone of support influence) by means of underground data.

EO 4 Characterise input parameters and design charts for support methodologies leading to improved support system design for quasi-static (rockfall) and dynamic (rockburst) conditions.

The four enabling outputs, as well as their associated principal findings, conclusions and recommendations for further work, are reviewed in Sections 10.1 to 10.4.

It should be remembered that this project is a preliminary investigation into the zone of support influence and stable span between support units. The authors are of the opinion that significant strides have been made in enhancing the understanding of zones of influence and quantifying optimised support spacing.

At this stage, however, the work is theoretical. Before its full acceptance and general practical implementation, the findings of this study should undergo field trials. This is considered an essential extension to the work. Past experience indicates that the ultimate solution to this problem can be achieved only if the research is approached pragmatically. The tributary area concept was the first step along a road that will have to be travelled step by step, if better hangingwall control is to be achieved in the stopes, the most vulnerable areas of the mines.

The final outcome of this work is a proposed design tool for the gold and platinum mining industry to assist the rock mechanics engineer to improve support design. Emphasis is placed on the estimation of optimised support spacing. These proposals are untried in practice and will have to be assessed and calibrated under realistic conditions. The authors hope that the rock engineers in the industry will provide sufficient feedback to facilitate further verification and calibration towards an even better support system design method.

10.1 Identification of relevant rock mass parameters to characterise the hangingwall integrity in various geotechnical areas

10.1.1 Summary

The objective of enabling output 1 is the identification of the relevant rock mass parameters to characterise the hangingwall integrity for use in the design of stope support layouts in various geotechnical areas as applicable to South African gold and platinum mines. To accomplish this, it was necessary to identify the relevant rock mass parameters that govern hangingwall stability, assess the accuracy and ease with which these parameters can be determined, and highlight characteristics of the most important geotechnical areas.

The relevant rock mass parameters, which govern hangingwall stability, were identified using previous SIMRAC work as a basis.

10.1.2 Principal findings and conclusions

Based on previous SIMRAC work, the most important parameters governing hangingwall stability were determined as:

1) The number of discontinuity sets present in the rock mass.
2) The dip angles/orientation of these discontinuities with respect to the horizontal.
3) The perpendicular spacing of the discontinuities, which include the beam thickness of hangingwall.
4) The properties of these discontinuities, such as apparent friction angle.
5) The horizontal clamping stress present in the hangingwall beam.

The input parameters, which are to be used in the design of support systems (Chapter 8), are:

- Extent of fracturing – discontinuities per metre of hangingwall (applicable to intermediate- and deep-level mines).
- Angle of extension (a) and shear fractures (b) (applicable to intermediate- and deep-level mines).
- Joint orientation and density (applicable to shallow mines).
- Bedding thickness (beam thickness), i.e.
    i) Fallout thickness (b) to prominent bedding plane (from rockfall back-analyses), or
    ii) 95% cumulative fallout thickness (b) from fatality database (Roberts, 1995).
- Friction angle (j).
- Density of the rock mass (r).
- *In situ* compressive hangingwall stress (s_x).

The number of discontinuity sets and their spacing can be determined fairly accurately, as can the dip/orientation of these discontinuities and the beam thickness. Friction angles and horizontal clamping stresses, however, cannot be determined accurately and are only

approximations. When using these parameters in designing a support system, as much data as possible must be obtained to give a good representation of the actual rock mass conditions.

Rock mass parameters are site specific and a good understanding of the geology of the area is required in order to estimate the rock mass parameters for the design process.

Using previous SIMRAC work, specifically GAP 330, the important geotechnical areas associated with the following Witwatersrand gold mine reefs were identified: Ventersdorp Contact Reef, Carbon Leader Reef, Vaal Reef, Leader Reef, B-Reef, Witpan Reef, and VS5. The main Bushveld reefs reviewed in this study are the Merensky Reef and the UG2.

10.1.3 Recommendations for further work

Further work is recommended to investigate the following:

- Improved techniques to estimate the *in situ* compressive hangingwall stresses.
- Joint interfaces, particularly in shallow mines, can include filler material and/or be welded. In this case the interface is cohesive, and measurement techniques are required to estimate the cohesive properties of joint interfaces. In future work, the cohesive properties of discontinuities should be considered as an input parameter, which might impact on support design.
- An electronic database should be established to facilitate easy access to critical rock engineering support design parameters for various reef types and geotechnical areas.

10.2 Quantifying zones of influence in a discontinuous rock mass

10.2.1 Summary

The objective of enabling output 2 is to develop a means of quantifying the zones of influence of support units, backfill and the stope face. This was achieved by using numerical techniques to gain qualitative insights into stress trajectories through fractured hangingwall beams, and to facilitate the formulation of mathematical models approximating the zone of influence stress profiles.

The zone of support influence is defined as the lateral extent of the vertical stress profile, induced in the hangingwall by a loaded support unit. The zone of influence can extend some distance away from the immediate support - hangingwall contact, and hence can contribute towards rock mass stability between adjacent support units.

Mining induced and geological discontinuities govern the behaviour and deformation of the rock mass surrounding stopes. The discontinuities affect the zones of influence, and hence extension fractures, shear fractures and bedding planes were considered in this study.

This report gives new and improved formulations of zones of influence of support units, backfill and the stope face in a discontinuous rock mass.

10.2.2 Principal findings and conclusions

The numerical, analytical and underground investigations indicate that mechanisms contributing towards hangingwall stability are: (i) the zones of support influence, and (ii) keyblock stability between adjacent support units. The interaction of these mechanisms gives rise to complex support – rock mass interactions. Support design based on these mechanisms requires in-depth insights into stress trajectories in a discontinuous hangingwall and understanding of limiting equilibrium requirements of keyblocks.

The zones of support influence and their characteristics are largely dependent on individual support units interacting with the hangingwall. A support system (i.e. multiple support units), however, needs to be considered when analysing the stability of keyblocks between adjacent support units.

From the various numerical and analytical models, it is apparent that the stress trajectories follow two principal paths, i.e. (i) parallel to the discontinuities, and (ii) perpendicular to the discontinuities. The orientation of the discontinuities and the magnitude of the horizontal clamping stress will determine the proportion of the stress that is transmitted in each direction.

The maximum extent of the zone of support influence, z, is governed by the friction angle, j, at the bedding plane interface and the bedding plane height, b, where $z = b \tan j$ is the maximum extent of the zone of influence.

Compressive hangingwall stresses affect the zone of influence by clamping hangingwall discontinuities together. As a consequence, stresses can be transmitted obliquely across discontinuities, and the zone of influence is extended to either side of the support unit. In intermediate- and deep-level mines, the typical hangingwall is characterised by face parallel, ubiquitous and closely spaced extension fractures, with face parallel conjugate shear fractures spaced between 1 and 3 m. In these mines, the hangingwall is generally compressed by clamping stresses in excess of 0,5 MPa, and the zones of influence correspond to those in homogeneous beams.

Elliptic paraboloids are chosen to conveniently describe three-dimensional zones of influence in a hangingwall beam arbitrarily discretised by two discontinuity sets. The zone of influence stress distribution in a homogeneous hangingwall beam is described by a circular paraboloid. The mathematical formulation of the zone of influence stress profiles is straightforward and can easily be incorporated into a support design computer program.

A novel probabilistic methodology is developed to quantify the zones of influence associated with hangingwall beams discretised by comparatively widely spaced discontinuities, as is typically the case in shallow mines.

The zone of influence of the stope face follows analogously to the support zone of influence. In intermediate- and deep-level mines the extent of the zone of stope face influence, z, can be approximated as $z = b \tan j$, where, as outlined before, j is the friction angle of the bedding plane and b is the bedding plane height.

In shallow mines, joint spacing and orientation govern the zone of influence of the stope face. Quantifying the zone of influence of the stope face in shallow mines is more complicated than in deeper mines, and falls beyond the scope of this project. Until such time as a clearer understanding of the zone of stope face influence in shallow mines is reached, it should be assumed to be zero.

The underlying theory of the zone of influence of backfill corresponds to the zone of influence induced by the stope face, i.e. $z = b \tan j$. In the case of backfill, however, the actual extent of the zone from the edge of the backfill is reduced due to two factors:

- Typically between 10 and 20 mm of closure is required in order to generate backfill stresses. This implies that for 4 to 12 hours (in an intermediate- or deep-level mine) after installation the stresses induced by the backfill into the hangingwall are negligible, and hence the zone of influence is negligible.

- Due to bulging of the backfill bag, the edge of the backfill does not generally correspond to the point of backfill – hangingwall contact. The work conducted as part of this project has shown that the point of contact is typically between 20 and 70 cm from the edge of the backfill. Since the extent of the zone of influence is measured from the edge of the support, the extent of the zone associated with backfill is reduced by, typically, 20 to 70 cm.

10.2.3 Recommendations for further work

To continue mining at ever-increasing depths with reduced rock-related risk and optimum productivity, support system design needs to be based upon sound engineering principles. Various tools have been developed to address support performance in quasi-static and dynamic conditions, support interaction with the hangingwall, and maximum stable spans between adjacent support units.

The various design criteria and engineering principles need to be incorporated into a unified design methodology. A computer program in the form of SDA II is required to engage the methodology and enable the rock engineer to conveniently optimise geotechnical area specific support systems.

In shallow mining environments, the determination of the exact shape of the zone of influence of the stope face and the associated stress distribution, is a complex problem, and falls outside the scope of this study. However, it is strongly recommended that further work concerning the quantification of these zones of influence should be undertaken.

10.3 Calibration and verification of theoretical models describing the zone of influence

10.3.1 Summary

For an analytical model to be useful in the industry, it needs to be verified by comparing the predicted results to actual cases, so that the model can be used with confidence in the design of support systems. The objective of enabling output 3 is to establish a procedure to verify and calibrate theoretical models, describing the zones of influence, by means of underground data.

In order to achieve this objective, the various methods, which can be used to estimate the *in situ* hangingwall strength in various geotechnical areas, are investigated. Furthermore, preliminary back-analyses of rockburst and rockfall accidents, using the CSIR accident database, are carried out in order to determine a statistical distribution of unstable hangingwall spans for various geotechnical areas. This information is used to establish a procedure to calibrate and verify the theoretical models.

10.3.2 Principal findings and conclusions

The fatality data has shown that, for the various reefs considered, on average, there is an increase in the number of fatalities, as the support density decreases.

Engineering judgement, past accident data, seismicity and hangingwall strength should be used to calibrate the theoretical models.

10.3.3 Recommendations for further work

To verify and calibrate the design methodology, it is recommended that several cases, taken from the accident database, be checked and back-analysed using the proposed design method. If the proposed methodology indicates that the actual support unit spacings used in these cases are sufficient, then it is not conservative enough, and steps should be taken to calibrate or modify the design method.

10.4 Characterising input parameters and design charts for support methodologies leading to improved support system design for quasi-static (rockfall) and (rockburst) conditions

10.4.1 Summary

The objective of enabling output 4 is to characterise the input parameters and provide improved support design methodologies for both rockfall and rockburst conditions. This is accomplished by integrating the tributary area-, zones of influence- and keyblock approaches to form a unified design methodology for stope support systems in intermediate- and deep-level mines. The proposed design procedure caters for both blocky hangingwalls and hangingwalls with face-parallel fractures (FPFs).

10.4.2 Principal findings and conclusions

The proposed design procedure provides a link between the continuous and discontinuous analyses. This is accomplished by making use of the zones of support influence to determine the length of the unsupported beam, *s*, and using this length in the discontinuous analysis. This method is not as conservative as the present design methodology, where the continuous and discontinuous analyses are independent of each other, and will allow for more optimal designs.

The assumption that the hangingwall will be stable if $d < 1{,}5s$ (based on probabilistic keyblock analyses indicating that, to ensure rock mass stability, the unsupported span in the dip direction, *d*, should not exceed 1,5 times the unsupported span in the strike direction, *s*), is also made in the new design procedure, as it simplifies the design by eliminating the need for complicated three-dimensional analyses. Furthermore, this relationship has been found to be valid in practice.

10.4.3 Recommendations for further work

The new design methodology combines the *tributary area*, *zone of influence* and *keyblock stability* theories, thus potentially providing an improved and further optimised design tool. It is recommended that the design methodology proposed here be evaluated underground and, if applicable, be incorporated in a design program such as SDA II for use in the industry.

11 References

Adams, G.R., Jager A.J. & Roering, C. 1981. Investigation of rock fracture around deep level gold mine stopes. *Proceedings of the 22nd U.S. Symposium on Rock Mechanics*. Boston, M.I.T., 28 June – 2 July, pp. 213-218.

Arnold, D.A., Legg, E.W. & Roberts, M.K.C. 1994. Reducing the unsupported stope span at Hartebeestfontein Gold Mine. *XV'th CMMI Congress*, Johannesburg: SAIMM, Vol. 1, pp. 159-165.

Bandis, S.C., Lumsden, A.C. & Barton, N.R. 1983. Fundamentals of rock joint deformation. *International Journal of Rock Mech. Min. Sci. & Geomech*. *Abstr*., 20(6), pp. 249 – 268.

Barton, N. and Choubey, V. 1978. The Shear Strength of Rock Joints in Theory and Practice. Norwegian Geotechnical Institute, Publication no. 119.

Beer, G. & Meek, J.L. 1982. Design curves for roofs and hangingwalls in bedded rock based on voussoir beam and plate solutions. *Trans Instn Min. Metall*., 91, pp. A18 – 22.

Brady, B.H.G. and Brown, E.T. 1985. Rock Mechanics For Underground Mining. London: George Allen and Unwin.

CSIR: Division of Mining Technology 1999. Support Design Analysis (SDA II) software. Rock Engineering, Carlow Rd. Auckland Park, South Africa.

Daehnke, A. 1997. Stress wave and fracture propagation in rock. Ph.D. Thesis, Vienna University of Technology.

Daehnke, A., Andersen, L.M., de Beer, D., Esterhuizen, E., Glisson, F.J., Jaku, E.P., Kuijpers, J.S., Peake, A.V., Piper, P., Quaye, G.B., Reddy, N., Roberts, M.K.C., Schweitzer, J.K., Stewart, R.D. 1998. SIMRAC Final Project Report (GAP 330). Stope Face Support Systems, CSIR: Division of Mining Technology.

Daehnke, A., Van Zyl, M., Le Bron, K.B. 1999a. Quantifying zones of support influence in a discontinuous rock mass. *Proceedings of the 2nd Southern African Rock Engineering Symposium*. Johannesburg, 13-15 September, pp. 194-203.

Daehnke, A., Salamon, M.D.G. & Roberts, M.K.C. 1999b. Investigating zones of support influence and quantifying stable hangingwall spans between support units. To be published in: *J. of South African Inst. of Mining and Metall.*

Esterhuizen, G.S. 1998. Improved support design through a keyblock approach. Interim Report for SIMRAC Project GAP 330, Stope face support systems, prepared by CSIR: Division of Mining Technology and University of Pretoria, pp. 1 – 83.

Esterhuizen, G.S. 1999. Analysis of keyblock rotation in Bushveld mines. Interim Report for SIMRAC Project GAP 613, Elongate support performance and requirements of blocky rock masses, Colorado, USA, pp. 1 – 18.

Evans, W.H. 1941. The strength of undermined strata. *Trans Instn Min. Metall*., 50, pp. 475 – 532.

Grimstad, E. & Barton, N. 1993. Updating of the Q-system for NMT. *Proceedings of the International Symposium on Sprayed Concrete - Modern Use of Wet Mix Sprayed Concrete for Underground Support*, Norwegian Concrete Institute.

Gürtunca, R.G., Squelch, A.P. & Gonlag, M.D. 1990. Results of a backfill monitoring program at harmony gold mine, 3 shaft, 27/18b stope. *COMRO internal note no. R04/90.* Johannesburg: Chamber of Mines Research Organisation.

Haile, A.T., Grave, D.M., Sevume, C. & Le Bron, K. 1998. SIMRAC Final Project Report. Strata control in tunnels and an evaluation of support units and systems currently used with a view to improving the effectiveness of support, stability and safety of tunnels. CSIR: Division of Mining Technology.

Herrmann, D.A. 1987. Fracture control in the hangingwall and the interaction between the support system and the overlying strata. M.Sc. Dissertation. Johannesburg: University of the Witwatersrand.

Hutchinson, D.J. & Diederichs, M.S. 1996. Cablebolting in Underground Mines. BiTech Publishers, pp. 265 – 269.

Itasca. (1993). Universal Distinct Element Code (UDEC) Version 2 Manual.

Jager, A.J. 1998. Personal communication on the structure of discontinuous hangingwalls in deep level mines. CSIR: Division of Mining Technology, Carlow Road, Auckland Park, Johannesburg, 2000.

Jager, A.J. & Roberts, M.K.C. 1986. Support systems in productive excavations. Gold 100. *Proc. of the Int. Conf. on Gold. Vol 1: Gold Mining Technology.*, SAIMM, Johannesburg, pp. 289 – 300.

Kuijpers, J.S. 1998. Identification of inelastic deformation mechanisms around deep level mining stopes and their application to improvements of mining techniques. PhD Thesis. Johannesburg: University of the Witwatersrand.

Palmstrøm, A, 1996. Characterising rock masses by the RMi for use in practical rock engineering Part 1: The development of the Rock Mass Index (RMi), *Tunnelling and Underground Space Technology*, Volume 11, No.2, Pergamon Press.

Roberts, M.K.C. 1995. Stope and gully support. Final Report for SIMRAC Project GAP 032, CSIR: Division of Mining Technology, pp. 1 – 45.

Roberts, M.K.C. 1999. Personal communication on the spacing of support units. CSIR: Division of Mining Technology, Carlow Road, Auckland Park, Johannesburg, 2000.

Rockfield 1996. ELFEN User Manual, Version 2.6, University College of Swansea.

Ryder, J.A., 1999. Personal communication, CSIR Mining Technology, December 1999.

Sellers, E.J. 1997 A tessellation approach for the simulation of the fracture zone around a stope. *Proceedings of SARES97.* Johannesburg: pp. 143-154.

Squelch, A.P. 1994. The determination of the influence of backfill on rockfalls in South African gold mines. M.Sc. Dissertation, University of Witwatersrand, Johannesburg.

Viljoen, M.J. & Hieber, R. 1986. The Rustenburg Section of Rustenburg Platinum Mines Limited, with reference to the Merensky Reef. In: Anhaeuser, C.R., and Maske, S. (Editors): *Mineral Deposits of Southern Africa*, Vol. 1, Geol. Soc. S. Afr., pp. 1107-1134.

Wagner, H. 1984. Support requirements for rockburst conditions. *Proc. of the 1st Int. Cong. on Rockbursts and Seismicity in Mines*, SAIMM, eds. N.C. Gay and E.H. Wainwright, Johannesburg, pp. 209 – 218.

York, G., Canbulat, I., Kabeya, K.K., Le Bron, K.B., Watson, B.P. & Williams, S.B., 1998. SIMRAC Final Project Report (GAP 334). Develop guidelines for the design of pillar systems for shallow and intermediate depth, tabular, hard rock mines and provide a methodology for assessing hangingwall stability and support requirements for the panels between pillars. CSIR: Division of Mining Technology.